

G9049

MICROWAVE ELECTRONICS

**DEVELOPMENT AND ANALYSIS OF
BROADBAND L-STRIP FED MICROSTRIP
ANTENNAS**



Thesis submitted by

LETHAKUMARY B

*In partial fulfilment of the requirements
for the degree of
DOCTOR OF PHILOSOPHY
under the Faculty of Technology*

**DEPARTMENT OF ELECTRONICS
COCHIN UNIVERSITY OF SCIENCE AND TECHNOLOGY
COCHIN 682 022, INDIA**

December 2004

Dedicated to the ones who paved the way for my achievements

- my parents & teachers

CERTIFICATE

This is to certify that this thesis entitled "**DEVELOPMENT AND ANALYSIS OF BROADBAND L-STRIP FED MICROSTRIP ANTENNAS**" is a bonafide record of the research work carried out by Ms. Lethakumary B, under my supervision in the Department of Electronics, Cochin University of Science and Technology. The results presented in this thesis or parts of it have not been presented for any other degree.



Dr. P. Mohanan

(Supervising Guide)

Professor

Cochin 682 022

30th December 2004

Department of Electronics

Cochin University of Science


and Technology

DECLARATION

I here by declare that the work presented in this thesis entitled **“DEVELOPMENT AND ANALYSIS OF BROADBAND L-STRIP FED MICROSTRIP ANTENNAS”** is based on the original work done by me under the supervision of Dr. P. Mohanan in the Department of Electronics, Cochin University of Science and Technology, and that no part thereof has been presented for any other degree.

Cochin 682 022

30th December 2004


Lethakumary B

ACKNOWLEDGEMENTS

I would like to express my sincere gratitude and indebtedness to Dr. P. Mohanan, Professor, Department of Electronics, Cochin University of Science and Technology for his valuable guidance and constant encouragement I received throughout my research work.

I would like to express my sincere thanks to Dr. K Vasudevan, Professor and Head, Dept. of Electronics for his valuable support and help during my research work.

Let me express my deep sense of gratitude to Dr. C. K. Aanandan, Reader, Dept. of Electronics, and Dr. K.T Mathew, Prof. Dept of Electronics, for their valuable suggestions and encouragements.

I also would like to thank Dr. P.R.S Pillai, and Dr. K. G. Balakrishnan, former Heads, Dept. of Electronics for their help during my research.

I am hereby recording my gratitude to Prof. K.G Nair, Director, Centre for Science in Society, Cochin University for his valuable suggestions.

Sincere thanks are due to, Dr. Tessamma Thomas, Mr. D. Rajaveerappa and Mr. James Kurian, faculty members of the Department of Electronics for the help and cooperation extended to me.

I am deeply indebted to my friend Ms. Supriya M.H, Lecturer, Department of Electronics for the encouragement and help rendered to me during my research work.

I would like to acknowledge with thanks Dr. Jacob George, Corning Inc. USA and Dr. Joe Jacob, Senior Lecturer, Newman College, Thodupuzha, for the help and valuable advices given to me for the successful completion of my work.

I take this occasion, to place on record the cooperation, help and encouragements I received from my former colleagues Ms. Sona O Kundukulam, Scientist, DRDO, Bangalore and Ms. Manju Paulson, Research fellow, University of Surrey, UK.

My words are boundless to thank research colleagues in the department, Ms. Sreedevi K .Menon, Ms. Mridula S, Ms. Binu Paul, Ms. Bindu G, Ms. Suma M. N, Mr. Rohit K. Raj, Mr. Anupam R. Chandran, Mr. Shynu S. V, Mr. Manoj Joseph, Mr. Gijo Augustine, Mr. Anil Lonappan, Dr. Jaimon Yohannan, Mr. Praveen Kumar, Mr. Vinu Thomas, and Mr. Dinesh Kumar V.P and other teaching, non-teaching, and technical staff of the Department of Electronics and all my well wishers who have extended their co-operation during my work.

LETHAKUAMRY B

OBJECTIVE AND OUTCOME

Objective : Design, development and analysis of a broad band microstrip antenna using modified feeding techniques.

Outcome : Designed and developed a broad band microstrip antenna using L-strip feeding technique with the following characteristics.

2: 1 VSWR BW % : ~20%, ~6 times larger than conventional rectangular patch antenna.

Gain : ~ 8.2dBi, slightly greater than conventional rectangular patch antenna.

Radiation pattern : Almost same as conventional rectangular patch antenna.

Analysis : Analyzed using FDTD method and found excellent agreement with experimental observations.
Computed resonant frequency, impedance bandwidth, input impedance, and radiation patterns.

CONTENTS

CHAPTER 1

INTRODUCTION	1
1.1 MICROSTRIP PATCH ANTENNAS	3
1.1.1 Radiation Mechanism Of Microstrip Antennas	3
1.1.2 Advantages And Disadvantages	6
1.1.3 Applications	6
1.1.4 Excitation techniques	7
1.1.5 Microstrip antenna configurations	10
1.1.6 Basic characteristics of rectangular patches	12
1.1.7 Theoretical methods for analysis of microstrip antennas	14
1.1.8 Broad band microstrip antennas	18
1.2 OUTLINE OF THE PRESENT WORK	18
1.3 CHAPTER ORGANIZATION	19

CHAPTER 2

REVIEW OF THE PAST WORK	20
2.1 DEVELOPMENT OF MICROSTRIP ANTENNAS	21
2.2 BROAD BAND MICROSTRIP ANTENNAS	24

CHAPTER 3

EXPERIMENTAL RESULTS AND OBSERVATIONS	32
SECTION I	
L-STRIP FED RECTANGULAR MICROSTRIP ANTENNAS	33
3.1 INTRODUCTION	33
3.1.1 ANTENNA GEOMETRY	33
3.2 METHODOLOGY	34
3.2.1 Input Impedance	37
3.2.2 Effect of feed parameters on reflection characteristics	48
3.2.2.1 Microstrip Antenna -2.4GHz	48

3.2.2.2	Microstrip Antenna – 2.7GHz	86
3.2.2.3	Microstrip Antenna – 3.2GHz	83
3.2.2.4	Microstrip Antenna – 3.3GHz	70
3.2.3	Effect of feed point location on reflection characteristics	77
3.2.4	Effect of permittivity on bandwidth	83
3.2.5	Radiation Pattern	87
3.2.6	Gain	93
3.2.7	Simulated Results	97
3.2.7.1	Return loss and bandwidth	97
3.2.7.2	Simulated radiation patterns	102

SECTION II

L-STRIP FED CIRCULAR MICROSTRIP ANTENNA	109
3.1 INTRODUCTION	109
3.1.1 Antenna Geometry	109
3.2 EXPERIMENTAL OBSERVATIONS	110
3.2.1 Circular patch –3.5GHz	110
3.2.2 Circular patch – 2.4GHz	116
3.2.3 Circular patch – 1.8GHz	122
3.2.4 Gain	126
3.2.5 Simulated Results	127

CHAPTER 4

THEORETICAL INVESTIGATIONS	130
4.1 Introduction	131
4.2 Theoretical Approach	131
4.2.1 FDTD Modelling Theory	131
4.2.2 FDTD Problem Definition	134
4.2.3 FDTD Principal Equations	135
4.2.4 Source Considerations	136
4.2.5 Absorbing Boundary Conditions	138

4.2.6	Scattering Parameters	140
4.2.7	Radiation pattern Calculation	140
4.3	ANALYSIS OF L-STRIP FED RECTNGULAR MICROSTRIP ANTENNA	144
4.3.1	Microstrip antenna – 3.3GHz	145
4.3.2	Microstrip Antenna – 3.2GHz	165
4.3.3	Effect of permittivity on bandwidth	178
CHAPTER 5		
CONCLUSIONS		
		185
APPENDIX A		
		189
APPENDIX B		
		197
APPENDIX C		
		203
REFERENCES		
		209
INDEX		
		220
LIST OF PUBLICATIONS OF THE CANDIDATE		
		222
RESUME OF THE CANDIDATE		
		225

CHAPTER 1

INTRODUCTION

In the year 1819, Hans Christian Oersted, a Danish Professor of Physics, [5] found that a current-carrying wire produces magnetism, and thus established the fact that electricity and magnetism are not two distinct phenomena but are interlinked. Later, Andre Marie Ampere, a French Physicist, carried out an in-depth study of the magnetic effects of electric currents. In 1831, Michel Faraday experimentally demonstrated the revolutionary concept; a changing magnetic field produces an electric current. The modern world is highly indebted to this invention. In the year 1873, based on Ampere's and Faraday's extensive experimental investigations, James Clerk Maxwell [5], the genius Mathematician, unified electricity and magnetism. The mathematical formulations of the interrelations between the electric and magnetic fields, led him into the prediction of the existence and propagation of electromagnetic waves. But more than a decade lapsed before his theories were vindicated by Hertz. In the year 1887, Heinrich Rudolph Hertz, [16], [20] assembled an apparatus which may now be called a complete *radio* system, using a top-loaded half-wave dipole as the transmitting antenna and resonant square loop as the receiving antenna. With the help of this apparatus working at 4 meters wavelength, he demonstrated the existence and propagation of electromagnetic waves. He also studied, employing 30cm wavelength, the reflection, refraction and polarization of electromagnetic waves, and showed that except for their much longer wavelength, radio waves are same as light waves. In the year 1897, Jagadish Chandra Bose [5], an Indian scientist, devised a horn antenna and hollow wave guide at a wavelength shorter than 30cm for the first time and demonstrated this in the Royal Society by setting up a radio communication link. Antennas were installed for the first time in a practical system by Marconi [16] in 1897 while he established the first system of wireless telegraphy and the Trans -Atlantic Communication system.

Hertz studied the fields of point dipoles. This work was carried on further by Sommerfield and others [16], and by 1914, the concept of retarded potential was extensively employed in calculations of the radiation patterns due to known currents on antennas. After the discovery of high frequency tubes by De Forest in 1920 [16], much interest was generated in resonant length antennas. Also this led to the theory and practice of simple arrays.

The contributions of J.D Kraus to the field of antennas are outstanding. He invented the helical and corner reflector antennas, which are widely used in space communications as well as television reception. He made extensive studies on the performance of various antennas and classified them as follows

- a. Wire antennas: dipoles, monopoles, helical antennas and Yagi-Uda antennas, commonly used for low frequency applications.
- b. Aperture antennas: wave guide horn, slot in wave guide, cavity or ground plane used for microwave frequencies.
- c. Reflector antennas: parabolic reflector antenna and cassegrain antenna operating at microwave frequencies.
- d. Printed planar antennas: microstrip antennas used in microwave frequency and Microwave Monolithic Integrated Circuit (MMIC) applications.
- e. Active antennas: used for MMIC applications.

The fast development in the field of communication systems demand planar, low profile, lightweight and conformal antennas. Microstrip patch antennas which exhibits all the above properties are the ideal choice and are replacing the conventional antennas in the above applications.

1.1 MICROSTRIP PATCH ANTENNAS

The concept of microstrip antennas was first proposed by Deschamp in 1953[13]. Howell [18] and Munson [19] developed the first practical antennas of this type in early 1970's. Conventional microstrip antennas consist of a single thin conducting material on a dielectric substrate above a ground plane. The patch conductor is normally of copper or gold and with any shape but regular geometrical shapes are generally used. Typically, rectangular or circular shapes with dimensions of the order of half wavelength are preferred. The basic configuration is shown in Figure 1.1.

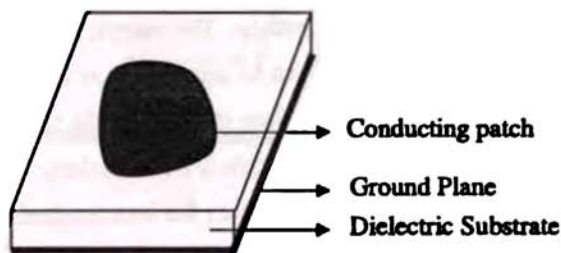


Figure 1.1 Microstrip Antenna

1.1.1 Radiation Mechanism of Microstrip Antenna

The radiations from a microstrip antenna can be determined from the field distributions between the patch and the ground plane. It can also be described in terms of the surface current distribution on the patch metalization. A microstrip patch antenna energized with a microwave source will establish a charge distribution on the upper and lower surfaces of the patch as well as on the ground plane surface. This is shown in Figure 1.2. The repulsive force between like charges, pushes back some of the charges from the bottom surface to its top surface. This movement of charges creates current densities J_b and J_t at the bottom and top surfaces of the patch [12].

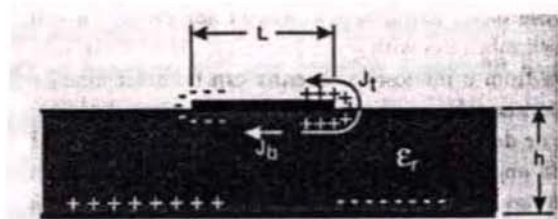


Figure 1.2 Charge distribution and current density creation on a microstrip patch.

Since the ratio of height to width of the microstrip patch is very small, most of the current and charge concentrates underneath the patch. A weak magnetic field tangential to the edge is formed due to a small amount of current flowing around the edges of its top surface. The electric field is normal to the patch surface and hence the antenna can be considered as a cavity with electric walls at the top and bottom surface and four magnetic walls along the edges. The cavity would not radiate if the material within it were lossless. The choice of the effective loss tangent of the material determines the loss mechanism of the cavity, which now behave as an antenna.

Since the thickness of the dielectric substrate is very small, the waves generated within it undergo reflections on reaching at the edge of the patch. Therefore only a small fraction of the energy is radiated. Since the height of the substrate is very small, the field variations along the height are constant. Also due to this, the fringing fields along the edges of the patch are also very small, so the electric field is normal to the surface of the patch. Therefore only TM^z field configurations can exist within the cavity. While the top and bottom walls of the cavity are perfectly electric conducting, the four side walls as perfectly conducting magnetic walls.

The antenna can be represented as two radiating slots along the length of the patch, each of width W and height h . Out of four slots representing the microstrip antenna, only two account for most of the radiation. The fields radiated by the other, which are separated by the width W of the patch, cancel along the

principal planes. The slots separated by the length of the patch are termed as the radiating slots. The slots are separated by parallel plate transmission line of length L , which acts as a transformer. The length of the transmission line is approximately $\lambda/2$ in order to have oppositely polarized fields at the aperture of the slots. This is illustrated in Figures 1.3 (a), (b) and (c). The two slots form an array with λ

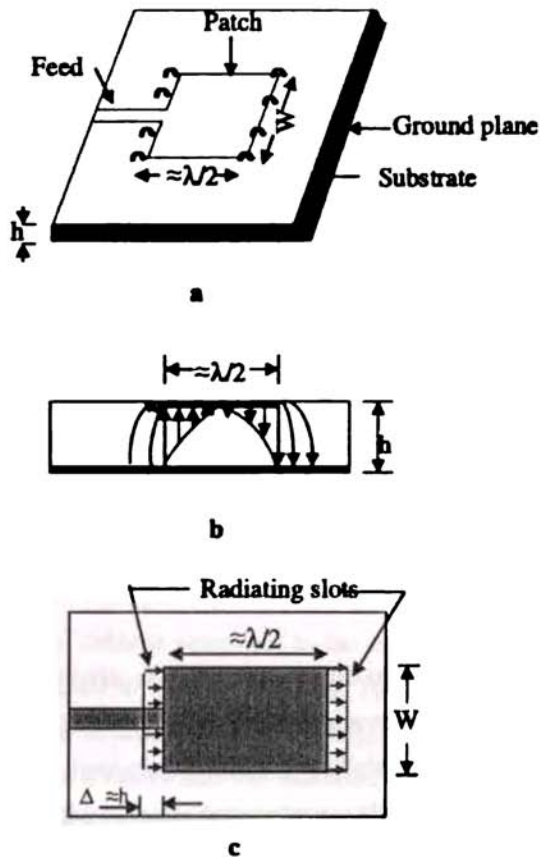


Figure 1.3(a) Rectangular microstrip patch antenna.

(b) Side view

(c) Top view

1.1.2 Advantages and Disadvantages

Microstrip antennas have many advantages. They are low-profile, light weight, easy to manufacture, conformable to planar and non planar surfaces, low cost, mechanically robust when mounted on rigid surfaces, and can be easily integrated with circuits. These antennas have applications in telemetry, satellite communications and various military radar systems. They can easily be integrated with solid state receiving or transmitting module. Linear and circular polarizations are possible by adjusting the antenna parameters and feeding networks or by placing shorting PIN diodes at appropriate positions.

Microstrip antennas suffer from some operational disadvantages also. They offer low efficiency, lower power handling capacity, low bandwidth, etc. Besides, the extraneous radiation from feeds, junctions and excitation of surface waves provides poor radiation performance. However some of these limitations can be overcome by proper choice of substrate and design parameters.

1.1.3 Applications

Mobile and wireless communications often require antennas having small size, lightweight, low profile and low cost. The practical applications of mobile systems are in moving vehicles and in portable systems. In ships and aircrafts, where conformal and lightweight antennas are desirable, microstrip antennas are considered to be suitable.

Microstrip antennas also find applications in satellite communications where circular polarization is required. The flat structure of microstrip antenna makes it suitable for array applications in satellite communications. Some of the commercial systems that presently use microstrip antennas with the corresponding frequency bands are listed below.

Applications	Frequency
Cellular phone	824-849 MHz and 869-895MHz
GPS	1575MHz and 1227MHz
Paging	931-932MHz
GSM	890-915MHz and 935-960MHz
Personal communication systems	1.85-1.99GHz and 2.18-2.2GHz
Wireless local area network	2.4-2.48GHz and 5.4GHz
Cellular video	28GHz
Direct broad cast satellite	11.7-12.5GHz
Automatic toll collection	905MHz and 5-6GHz
Collision advance Radar	60GHz, 77GHz and 94GHz
Wide area computer networks	60GHz

1.1.4 Excitation Techniques

Microstrip antennas are excited by one of the four methods: (a) coaxial probe, (b) microstrip line feed connected to the edge of the patch, (c) microstrip line coupled to the patch through electromagnetic method, and (d) microstrip line coupled to the patch through an aperture.

1.1.4.1 Coaxial feed

One of the common methods of feeding the microstrip antenna employs coaxial probe. The basic configuration is shown in Figure 1.5. Here the central conductor of the coaxial cable is connected to the radiating patch where as the outer conductor is attached to the ground plane. This type of feeding has the flexibility of impedance matching with low spurious radiation. Coaxially fed antenna has low impedance bandwidth. For increased bandwidth, thick substrates are to be used and which requires a longer probe. But, this gives rise to an increase in spurious radiation form the probe, increased surface wave power and increased feed inductance.

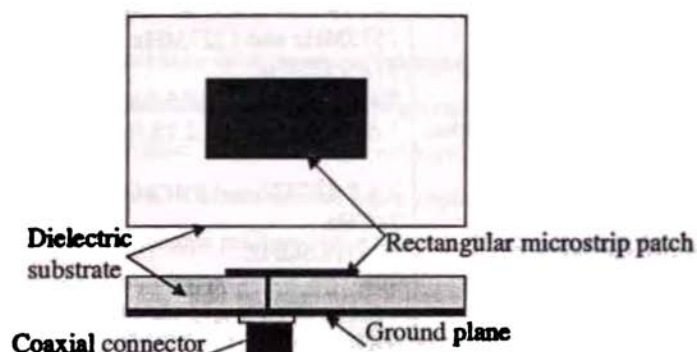
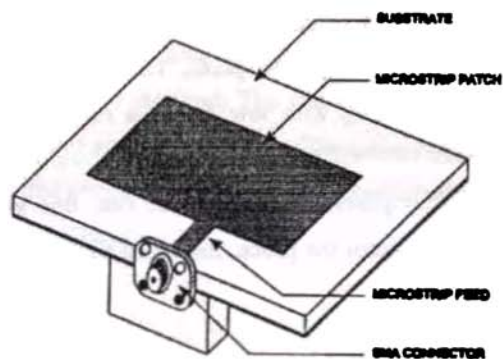


Figure 1.5 Co-axial fed Rectangular microstrip patch.

1.1.4.2 Microstrip Line Feed

Microstrip line feed is the simplest of the excitation techniques. Here, the feed line is fabricated along with the patch on the same side. Figure 1.6 shows the feeding arrangement. This method of directly connecting a strip to the edge of a patch is highly convenient when integrating the feeding network for large arrays. However the spurious radiation from the feed often creates problems. This can be reduced by choosing a high dielectric constant substrate. In this type of excitation the prior knowledge of the feed point location is absolutely required for impedance matching.



1.1.4.3 Electromagnetic (Proximity) Coupling

In this type of feeding system, the radiating patch is etched on another substrate and placed above the open-ended feed line. Thus the element is parasitically coupled to the feed network. Figure 1.7 depicts such a feeding mechanism. It has large bandwidth, low spurious radiation and easy to fabricate. The system consists of two substrates separated by a ground plane. Energy from the microstrip feed line on the bottom side of the lower substrate is coupled to the patch through the slot on the ground plane separating the two.

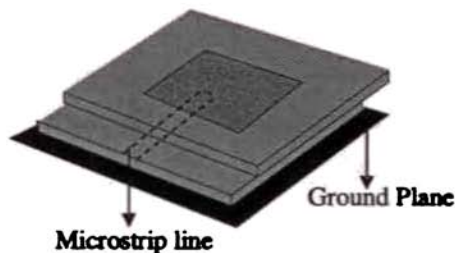


Figure 1.7 Proximity Coupling.

1.1.4.4 Aperture Coupling

A feeding method, which has become very popular, involves coupling of energy from a microstrip line through an aperture (slot) in the ground plane. This method is known as the aperture coupling and is shown in Figure 1.8. The slot couples energy from the strip line to the patch. Typically high dielectric constant material is used for the bottom substrate and thick low dielectric constant material for the top substrate. The spurious radiation from the feed network is low because the radiating element is isolated from the feed by the ground plane.

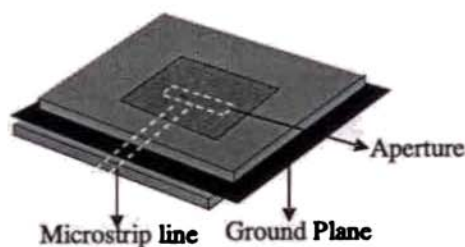


Figure 1.8 Aperture Coupling.

1.1.5 Microstrip Antenna Configurations

Microstrip antennas can be divided into three basic categories: microstrip patch antennas, microstrip traveling wave antennas, and microstrip slot antennas. Their characteristics are discussed below.

1.1.5.1 Microstrip Patch Antennas

A microstrip patch antenna consists of a conducting patch of any planar geometry on one side of a dielectric substrate backed by a ground plane. Various microstrip patch configurations are shown in Figure 1.9.

1.1.5.2 Microstrip Traveling Wave Antennas

Microstrip Traveling Wave Antennas consists of chain shaped periodic conductors or an ordinary long TEM line which also supports a TE mode, on a substrate backed by a ground plane. The open end of the TEM line is terminated in a matched resistive load. As antenna supports traveling waves, their structures may be designed so that the main beam lies in any direction from broadside to end-fire. Various configurations are shown in Figure 1.10.

1.1.5.3 Microstrip Slot Antennas

Microstrip slot antenna comprises of a slot in the ground plane fed by a microstrip line. The slot may have the shape of a rectangle or a circle as shown in the Figure 1.11.

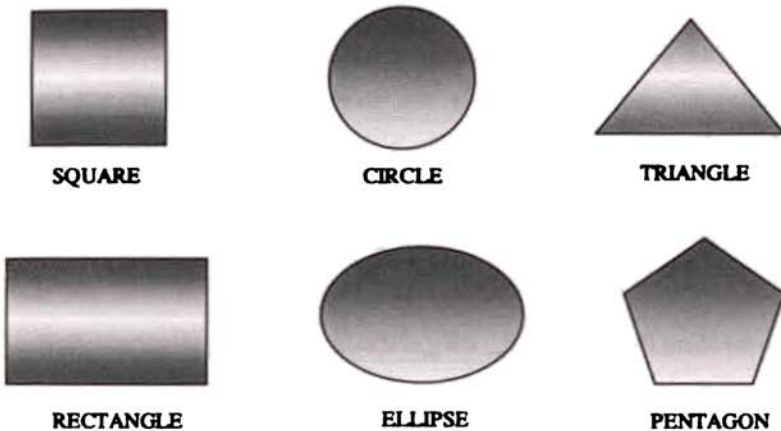


Figure 1.9 Microstrip Patch Antennas.

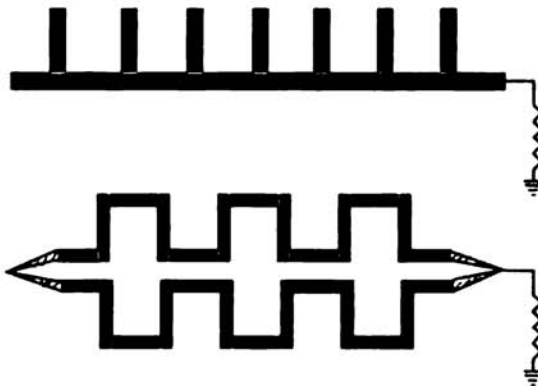


Figure 1.10 Microstrip Traveling Wave Antennas.

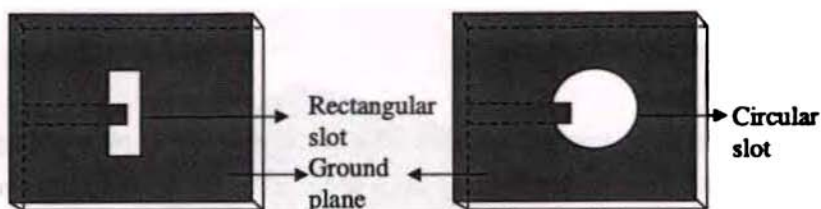


Figure 1.11 Microstrip Slot Antennas.

1.1.6 Basic Characteristics of Rectangular patches

Rectangular patch is probably the most commonly used microstrip antenna. It is characterized by the length 'a' and width 'b'. Geometry can be analyzed by the application of cavity model. The electric and magnetic field of a resonant mode in the cavity under the patch is given by

$$E_z = E_0 \cos(m\pi x/a) \cos(n\pi y/b), \text{ where } m, n = 0, 1, 2, \dots \quad (1.1)$$

$$\text{The resonant frequency is } f_{mn} = k_{mn} c / 2\pi \sqrt{\epsilon_r}, \quad (1.2)$$

$$\text{where } k_{mn}^2 = (m\pi/a)^2 + (n\pi/b)^2 \quad (1.3)$$

eqn (1.2) is based on the assumption of a perfect magnetic wall. To account for fringing field at the perimeter of the patch effective length and width are to be considered.

1.1.6.1 Current Distribution

The lowest modes which are commonly used for antenna radiation are TM_{10} and TM_{01} and TM_{20} . The electric and magnetic surface current distributions on the side wall for TM_{10} and TM_{01} and TM_{20} modes are illustrated in Figure 1.12. For the TM_{10} mode the magnetic currents along 'b' are constant and in phase while those along 'a' vary sinusoidally and are out of phase. That is why the edge 'b' is known as the radiating edge and 'a' as non-radiating edge. Similarly for the TM_{01} mode the magnetic currents are constant and in phase along 'a' and are out of phase and vary sinusoidally along 'b'. The edge 'a' is thus the radiating edge for this mode.

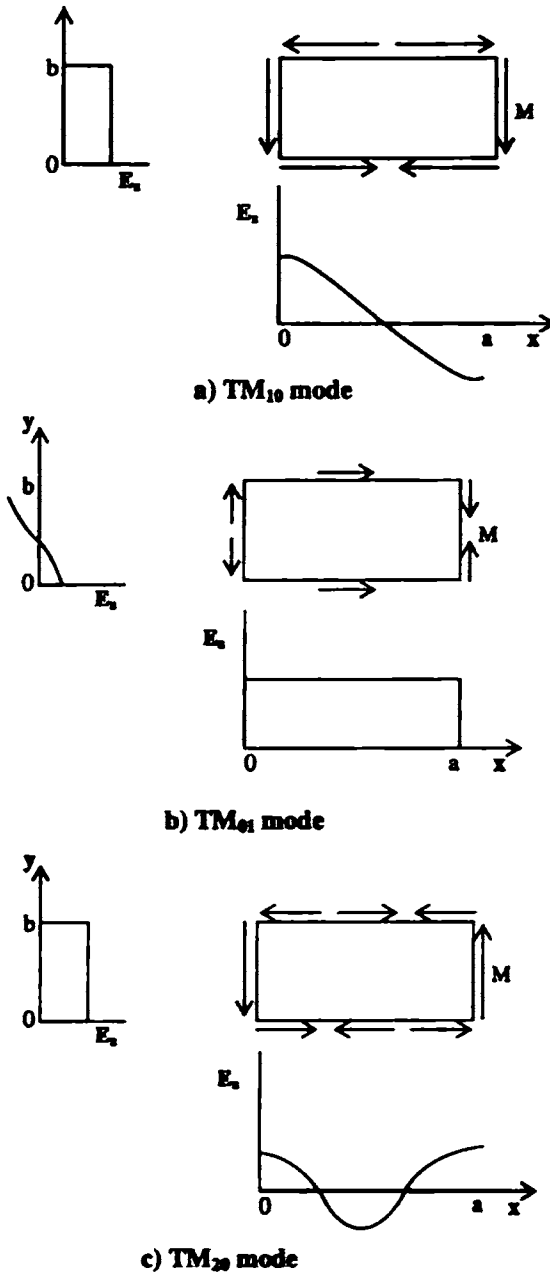


Figure 1.12 Electric field and magnetic surface current distributions for different modes of a rectangular microstrip patch antenna.

1.1.7 Theoretical Methods for Analysis of Microstrip Antennas

Numerous methods are employed for the analysis of microstrip antennas. The most popular methods for antennas having regular geometrical shapes are the transmission line and the cavity methods. These techniques maintain simplicity and accuracy, but not suitable for antennas having irregular shapes. To analyze such antennas, numerical techniques like Finite Element Method (FEM), Finite-Difference Time –Domain Method (FDTD), Integral Equation (IE) method etc., are used.

1.1.7.1 Transmission Line model

Transmission line model is the easiest one for the analysis of rectangular and square patch geometries. Here these antennas are modeled as sections of transmission lines. Similarly circular patches, annular rings and sectors can be modeled in terms of sections of radial transmission lines. The transmission line method is one of the most intuitively attractive models for microstrip antenna analysis. The characteristic impedance and the propagation constant of the transmission line are determined from the patch size and substrate parameters

For a rectangular patch with dimension $L \times W$, the periphery of the patch is described by four walls or edges at $x = 0, L$ and $y = 0, W$. The four edges of the patch are classified as radiating or non radiating edges depending upon the field variations along their length. The radiating edge is associated with a slow field variation along its length. The non-radiating edges should have an integral multiple of half wave variations along the edge such that there is almost complete cancellation of the radiated power from the edge. For the TM_{10} mode in the patch, the edges at $x = 0, L$ are the radiating edges and the walls at $y = 0, W$ are the non-radiating edges. The radiating edges radiate most of the power and are characterized by the load admittance. The radiation patterns of the antennas are assumed to be the same as that of an array of two narrow slots separated by a distance equal to the length of the patch. The input admittance at the feed port is

obtained by transforming the edge admittance to the feed point. The major drawback of this model is that the fields along the width of the patch and substrate thickness are assumed to be uniform. Therefore the model is restricted to rectangular patch geometry, thin substrates, single layer, linearly polarized antennas, and to probe fed or microstrip edge fed antennas.

1.1.7.2 Cavity Model

Microstrip patch antennas are narrow band resonant antennas. They can be termed as lossy cavities. Therefore the cavity model becomes a natural choice to analyze the patch antennas. In this model, the interior region of the patch is modeled as a cavity bounded by electric walls on the top and bottom, and magnetic walls along the periphery. The bases for these assumptions are the following:

For thin substrates,

- The fields in the interior region do not vary with z because the substrate is very thin.
- Electric field is z directed only, and the magnetic field has only the transverse components in the region bounded by the patch metalization and the ground plane.
- The electric current in the patch has no component normal to the edges of the patch metalization, which implies that the tangential component of \hat{H} along the edge is negligible, and the magnetic wall can be placed along the periphery.

The variation along the width of the patch is included in this model. The mutual coupling between the radiating edges are included implicitly in the form of radiated power, which accounts for the effect of mutual conductance. Its main limitation is that the variation of fields along the substrate thickness is not included. The application of this model to the arrays is limited, because the fields from various apertures are assumed to be in phase.

1.1.7.3 Method of Moments

Numerical techniques based on the method of weighted residuals are known as moment method. Method of moment analysis can be carried out either in spatial domain or in spectral domain. The spatial domain analysis involves the Sommerfeld type of integral, while the spectral domain approach uses the closed form Green's function in its formulation [9]. This technique is well suited for planar microstrip structures mounted on large ground planes and is capable of modeling variety of feed structures. This technique is analytically simple and versatile, but it requires large amount of computation. The limitations of this technique are that it requires large storage capacity computers, speed is a limiting factor and also they are not suited for analyzing complex inhomogeneous geometries.

1.1.7.4 Finite Element Method

Finite Element Method (FEM) is a volumetric approach, which enables it to conveniently model various inhomogeneities in the problem. The ability to use tetrahedral and prismatic elements allows for an accurate geometric characterization of the structure. Another attractive feature of this method is the ability to visualize the filed domain over which the problem is being solved. This method can be applied to arbitrary shaped structures also. While its application for the analysis of microstrip antennas in complex environment is difficult, it can model unbounded radiation problems as effectively as moment method.

1.1.7.5 Finite Difference Time Domain (FDTD) method

The finite difference time domain (FDTD) method first proposed by Yee [113], is a powerful yet simple algorithm to solve the Maxwell's equation in time domain. This method calculates the electric and magnetic fields on a discrete mesh by approximating the first order Maxwell's two-dimensional curl equation.

The discrete electric and magnetic fields are interleaved in space to obtain centered difference approximations to the spatial derivatives. The time derivatives are calculated in 'leap-frog' manner to obtain centered differences in time.

FDTD method can be applied to the problems of modeling different types of antenna structures and different feeding methods. The FDTD technique has the following advantage over other methods

- From a mathematical point of view it is a direct implementation of Maxwell's curl equation. Therefore analytical processing is almost negligible.
- It is capable of predicting broadband frequency response because the analysis is carried out in time domain.
- It has the capability to analyze complex systems.
- It is capable of analyzing structures using different types of materials.
- It provides real-time animation display; it is a powerful tool for electromagnetic design.

However this method requires large computational domain when the structure is complex.

1.1.7.6 Green's Function Method

Green's function method is suitable when the shape of the radiating structure is simple, like rectangle, triangle or circle. The Green's function is employed in the electric field integral equation formulation to satisfy the boundary conditions at the patch metallization. The resulting integral equations are discretized into a set of linear equations by means of the moment method to yield a matrix equation. The solution of the matrix equation provides the current distribution on the patch metallization. The near-field and far-field characteristics of antenna are then obtained from the current distribution and the Green's function. The input impedance is calculated by evaluating the electric field inside

the cavity using Green's function. This method is not suitable for arbitrary geometrical shapes.

1.1.8 Broadband Microstrip Antennas

The inherent drawback of microstrip antenna is its narrow impedance bandwidth. Different approaches for increasing the bandwidth are available in the literature. They include thick substrate with low dielectric constant, using multiple patches stacked vertically, using multiple patches in one plane, and using broadband impedance matching networks [6]. By using thick substrate the enhancement of bandwidth is limited because of the large inductance and radiation associated with the feed junction, and increased excitation of surface waves. By using parasitic patches the overall volume of the antenna increases.

Use of multiple resonators in the same plane is another method to increase the bandwidth. Stagger tuned resonators leads to wider bandwidth. But the two associated problems are large area requirement and deterioration of radiation pattern over bandwidth. A method to overcome these two problems is by using multiple resonators gap-coupled along the non-radiating edges. Techniques like U-shaped slot and L-probe are also used for the enhancement of bandwidth [81], [88]. These methods also increase the volume of the antenna substantially. A novel technique to enhance the bandwidth of microstrip antenna without much increase in volume is presented in this thesis.

1.2 OUT LINE OF THE PRESENT WORK

In this thesis, the theoretical and experimental investigations towards the development of a new broadband compact microstrip antenna are presented. The technique adopted is by changing the feed structure without altering the basic shape of the radiating patch. The resonant frequency of the microstrip antenna is shifting down when it is excited with L-strip feed. The patches used for study are selected to incorporating this frequency shift with bandwidth enhancement. All the patches used for study offered bandwidth enhancement. The bandwidth enhancement is achieved without affecting the radiation characteristics of the

antenna. The experimental and theoretical studies reveal that the present antenna is broadband and compact. These desirable characteristics make the present antenna suitable for broadband communication systems. The method is applied to circular microstrip patches also to validate the observations.

For the theoretical analysis, Finite Difference Time Domain method (FDTD) is employed. Radiation and reflection characteristics of the newly developed antenna are studied using FDTD.

1.3 CHAPTER ORGANIZATION

Followed by an introductory Chapter, a brief review of the past work in the field of microstrip antennas with due emphasis on bandwidth enhancement is presented in Chapter 2. Chapter 3 deals with the outcome of the experimental studies carried out on different antenna configurations. Bandwidth enhancement for different configurations along with other radiation properties is presented in this chapter.

Chapter 4 describes the analysis of the proposed antenna using FDTD. The comparisons between the theoretical and experimental results on various antenna configurations are also presented. Excellent agreement between theory and experiment is observed and narrated in this chapter.

The conclusions derived from the theoretical and experimental studies are described in Chapter 5. The scope of further work is also outlined.

L-strip feed is modified into T-strip and hook strip feed. Appendix A deals with the experimental and theoretical results of the studies conducted on T-strip fed rectangular microstrip antennas.

Outcome of the experimental and theoretical studies conducted on rectangular microstrip patches antenna using hook-strip feed is described in Appendix B.

Appendix C depicts the antenna measurement techniques using the Network Analyzer.

CHAPTER 2

REVIEW OF THE PAST WORK

The development of microstrip antenna technology began in 1970's. Historical development of the experimental and theoretical studies on microstrip antenna during the last few decades is explained in this chapter. The relevant research works in the field are reviewed with emphasis given to bandwidth enhancement techniques.

2.1 Development of microstrip antennas

The concept of microstrip antennas was conceived by Deschamp's [13] in 1953. In 1955, Gluton and Bassinot [14] patented a flat aerial that can be used in the UHF region. Lewin [15] studied the radiation from discontinuities in strip line. However, serious attention was given to this element only in the early 1970's. The first microstrip radiator was constructed by Byron [17] in the early 1970's. It was a strip radiator of several wave lengths long and half wave length wide and fed at periodic intervals using coaxial connectors. Howell [18] in 1972, designed basic rectangular and circular microstrip patches. Munson [19] in 1974 demonstrated a new classes of microstrip wrap around antenna suitable for missiles using microstrip radiator and microstrip feed networks on the same substrate.

Sanford [21] presented the use of conformal microstrip arrays for L-band communication. Weinschel [22] reported a practical pentagonal antenna in 1975.

Mathematical modeling of microstrip antenna was first proposed by Munson [19] and Derneryd [23-24] by applying transmission line analogy. This gives an approximate explanation of the radiation mechanism and provides the expressions for the radiation fields, radiation resistance, and input impedance. Radiation mechanism of an open circuited termination was studied by James and Wilson [25]. They observed that the terminal plane region is the dominant radiating aperture.

Agarwall and Bailey [26] suggested the wire grid model for the evaluation of microstrip antenna characteristics. Here the radiating structure is modeled as a fine grid of wire segments. This technique is useful for the design of microstrip antennas of different geometries.

Long *et al.* [27-28] measured the driving point impedance of a printed circuit antenna consisting of a circular disc separated by a dielectric from a ground plane.

Ker [29] investigated the rectangular and circular patches with a central diagonal slot. He obtained polarized radiation with a very good axial ratio. The bandwidth obtained was nearly 2%.

Newman *et al.* [30-31] proposed the method of moments for the analysis of microstrip antennas. They used Richmond's reaction method in connection with the method of moments for the calculation of unknown surface currents flowing on the walls forming the microstrip patch, ground plane and magnetic walls.

A more accurate mathematical cavity model was suggested by Lo *et al.* [32-34] for the analysis of microstrip antennas. In this model, the upper patch and the section of the ground plane are located below it, is joined by a magnetic wall under the edge of the patch. The antenna parameters for different geometries with arbitrary feed points can be calculated using this model. The effects of radiation and other losses are introduced in terms of either an artificially increased substrate loss tangent [34] or by employing the impedance boundary conditions.

Caver and Coffey [35-37] proposed the modal expansion model, which is similar to cavity model. The patch is considered as a thin cavity with leaky magnetic walls. The impedance boundary conditions are imposed on the four walls and the stored and radiated energy were calculated in terms of complex wall admittances.

Hammer *et al.* [38] developed an aperture model for radiation field calculations of the microstrip antenna. This method accounts radiation from all the edges of the patch and gives the radiation fields and radiation resistance of any mode in the microstrip resonator antenna.

Mosig and Gardiol [39] developed a vector potential approach and applied the numerical technique to evaluate the fields produced by microstrip antennas of any shape.

Microstrip disc has been analyzed by Derneryd [40] by calculating the radiation conductance, antenna efficiency and quality factor associated with circular disc antenna.

Alexopolus *et al.* [41] developed a dyadic Green's function technique for the calculation of the field radiated by a Hertzian dipole printed on a grounded substrate.

The circular microstrip antenna was rigorously treated by Butler [42]. He solved the problem of central fed circular microstrip antenna by treating patch as a radiating annular slot, in which the radius of the outer ring is very large. Butler and Yung [43] analyzed the rectangular microstrip antenna employing this method.

Mink [44] developed a circular microstrip antenna, which operates at a low frequency compared to a circular patch antenna of the same size.

Electric probe measurements on microstrip were proposed by J.S Dabelle and A.L. Cullen [45]. By this method the field of microstrip is determined using a field probe.

Shen [46] analyzed the elliptical microstrip patch and proved that the radiation pattern from this antenna is circularly polarized in a narrow band when eccentricity of the ellipse is small.

R.Chadha and K.C Gupta [47] developed Green's function of circular sector and annular sector shaped segments in microwave planar circuits and microstrip antennas.

Lo and Richard [48] applied the perturbation model approach to the design of circularly polarized antenna. Critical dimensions needed to produce circularly polarization from nearly circular patches were determined by trial and error method.

Newman and Tulyathan [49] analyzed microstrip patch antennas of different shapes using moment method. The patch is modeled by surface currents and dielectric by volume polarization current.

Schaubert *et al.* [50] was reported a method for controlling the operating frequency and polarization of microstrip antennas. The control is achieved by placing shorting posts within the antenna boundary.

A full wave analysis of a circular disc conductor on printed substrate backed by ground plane was presented by Araki and Itoh [51].

Chew and Kong [52] analyzed the problem of circular microstrip disc antenna excited by a probe on thin and thick substrate. Here the unknown current was solved by vector Hankel Transform.

Itoh and Mentzel [53] suggested a method for analyzing the characteristics of open microstrip disk antenna. This method provides a number of unique and convenient features in analytical and numerical phase.

Kuester *et al.* [54] suggested a thin substrate approximation applied to microstrip antennas. The formulae suggested by them were found to be useful in simplifying the expression for the antenna parameters considerably.

Microstrip antenna covered with a dielectric layer was proposed by Bahl *et al.* [55]. They suggested an appropriate correction for the calculation of resonant frequency of a microstrip antenna coated with protective dielectric layer.

2.2 Broadband Microstrip Antennas

The narrow bandwidth available from microstrip patch antenna is recognized as the most significant factor limiting the applications of this class of antennas. Some of the researchers world wide are working towards overcoming this inherent disadvantage.

Hall *et al.* [56] reported the concept of multilayer substrate antennas to achieve broader bandwidth. These antennas constructed on alumina substrates which gave a bandwidth of 16 times that of a standard patch antenna with an increase in overall height.

C. Wood [57] suggested the use of circular and spiral microstrip lines as compact wide band circularly polarized microstrip antennas.

C. Wood [58] suggested a method for doubling the bandwidth of microstrip patch antennas by locating capacitively excited $\lambda/4$ short circuit parasitic elements at their radiating edges.

Derneryd and Karlsson [59] have made a broad band microstrip antenna by using thicker substrates of low dielectric constant.

Pandharipande and Verma [60] suggested a new feeding scheme for the excitation of patch array which gave broader bandwidth. The feeding network consists of a strip line power divider using hybrid rings and the coupling from strip line to feed point is achieved by thin metal probe.

Poddar *et al.* [61] has obtained an increase in bandwidth of microstrip antenna constructing the patch antenna on a stepped wedge shaped dielectric substrate.

Das and Chatterjee [62] reported a conical microstrip antenna with much larger bandwidth than that of an identical circular patch antenna. The conical patch antenna is obtained by modifying the circular patch antenna by slightly depressing the patch configuration conically into the substrate.

Sabban [63] reported a stacked two layer microstrip antenna with an increase in bandwidth of 15%. This antenna has been used as an element for 64 element Ku band array.

Long S A *et al.* [64] described that cylindrical dielectric cavity resonator can effectively be used as an antenna.

Bhatnagar *et al.* [65] proposed a stacked configuration of triangular microstrip antennas to obtain larger bandwidth.

Girish Kumar and K. C. Gupta [66] described two configurations for bandwidth enhancement of microstrip patch antennas. One of these configurations uses two additional resonators which are gap coupled to the non radiating edges of rectangular patch, whereas in the second case four additional resonators are gap coupled to the four radiating edges of a rectangular patch.

Hori and Nakagima [67] designed a broadband circularly polarized microstrip antenna for public radio communication system.

A microstrip antenna with double bandwidth has proposed by Prior and Hall [68], by the addition of a short circuited ring to a microstrip disc antenna.

C.K. Aanandan and K.G Nair [69] developed a compact broad band microstrip antenna configuration. The system uses number of parasitic elements which are gap coupled to a driven patch element. By using this technique they acquire an impedance bandwidth of 6% without deteriorating the radiating characteristics.

Bhatnagar *et al.* [70] has obtained a large bandwidth in triangular microstrip antennas using two parasitic resonators directly coupled to the non radiating edges and a third one gap coupled to the radiating edge.

T. Huynh and K.F. Lee [71] has described a coaxially fed single-layer wideband microstrip antenna in the form of rectangular patch with a U-shaped slot. The antenna attained an impedance bandwidth of 10 - 40%.

L. Gaiuffret *et al.* [72] proposed an efficient method for bandwidth enhancement by coupling a CPW line fed slot to a microstrip antenna. This antenna has a large bandwidth with high gain and low cores polarization levels.

S.D Targonski *et al.* [73] presented a wide band aperture coupled stacked patch microstrip antenna. This has the capability of operating over a bandwidth in excess of 50%.

M.Deepu Kumar *et al.* [74] developed dual port microstrip antenna geometry for dual frequency operation. This antenna has wide impedance bandwidth and excellent isolation between ports.

Kin-Lu and Wen-Hsiu Hsu [75] designed a broad band triangular microstrip antenna with a U-shaped slot. It consists of a foam substrate of thickness $\sim 0.08\lambda_0$, a slotted triangular microstrip antenna.

Kin-Lu Wong and Jian-Yi Wu [76] designed a circularly polarized square microstrip antenna fed along a diagonal with a pair of suitable chip resistors. This antenna provided a wide bandwidth for circular polarization about two times that of a similar design with a pair of shorting pins.

K.P Ray and G. Kumar [77] presented the experimental investigations on a hybrid circular microstrip antenna. The geometry constitutes circular patches with different radii with a small gap between them. Shorting strips of different widths are used to adjust the coupling between the central fed patch and two parasitic patches, yielding dual band, triple band and broad band operations.

K.M Luk *et al.* [78] designed a proximity fed stacked circular disc antenna with an impedance bandwidth of 26% and gain of 8dBi. The essential feature of this design is the presence of four linear slots in the bottom patch of the stacked arrangement.

Chih-Yu Huang *et al.* [79] presented a compact rectangular microstrip antenna enhanced gain and wider bandwidth. The compact antenna is obtained by

loading a high permittivity superstrate layer and a 1Ω chip resistor. This design has an operating bandwidth of six times that of conventional patch antenna.

Y.Kim *et al.* [80] designed a wide band microstrip antenna with dual frequency dual polarization operation. A parasitic element is stacked above the fed element for widening the bandwidth. The measured bandwidth at 15dB return loss at dual frequencies are 9.02 and 12.4 & respectively.

C.L Mak, *et al.* [81] designed a proximity coupled U-slot microstrip antenna with an impedance bandwidth of 20%. The antenna has an average gain of 7.5 dBi and cross-polarization of about ~ 20 dB.

A novel broad band probe fed rectangular microstrip antenna with a pair of toothbrush shaped slots embedded close to the non radiating edges of the patch is presented by Jia-Yi Sze and Kin-Lu Wong [82]. An antenna bandwidth as large as ~ 2.6 times that of a conventional rectangular microstrip has been obtained.

Shyh-Ting Fang *et al.* [83] presented a broad band antenna by embedding a pair of properly-bent narrow slots in an equilateral triangular microstrip patch, broadband operation of microstrip antenna can be achieved with an inset microstrip line feed, and the proposed design has an impedance bandwidth as large as ~ 3 times that of a corresponding simple triangular microstrip antenna.

K.M. Luk *et al.* [84] investigated an L-shaped probe fed broadband rectangular microstrip. It consists of a foam layer with a thickness of around 10% of the wave length is used as the supporting substrate. The proposed antenna has an impedance bandwidth of 35% and an average gain of 7.5 dBi.

K.M. Luk *et al.* [85] designed a rectangular U-slot patch antenna proximity fed by an L-shaped probe using a foam layer of thickness of $\sim 7\%$ of the wavelength as supporting substrate.

Kin-Lu and Jen-Yea Jan [86] proposed a broad band design for a circular microstrip antenna with reactive loading integrated with a circular patch. Using this method bandwidth of ~ 3.2 times that of a conventional circular microstrip antenna has been achieved.

Y.X Guo *et al.* [87] presented a broad band U-slot circular patch antenna with L-probe feeding with a foam layer of thickness $\sim 0.1\lambda_0$ a supported substrate. An impedance bandwidth of 38% and gain of 6.8dBi have been achieved.

L-probe proximity fed short circuited quarter wave length patch antenna is presented by Y.X.Guo *et al.* [88]. The antenna provided an impedance bandwidth of 39% and a gain of >7dBi.

R.B Waterhouse [89] developed a stacked shorted patch antenna for broad band operation. This proposed antenna has an impedance bandwidth greater than 30%.

Lakhdar Zaid *et al.* [90] designed a dual frequency broad band antenna with stacked quarter wave length elements. The structure offers two modes with different radiation characteristics with a bandwidth of 30% for a VSWR<2.

W.K. Lo *et al.* [91] proposed a circularly polarized circular patch microstrip antenna with a cross slot using an L-shaped probe fed by a microstrip line. With single L-probe, the impedance bandwidth, axial ratio bandwidth and gain bandwidth are 27, 3.47 and 26% respectively.

Kin-Fai Tong *et al.* [92] developed a broad band U-slot rectangular microstrip patch antenna on microwave substrate. The dielectric constant of the substrate is 2.33. The antenna has achieved a maximum impedance bandwidth of 27%. They presented the theoretical analysis also.

Sean M. Duffy [93] described a bandwidth enhancement design technique for electromagnetically coupled microstrip antennas by utilizing a tuning stub. Using this method the bandwidth of a conventional proximity coupled antenna is increased from 4.8 to 8.4 % and the bandwidth of a stacked aperture coupled antenna is increased from 27.5 to 34.5%.

Jia-Yi Sze and Kin-Lu Wong [94] demonstrated a novel bandwidth enhancement method of microstrip antennas by loading a pair of right angled slots and a modified U-shaped slot in a rectangular microstrip patch. They have achieved a bandwidth as large as about 2.4 times that of a corresponding unslotted rectangular microstrip antenna.

J.S Baligar *et al.* [95] presented a novel microstrip antenna consisting of a stacked annular ring coupled to a shorted circular patch. This new geometry offers a large bandwidth, higher gain and lower cross polarization levels.

Y.W Jang [96] described a cross shaped microstrip line fed slot antenna of large bandwidth. The antenna offers a bandwidth of 98.95%.

Wen-Hsiu Hsu and Kin-Lu Wong [97] designed a new circular patch antenna with an impedance bandwidth greater than 25% and a peak antenna gain about 8.3 dBi. The circular patch antenna has a thick air substrate and pair of wide slits are cut in the circular patch to facilitate the antenna's impedance matching. The circular patch is supported by a conducting post, which is also connected to a 50Ω microstrip feed line.

M.D Van Wyk and K.D Palmer [98] described a novel single layer rectangular patch antenna using a coupled line feed. This coupled line matching technique increases the bandwidth of the patch antenna by a factor of more than 2.5 times as compared to the normal edge fed patch with the same geometrical dimensions.

Yong-Xin Guo *et al.* [99] designed and studied a broad band single layer annular ring microstrip antenna fed by an L-shaped probe. It achieved, for the TM_{11} an impedance bandwidth of about 33% and a maximum gain of 7.5 dBi, and for the TM_{12} mode 27% bandwidth. A foam layer substrate of thickness around 10% of the operating wavelength in free space is used as the supporting substrate.

Yong-Woong Jang [100] presented a wide band T-shaped microstrip fed printed slot array antenna. This antenna is fabricated on a substrate having permittivity 4.3 and thickness 1mm. The antenna offers a bandwidth of approximately 53.9% for return loss less than or equal to -10dB. The bandwidth of the twin slot is ~1.06% larger than that of single slot antenna.

Yong-Woong Jang [101] proposed a new structure of an aperture coupled T-shaped patch microstrip fed triangular patch antenna, which has a similar radiation properties, with an advantage of being smaller than the aperture coupled rectangular antenna or microstrip slot antenna. The antenna has a bandwidth of 44.5 %.

Y.X Guo *et al.* [102] developed wide band T-probe proximity fed regular circular and compact semicircular antennas. For the regular circular patch antenna, using a foam thickness $\sim 0.13\lambda_0$ as a supported substrate an impedance bandwidth of 35% and a gain of over 8 dBi have been obtained. For the semicircular patch antenna, an impedance bandwidth of 56% and a gain of over 4.5 dBi are achieved with the same substrate.

A.K. Shackelford *et al.* [103] presented a small size probe fed notched patch antenna with a shorting post. The area of the patch has been reduced to 94 % with a bandwidth of 13.2%.

Fa -Shian Chang and Kin -Lu Wong [104] proposed a novel broad band design of probe fed patch antenna suitable for applications in DCS cellular system base station. The antenna has a thicker air substrate for broad band operation, and is fed by a probe feed with a short probe pin, which is connected through a triangular conducting patch to one of the patch's radiating edges.

Yong-Woong Jang [105] developed a wide band double T-shaped microstrip line fed slot antenna. The antenna offers a bandwidth of 114% ($VSWR < 2$).

B.L.Ooi *et al.* [106] investigated the characteristics of a novel rectangular patch with an offset F-shaped probe. The patch height is approximately 9% of the designed wave length. An impedance bandwidth of 36% and an average measured gain of approximately 5dBi are achieved for the first dominant mode. For the higher order mode the impedance bandwidth extends to 64% and provides an average gain of 3dBi.

Y.X Guo *et al.* [107] designed a wide band L-probe fed shorted triangular patch antenna. Using a foam layer of thickness $\sim 0.13\lambda_0$ as a supported substrate, an impedance bandwidth of 61% ($SWR < 2$) and a gain of over 4dBi have been obtained.

Yong-Xin Guo *et al.* [108] presented the design of L-probe proximity fed patch antenna. An impedance bandwidth of 30% and an average gain of 7.5 dBi have been achieved for the design. They also presented the FDTD analysis of the L-probe fed antenna.

SECTION I

L-STRIP FED RECTANGULAR MICROSTRIP ANTENNA

3.1 INTRODUCTION

The present work is intended to develop a new feeding technique to enhance the bandwidth of basic microstrip patches without deteriorating the efficiency and radiation characteristics of the antenna. New L-shaped microstrip feed structure is applied to microstrip patches for improving the bandwidth. Since the excitation is using an 'L' strip, the antenna is named as L-strip fed microstrip rectangular patch antenna.

3.1.1 Antenna Geometry

The geometry of the new L-strip fed microstrip antenna is shown in Figure 3.1. A 50Ω 'L' shaped line is etched on a substrate having permittivity ' ϵ_{r1} ' and height ' h_1 '. The different geometrical parameters of the L-strip are the feed length ' S_1 ', feed segment length ' S_2 ' and the width ' w '. A rectangular microstrip antenna of dimension $L \times W$ etched on dielectric substrate of dielectric constant ' ϵ_{r2} ' and height ' h_2 ' is electromagnetically coupled with the L-shaped microstrip feed. This allows reduction in feed radiation by locating it closer to the ground plane than the patch. Moreover this facilitates easy adjustment of the position of the patch over the feed to obtain the optimum impedance bandwidth. Finally the two substrates are joined together at the optimum feed position with low loss epoxies without any air gap. The feed parameters that control the antenna characteristics are feed length ' S_1 ', feed segment length ' S_2 ', the feed offset distance d_1 and d_2 .

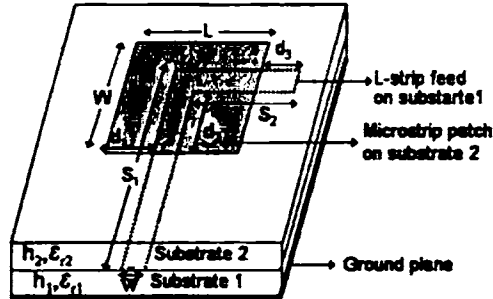


Figure 3.1 Geometry of the L-strip fed rectangular microstrip antenna

3.2 Methodology

The variation of the following antenna characteristics with different feed parameters are studied in detail.

- a. Input Impedance
- b. Resonant frequency
- c. Impedance bandwidth
- d. Radiation pattern
- e. Gain

These studies have enabled the development of a wide band microstrip antenna with less feed complexity and compactness. HP 8510C Vector Network Analyzer is used for the measurement of antenna characteristics. [See Appendix C]

Selection of radiating patches employed for the experimental study is discussed in the following part.

A rectangular microstrip antenna resonating at 2.4GHz is considered for initial experimental studies, since this frequency is commonly used for wireless LAN applications. Patch with size $L = 3.9\text{cm}$ and $W = 3\text{cm}$ resonating at 2.4 GHz is fabricated on a substrate of $\epsilon_r = 4.28$ and height $h = 0.16\text{cm}$. When it is electromagnetically fed with L-strip having a particular feed length S_1 / λ_g and

S_2 / λ_d (λ_d is the wave length in the dielectric) is varied, the patch is found to be resonating in the band 2.215GHz to 2.32GHz. This shifting of the resonant frequency to lower side is observed when the feed parameters S_1 / λ_d and S_2 / λ_d are varied.

To achieve a resonant frequency of ≈ 2.4 GHz and to compensate the above frequency shift, the patch size is iteratively reduced to $L = 3.6$ cm and $W = 2.6$ cm. When the patch is fed with L-strip, it is resonating between 2.405GHz and 2.55 GHz as S_2 / λ_d is varied. Under this condition the bandwidth is also increased.

To verify and ascertain the effect of L-strip feed on the antenna characteristics, microstrip patches resonating at frequencies 2.7GHz, 2.9GHz, 3.4GHz and 3.5GHz were subjected to detailed experimental studies. All the antennas provided bandwidth enhancements when fed with L-strip without deteriorating other characteristics. The feed length and feed segment lengths are systematically varied, and a maximum bandwidth of $\sim 20\%$ is observed for the patch resonating at 3.4GHz, with dimension $L = 4$ cm, $W = 2$ cm, while other patches offered between 16 to 19%. Hence this patch is selected for detailed study. Characteristics of other patches with L-strip feed are also outlined in this thesis.

Characteristics of microstrip antennas with conventional microstrip line feed are studied for comparison. The bandwidths of these patches with ordinary microstrip line are found to be approximately 3%. The return loss characteristic of a typical patch with proximity coupling using conventional feed is shown in Figure 3.2. The antenna is resonating at 3.4GHz with a bandwidth of 3.9%.

Resonant frequency variations with the feed point variations for the antenna of dimensions $L = 4$ cm and $W = 2$ cm fed with a conventional feed are studied. When the feed point is moved along the X-axis, it is observed that the impedance is varying with a slight change in resonant frequency. The same effect is observed along the Y-axis also. The variation of resonant frequency as a function of the feed point for the microstrip antenna fed with conventional microstrip line is shown in Figure 3.3.

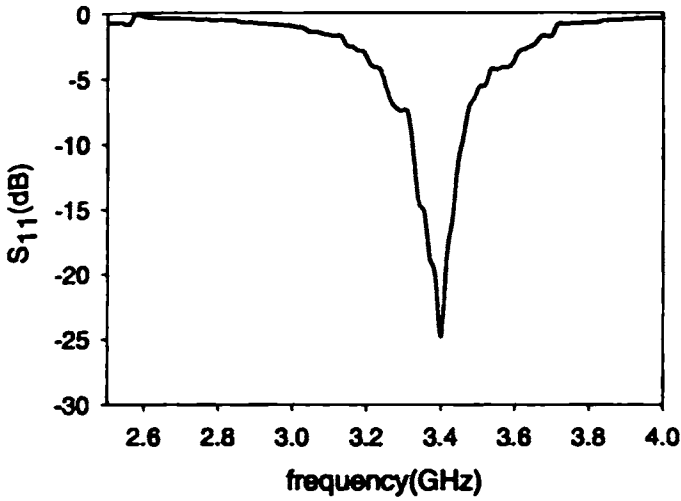


Figure 3.2 Return loss variation with frequency of the antenna ($L = 4\text{cm}$, $W = 2\text{cm}$, $\epsilon_{r1} = \epsilon_{r2} = 4.28$, $h_1 = h_2 = 0.16\text{cm}$) fed with simple microstrip line

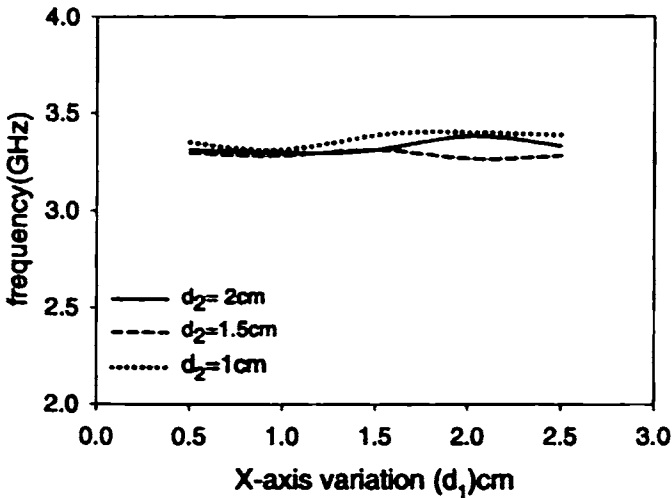


Figure 3.3 Resonant frequency variations as a function of the feed points d_1 , d_2 for the patch ($L = 4\text{cm}$, $W = 2\text{cm}$, $\epsilon_{r1} = \epsilon_{r2} = 4.28$, $h_1 = h_2 = 0.16\text{cm}$.) fed with simple microstrip feed.

Microstrip patches resonating at different resonant frequencies, with dimensions $L \times W = 3.6 \times 2.6 \text{ cm}^2, 3 \times 2.4 \text{ cm}^2, 3 \times 2 \text{ cm}^2$ and $4 \times 2 \text{ cm}^2$ are excited with L-strip feed and their reflection and radiation characteristics are studied in detail. To study the effect of feed parameters on the antenna characteristics, generally S_1 is varied from $0.5\lambda_d$ to $2\lambda_d$. For each S_1 , S_2 is varied from $0.05\lambda_d$ to $1.2\lambda_d$ where λ_d is the wavelength inside the dielectric. The following sections deal with the experimental results obtained for various L-strip fed antennas.

3.2.1 Input Impedance

Input impedance variation of the L-strip fed microstrip antenna is studied for various feed parameters. Microstrip patch with dimension $L \times W = 4 \times 2 \text{ cm}^2$ is used for studying the impedance variations. Antenna resonant mode and the input impedance variations as a function of the feed points d_1 and d_2 are studied. By suitably selecting the feed point, we can excite the desired mode. The input impedance also varies with the feed point (d_1, d_2). As the feed point is moved along the non radiating edge to the centre, the impedance at resonance varies from a maximum to minimum values as in the case of conventional microstrip proximity coupling. By proper selection of the feed point, the antenna can be matched to a 50Ω transmission line.

(a) Feed length – $0.862\lambda_d$

The input impedance of the antenna is highly dependent on the feed parameters like S_1, S_2, d_1 and d_2 . Impedance loci variations for the antenna for various feed positions when the feed length S_1 is $0.862\lambda_d$ and S_2 is $0.754\lambda_d$ are shown in Figure 3.4 (i). From the observations it is evident that as in the case of a rectangular patch fed with a microstrip line, here also the location of the feed point determines the input impedance of the antenna. By suitably selecting the feed point location, the impedance curve can be brought to the centre of the Smith chart. At this location the antenna offers perfect matching to the line with broad bandwidth.

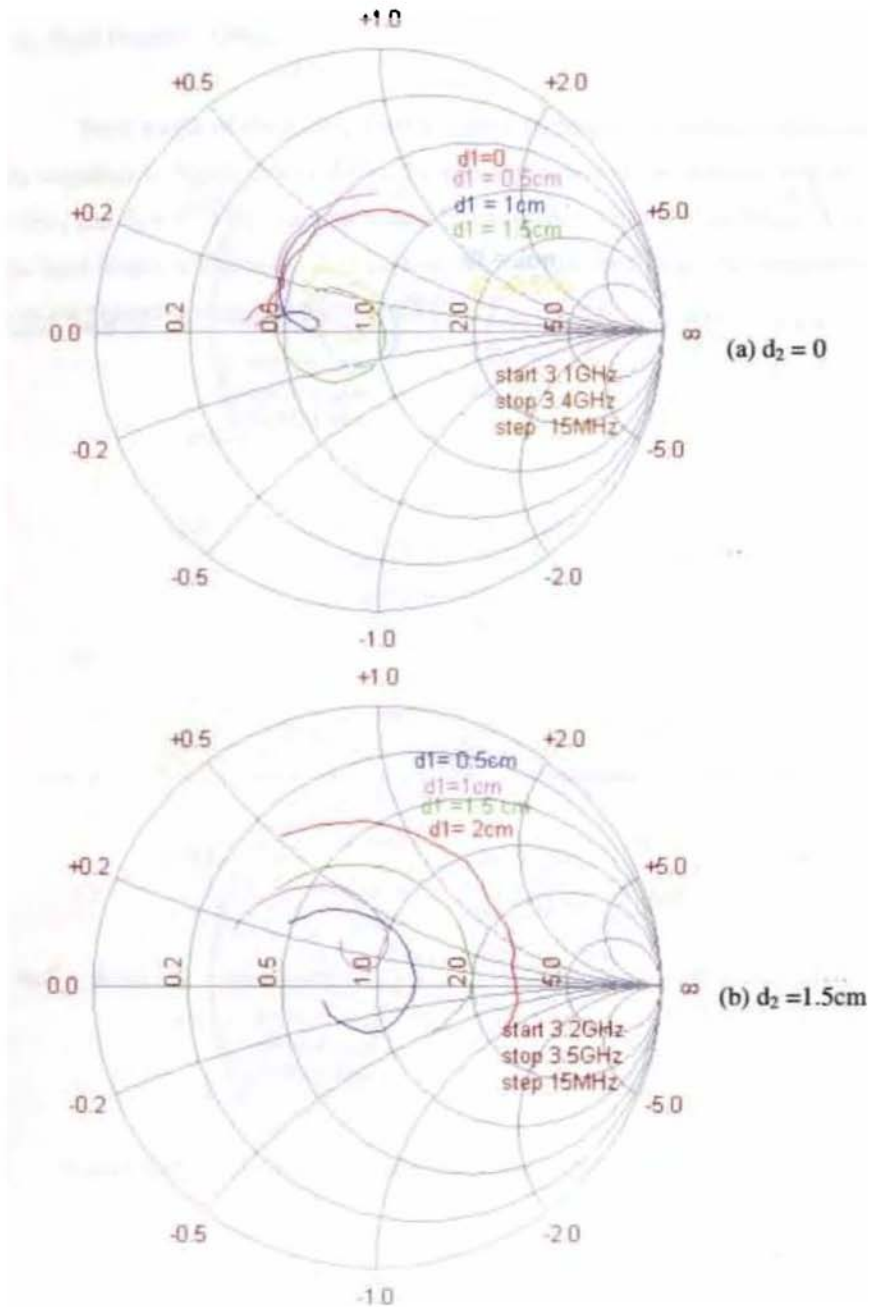


Figure 3.4(i) Impedance loci of the L-strip fed antenna at different feed point locations, $L = 4 \text{ cm}$, $W = 2 \text{ cm}$, $S_1 = 0.862\lambda_d$, and $S_2 = 0.754\lambda_d$.

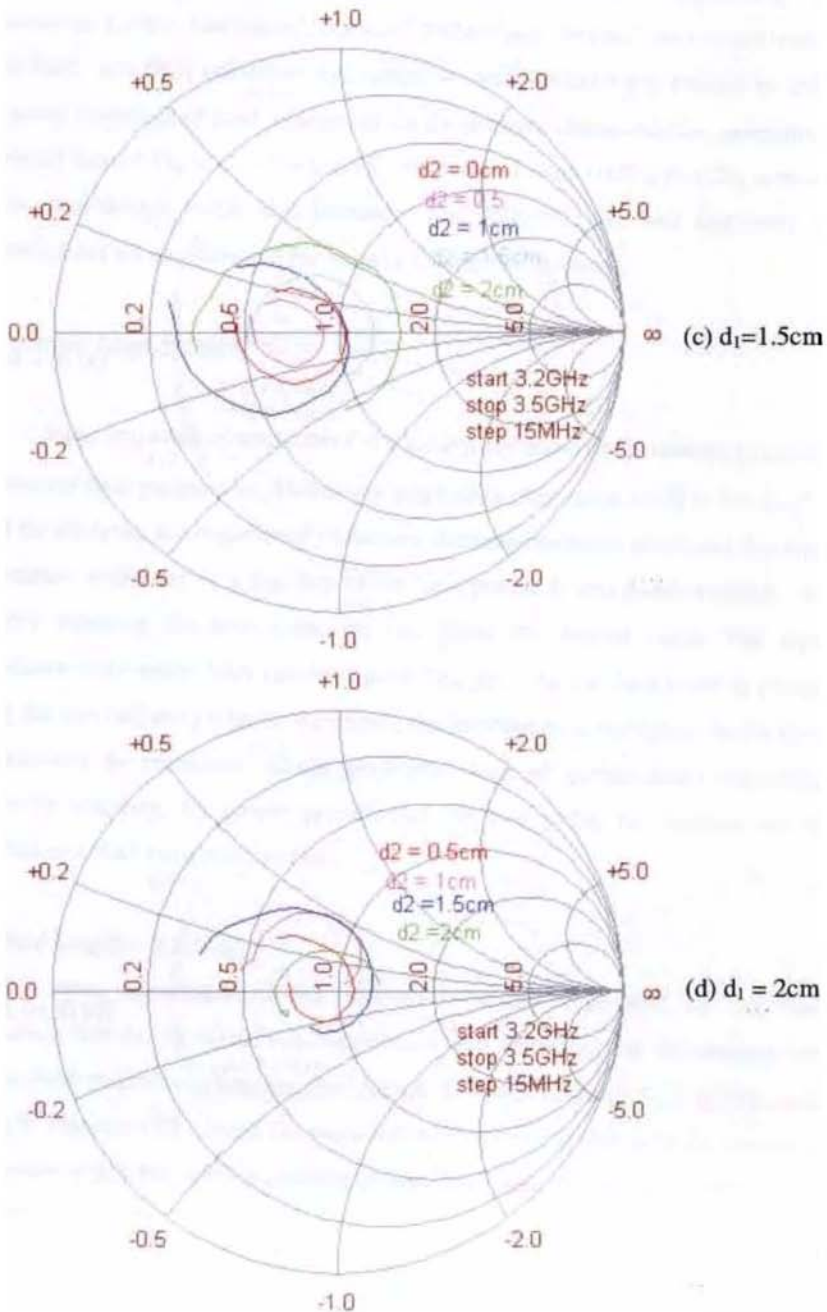


Figure 3.4(i) Impedance loci of the antenna at different feed point locations, $L = 4\text{ cm}$, $W = 2\text{ cm}$, $S_1 = 0.862\lambda_d$, and $S_2 = 0.754\lambda_d$.

(b) Feed length – $1.08\lambda_d$

Feed length of the L-strip feed is further increased to observe its effect on the impedance. Figure 3.4(ii) shows the impedance loci of the antenna with $S_1 = 1.08\lambda_d$ and $S_2 = 0.754\lambda_d$. Similar nature of impedance variations are found when the feed length is increased. It is noticed that for this feed length the impedance loci are expanded more compared to $0.862\lambda_d$.

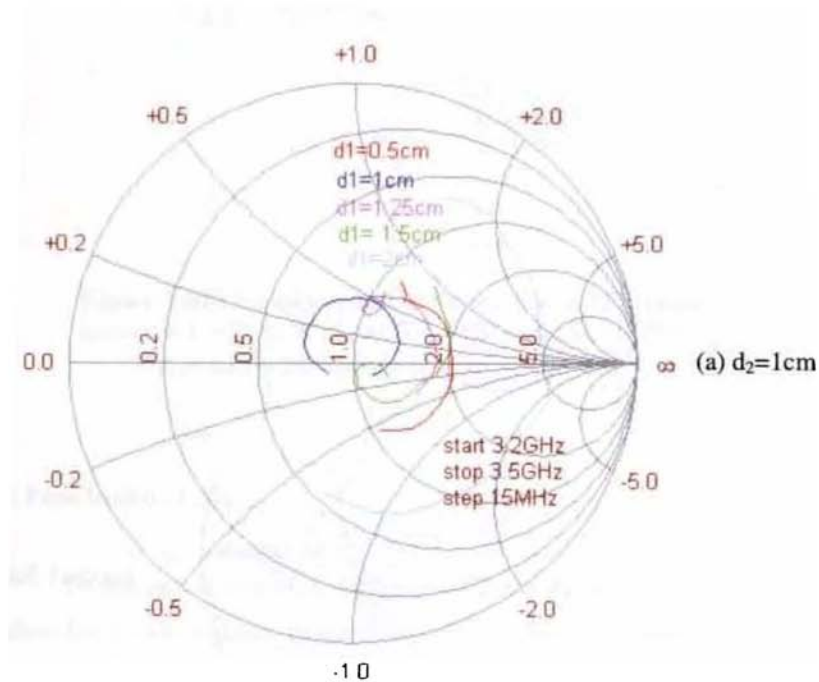


Figure 3.4(ii) Impedance loci of the antenna at different feed point locations, $L = 4\text{cm}$, $W = 2\text{cm}$, $S_1 = 1.08\lambda_d$, and $S_2 = 0.754\lambda_d$

$$\epsilon_{r1} = \epsilon_{r2} = 4.28, h_1 = h_2 = 0.16\text{cm}.$$

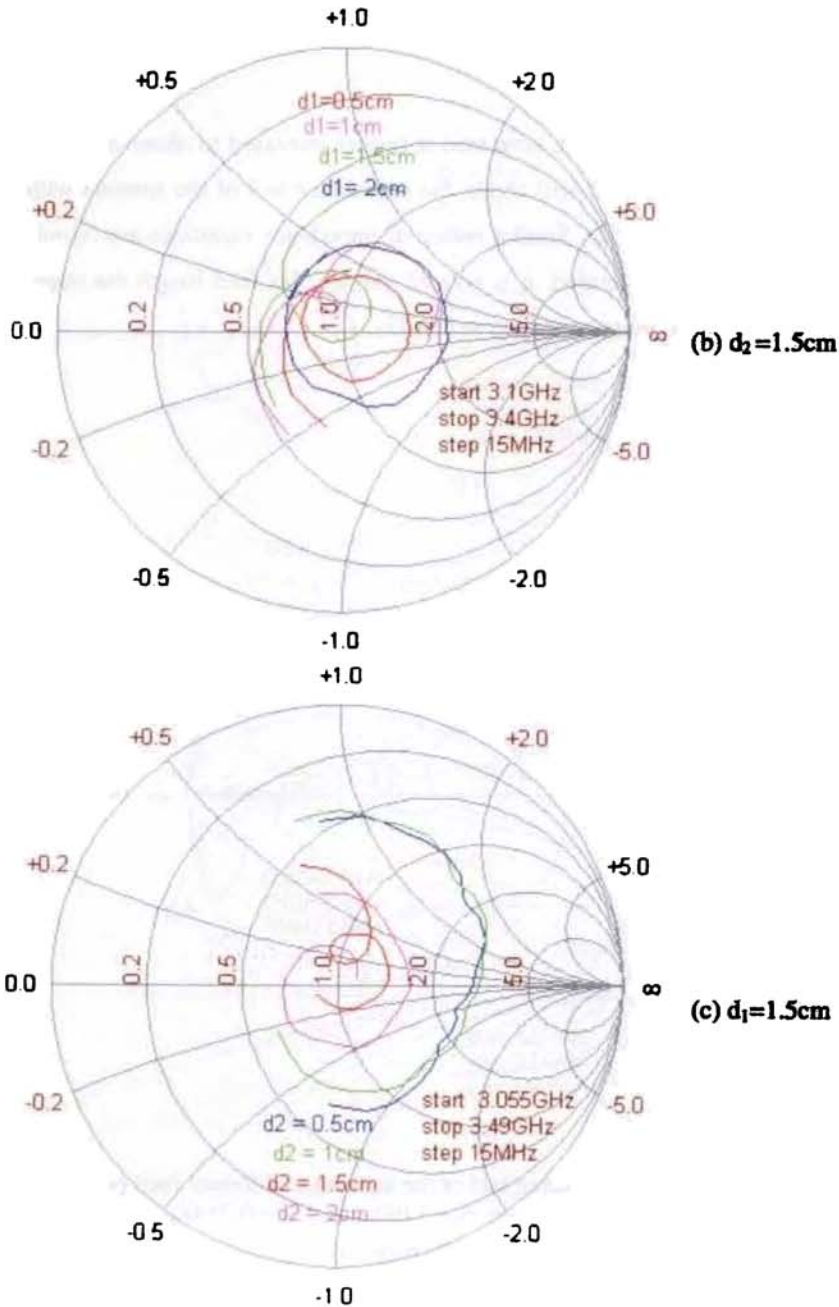


Figure 3.4(ii) Impedance loci of the antenna at different feed point locations, $L = 4\text{cm}$, $W = 2\text{cm}$, $S_1 = 1.08\lambda_d$, and $S_2 = 0.754\lambda_d$.
 $\epsilon_{r1} = \epsilon_{r2} = 4.28$, $h_1 = h_2 = 0.16\text{cm}$.

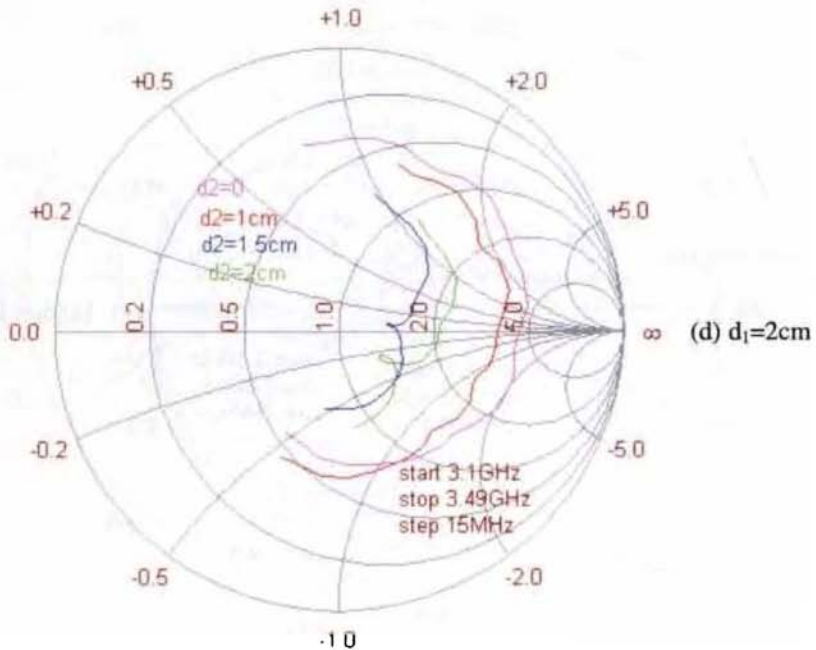
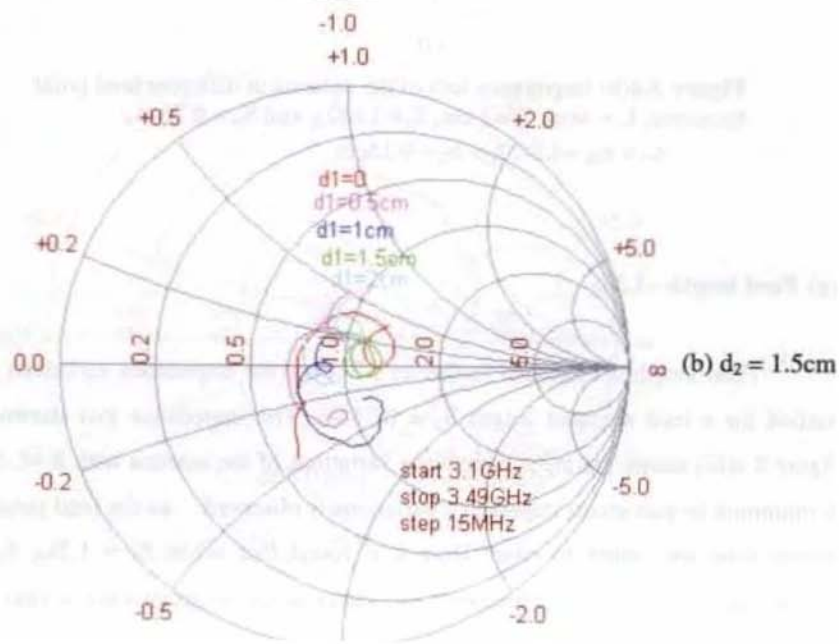
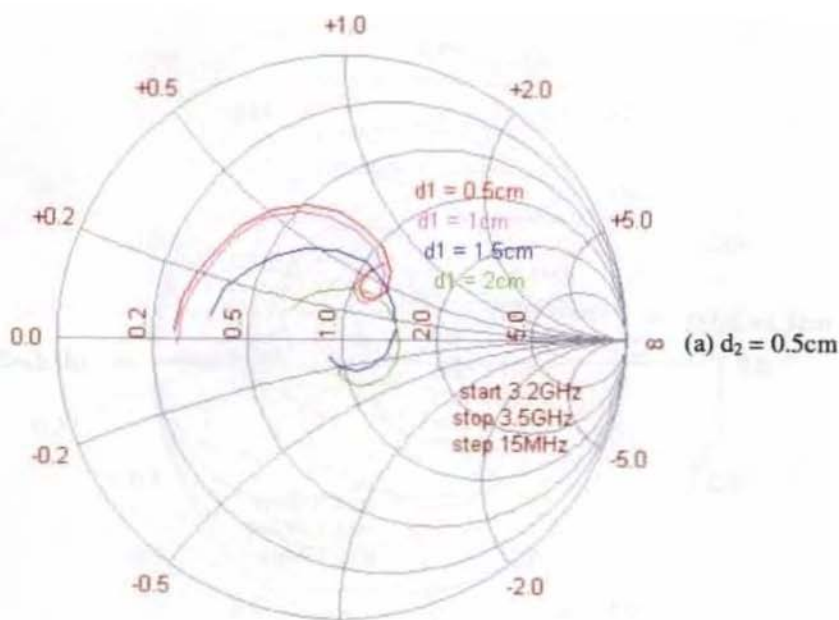


Figure 3.4(ii) Impedance loci of the antenna at different feed point locations, $L = 4\text{cm}$, $W = 2\text{ cm}$, $S_1 = 1.08\lambda_d$, and $S_2 = 0.754\lambda_d$
 $\epsilon_{r1} = \epsilon_{r2} = 4.28$, $h_1 = h_2 = 0.16\text{cm}$.

(c) Feed length $-1.3\lambda_d$

Feed length is increased further to $1.3\lambda_d$ and the impedance variations are studied for a feed segment length $S_2 = 0.754\lambda_d$. The impedance loci shown in Figure 3.4(iii) shows the input impedance variations of the antenna with $S_1 = 1.3\lambda_d$. A minimum to maximum impedance variations is observed as the feed point is moved from the centre to edge. Here it is found that when $S_1 = 1.3\lambda_d$, $S_2 = 0.754\lambda_d$, $d_2 = 1.5\text{cm}$ all the impedance loci varies in the neighborhood of 50Ω for certain values of d_1 .



10

Figure 3.4(iii) Impedance loci of the antenna at different feed point locations, $L = 4\text{cm}$, $W = 2\text{cm}$, $S_1 = 1.3\lambda_d$, and $S_2 = 0.754\lambda_d$
 $\epsilon_r = \epsilon_0 = 4.28$, $h_1 = h_2 = 0.16\text{cm}$

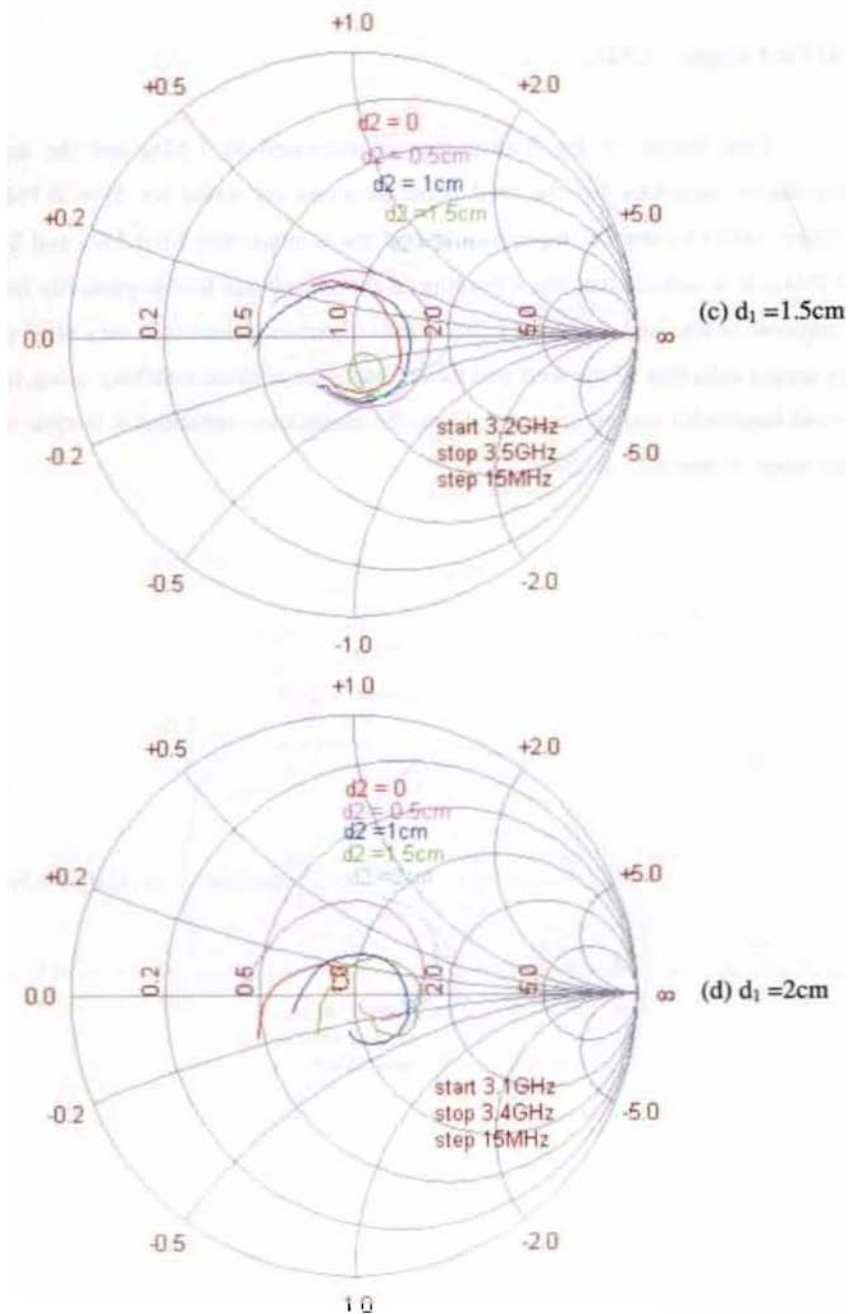


Figure 3.4(iii) Impedance loci of the antenna at different feed point locations, $L = 4\text{cm}$, $W = 2\text{cm}$, $S_1 = 1.3\lambda_d$, and $S_2 = 0.754\lambda_d$, $\epsilon_{r1} = \epsilon_{r2} = 4.28$, $h_1 = h_2 = 0.16\text{cm}$.

(d) Feed length – $1.52\lambda_d$

Feed length of the L-strip feed is increased to $1.52\lambda_d$ and the input impedance variations for the feed point locations are noted for $S_2 = 0.754\lambda_d$. Figure 3.4(iv) shows the impedance loci of the antenna with $S_1=1.52\lambda_d$ and $S_2 = 0.754\lambda_d$. It is noticed that the spreading of the impedance loci is generally more compared to the feed length of $1.3\lambda_d$. From the observations it is very clear that by proper selection of the feed parameters better impedance matching along with broad bandwidth can be achieved. From the impedance variations it is clear that the mode of operation is TM_{01} .

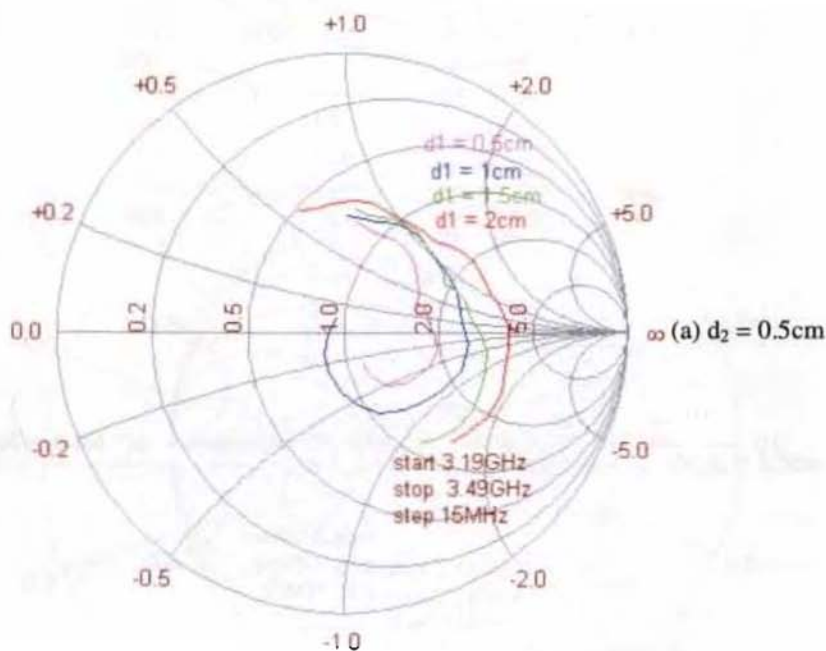


Figure 3.4(iv) Impedance variations of the antenna at different feed point locations, $L= 4\text{cm}$, $W= 2\text{cm}$ $S_1=1.52\lambda_d$, and $S_2 = 0.758\lambda_d$.

$$\epsilon_{r1} = \epsilon_{r2} = 4.28, h_1 = h_2 = 0.16\text{cm}.$$

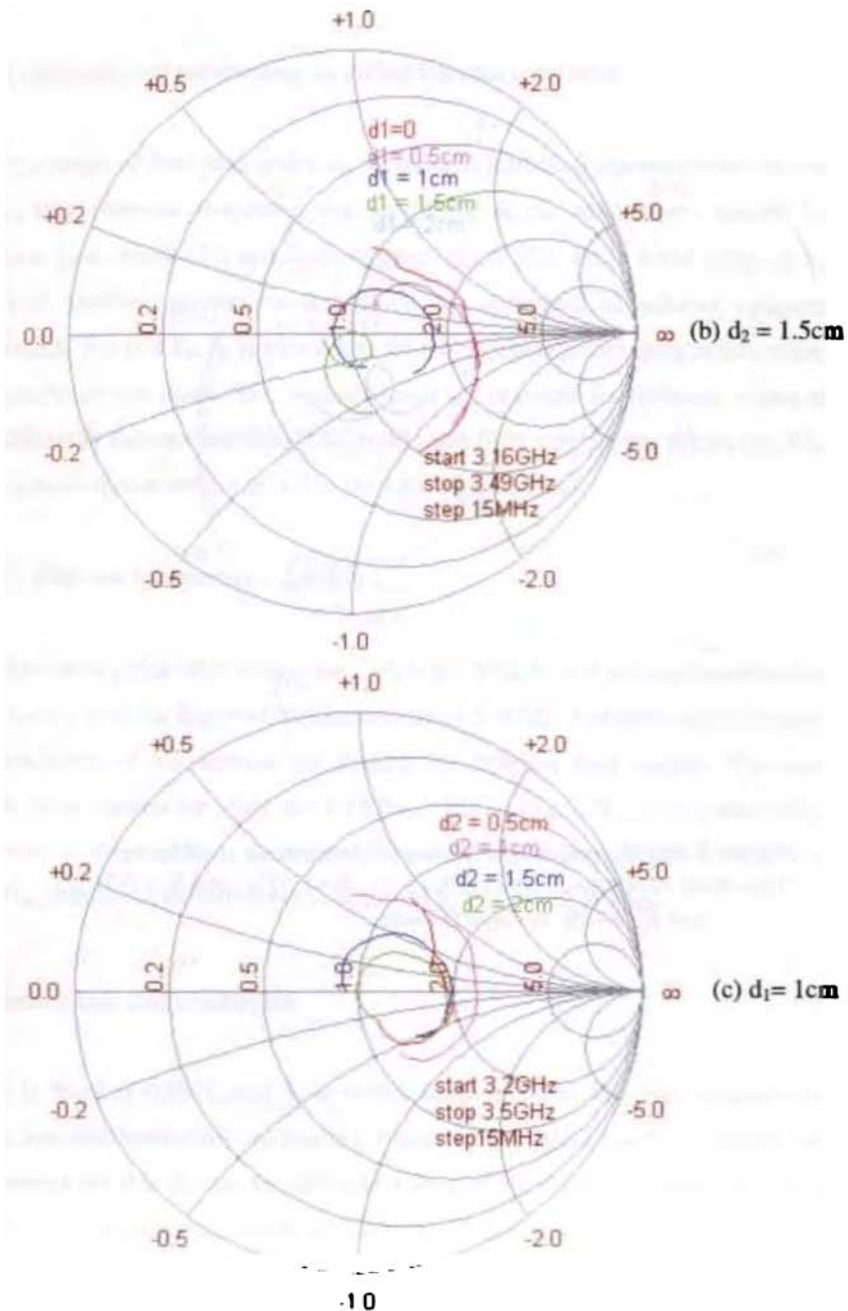


Figure 3.4(iv) Impedance variations of the antenna at different feed point locations, $L = 4\text{cm}$, $W = 2\text{cm}$, $S_1 = 1.52\lambda_d$, and $S_2 = 0.758\lambda_d$
 $\epsilon_{r1} = \epsilon_{r2} = 4.28$, $h_1 = h_2 = 0.16\text{cm}$.

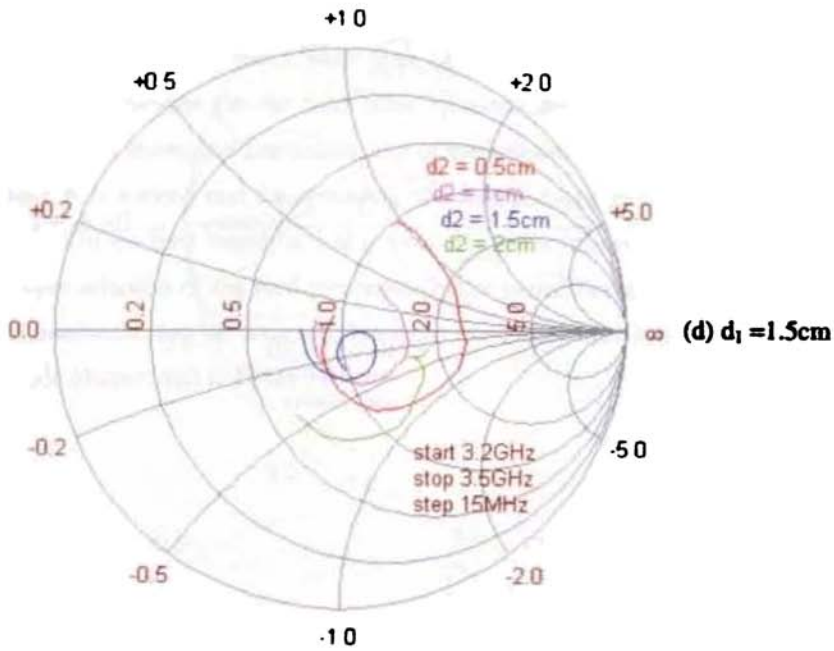


Figure 3.4(iv) Impedance variations of the antenna at different feed point locations, $L = 4$ cm, $W = 2$ cm, $S_1 = 1.52\lambda_d$, and $S_2 = 0.758\lambda_d$, $\epsilon_{r1} = \epsilon_{r2} = 4.28$, $h_1 = h_2 = 0.16$ cm.

3.2.2 Effect of feed parameters on reflection characteristics

The effect of feed parameters on the antenna reflection characteristics such as return loss, resonant frequency and bandwidth of the antenna are studied for different feed length (S_1) and feed segment length (S_2). For a fixed value of S_1 , the feed position parameters d_1 , d_2 , d_3 are optimized to achieve optimum bandwidth. For this S_1 , S_2 is varied and the corresponding variations in return loss characteristics are noted. The measurements are repeated for different values of S_1 . Generally S_1 is varied from $0.5\lambda_d$ to $2\lambda_d$ and S_2 is varied from $0.05\lambda_d$ to $1.2\lambda_d$. The detailed results are presented in the following sections.

3.2.2.1 Microstrip antenna – 2.4GHz

Microstrip patch with dimension $L=3.6\text{cm}$, $W=2.6\text{cm}$ is selected and excited with L-strip feed for bandwidth enhancement at 2.4GHz. Radiation and reflection characteristics of the antenna are studied for different feed lengths. The feed length value chosen for study are $0.637\lambda_d$, $0.821\lambda_d$, $1\lambda_d$, $1.2\lambda_d$, $1.32\lambda_d$ and $1.5\lambda_d$. For each of these values, S_2 is varied from $0.05\lambda_d$ to $1\lambda_d$. When S_1 is below $0.637\lambda_d$, bandwidth enhancement is observed to be is 4 to 5 % only.

(a) Return loss and bandwidth

S_1 is fixed as $0.637\lambda_d$ and S_2 is varied from $0.05\lambda_d$ to $1\lambda_d$, and variations in return loss and bandwidth are studied. Figure 3.5(a) shows the S_{11} variations of the antenna for this S_1 and for different values of S_2 . From the observation it is found that maximum bandwidth of 8.5% is obtained when S_2 is $0.4\lambda_d$. For this case the resonant frequency is also minimum and equal to 2.425GHz. Hence bandwidth enhancement along with lower resonant frequency is achieved.

S_1 value is increased to $0.821\lambda_d$ and the return loss and bandwidth variations are observed for different S_2 and the result is presented in Figure 3.5(b). From the

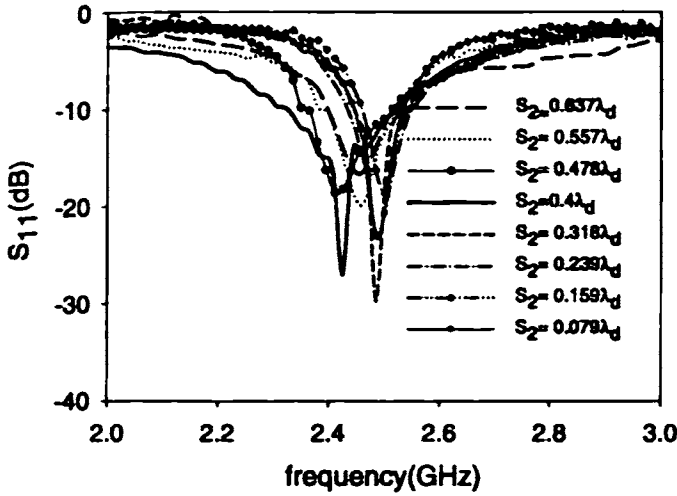
figure, it is observed that a maximum bandwidth of 11.5 % is obtained at 2.5GHz. Maximum bandwidth is achieved when the value of $S_2 = 0.41\lambda_d$. The bandwidth of the patch is improved as the feed length increases with a slight increase in resonant frequency.

S_1 is increased further to $1\lambda_d$ to find the optimum value to attain maximum bandwidth. Return loss variation for different S_2 segment length for the increased S_1 is shown in Figures 3.5 (c). From the figure it is observed that a maximum bandwidth of 16.8% is obtained when $S_2 = 0.4\lambda_d$ at the resonant frequency 2.425GHz.

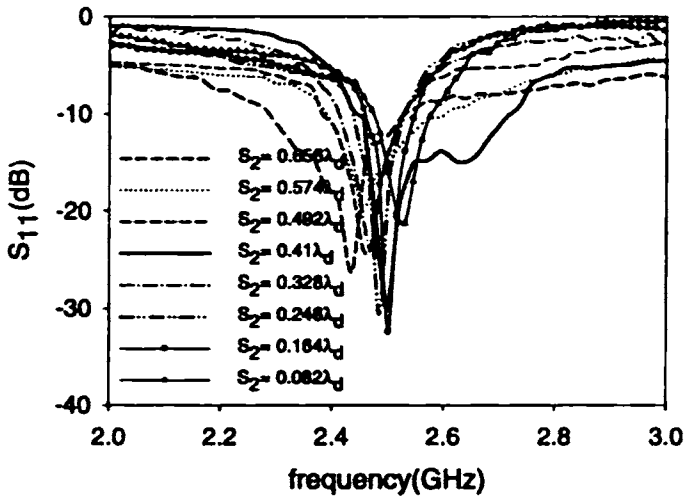
Figure 3.5 (d) shows the return loss variations for different S_2 for $1.2\lambda_d$. It is found that bandwidth of the antenna is decreases slightly for this feed length. Maximum bandwidth is obtained when the value of $S_2 = 0.404\lambda_d$. To confirm the result, S_1 is increased to $1.32\lambda_d$ and then to $1.5\lambda_d$, S_2 is varied from $0.05\lambda_d$ to $1\lambda_d$. It is observed that bandwidth of the antenna is decreasing for these values of S_1 .

Measured results are summarized in Table 3.1. The feed parameters for maximum bandwidth is $S_1/\lambda_d=1$, $S_2/\lambda_d = 0.4$, $d_1/\lambda_d = 0.1$, $d_2/\lambda_d = 0.2$ and $d_3/\lambda_d = 0.01$. Figure 3.6 consolidates the return loss curves for the S_2 values offering maximum bandwidth, for different S_1 .

Figure 3.7 shows the bandwidth variations with S_2 for different S_1 . From the figure it is clear that maximum bandwidth enhancement is obtained when the value of $S_1 = 1\lambda_d$. The feed parameters for maximum bandwidth are $S_1 + S_2 = 1.4\lambda_d$ and $S_2 = 0.4\lambda_d$.



(a)

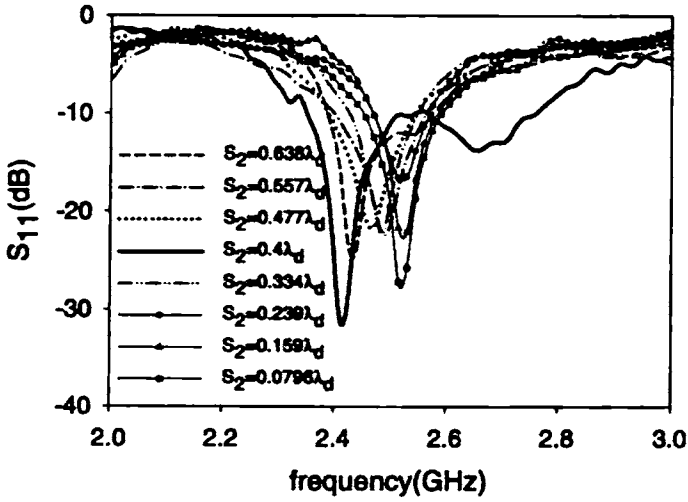


(b)

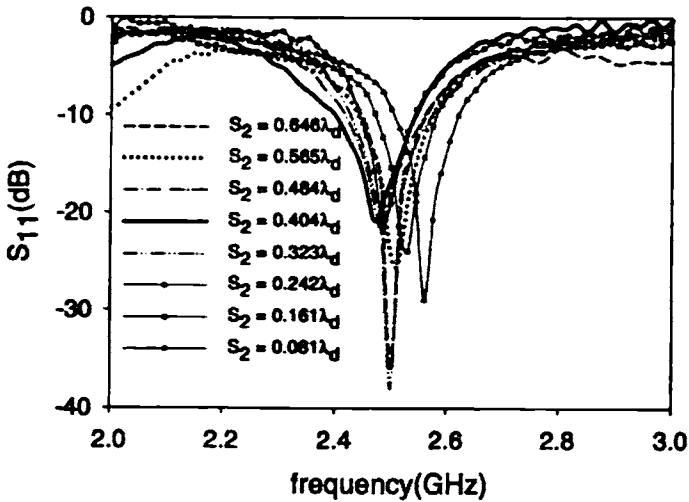
Figure 3.5(a) Return loss variations with frequency of the patch $L = 3.6$ cm, $W = 2.6$ cm, for different S_2

(a) $S_1 = 0.637\lambda_d$

(b) $S_1 = 0.821\lambda_d$



(c)



(d)

Figure 3.5 Return loss variations with frequency of the patch $L = 3.6\text{cm}$, $W = 2.6\text{cm}$, for different S_2

(c) $S_1 = 1\lambda_d$

(d) $S_1 = 1.2\lambda_d$

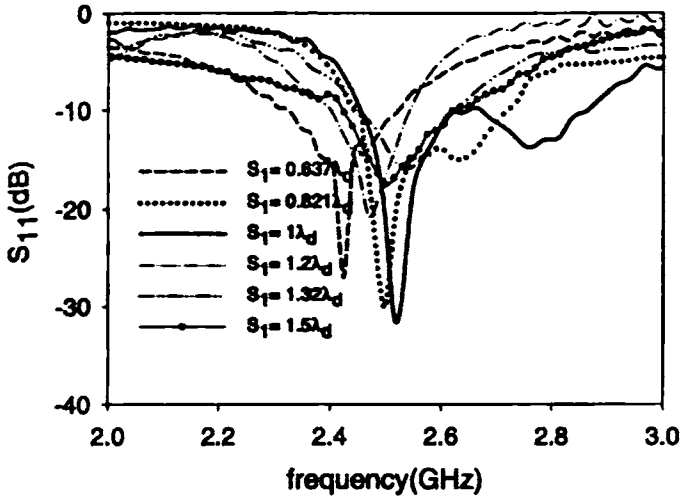


Figure 3.6 Return loss variations with frequency at the maximum bandwidth position for different S_1

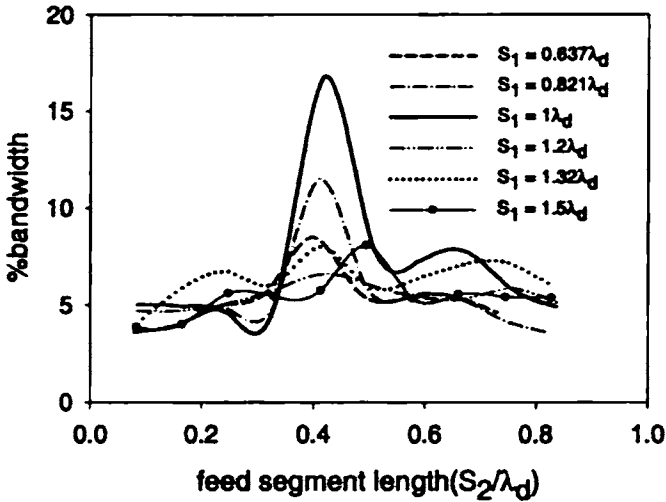


Figure 3.7 Bandwidth variations with S_2 for different S_1
 $L = 3.6\text{cm}$, $W = 2.6\text{cm}$, $\epsilon_{r1} = \epsilon_{r2} = 4.28$, $h_1 = h_2 = 0.16\text{cm}$

(b) Resonant frequency

To study the influence of feed parameters on resonant frequency, keeping S_1 fixed, S_2 is varied from $0.05\lambda_d$ to $1\lambda_d$. The variations of the resonant frequency of the antenna with S_2 for different S_1 are shown in the Table 3.1. Figure 3.8 also shows the resonant frequency variations for different S_1 . From the figure and table it is clear that the resonant frequency is not much affected by variation of S_1 and depends mainly on S_2 . It is again noted that the percentage bandwidth is highly depending on S_2 .

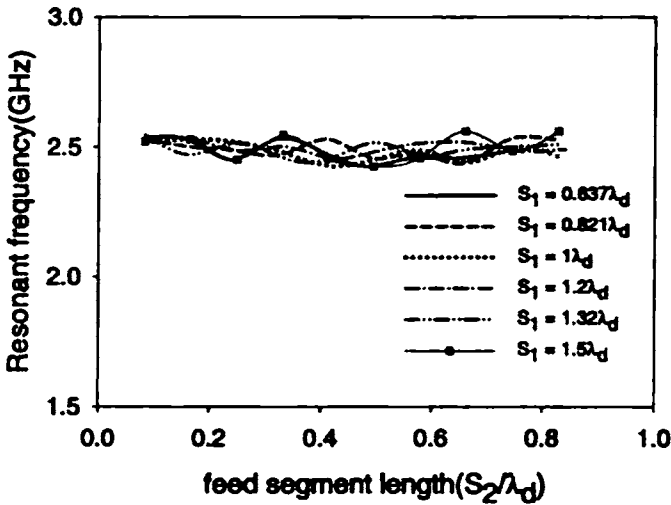


Figure 3.8 Resonant frequency variations with S_2 for different S_1 $L = 3.6\text{cm}$, $W = 2.6\text{cm}$, $\epsilon r1 = \epsilon r2 = 4.28$, $h_1 = h_2 = 0.16\text{cm}$

Table 3.1 Bandwidth and resonant frequency variations with S_2/λ_d for different S_1/λ_d of the L-strip fed antenna with $L = 3.6\text{cm}$, $W = 2.6\text{cm}$, $\epsilon_{r1} = \epsilon_{r2} = 4.28$, $h_1 = h_2 = 0.16\text{cm}$

Feed length (S_1/λ_d)	Feed segment length (S_2/λ_d)	Resonant frequency (GHz)	%bandwidth
0.637	0.079	2.485	3.6
	0.159	2.50	4.0
	0.239	2.45	5.0
	0.318	2.485	5.71
	0.40	2.425	8.5
	0.478	2.425	5.75
	0.557	2.455	5.29
	0.637	2.455	5.5
0.821	0.082	2.53	3.6
	0.164	2.5	4.0
	0.246	2.485	4.8
	0.328	2.47	5.86
	0.410	2.50	11.5
	0.492	2.455	6.1
	0.574	2.475	5.75
	0.656	2.436	5.37
	0.739	2.53	4.22
0.82	2.53	3.8	
1	0.0796	2.515	5.0
	0.159	2.53	4.9
	0.239	2.515	4.5
	0.334	2.475	6.2
	0.40	2.425	16.8
	0.477	2.454	8.5
	0.557	2.485	7.2
	0.638	2.44	7.08
	0.717	2.50	5.9
	0.796	2.455	4.9
1.2	0.081	2.54	4.69
	0.161	2.53	4.7
	0.242	2.485	5.1
	0.323	2.50	5.83
	0.404	2.455	7.6
	0.484	2.485	6.0
	0.565	2.515	5.43
	0.646	2.515	5.03
	0.726	2.485	5.83
	0.807	2.49	5.08

Table 3.1contd.. Bandwidth and resonant frequency variations with S_2/λ_d for different S_1/λ_d of the L-strip fed antenna with $L = 3.6\text{cm}$, $W = 2.6\text{cm}$, $\epsilon_{r1} = \epsilon_{r2} = 4.28$, $h_1 = h_2 = 0.16\text{cm}$

Feed length (S_1/λ_d)	Feed segment length (S_2/λ_d)	Resonant frequency (GHz)	%bandwidth
1.32	0.0826	2.545	4.0
	0.165	2.47	5.87
	0.248	2.515	6.7
	0.330	2.456	6.05
	0.413	2.452	8.1
	0.495	2.516	6.1
	0.578	2.47	6.26
	0.660	2.49	7.0
	0.743	2.50	7.21
	0.826	2.51	6.04
1.5	0.083	2.52	3.85
	0.165	2.53	4.0
	0.248	2.451	5.6
	0.330	2.545	5.44
	0.413	2.455	5.74
	0.495	2.423	8.08
	0.578	2.456	5.32
	0.660	2.513	5.54
	0.745	2.485	5.34
	0.828	2.56	5.36

From the experimental observations it can be concluded that microstrip patch with dimension $L = 3.6\text{cm}$, $W = 2.6\text{cm}$ is offering a bandwidth enhancement of $\sim 17\%$ when it is excited with L-strip feed. The feed parameters for maximum bandwidth are $S_1 + S_2 = 1.4\lambda_d$ and $S_2 = 0.4\lambda_d$.

3.2.2.2 Microstrip antenna – 2.7GHz

To confirm the above results the experiments are repeated at another antenna operating at 2.7GHz. Microstrip antenna with dimensions $L = 3\text{cm}$, $W = 2.4\text{cm}$ is excited with an L-strip feed and the reflection characteristics of the antenna are studied for different feed lengths. The feed length values chosen for study are $0.73\lambda_d$, $0.917\lambda_d$, $1.07\lambda_d$, $1.32\lambda_d$, $1.47\lambda_d$ and $1.6\lambda_d$. For each of this S_1 value, S_2 is varied from $0.05\lambda_d$ to $1\lambda_d$ and its effect are studied on the return loss of the antenna. The results are discussed in the following sections.

(a) Return loss and bandwidth

S_1 is fixed as $0.73\lambda_d$, return loss and bandwidth variations are studied for different S_2 . The S_{11} variations are given in Figure 3.9(a). Maximum bandwidth of 8.6% is achieved when S_2 is $0.73\lambda_d$. Bandwidth enhancement is achieved at the resonant frequency 2.785GHz.

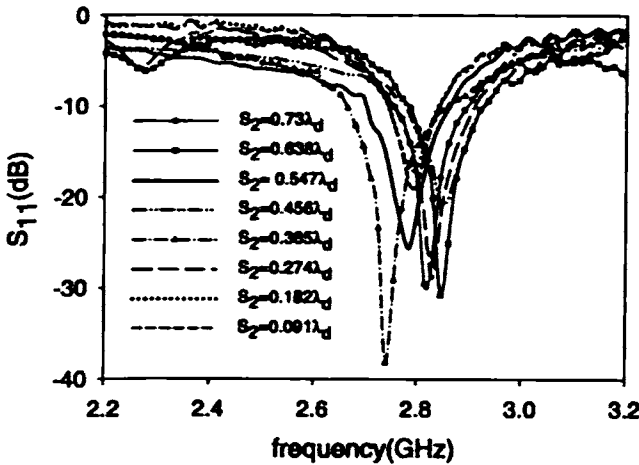
S_1 is further increased to $0.92\lambda_d$ and measurements are repeated. Figure 3.9(b) shows the S_{11} variation of this antenna for different values of S_2 . From the figure, it is found that the bandwidth improves from 8.6% to 10.5%, when the feed length is increased from $0.73\lambda_d$ to $0.92\lambda_d$. For this case the resonant frequency is 2.79GHz. The value of S_2 for maximum bandwidth is $0.734\lambda_d$.

S_1 is further increased to $1.07\lambda_d$ and by varying S_2 return loss and bandwidth variations are again noted. Figure 3.9(c) shows the return loss variations of the antenna for different S_2 values. This configuration offers a maximum bandwidth of 19 % when the value of $S_2 = 0.717\lambda_d$. It is observed that the bandwidth of the antenna increases as S_1 increases.

S_1 is further increased to $1.32\lambda_d$ and the corresponding return loss variations are given in Figure 3.9(d). Maximum bandwidth of 10% is achieved when $S_2 = 0.753\lambda_d$. It is found that the bandwidth of the antenna shows a decline for this S_1 . Hence the optimum value of S_1 for $3 \times 2.4\text{cm}^2$ patch is $1.07\lambda_d$.

To confirm the result, S_1 value is increased to $1.47\lambda_d$ and then to $1.6\lambda_d$. Results given in Table 3.2, also indicates a decline in bandwidth as S_1 increases. The optimum feed parameters for this patch to attain optimum bandwidth are $S_1/\lambda_d = 1.07$, $S_2/\lambda_d = 0.717$, $d_1/\lambda_d = 0.107$, $d_2/\lambda_d = 0.125$ and $d_3/\lambda_d = 0.322$.

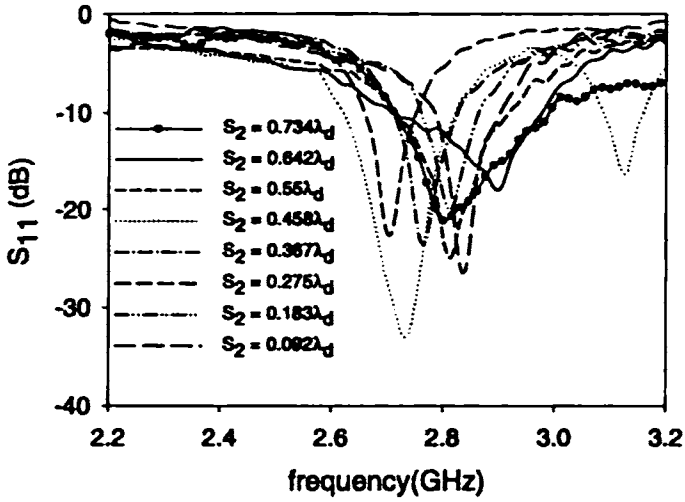
Figure 3.10 shows the consolidation of return loss curves for S_2 offering maximum bandwidth positions for different S_1 . From the figure it is clear that maximum bandwidth is obtained when $S_1 = 1.07\lambda_d$. Bandwidth variations for different S_1 are shown in Figure 3.11.



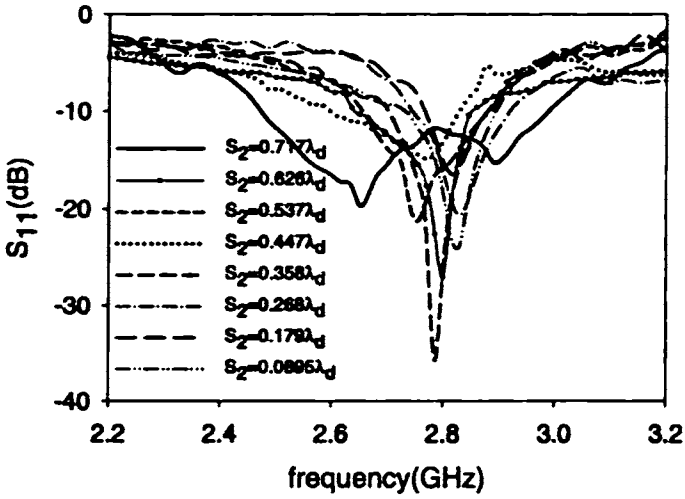
(a)

Figure 3.9 Return loss variations with frequency for the patch $L = 3\text{cm}$, $W = 2.4\text{cm}$, for different S_2 .

(a) $S_1 = 0.73\lambda_d$



(b)



(c)

Figure 3.9 Return loss variations with frequency for the patch $L = 3\text{cm}$, $W = 2.4\text{cm}$, for different S_2

(b) $S_1 = 0.917\lambda_d$

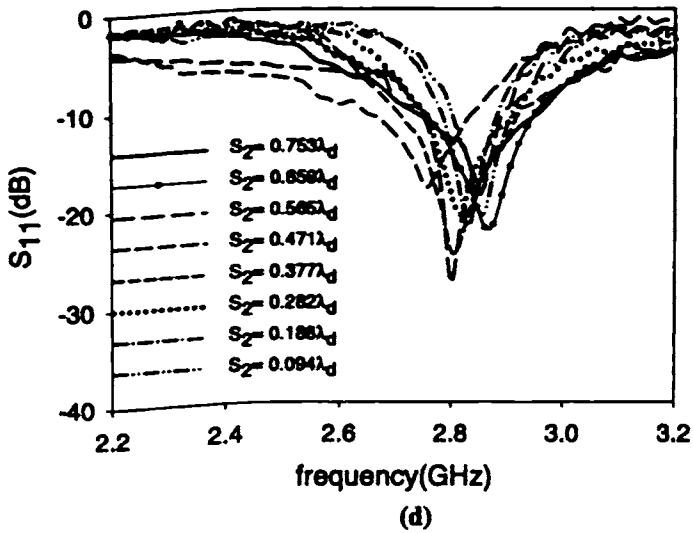


Figure 3.9 Return loss variations with frequency for the patch $L = 3\text{cm}$, $W = 2.4\text{ cm}$, for different S_2
 (d) $S_1 = 1.32\lambda_d$

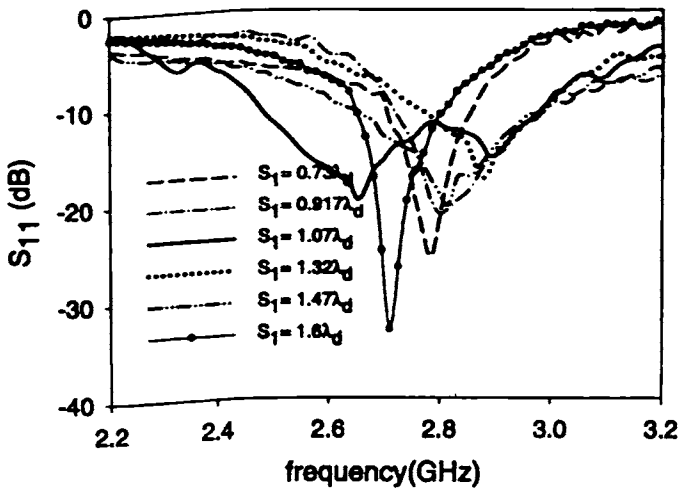


Figure 3.10 Return loss variations of the antenna at the maximum bandwidth position for different S_1 , with $L = 3\text{cm}$, $W = 2.4\text{cm}$
 $\epsilon_{r1} = \epsilon_{r2} = 4.28$, $h_1 = h_2 = 0.16\text{cm}$.

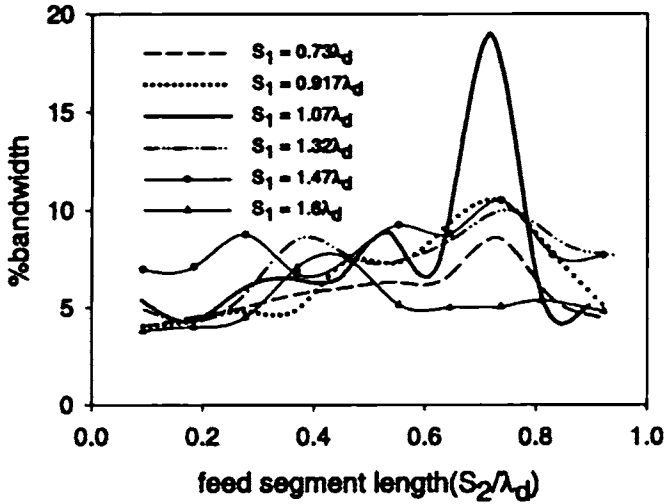


Figure 3.11 Bandwidth variations with S_2 of the patch
 $L = 3\text{cm}$, $W = 2.4\text{cm}$, $\epsilon_{r1} = \epsilon_{r2} = 4.28$, $h_1 = h_2 = 0.16\text{cm}$.
 for different S_1

(b) Resonant frequency

To study the influence of feed parameters on resonant frequency, keeping S_1 fixed, S_2 is varied from $0.05\lambda_d$ to $1\lambda_d$. The variations of the resonant frequency of the antenna with S_2 for different S_1 are shown in the Table 3.2. Also Figure 3.12 shows the resonant frequency variations for different S_1 . From the figure and table it is clear that the resonant frequency variations are less with S_1 as observed in the previous case.

From the measured results it is observed that the patch resonating at 2.9GHz when excited with L-strip feed, the resonant frequency of the patch is shifting to 2.7GHz, with slight bandwidth enhancement. Maximum bandwidth obtained is 19%, which is ~ 6 times higher than that with conventional feed.

Table 3.2 Bandwidth and resonant frequency variations with S_2/λ_d for different S_1/λ_d of the L-strip fed antenna with

$L = 3\text{cm}$, $W = 2.4\text{cm}$, $\epsilon_{r1} = \epsilon_{r2} = 4.28$, $h_1 = h_2 = 0.16\text{cm}$

Feed length (S_1/λ_d)	Feed segment length (S_2/λ_d)	Resonant frequency (GHz)	%bandwidth
0.73	0.091	2.815	4.02
	0.182	2.815	4.5
	0.274	2.785	5.0
	0.365	2.74	5.65
	0.456	2.815	6.0
	0.547	2.785	6.3
	0.638	2.83	6.5
	0.730	2.785	8.6
0.917	0.092	2.83	4.04
	0.183	2.815	4.29
	0.275	2.71	4.8
	0.367	2.77	4.83
	0.458	2.74	7.35
	0.55	2.71	7.27
	0.642	2.80	9.27
	0.734	2.79	10.9
	0.825	2.815	7.96
	0.92	2.8	5.14
1.07	0.089	2.83	5.39
	0.179	2.815	4.29
	0.268	2.83	5.88
	0.358	2.80	6.48
	0.447	2.77	6.5
	0.537	2.755	8.86
	0.626	2.80	7.38
	0.717	2.733	19.0
	0.805	2.755	6.06
	0.895	2.71	5.09
1.32	0.094	2.83	4.89
	0.188	2.83	4.29
	0.282	2.815	5.86
	0.377	2.80	8.6
	0.471	2.755	7.49
	0.565	2.80	7.5
	0.659	2.815	8.8
	0.753	2.785	10.0
	0.847	2.815	8.31
	0.941	2.80	7.67

Table 3.2contd.. Bandwidth and resonant frequency variations with S_2/λ_d for different S_1/λ_d of the L-strip fed antenna with $L = 3\text{cm}$, $W = 2.4\text{cm}$, $\epsilon_{r1} = \epsilon_{r2} = 4.28$, $h_1 = h_2 = 0.16\text{cm}$

Feed length (S_1/λ_d)	Feed segment length (S_2/λ_d)	Resonant frequency (GHz)	%bandwidth
1.47	0.092	2.815	6.94
	0.184	2.815	7.07
	0.277	2.815	8.76
	0.369	2.80	6.7
	0.461	2.755	7.5
	0.553	2.815	9.24
	0.645	2.785	8.78
	0.737	2.785	10.5
	0.83	2.77	7.7
	0.922	2.755	7.67
1.6	0.092	2.815	3.8
	0.184	2.83	4.0
	0.277	2.785	4.5
	0.369	2.815	7.04
	0.461	2.73	7.5
	0.553	2.815	5.13
	0.645	2.80	5.0
	0.737	2.71	5.03
	0.81	2.74	5.36
	0.922	2.80	4.8

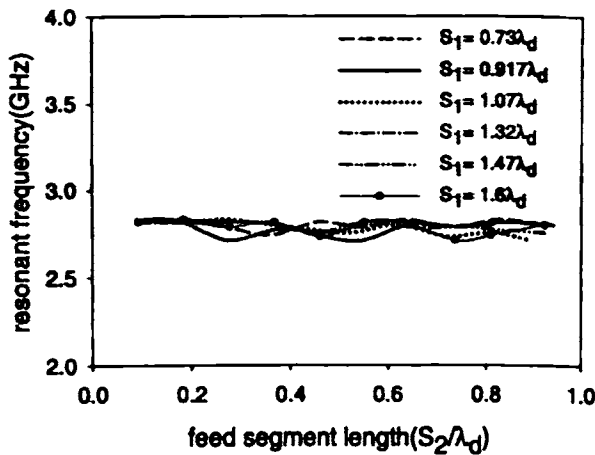


Figure 3.12 Resonant frequency variations with S_2 for different S_1 of the patch $L = 3\text{cm}$, $W = 2.4\text{cm}$
 $\epsilon_{r1} = \epsilon_{r2} = 4.28$, $h_1 = h_2 = 0.16\text{cm}$

3.2.2.3 Microstrip antenna – 3.2GHz

Microstrip patch with dimensions $L = 3\text{cm}$, $W = 2\text{cm}$, resonating at 3.5GHz is excited with L-strip feed and the effect of feed parameters on the reflection characteristics of the antenna are studied. To study the effect of feed parameters on the return loss of the antenna, for a fixed value of S_1 , say $0.833\lambda_d$, S_2 is varied between $0.1\lambda_d$ to $1.1\lambda_d$ and the experiments are repeated. The other feed parameters like d_1 , d_2 , d_3 are optimized to achieve maximum bandwidth as in the previous cases. The experiments are repeated for S_1 values $1.06\lambda_d$, $1.27\lambda_d$, $1.5\lambda_d$, $1.7\lambda_d$ and $1.85\lambda_d$. When S_1 is below $0.833\lambda_d$ bandwidth enhancement is observed to be 5 to 6% only. The experimental observations are discussed in the following sections.

(a) Return loss characteristics and bandwidth

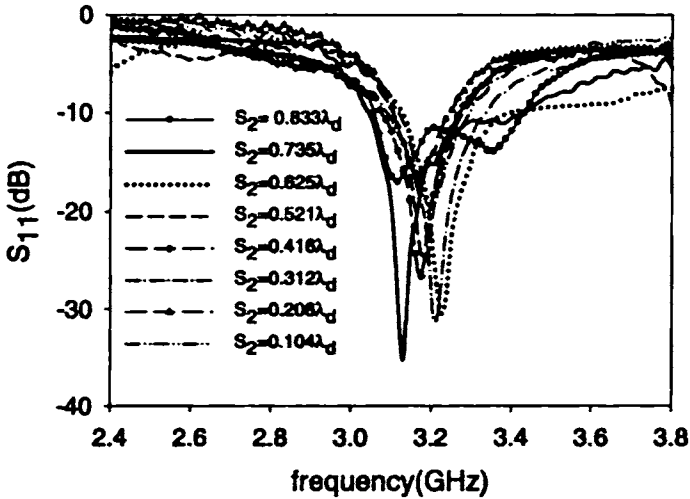
Return loss characteristics of the antenna are studied for the above mentioned S_1 values. Figure 3.13(a) shows the return loss variation for different values of S_2 when $S_1 = 0.833\lambda_d$. It is found that the bandwidth of the antenna is improved when it is fed with the L-strip. From the return loss curve the resonance frequency can be identified as 3.1GHz. The frequency is shifted from 3.5GHz to 3.1GHz due to the L-strip feeding. Maximum bandwidth of 12.52%, four times higher than that with a conventional feed is achieved for this particular S_1 when $S_2 = 0.734\lambda_d$.

S_1 is increased to $1.06\lambda_d$ and return loss variations are observed and are presented in Figure 3.13(b). It is observed that the bandwidth increases with S_1 . Maximum bandwidth of 18.12% is obtained when $S_2 = 0.746\lambda_d$.

Figure 3.13(c) gives the return loss variations when S_1 is $1.27\lambda_d$ for different S_2 . It is observed that the bandwidth is decreased for this value of S_1 . S_1 is further increased to $1.5\lambda_d$ and the return loss variations are presented in Figure 3.13(d). Return loss variations are studied for feed lengths $1.7\lambda_d$ and $1.85\lambda_d$ also.

Experimental results are presented in Table 3.3. From the results, it is clear that the bandwidth decrease if we increase S_1 above $1.06\lambda_d$. So the optimum value of S_1 is chosen as $1.06\lambda_d$. The other feed parameters for maximum bandwidth are $S_2/\lambda_d = 0.746$, $d_1/\lambda_d = 0.148$, $d_2/\lambda_d = 0.254$ and $d_3/\lambda_d = 0.336$.

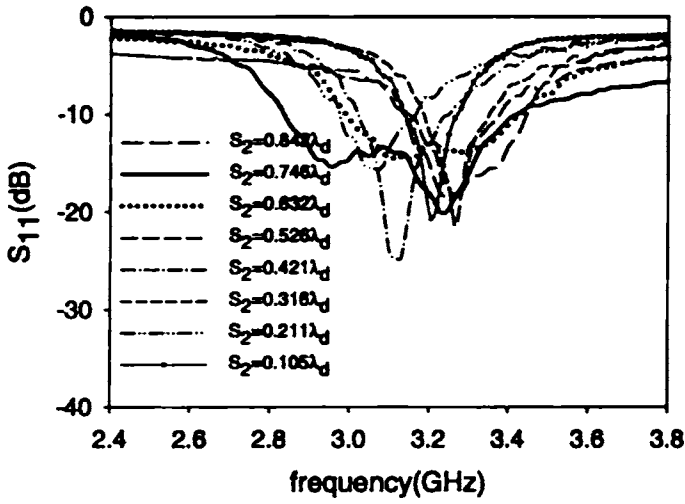
Figure 3.14 shows the consolidation of return loss curves for S_2 offering maximum bandwidth, for different S_1 . Figure 3.15 shows the bandwidth variations with S_2 for different S_1 . It is found that maximum bandwidth of 18.20% is obtained when $S_1 = 1.06\lambda_d$ and $S_2 = 0.746\lambda_d$.



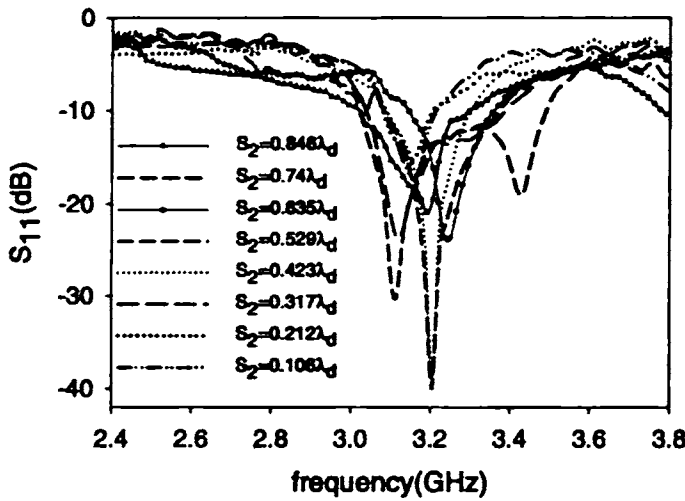
(a)

Figure 3.13 Return loss variations with frequency for the patch $L = 3\text{cm}$, $W = 2\text{cm}$, for different S_2 .

(a) $S_1 = 0.833\lambda_d$



(b)



(c)

Figure 3.13 Return loss variations with frequency for the patch $L = 3\text{cm}$, $W = 2\text{cm}$, for different S_2
 (b) $S_1 = 1.06\lambda_d$
 (c) $S_1 = 1.27\lambda_d$

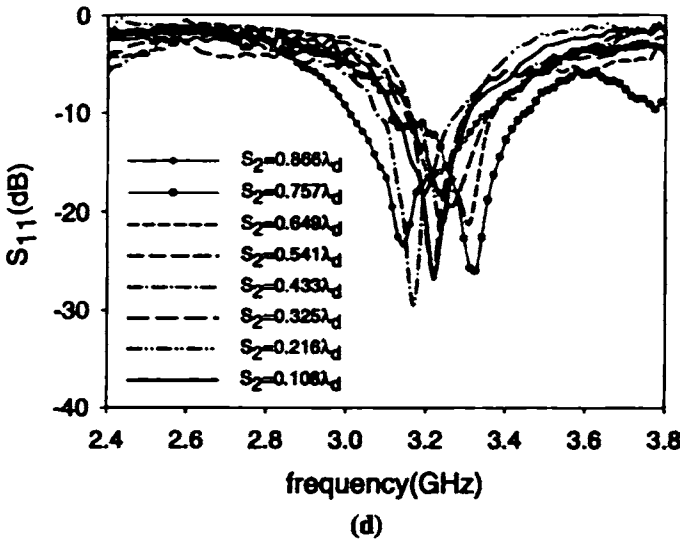


Figure 3.13 Return loss variations with frequency for the patch $L = 3\text{cm}$, $W = 2\text{cm}$, for different S_2 .
(d) $S_1 = 1.5\lambda_d$

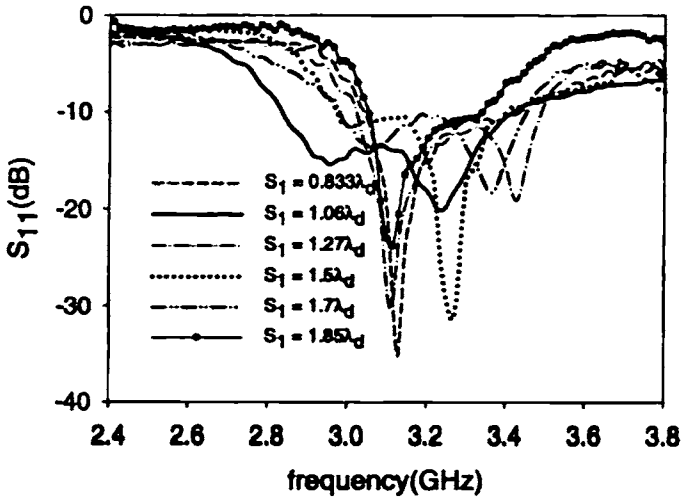


Figure 3.14 Return loss variations with frequency at the maximum bandwidth position for different S_1 , $L = 3\text{cm}$, $W = 2\text{cm}$, $\epsilon_{r1} = \epsilon_{r2} = 4.28$, $h_1 = h_2 = 0.16\text{cm}$.

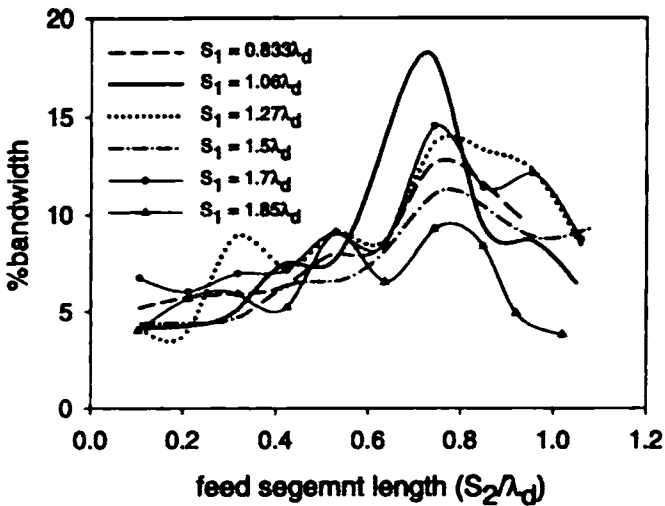


Figure 3.15 Bandwidth variations with S_2 of the patch $L = 3\text{cm}$, $W = 2\text{cm}$, $\epsilon_{r1} = \epsilon_{r2} = 4.28$, $h_1 = h_2 = 0.16\text{cm}$, for different S_1 .

(b) Resonant frequency

To study the influence of feed parameters on resonant frequency, keeping S_1 fixed, S_2 is varied from $0.1\lambda_d$ to $1.1\lambda_d$. The variations of the resonant frequency of the patch having dimensions $L \times W = 3 \times 2\text{cm}^2$ with respect to S_2 for different S_1 are shown in the Table 3.3. Figure 3.16 shows the resonant frequency variations for different S_1 . From the figure it is clear that the resonant frequency is not much affected by variation of S_1 and S_2 .

Table 3.3 Bandwidth and resonant frequency variations with S_2/λ_d for different S_1/λ_d of the L-strip fed antenna with $L = 3\text{cm}$, $W = 2\text{cm}$, $\epsilon_{r1} = \epsilon_{r2} = 4.28$, $h_1 = h_2 = 0.16\text{cm}$

Feed length S_1/λ_d	Feed segment length S_2/λ_d	Resonant frequency(GHz)	%bandwidth
0.833	0.105	3.22	5.19
	0.209	3.205	5.74
	0.314	3.205	5.95
	0.419	3.175	6.35
	0.524	3.19	7.98
	0.628	3.22	8.35
	0.734	3.22	12.52
	0.838	3.25	11.86
1.06	0.106	3.205	4.16
	0.211	3.205	4.26
	0.316	3.265	5.08
	0.421	3.205	7.52
	0.526	3.22	7.66
	0.632	3.205	13.62
	0.746	3.235	18.12
	0.842	3.25	9.80
	0.947	3.24	8.76
	1.06	3.19	6.49
1.27	0.106	3.16	4.16
	0.212	3.145	4.04
	0.312	3.19	8.91
	0.423	3.205	7.23
	0.529	3.205	9.16
	0.635	3.22	8.65
	0.74	3.254	14.29
	0.846	3.26	13.35
	0.952	3.28	12.4
	1.06	3.216	8.47
1.5	0.108	3.22	4.39
	0.216	3.145	4.41
	0.325	3.235	4.77
	0.433	3.22	6.43
	0.541	3.205	6.65
	0.649	3.310	8.52
	0.757	3.32	11.25
	0.866	3.28	10.14
	0.974	3.235	8.81
	1.08	3.145	9.31

Table 3.3 contd.. Bandwidth and resonant frequency variations with S_2/λ_d for different S_1/λ_d of the L-strip fed antenna with $L = 3\text{cm}$, $W = 2\text{cm}$, $\epsilon_{r1} = \epsilon_{r2} = 4.28$, $h_1 = h_2 = 0.16\text{cm}$

Feed length S_1/λ_d	Feed segment length S_2/λ_d	Resonant frequency(GHz)	%bandwidth
1.7	0.106	3.175	6.75
	0.212	3.145	6.05
	0.318	3.22	6.98
	0.424	3.245	7.16
	0.530	3.175	9.1
	0.636	3.175	8.52
	0.743	3.26	14.55
	0.849	3.22	11.41
	0.955	3.145	12.15
	1.06	3.205	8.74
1.85	0.102	3.22	4.0
	0.212	3.22	5.68
	0.318	3.205	5.94
	0.424	3.19	5.22
	0.530	3.175	9.1
	0.636	3.25	7.5
	0.743	3.145	9.29
	0.849	3.145	8.4
	0.92	3.145	4.91
	1.02	3.1	3.8

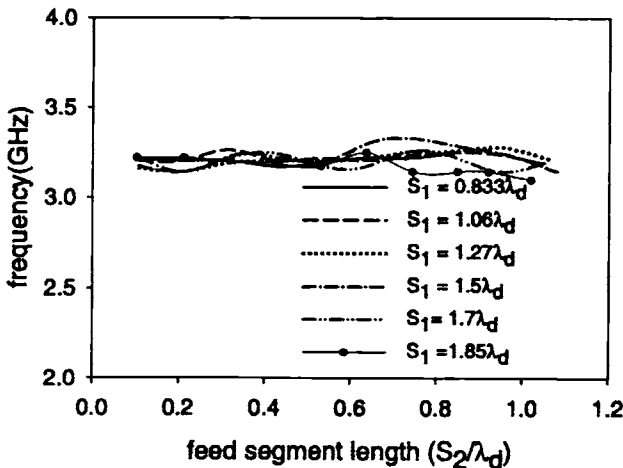


Figure 3.16 Resonant frequency variations of the antenna for different S_1 , $L = 3\text{cm}$, $W = 2\text{cm}$, $\epsilon_{r1} = \epsilon_{r2} = 4.28$, $h_1 = h_2 = 0.16\text{cm}$

3.2.2.4 Microstrip antenna –3.3GHz

To reconfirm the experimental observations, the experiments are repeated on another microstrip antenna resonating at 3.3GHz ($L = 4\text{cm}$, $W=2\text{cm}$). For a fixed value of S_1 , the feed position parameters d_1 , d_2 , d_3 are optimized to achieve maximum bandwidth. For this S_1 , S_2 is varied and the corresponding variations in return loss characteristics are noted. The measurements are repeated for different values of S_1 .

(a) Return loss characteristics and bandwidth

The feed length value chosen for study are $0.862\lambda_d$, $1.08\lambda_d$, $1.3\lambda_d$, $1.52\lambda_d$, $1.75\lambda_d$ and $1.95\lambda_d$. For each of these S_1 values, S_2 is varied from $0.1\lambda_d$ to $1.2\lambda_d$. When the feed length is below $0.8\lambda_d$ the maximum bandwidth enhancement is observed to be 5 to 6%. Figure 3.17 (a) shows the return loss variations with frequency for $S_1 = 0.862\lambda_d$, for different S_2 . Here maximum bandwidth of 12.62% is obtained when S_2 is $0.754\lambda_d$ ($\approx \frac{3}{4}\lambda_d$). From the return loss curve the resonance frequency is identified as 3.31GHz.

The feed length is increased to $1.08\lambda_d$ and the return loss of the antenna is measured for different feed segment lengths (S_2) and plotted in Figure 3.17(b). Maximum bandwidth of 15.8% is obtained for this case also when $S_2 = \frac{3}{4}\lambda_d$. The bandwidth of the antenna is found to be increasing with increasing S_1 .

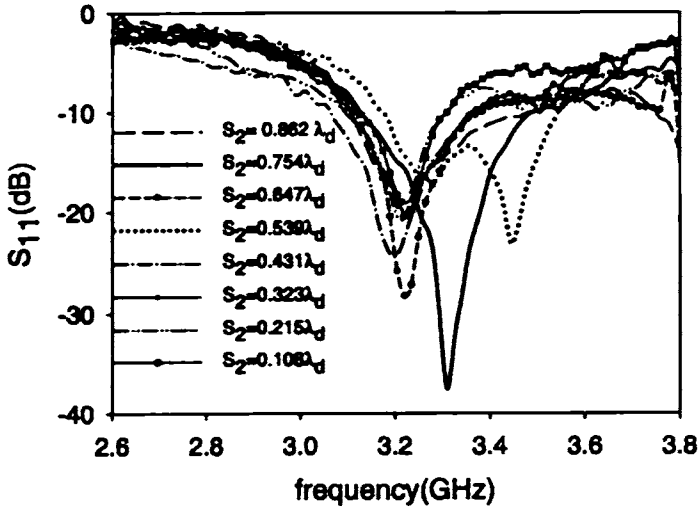
Figure 3.17(c) shows the return loss variations of the antenna with $S_1 = 1.3\lambda_d$. Bandwidth of the antenna is further increased and a maximum bandwidth of 20% is obtained for $S_2 \approx \frac{3}{4}\lambda_d$.

Figure 3.17(d) shows the return loss variation of the antenna with $S_1 = 1.52\lambda_d$ for different S_2 . For this case also maximum bandwidth of 19% is obtained when $S_2 \approx \frac{3}{4}\lambda_d$. Maximum bandwidth of the antenna is found remain almost constant. To find the optimum value of S_1 , it is increased further to $1.95\lambda_d$. Then the bandwidth is found to be less than that obtained for $S_1 = 1.75\lambda_d$ and hence the experiment is not repeated for further S_1 values. It is observed that for all the S_1

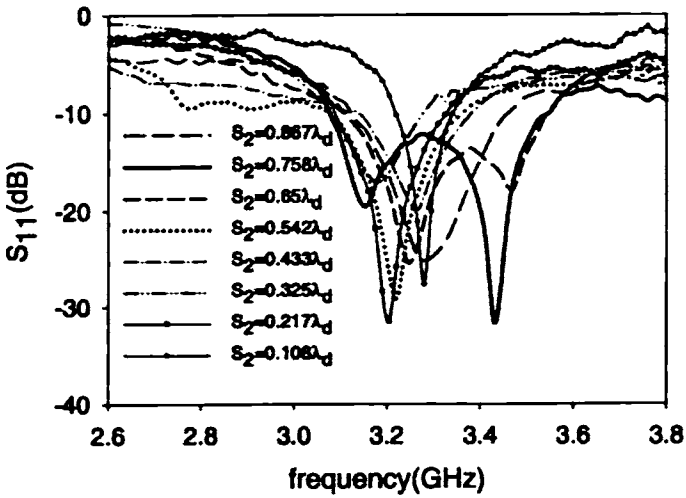
values, maximum bandwidth is achieved when $S_2 \approx 0.75\lambda_d$. From the experimental studies it is found that the other feed parameters to achieve maximum bandwidth are $d_1/\lambda_d = 0.271$, $d_2/\lambda_d = 0.325$ and $d_3/\lambda_d = 0.217$. Experimental results are summarized in Table 3.4. From the table it is clear that the bandwidth of the antenna is optimum when the feed length is $1.3\lambda_d$.

Figure 3.18 consolidates the return loss curves for the S_2 values offering maximum bandwidth, for different S_1 . From the figure it is observed that maximum impedance bandwidth is achieved when $S_1 = 1.3\lambda_d$.

From the experimental studies it is observed that the L-strip fed rectangular microstrip antenna having dimensions $L = 4\text{cm}$, $W = 2\text{cm}$ is offering a large impedance bandwidth of the order of $\sim 20\%$, which is 6.5 times higher than that of conventional microstrip feed.



(a)

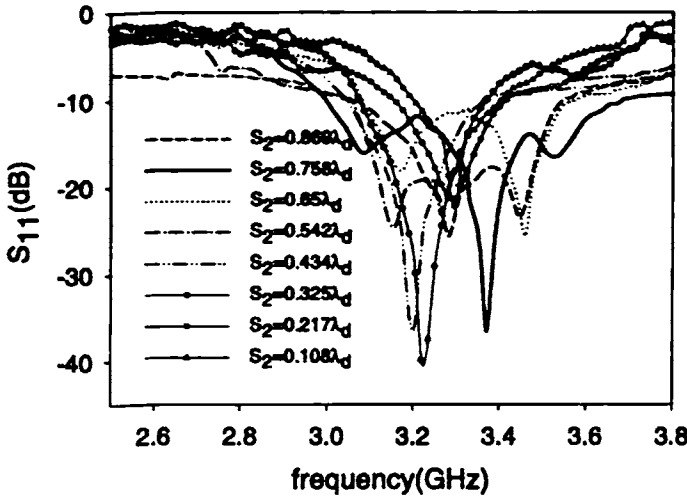


(b)

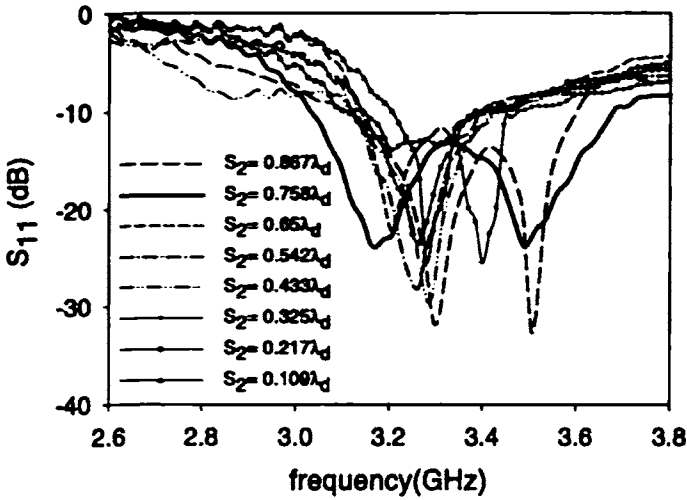
Figure 3.17 Return loss variations with frequency for the patch with $L = 4\text{cm}$, $W = 2\text{cm}$, for different S_2

(a) $S_1 = 0.862\lambda_d$

(b) $S_1 = 1.08\lambda_d$



(c)



(d)

Figure 3.17 Return loss variations with frequency for different S_2 with $L = 4\text{cm}$, $W=2\text{cm}$, for different S_2

(c) $S_1 = 1.3\lambda_d$

(d) $S_1 = 1.52\lambda_d$

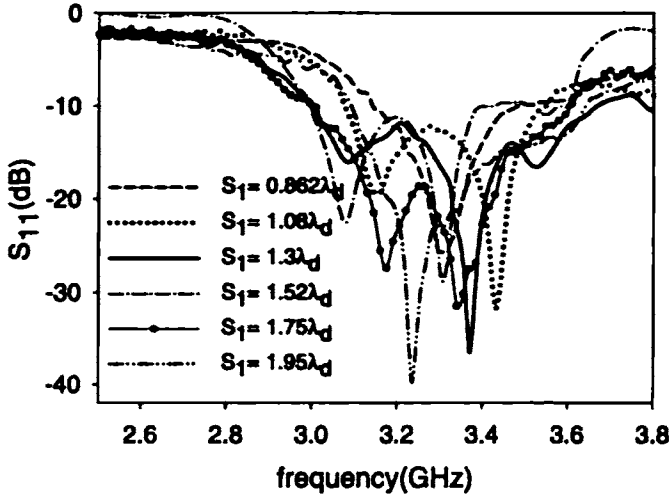


Figure 3.18 Return loss variations of the L-strip fed antenna at the maximum bandwidth position for different S_1 , with $L = 4\text{cm}$, $W = 2\text{cm}$, $\epsilon_{r1} = \epsilon_{r2} = 4.28$, $h_1 = h_2 = 0.16\text{cm}$, $S_2 = 0.75\lambda_d$

(b) Resonant frequency

To study the influence of feed parameters on resonant frequency, keeping S_1 fixed, S_2 is varied from $0.1\lambda_d$ to $1.2\lambda_d$. The variations of the corresponding resonant frequency of the antenna of dimension $4 \times 2\text{cm}^2$ are shown in the Table 3.4. Resonant frequency variations of the patch are found to be almost invariant with S_1 , but the bandwidth and resonant frequency are highly depending on S_2 .

Table 3.4 Bandwidth and resonant frequency variations with S_2/λ_d for different S_1/λ_d of the L-strip fed antenna with $L = 4\text{cm}$, $W = 2\text{cm}$, $\epsilon_{r1} = \epsilon_{r2} = 4.28$, $h_1 = h_2 = 0.16\text{cm}$

Feed length S_1/λ_d	Feed segment length S_2/λ_d	Resonant frequency (GHz)	%Bandwidth
0.862	0.108	3.205	5.78
	0.216	3.20	6.0
	0.325	3.24	8.29
	0.431	3.205	9.39
	0.539	3.22	9.89
	0.647	3.25	10.62
	0.754	3.31	12.62
	0.862	3.211	8.19
1.08	0.108	3.25	4.00
	0.217	3.20	6.57
	0.325	3.20	7.02
	0.433	3.262	7.29
	0.542	3.245	9.76
	0.650	3.245	13.25
	0.758	3.33	15.80
	0.867	3.311	10.03
	0.975	3.30	9.62
1.08	3.33	8.65	
1.3	0.108	3.235	5.68
	0.217	3.25	6.68
	0.325	3.235	9.08
	0.433	3.215	10.16
	0.542	3.231	10.8
	0.650	3.319	14.4
	0.758	3.331	20.0
	0.867	3.32	14.31
	0.975	3.34	13.79
1.08	3.34	11.7	
1.52	0.108	3.28	4.5
	0.217	3.265	5.68
	0.325	3.31	9.07
	0.433	3.295	9.22
	0.542	3.26	9.21
	0.650	3.205	11.24
	0.758	3.33	19.0
	0.867	3.34	14.5
	0.975	3.383	12.08
1.08	3.298	13.89	

Table 3.4 contd.. Bandwidth and resonant frequency variations with S_2/λ_d for different S_1/λ_d of the L-strip fed antenna with $L = 4\text{cm}$, $W = 2\text{cm}$,

$$\epsilon_{r1} = \epsilon_{r2} = 4.28, h_1 = h_2 = 0.16\text{cm}$$

Feed length S_1/λ_d	Feed segment length S_2/λ_d	Resonant frequency (GHz)	%Bandwidth
1.75	0.109	3.265	4.3
	0.217	3.235	5.93
	0.326	3.295	8.33
	0.434	3.205	9.09
	0.543	3.235	11.6
	0.652	3.33	13.0
	0.76	3.38	18.5
	0.869	3.319	15.7
	0.978	3.34	13.38
	1.086	3.37	10.94
1.95	0.109	3.265	4.82
	0.217	3.25	6.14
	0.326	3.22	8.36
	0.434	3.251	9.04
	0.543	3.235	11.6
	0.652	3.238	11.0
	0.76	3.364	16.35
	0.869	3.215	12.35
	0.976	3.299	10.09
	1.08	3.34	9.99

From the experiments, it is concluded that if the resonant frequency of the microstrip patch is of the order of 2.7GHz - 4GHz, for maximum bandwidth, the value of S_2 is of the order of $0.75\lambda_d$. The optimum feed parameters to attain maximum bandwidth for the patch with dimension $L = 4\text{cm}$, $W = 2\text{cm}$ is $S_1 + S_2 = 2\lambda_d$ and $S_2 = \frac{3}{4}\lambda_d$.

3.2.3 Effect of feed point location on reflection characteristics

The lengths d_1 and d_2 determines the co-ordinates of the feed point location. The bandwidth as well as the resonant frequency of the L-strip fed antenna varies with d_1 and d_2 . Effect of the feed point locations on these parameters are studied for the patch which gave optimum bandwidth. The detailed results are discussed below.

(a) Feed length – $0.862\lambda_d$

Here S_1 and S_2 are fixed as $0.862\lambda_d$ and $0.754\lambda_d$ respectively and d_1 and d_2 are systematically varied. Figure 3.19 and 3.20 shows the variation of resonant frequency and bandwidth with respect to d_1 and d_2 . It is found that when $d_1 = 0.217\lambda_d$ and $d_2 = 0.325\lambda_d$ the antenna is resonating with minimum frequency of 3.295 GHz. But when $d_1 = 0.271\lambda_d$ and $d_2 = 0.325\lambda_d$ the antenna offers maximum bandwidth even though the resonant frequency is slightly higher.

(b) Feed length – $1.08\lambda_d$

Feed length of the L-strip feed is increased to $1.08\lambda_d$ and the experiments are repeated. Figure 3.21 and 3.22 shows the influence of d_1 and d_2 on resonant frequency and bandwidth. Here it seems that resonant frequency variations are appreciable with the feed position parameters. The condition for minimum resonant frequency is $d_1 = 0.108\lambda_d$ and $d_2 = 0.325\lambda_d$ and that for maximum bandwidth is $d_1 = 0.271\lambda_d$, $d_2 = 0.325\lambda_d$

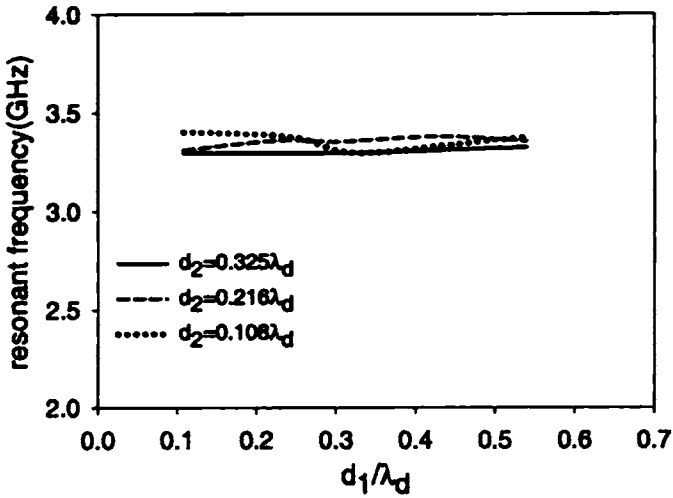


Figure 3.19 Variation of resonant frequency with d_1 and d_2 for the patch $L = 4\text{cm}$, $W = 2\text{cm}$, $S_1 = 0.862\lambda_d$, $S_2 = 0.754\lambda_d$

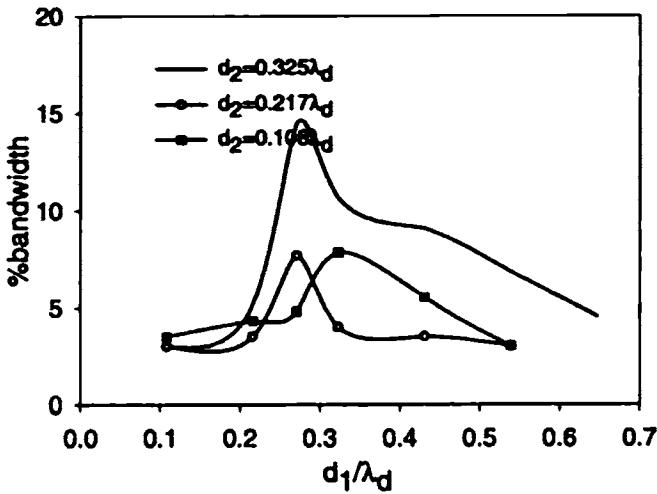


Figure 3.20 Bandwidth variations with d_1 and d_2 for the patch $L = 4\text{cm}$, $W = 2\text{cm}$, $S_1 = 0.862\lambda_d$ and $S_2 = 0.754\lambda_d$

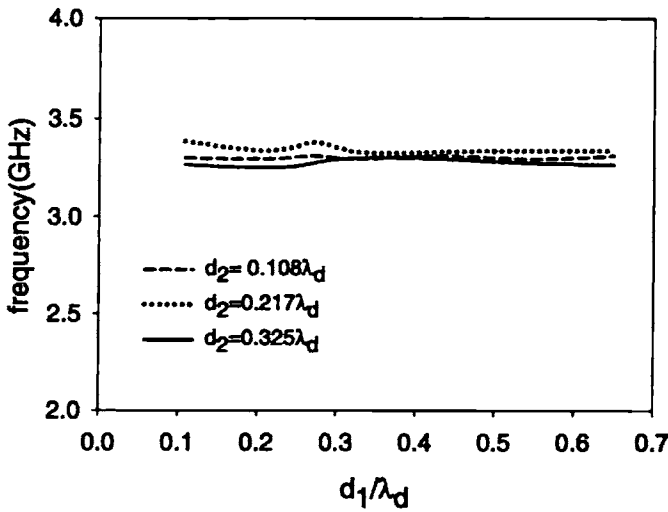


Figure 3.21 Resonant frequency variations with d_1 and d_2 for the patch $L = 4\text{cm}$, $W = 2\text{cm}$, $S_1 = 1.08\lambda_D$, $S_2 = 0.754\lambda_D$

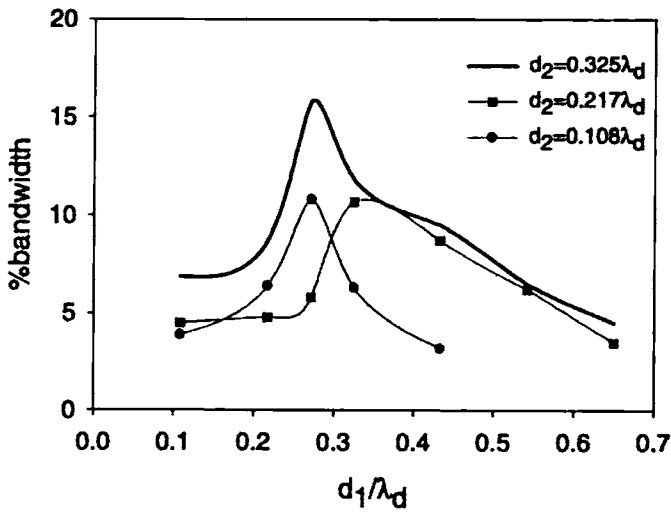


Figure 3.22 Bandwidth variations with d_1 and d_2 for the patch $L = 4\text{cm}$, $W = 2\text{cm}$, $S_1 = 1.08\lambda_D$ and $S_2 = 0.758\lambda_D$.

(c) Feed length – $1.3\lambda_d$

Feed length is further increased to $1.3\lambda_d$ and resonant frequency variations with the feed point parameters d_1 and d_2 are noted and are presented in Figure 3.23. Bandwidth variations with the change in feed position parameters are shown in Figure 3.24. Minimum resonant frequency condition is $d_2 = 0.108\lambda_d$ and $d_1 = 0.325\lambda_d$ and that for maximum bandwidth the parameters are $d_1 = 0.271\lambda_d$ and $d_2 = 0.325\lambda_d$ respectively.

(d) Feed length – $1.52\lambda_d$

Resonant frequency variations with the feed position parameters d_1 and d_2 are noted and are plotted in Figure 3.25. From the figure it observed that the resonant frequency is almost invariant with d_1 and d_2 . Bandwidth variations with the feed points are presented in Figure 3.26. Minimum resonant frequency and maximum bandwidth occurs when $d_2 = 0.108\lambda_d$, $d_1 = 0.325\lambda_d$ and $d_1 = 0.271\lambda_d$, $d_2 = 0.325\lambda_d$ respectively.

From the experimental studies, it is concluded that for all feed lengths the condition for maximum bandwidth for the patch with dimensions $L = 4\text{cm}$, $W = 2\text{cm}$ is $S_2 \approx \frac{3}{4}\lambda_d$, $d_1 = 0.271\lambda_d$, $d_2 = 0.325\lambda_d$.

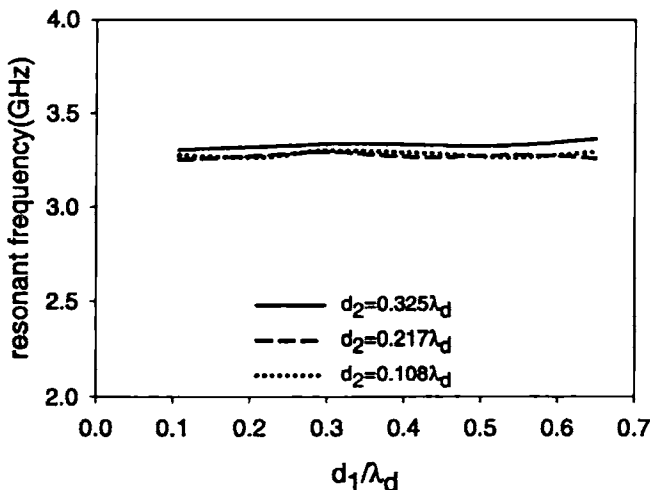


Figure 3.23 Resonant frequency variations with d_1 and d_2 for the patch $L = 4\text{cm}$, $W = 2\text{cm}$, $S_1 = 1.30\lambda_d$, $S_2 = 0.758\lambda_d$

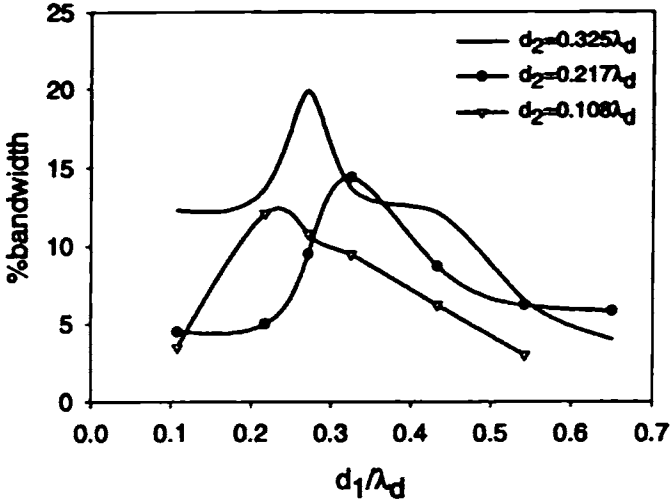


Figure 3.24 Variation of percentage bandwidth with d_1 and d_2 for the patch $L = 4\text{cm}$, $W = 2\text{cm}$, $S_1 = 1.30\lambda_d$, $S_2 = 0.758\lambda_d$

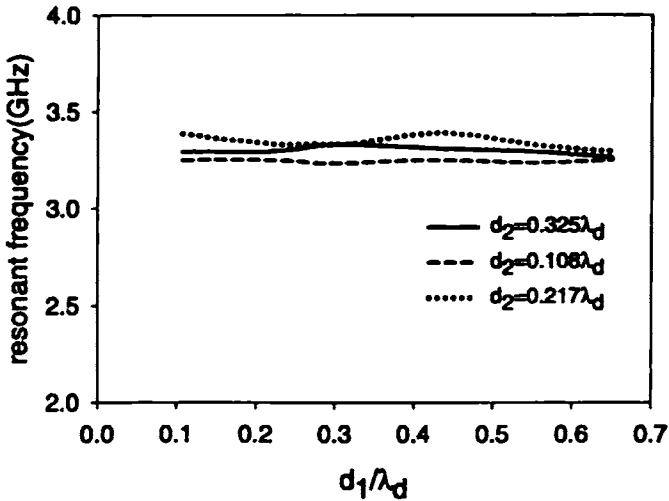


Figure 3.25 Variation of resonant frequency with d_1 and d_2 for the patch $L = 4\text{cm}$, $W = 2\text{cm}$, $S_1 = 1.52\lambda_d$ and $S_2 = 0.758\lambda_d$

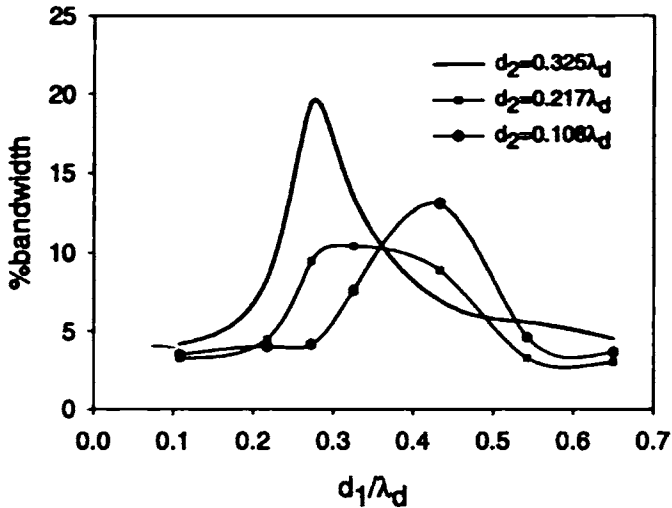


Figure 3.26 Variation of percentage bandwidth with d_1 and d_2 for the patch $L = 4\text{cm}$, $W=2\text{cm}$, $S_1=1.52\lambda_d$ and $S_2 = 0.758\lambda_d$

The Experimental observations reveal that all the patches offered maximum bandwidth of 17 to 20% when it is excited with L-strip feed, which ~ 6 to 7 times higher than that with conventional feed. The resonant frequency of the patches is found to be shifting to the lower side. This indicates that the L-strip feeding technique can increase the bandwidth of microstrip antenna considerably.

3.2.4 Effect of permittivity on bandwidth

Rectangular patch resonating at 3.3GHz and fabricated on different substrates are also investigated to observe the influence of permittivity on the characteristics of the antenna. Experimental results for selected feed lengths are discussed in the following sections.

(a) Feed length – $0.862\lambda_d$

Rectangular patches resonating at same frequencies are made on substrates with permittivity $\epsilon_r = 10.2$ with height $h = 0.065\text{cm}$ and $\epsilon_r = 2.2$ with height $h = 0.08\text{cm}$. Bandwidth variations are studied with L-strip feed excitation. The results are presented in Figure 3.27. Maximum bandwidth of 10.5% is obtained when the feed and the patch are on substrates having different permittivity, while 12.5% is obtained when both the feed and the patch are on same type of substrates.

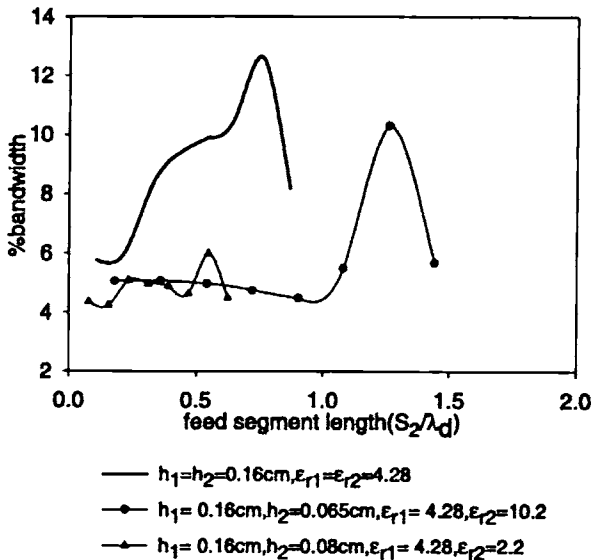


Figure 3.27 Bandwidth variations with permittivity when $S_1 = 0.862\lambda_d$

(b) Feed length – $1.08\lambda_d$

S_1 is increased to $1.08\lambda_d$ and studies are repeated to observe the variation of bandwidth with permittivity. The variation in impedance bandwidth with the dielectric constant with the increased feed length is shown in Figure 3.28. Maximum impedance bandwidth obtained when feed and patch are on substrate having different permittivity is 10.8% while 15.8% is obtained when both feed and patch are on same substrate. It is observed that when the feed and the patch are on substrates with different permittivity, there is no appreciable bandwidth increase as S_1 increases.

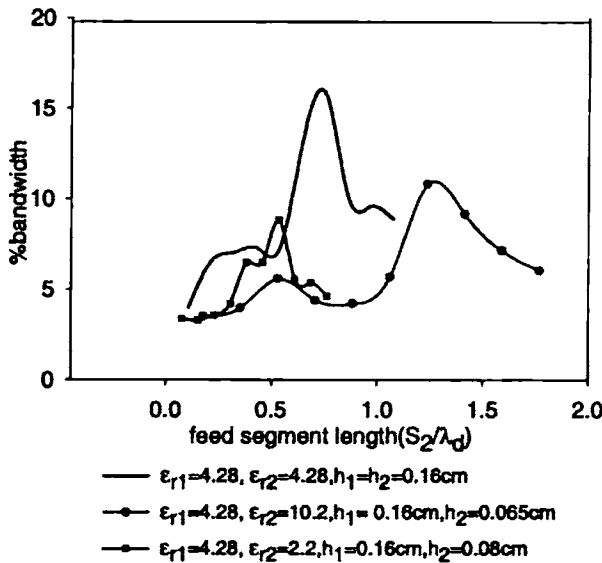


Figure 3.28 Bandwidth variations with permittivity for different S_2 when $S_1 = 1.08\lambda_d$

(c) Feed length – $1.3\lambda_d$

S_1 value is increased to $1.3\lambda_d$ and the effect of permittivity on bandwidth is noted. Results obtained are presented in Figure 3.29. Maximum bandwidth of 12% is attained when the feed and the patch are on substrates having different permittivity while 20% is obtained when the feed and the patch are on substrates having same permittivity. Here the bandwidth is increasing as S_1 is increasing.

(d) Feed length - $1.52\lambda_d$

To find the optimum bandwidth when the feed and the patch are fabricated on substrates with different permittivity, S_1 is increased further to $1.52\lambda_d$ and the observations are repeated. Figure 3.30 shows the bandwidth variations for the enhanced S_1 value. Maximum bandwidth of 10% is attained when the feed and the patch are on substrates having different permittivity and 19% is when the feed and the patch are on substrates with same permittivity.

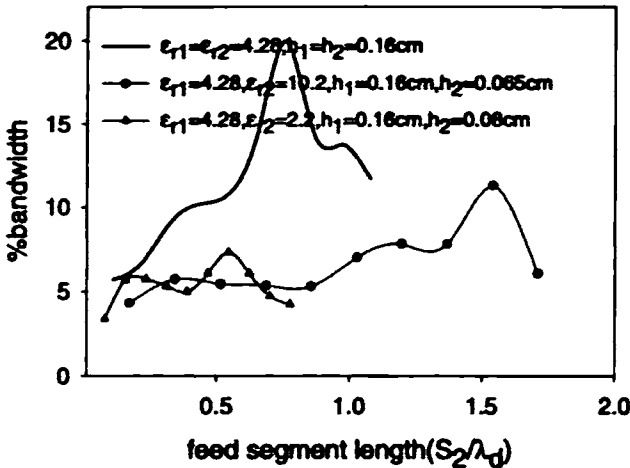


Figure 3.29 Bandwidth variations with permittivity for different S_2 with $S_1=1.3\lambda_d$

From the observations it is clear that the bandwidth improvement is only 10 to 12% when feed and patch substrates permittivities are different. But 20% bandwidth enhancement is achieved when feed and patch substrates permittivities are same. Optimum feed length for both the cases is $1.3\lambda_d$. It seems that permittivity and thickness of the substrate have significant effect on the bandwidth of the antenna.

Patches resonating at the same frequency fabricated on substrates with permittivity $\epsilon_r = 2.2$ and height $h = 0.08\text{cm}$ is excited with L-strip feed fabricated on similar substrates with the optimized feed length, then the antenna offers an

impedance bandwidth of only 3.5 to 5.5%. The variation of the bandwidth is shown in Figure 3.31. From the results it can be concluded that bandwidth is high for a given frequency when thicker substrates are used.

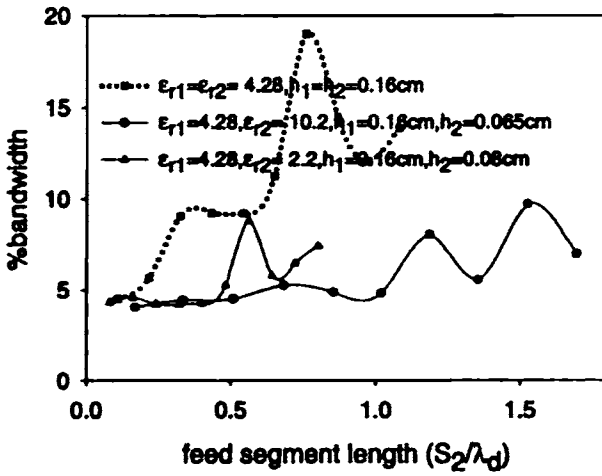


Figure 3.30 Bandwidth variations of different patches with permittivity with $S_1 = 1.52\lambda_d$

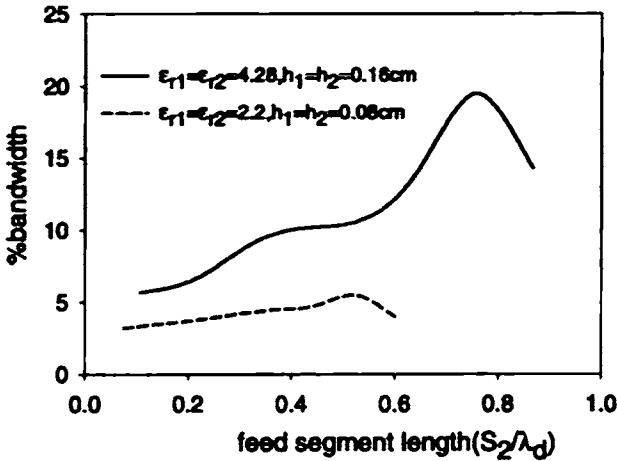


Figure 3.31 Variation of percentage bandwidth for different substrates for with the optimized feed.

3.2.5 Radiation pattern

Radiation patterns of the L-strip fed antennas configurations offering maximum bandwidth are studied in detail. Radiation characteristics such as 3dB beam width and cross-polar levels can be deduced from the radiation patterns.

(a) Microstrip antenna – 2.4GHz

The microstrip antenna with dimensions $L=3.6\text{cm}$, $W=2.6\text{cm}$ offered maximum bandwidth of 17% when $S_1 = 1\lambda_d$ and $S_2 = 0.4\lambda_d$. The co-polar and cross-polar radiation patterns of these antenna configurations in the principal planes are taken at 51 frequency points in the operating band of each antenna. The measured co-polar and cross-polar radiation patterns at the typical frequencies are shown in Figure 3.32(i). Also the radiation patterns are broad with low cross polar level -32dB. Radiation characteristics of L-strip fed antennas are given in Table 3.5.

(b) Microstrip antenna – 2.7GHz

The antenna with dimensions $L=3\text{cm}$, $W=2.4\text{cm}$ offered maximum bandwidth of 19% when $S_1 = 1.07\lambda_d$ and $S_2 = 0.717\lambda_d$. The co-polar and cross-polar radiation patterns of this particular antenna configuration in the principal planes are taken. The measured co-polar and cross-polar radiation patterns at the typical frequencies are shown in Figure 3.32(ii). Also the radiation patterns are broad with low cross polar level -34dB. Radiation characteristics of L-strip fed antennas are given in Table 3.5.

(c) Microstrip antenna – 3.2GHz

The antenna with dimensions $L \times W = 3 \times 2\text{cm}^2$ offered maximum bandwidth of 18% when $S_1 = 1.06\lambda_d$ and $S_2 = 0.746\lambda_d$. The co-polar and cross-polar radiation patterns of this optimum antenna configuration in the principal planes are taken.

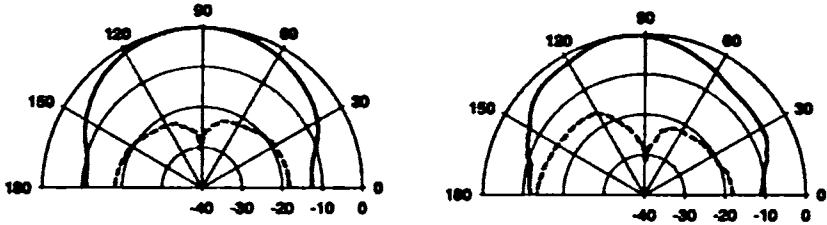
The measured co-polar and cross-polar radiation patterns at the typical frequencies are shown in Figure 3.32(iii). The radiation patterns are broad with low cross polar level of -40dB along the bore-sight direction.

(c) Microstrip antenna – 3.3GHz

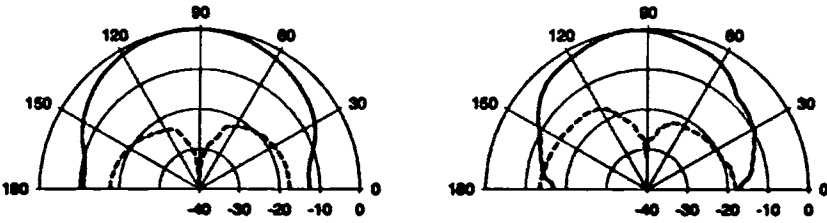
The antenna with dimensions $L = 4\text{cm}$, $W=2\text{cm}$ offered maximum bandwidth of 20% when $S_1 = 1.3\lambda_d$ and $S_2 = 0.758\lambda_d$. The measured co-polar and cross-polar radiation patterns at the typical frequencies are shown in Figure 3.32(iv). Radiation patterns are similar to that of a rectangular patch fed with simple microstrip feed. The radiation patterns are broad with low cross polar level -39dB. All the above observations confirm that the antenna is offering excellent radiation characteristics with improved bandwidth.

Table 3.5 Radiation characteristics of L-strip fed antennas at different frequencies in the operating band given in Figure 3.32

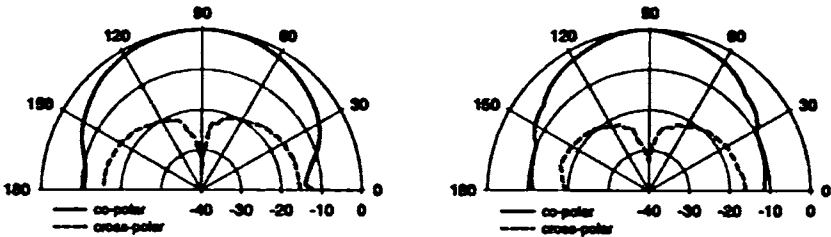
L(cm)	W(cm)	Frequency (GHz)	3-dB beam width(deg)		Cross-polar level(dB)	
			E-plane	H-plane	E-plane	H-plane
3.6	2.6	2.38	79	65	-30	-31
		2.45	79	64	-33	-31
		2.6	85	60	-33	-31
3	2.4	2.6	88	82	-29	-34
		2.73	91	82	-25	-30
		2.85	97	82	-25	-32
3	2	2.9	74	86	-40	-40
		3.247	98	76	-40	-38
		3.42	80	72	-40	-30
4	2	3.0	72	76	-32	-36
		3.33	78	70	-32	-37
		3.58	76	70	-27	-37



(a)



(b)



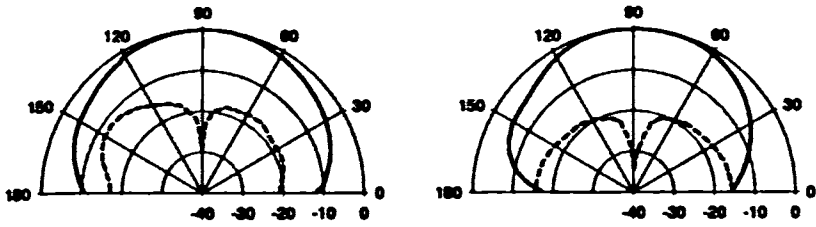
(c)

E-plane

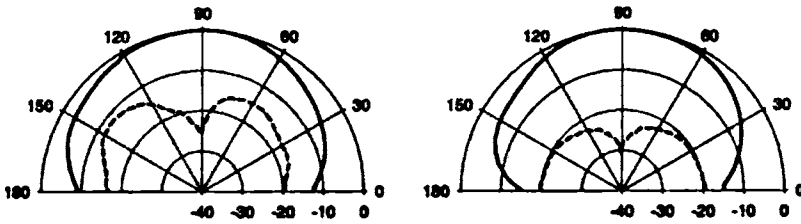
H-plane

Figure 3.32(f) Radiation patterns of the antenna with $L = 3.6\text{cm}$, $W = 2.6\text{cm}$, $S_1 = 1\lambda_d$, $S_2 = 0.4\lambda_d$, $d_1 = 0.1\lambda_d$, $d_2 = 0.2\lambda_d$ and $d_3 = 0.01\lambda_d$

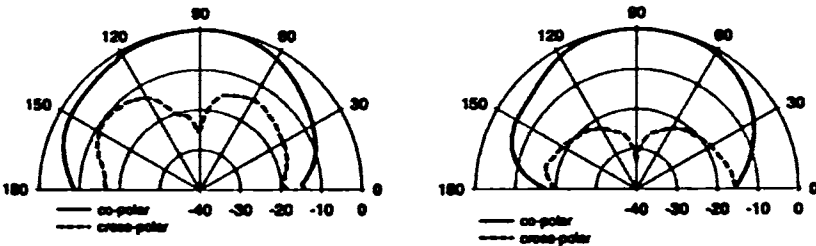
(a) 2.38 GHz (b) 2.45GHz (c) 2.6GHz



(a)



(b)



(c)

E-plane

H-plane

Figure 3.32 (ii) Radiation patterns of the antenna at different frequencies,

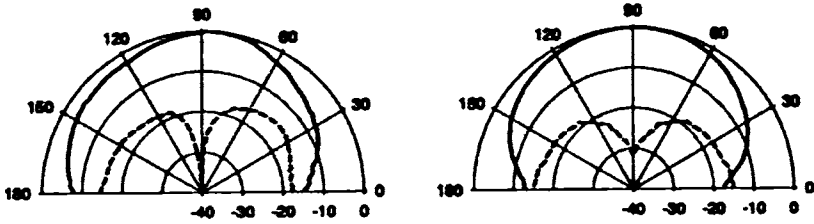
$L = 3\text{cm}$, $W = 2.4\text{cm}$, $S_1 = 1.07\lambda_d$, $S_2 = 0.717\lambda_d$, $d_1 = 0.107\lambda_d$,

$d_2 = 0.125\lambda_d$ and $d_3 = 0.322\lambda_d$.

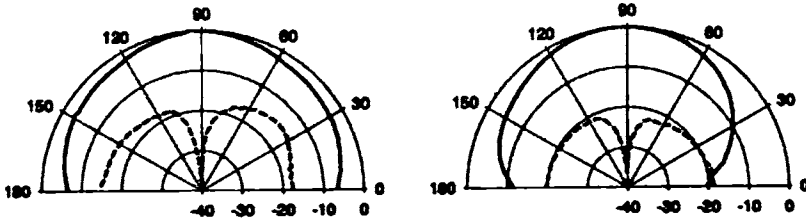
(a) 2.6 GHz

(b) 2.73GHz

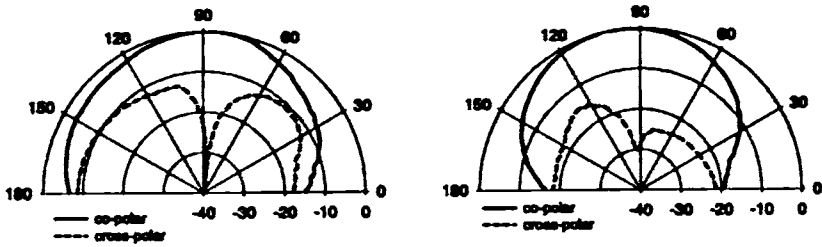
(c) 2.85GHz



(a)



(b)



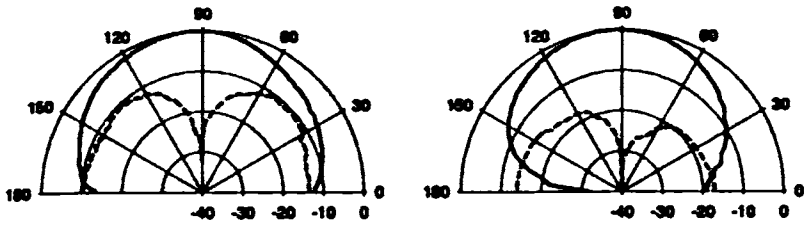
(c)

E-plane

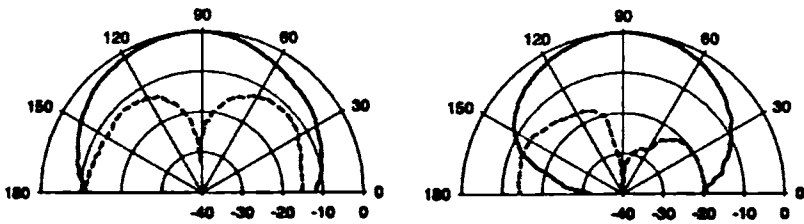
H-plane

Figure 3.32(iii) Radiation patterns of antenna at different frequencies,
 $L = 3\text{cm}$, $W = 2\text{cm}$, $S_1 = 1.06\lambda_d$, $S_2 = 0.746\lambda_d$, $d_1 = 0.148\lambda_d$, $d_2 = 0.254\lambda_d$,
 $d_3 = 0.336\lambda_d$.

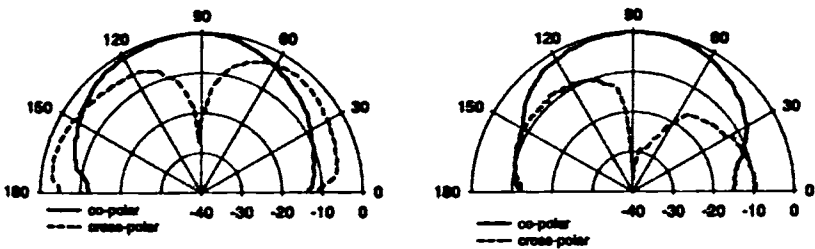
(a) 2.9GHz (b) 3.247GHz (c) 3.42GHz



(a)



(b)



(c)

E-plane

H-plane

**Figure 3.32 (iv) Radiation patterns of the antenna at different frequencies, $L=4\text{cm}$, $W=2\text{cm}$ $S_1=1.30\lambda_d$, $S_2=0.758\lambda_d$, $d_1=0.271\lambda_d$, $d_2=0.325\lambda_d$ and $d_3=0.217\lambda_d$
 (a) 3 GHz (b) 3.33GHz (c) 3.58GHz**

3.2.6 Gain

Gain of the antenna for different configurations is studied in detail. Gain transfer method is used to find the gain of the antenna. Variations of the antenna gain for different feed lengths are presented in Figure 3.33. The antenna has a maximum gain of 8.2dBi when $S_1 = 1.08\lambda_d$, $S_2 = 0.758\lambda_d$ and most of the cases the gain is greater than 5dBi. In certain cases the gain of the present antenna is greater than conventional rectangular antenna. This may be due to the radiation from the L-strip feed. If the radiation from the feed and the antenna are in phase, constructive interference will take place and hence increase in gain of the antenna.

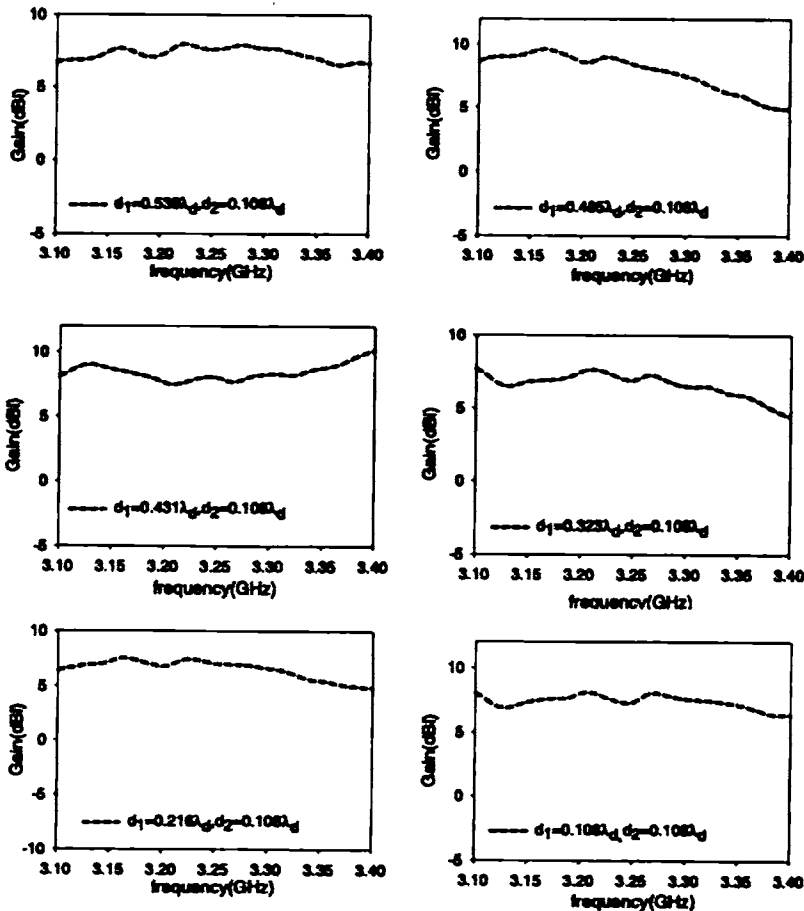


Figure 3.33 (D) S₁ plots of the antenna for different lengths of d₁ and d₂

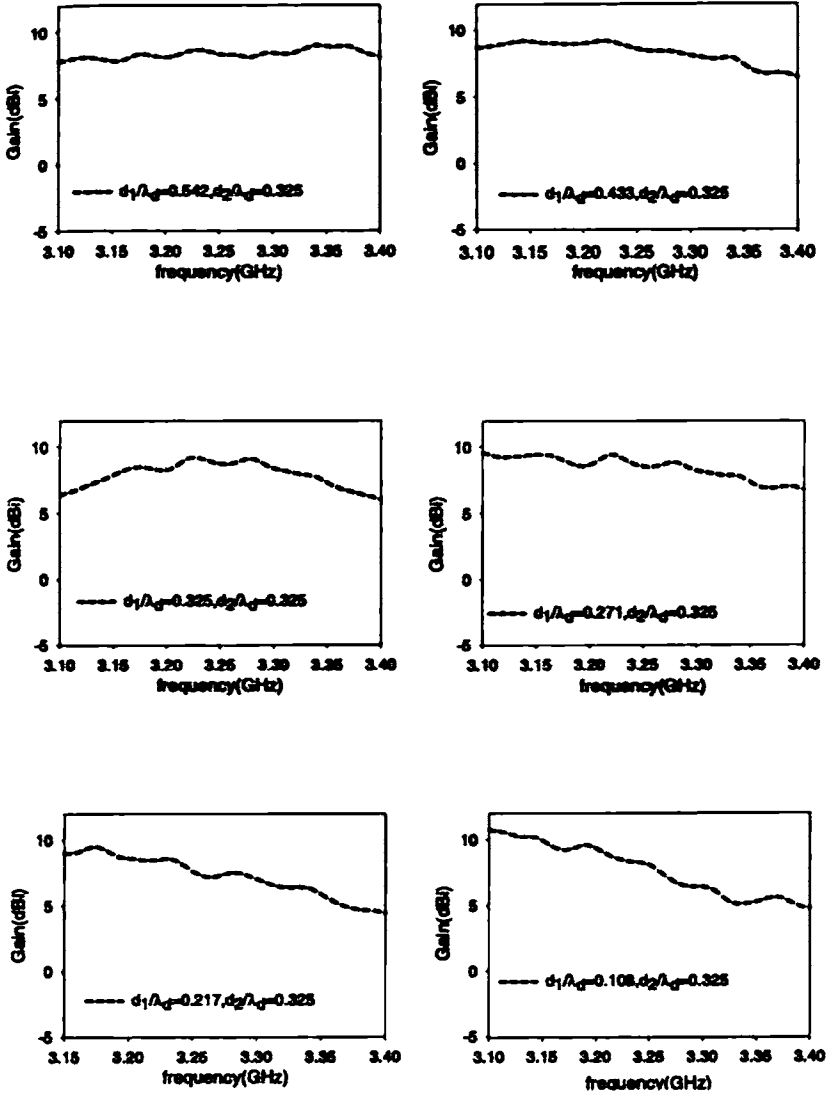


Figure 3.33(ii) S_{21} plots of the antenna for different lengths of d_1 and d_2 , $L = 4\text{cm}$, $W = 2\text{cm}$, $S_1 = 1.08\lambda_d$ and $S_2 = 0.758\lambda_d$

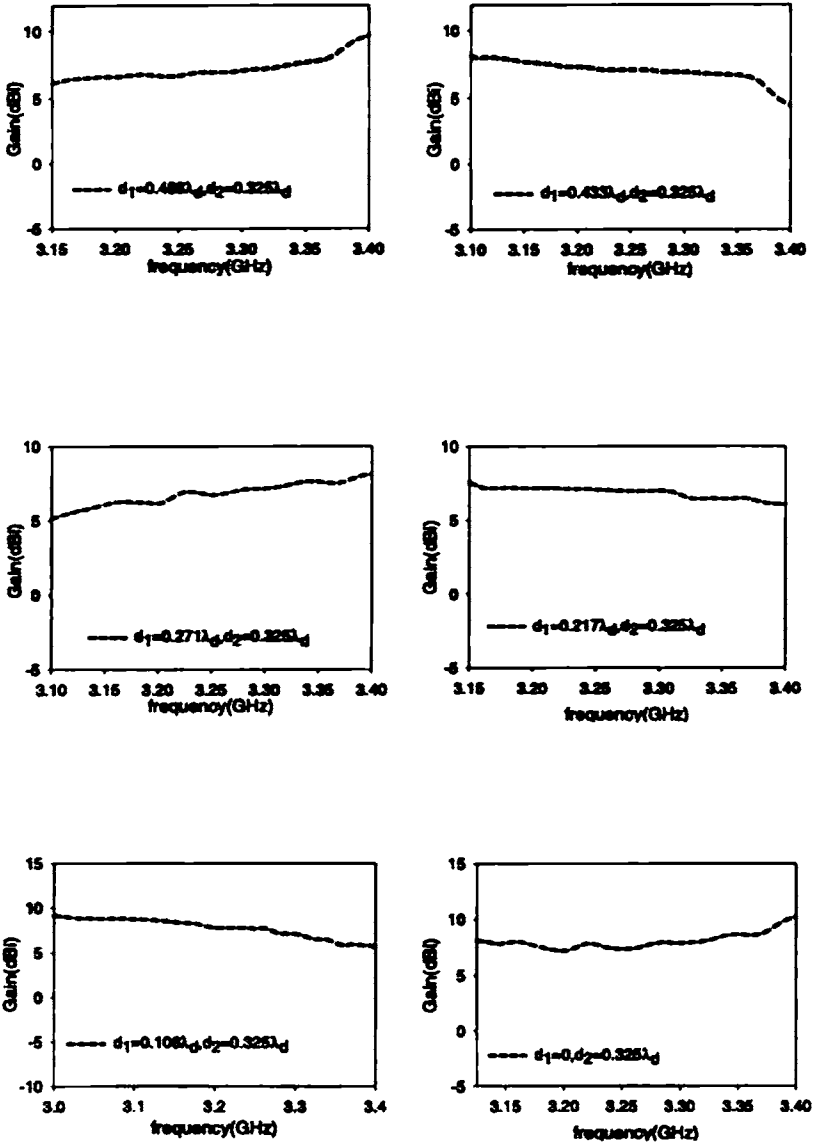


Figure 3.33(iii) S_{21} plots of the antenna for different d_1 and d_2 ,
 $L = 4\text{cm}$, $W = 2\text{cm}$, $S_1 = 1.3\lambda_d$ and $S_2 = 0.758\lambda_d$

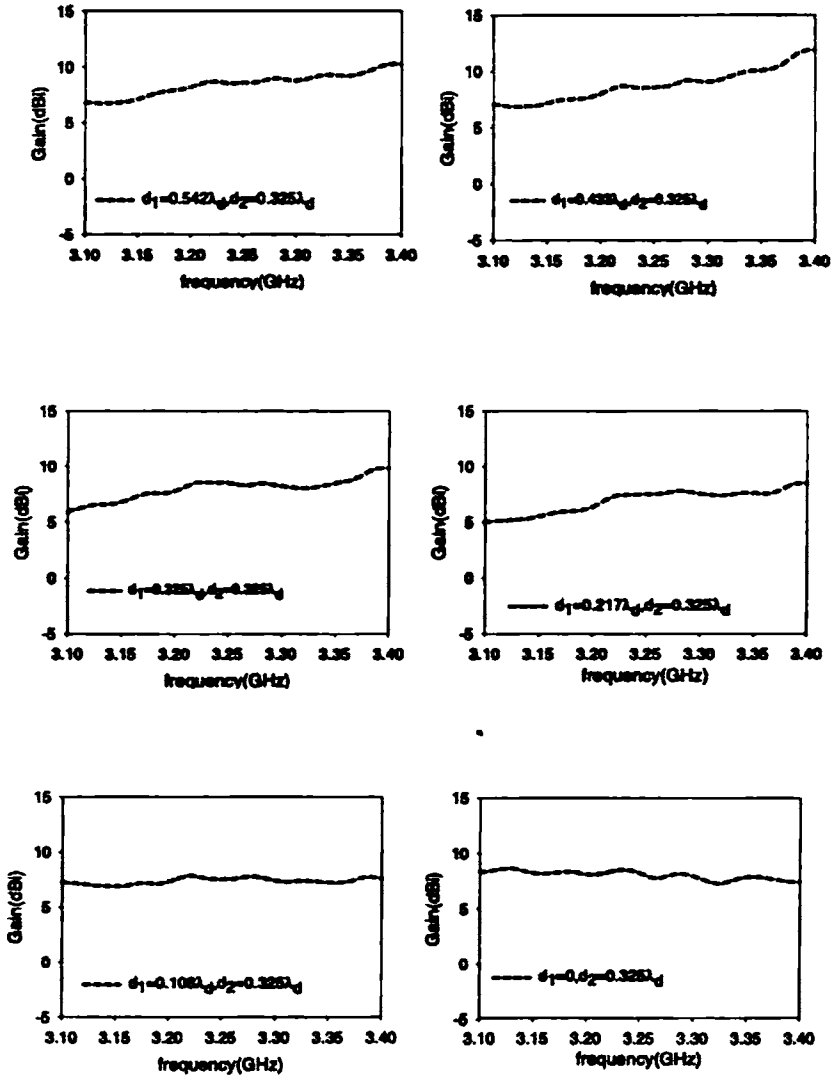


Figure 3.33(iv) S_{21} plots of the antenna for different d_1 and d_2
 $L = 4\text{cm}$ $W = 2\text{cm}$, $S_1 = 1.52\lambda_d$ and $S_2 = 0.758\lambda_d$

3.2.7 Simulated Results

Selected L-strip fed antenna configurations which offered maximum bandwidth are simulated using IE3D software. Simulated reflection and radiation characteristics are discussed in the following sections.

3.2.7.1 Return loss and bandwidth

(a) Microstrip antenna – 3.3GHz

Experimentally, microstrip antenna with dimension $4 \times 2 \text{cm}^2$ offered a maximum impedance bandwidth of 20% when S_1 and S_2 are $1.3\lambda_d$ and $0.758\lambda_d$ respectively. This particular configuration is simulated and the results are verified with experimental ones. Return loss variations for different S_2 are shown in Figure 3.34, and return loss variation at the maximum bandwidth position is presented in Figure 3.35. An impedance bandwidth of 14.5% in the operating band 2.97GHz-3.45GHz with a centre frequency of 3.3GHz is obtained by simulation which is close agreement with the experimental results. Comparison of simulated and experimental resonant frequencies is given in Table 3.6. Worst case error between the simulated and experimental frequencies is less than 2%. The main cause of error may be due to the uncertainty in the permittivity values of the substrates used for simulation or the slight anisotropic character of the substrate.

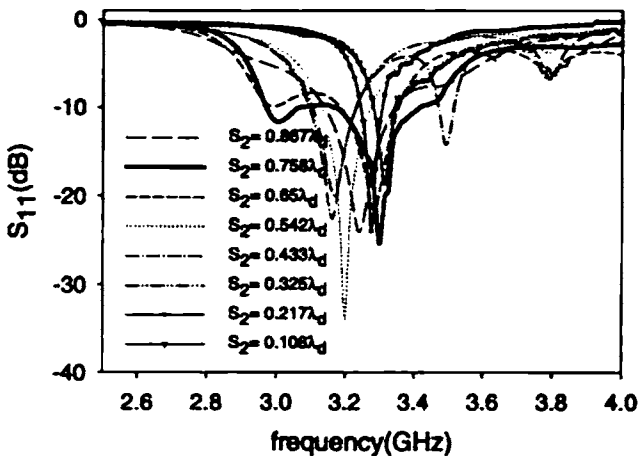


Figure 3.34 Simulated return loss variations of the antenna with $S_1 = 1.3\lambda_d$ and for different S_2 with $L = 4 \text{cm}$, $W = 2 \text{cm}$

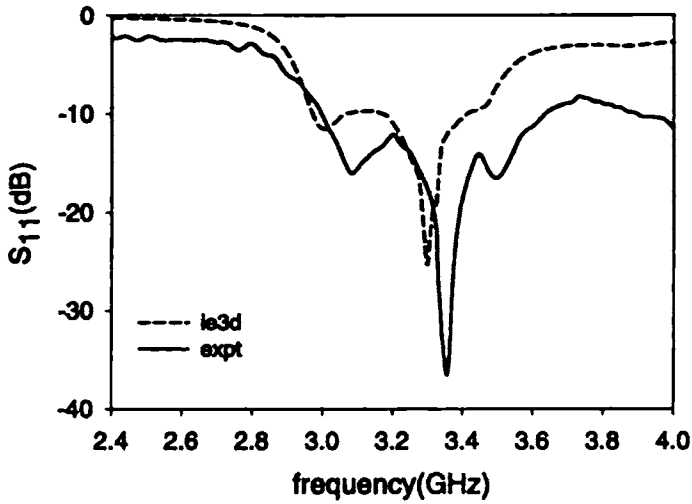


Figure 3.35 Experimental and simulated S_{11} variation of the patch $L = 4\text{cm}$, $W = 2\text{cm}$, $S_1 = 1.30\lambda_d$, $S_2 = 0.758\lambda_d$, $d_1 = 0.271\lambda_d$, $d_2 = 0.325\lambda_d$ and $d_3 = 0.217\lambda_d$

Table 3.6 Comparison of simulated and experimental resonant frequencies of the patch $L = 4\text{cm}$, $W = 2\text{cm}$, $S_1 = 1.3\lambda_d$

Patch parameters				Feed segment length (S_2/λ_d)	Simulated Resonant frequency (GHz)	Experimental resonant frequency (GHz)
L(cm)	W(cm)	h(cm)	ϵ_r			
4.0	2.0	0.16	4.28	0.108	3.25	3.235
				0.217	3.225	3.25
				0.325	3.212	3.235
				0.433	3.175	3.215
				0.542	3.20	3.231
				0.650	3.30	3.319
				0.758	3.30	3.331
				0.867	3.288	3.32
				0.975	3.275	3.34
				1.08	3.313	3.34



G9049

(b) Microstrip antenna – 3.2GHz

Maximum impedance bandwidth of 18% is obtained for L-strip fed microstrip antenna with dimension $3 \times 2 \text{cm}^2$ when S_1 and S_2 are $1.06\lambda_d$ and $0.746\lambda_d$ respectively. This particular configuration is simulated and the results are verified with experimental ones. Return loss variations with $S_1 = 1.06\lambda_d$ and for different S_2 are shown in Figure 3.36. The variations of impedance bandwidth for different feed segment lengths are studied. From the return loss variations, it is found that the maximum bandwidth for this configuration is obtained when the feed segment length is $0.746\lambda_d$ with good resonance curve.

Return loss curve of the antenna at the optimum position is shown in Figure 3.37. An impedance bandwidth of 12% in the operating band 3.04GHz-3.43GHz with a centre frequency of 3.26GHz is obtained by simulation. The resonance curves are also in good matching.

Comparison of simulated and experimental resonant frequencies is given in Table 3.7. Worst case error between the simulated and experimental frequencies is less than 2%. The simulated results are in good agreement with the experimental results.

Table 3.7 Comparison of simulated and experimental resonant frequencies of the patch $L=3\text{cm}$ and $W=2\text{cm}$, $S_1 = 1.06\lambda_d$

Patch parameters				Feed segment length (S_2/λ_d)	Simulated Resonant frequency (GHz)	Experimental resonant frequency (GHz)
L(cm)	W(cm)	h(cm)	ϵ_r			
3.0	2.0	0.16	4.28	0.107	3.235	3.205
				0.213	3.225	3.205
				0.32	3.235	3.265
				0.427	3.237	3.205
				0.533	3.188	3.22
				0.639	3.25	3.205
				0.746	3.26	3.235
				0.852	3.28	3.25

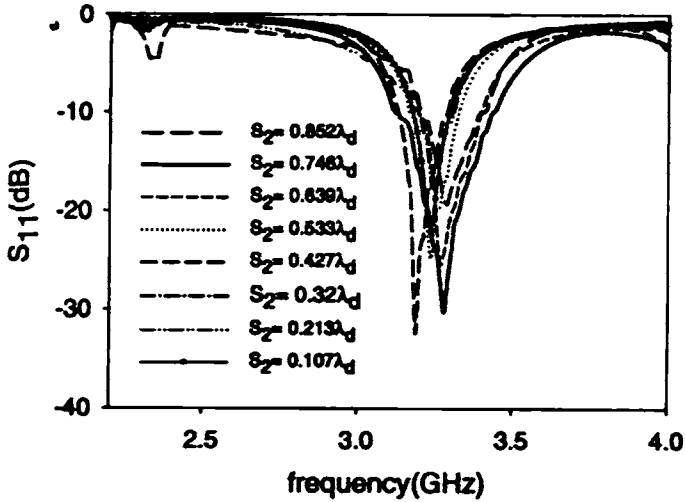


Figure 3.36 Simulated Return loss variations with frequency for different feed segment lengths for the patch $L = 3\text{cm}$, $W = 2\text{cm}$, $S_1 = 1.06\lambda_d$ and for different S_2

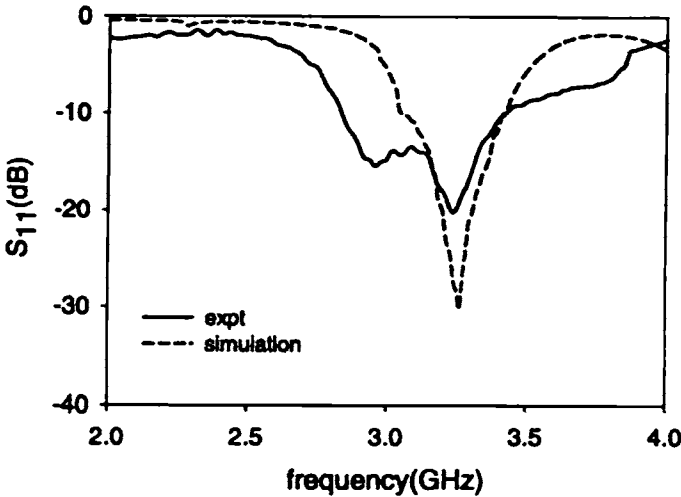


Figure 3.37 Return loss of the L-strip fed antenna at the optimum position with $L = 3\text{cm}$, $W = 2\text{cm}$, $S_1 = 1.06\lambda_d$, $S_2 = 0.746\lambda_d$, $d_1 = 0.148 \lambda_d$, $d_2 = 0.254\lambda_d$, $d_3 = 0.336\lambda_d$

(c) Microstrip antenna – 2.7GHz

Experimentally the patch $3 \times 2.4 \text{ cm}^2$ offered a maximum bandwidth of 19% when $S_1 = 1.074\lambda_d$ and $S_2 = 0.717\lambda_d$. These results are verified using the Zeland IE3D software. Simulated return loss variation at the maximum bandwidth positions is shown in Figures 3.38. An impedance bandwidth of 13.14% in the operating band 2.514GHz-2.87GHz with a centre frequency of 2.7GHz is obtained by simulation. Comparison of simulated and experimental resonant frequency variations for different S_2 is given in Table 3.8. Maximum error between simulated and experimental results is 2%.

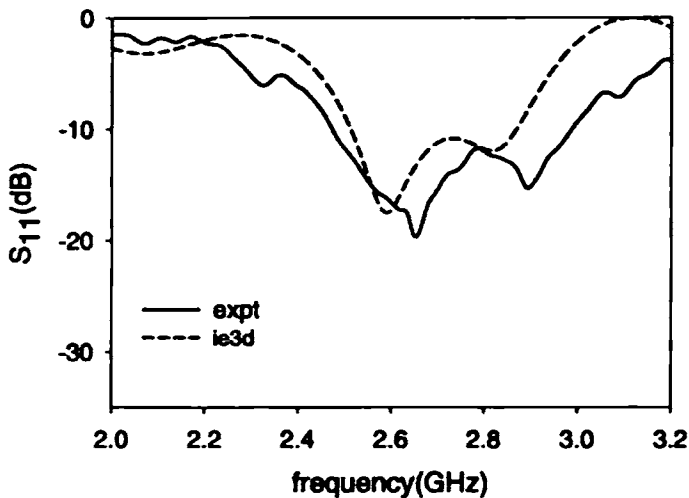


Figure 3.38 Return loss variation of the patch at the optimum bandwidth position $L = 3 \text{ cm}$, $W = 2.4 \text{ cm}$, $S_1 = 1.07\lambda_d$, $S_2 = 0.717\lambda_d$, $d_1 = 0.107\lambda_d$, $d_2 = 0.125\lambda_d$ and $d_3 = 0.322\lambda_d$

Table 3.8 Comparison of simulated and experimental resonant frequencies of the patch $L = 3\text{cm}$, $W = 2.4\text{cm}$ and $S_1 = 1.07\lambda_d$

Patch parameters				Feed segment length (S_2/λ_d)	Simulated Resonant frequency (GHz)	Experimental resonant frequency (GHz)
L(cm)	W(cm)	h(cm)	ϵ_r			
3.0	2.4	0.16	4.28	0.089	2.813	2.83
				0.179	2.788	2.815
				0.268	2.785	2.83
				0.358	2.763	2.80
				0.447	2.80	2.77
				0.537	2.775	2.755
				0.626	2.813	2.80
				0.717	2.70	2.733
				0.805	2.737	2.755
				0.895	2.788	2.71

3.2.7.2 Simulated radiation patterns

Simulated and experimental radiation patterns of the above mentioned patches at the maximum bandwidth position at different frequencies in the operating band are shown in Figure 3.39. Simulated radiation characteristics are given in Table 3.9. From the table it is clear that the radiation patterns are broad with cross polar level of -42 dB.

Table 3.9 Simulated radiation characteristics of L-strip fed antennas at different frequencies in the operating band

L(cm)	W(cm)	Frequency (GHz)	3-dB beam width(deg)		Cross-polar level(dB)	
			E-plane	H-plane	E-plane	H-plane
4	2	3.0	107	74	-41	-41
		3.334	105	73	-41	-43
		3.425	115	76	-39	-42
3	2	2.9	74	86	-40	-40
		3.247	98	76	-40	-38
		3.42	80	72	-40	-30
3	2.4	2.6	125	100	-30	-35
		2.723	135	90	-36	-35
		2.8	125	90	-35	-36

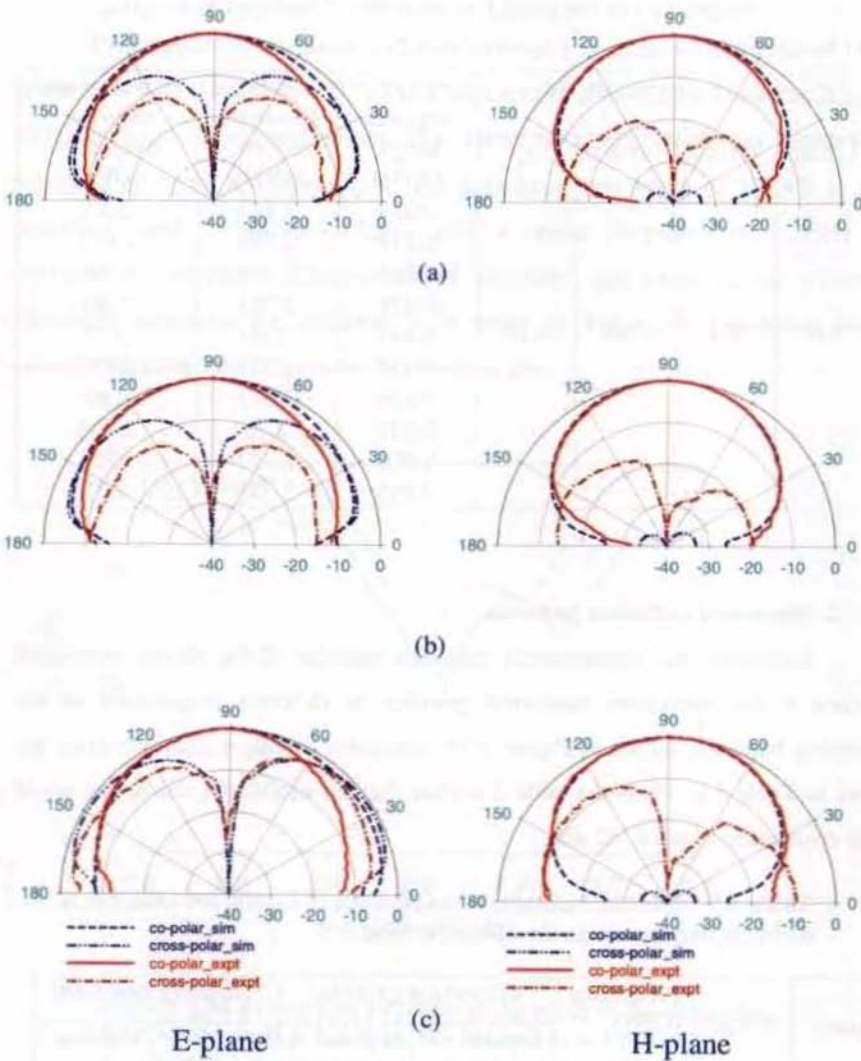


Figure 3.39(i) Simulated and experimental radiation patterns of the antenna at different frequencies

$L = 4\text{cm}$, $W = 2\text{cm}$, $S_1 = 1.30\lambda_d$, $S_2 = 0.758\lambda_d$, $d_1 = 0.271\lambda_d$, $d_2 = 0.325\lambda_d$ and $d_3 = 0.217\lambda_d$

(a) 3.0GHz

(b) 3.334GHz

(c) 3.425GHz

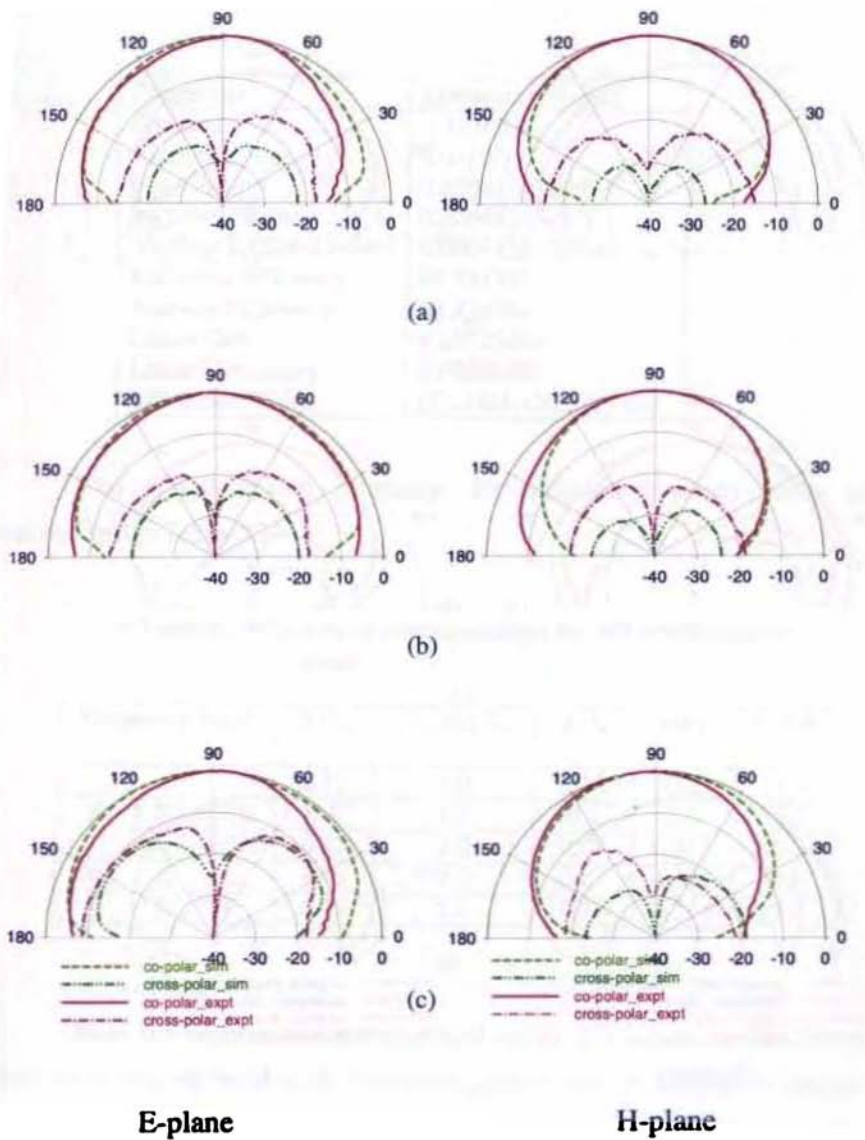
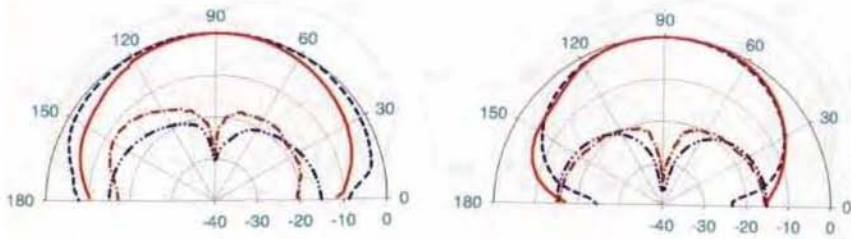
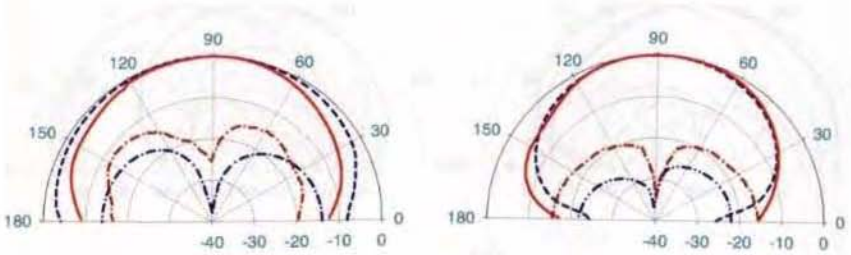


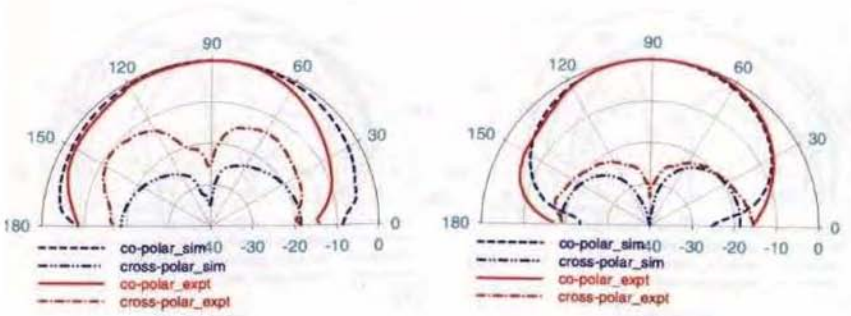
Figure 3.39(ii) Simulated and experimental radiation patterns of the antenna at different frequencies in the operating band
 $L = 3\text{cm}$, $W = 2\text{cm}$, $S_1 = 1.06\lambda_d$, $S_2 = 0.746\lambda_d$, $d_1 = 0.148\lambda_d$, $d_2 = 0.254\lambda_d$, $d_3 = 0.336\lambda_d$
 (a) 2.9 GHz (b) 3.288GHz (c) 3.4 GHz



(a)



(b)



E-plane

(c)

H-plane

Figure3.39 (iii) Simulated and experimental radiation patterns of the antenna at the maximum bandwidth position.

$L = 3\text{cm}$, $W = 2.4\text{cm}$, $S_1 = 1.07\lambda_d$, $S_2 = 0.717\lambda_d$, $d_1 = 0.107\lambda_d$, $d_2 = 0.125\lambda_d$ and $d_3 = 0.322\lambda_d$

(a) 2.6GHz

(b) 2.723GHz

(c) 2.85GHz

Properties of the L-strip fed antenna with $L = 4\text{cm}$, $W = 2\text{cm}$, $S_1 = 0.862\lambda_d$ and $S_2 = 0.754\lambda_d$ at the resonant frequency obtained by simulation are shown below.

Properties	Frequency (GHz)
Frequency	3.33 (GHz)
Incident Power	0.01(W)
Input Power	0.009431357(W)
Radiated Power	0.00648245(W)
Average Radiated Power	0.000515857(W/s)
Radiation Efficiency	68.7313%
Antenna Efficiency	64.8245%
Linear Gain	4.15825dBi
Linear Directivity	6.04086dBi
3dB Beam Width	(72.3428,130.771) deg

The optimized feed parameters for different frequency bands are summarized in Table. 3.10

Table 3.10 Optimized feed parameters for different frequency bands

Frequency Band	S_2/λ_d	$(S_1+S_2)/\lambda_d$	d_1/λ_d	d_2/λ_d	% BW	
L	0.25	1.0	0.16	0.2	11.0	
S	2-2.6GHz	0.5	1.5	0.1	0.2	17.0
	2.7-4GHz	0.75	2.0	0.27	0.325	20.0
C	0.75	2.0	0.27	0.325	19.0	
X	0.75	2.0	0.27	0.325	20.0	

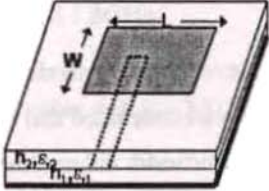
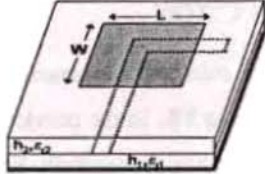
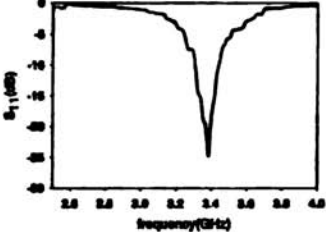
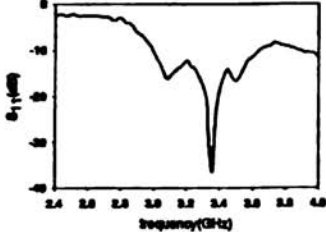
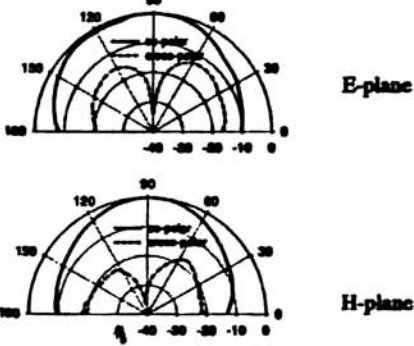
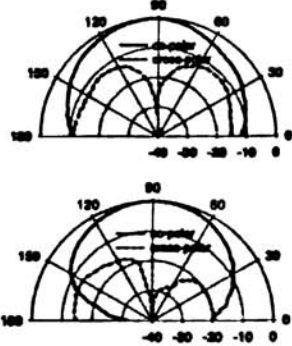
From the experimental and simulated results it is concluded that L-strip feed can effectively be used for bandwidth enhancement of rectangular patches. Bandwidth enhancement is achieved for all the patches used for study. Bandwidth enhancement is achieved with slight improvement in gain and the radiation coverage of L-strip fed antennas is similar to that of conventionally fed microstrip patch antennas. The present feeding method can effectively be used for

L, S, C and X band frequencies. Resonant frequency of the patch has a lower shift when it is excited with L-strip feed.

Permittivity and height of the substrates used for fabricating the patch and feed is also having influence on the bandwidth of the L-strip fed antenna. If they are on substrates with different permittivity, bandwidth enhancement is limited to 10 -12%.

Comparison of the characteristics of the L-strip fed antenna of patch dimensions $4 \times 2 \text{cm}^2$ with a similar patch fed with simple microstrip feed is given in Table 3.11.

Table 3.11 Comparison of L-strip fed antenna with simple microstrip line fed antenna

<p style="text-align: center;">Simple Microstrip feed</p> <p>(a) Geometry</p> 	<p style="text-align: center;">L-strip feed</p> 
<p>(b) Return loss</p>  <p style="text-align: center;">Resonant frequency 3.4 GHz Bandwidth 3.9%</p>	<p>(b) Return loss</p>  <p style="text-align: center;">Resonant frequency 3.33GHz Bandwidth 20%</p>
<p>(c) Radiation pattern</p>  <p style="text-align: center;">HPBW E-plane 92° H-plane 62°</p>	<p>(c) Radiation pattern</p>  <p style="text-align: center;">HPBW E-plane 78° H-plane 70°</p>
<p>(d) Gain 7.07dB</p>	<p>Gain 8.2dBi</p>
<p>(e) Linear polarization Cross - polar level -6dB</p>	<p>Linear polarization Cross - polar level -37dB</p>
<p>(f) Area at 2.4GHz - 27.5cm²</p>	<p>Area at 2.4GHz - 25.5cm²</p>

SECTION II

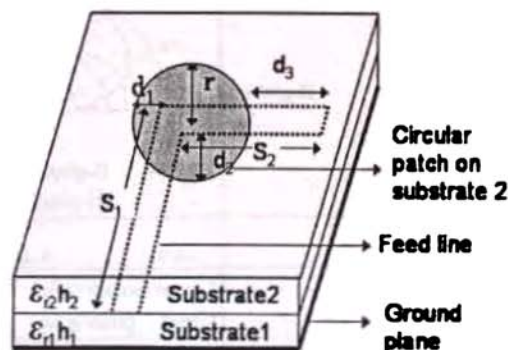
L-STRIP FED CIRCULAR MICROSTRIP ANTENNA

3.1 INTRODUCTION

Circular microstrip antennas excited using conventional methods have a bandwidth of ~2 to 3%. In the previous sections it has been concluded that L-strip feeding technique has successfully been used for the bandwidth enhancement of rectangular microstrip patches. In this section, the results of L-strip feeding applied to circular microstrip patches are discussed. By using L-strip feeding techniques circular microstrip patches gave a bandwidth of ~17%, which is approximately six times higher than that obtained by using conventional methods. Experimental studies conducted on different circular patches are described in detail in the following sections.

3.1.1 Antenna Geometry

Geometry of the L-strip fed circular microstrip antenna is shown in Figure 3.1. The feed parameters that affect the characteristics of the antenna are S_1 and S_2 , the feed length and feed segment length respectively. Feed is fabricated on a substrate with permittivity 4.28 and height 0.16 cm. Circular microstrip patches are fabricated on another substrate having the same electrical characteristics.



3.2 Experimental Observations

Resonant frequency and bandwidth variations with feed length S_1 and feed segment length S_2 are studied in detail for circular patches resonating at 3.5GHz, 2.4 GHz and 1.8GHz.

3.2.1 Circular patch – 3.5GHz

When the circular patch with radius $r = 1.22$, resonating at 3.5 GHz is electromagnetically coupled with a simple microstrip line, its frequency is shifting to 3.37GHz giving an impedance bandwidth of 3.7%. The same patch is excited with L-strip feed, the resonant frequency have a further shift to the lower side with an increased bandwidth. Experimental variations of bandwidth and resonant frequency with feed segment length for different feed lengths of the circular patch with radius $r = 1.22$ cm is discussed in the following sections.

To study the effect of L-strip feed parameters on antenna characteristics, feed length (S_1) is varied from $1\lambda_d$ to $2\lambda_d$ and the feed segment length (S_2) from $0.1\lambda_d$ to $1\lambda_d$. For each combination of S_1 and S_2 return loss and bandwidth variations are measured.

Figure 3.2 (a) shows the S_{11} variations of the L-strip fed circular patch with radius 1.22 cm when $S_1 = 1.05\lambda_d$ for different values of S_2 . This feed length configuration of L-strip offers a bandwidth of 16.66% when $S_2 = 0.732\lambda_d$.

S_1 is increased to $1.25\lambda_d$ and the return loss variations of the antenna are noted. Figure 3.2(b) shows the return loss variations for different S_2 . Maximum bandwidth is achieved when $S_2 = 0.728\lambda_d$.

Figure 3.2(c) and (d) shows the return loss variations with $S_1 = 1.45\lambda_d$ and $1.65\lambda_d$ respectively. Here also maximum bandwidth is achieved when $S_2 = 0.725\lambda_d$. Table 3.1 gives the resonant frequency and bandwidth variations with feed parameters. From the Table it is observed that maximum bandwidth is achieved when the $S_2 = \frac{3}{4}\lambda_d$ for the patch with radius $r = 1.22$ cm. The feed parameters for optimum bandwidth are $S_1/\lambda_d = 1.05$ and $S_2/\lambda_d = 0.732$, $d_1/\lambda_d =$

0.01, $d_2/\lambda_d = 0.251$, $d_3/\lambda_d = 0.209$. The bandwidth variations with S_2 for different S_1 are shown in Figure 3.3. Figure 3.4 gives consolidation of the return loss curves obtained for S_2 offering maximum bandwidth, for different S_1 .

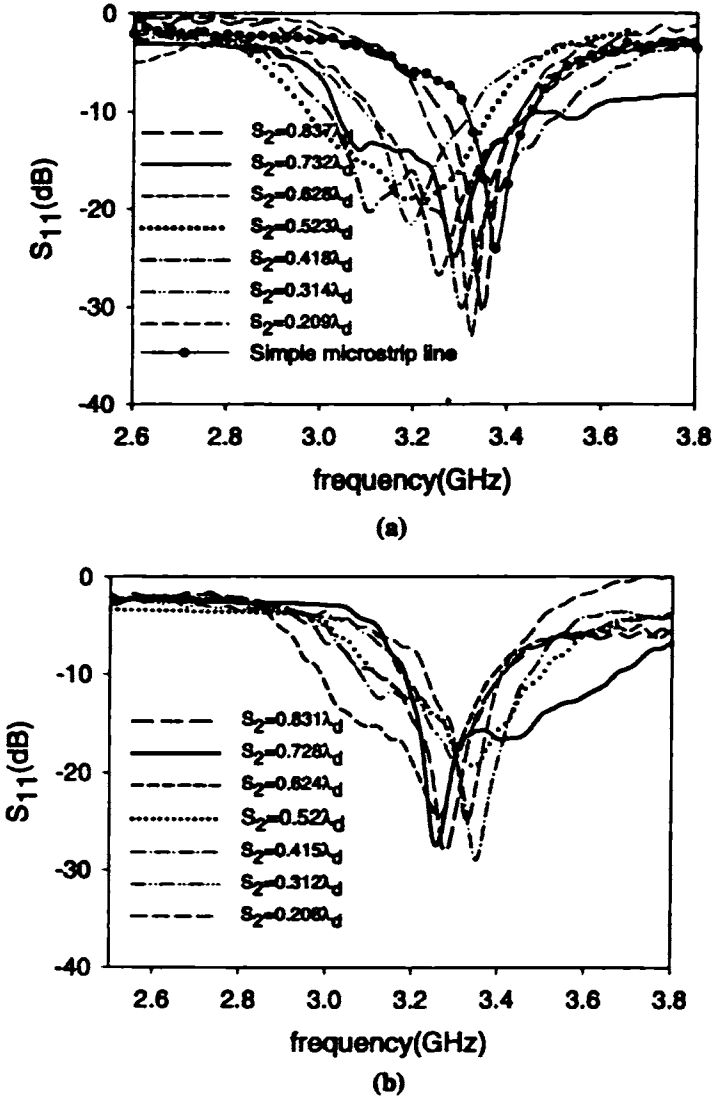
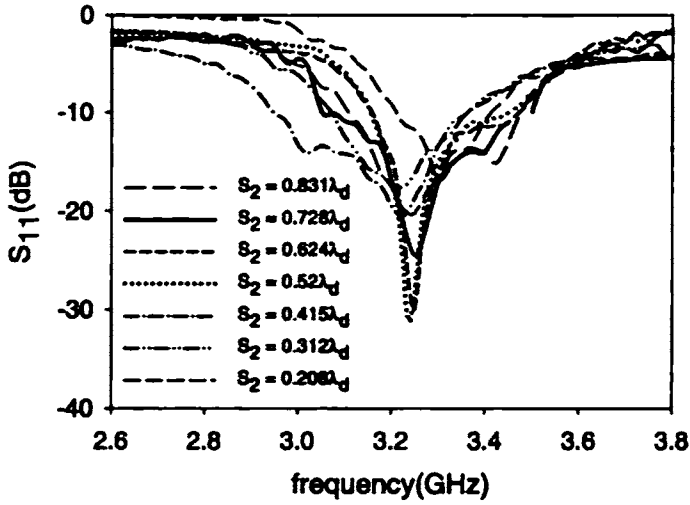
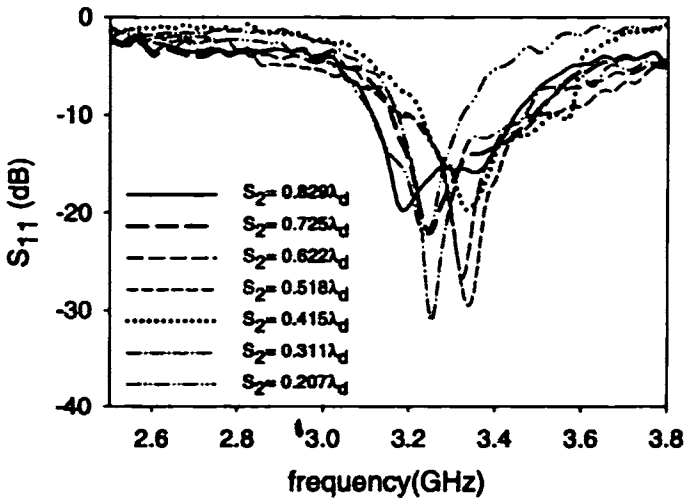


Figure 3.2 Return loss variations with frequency of the circular patch $r = 1.22$ cm, for different S_2
 (a) $S_1 = 1.05\lambda_d$
 (b) $S_1 = 1.25\lambda_d$



(c)



(d)

Figure 3.2 Return loss variations of the L-strip fed antenna with $r = 1.22$ cm, for different S_2

(c) $S_1 = 1.45\lambda_d$

(d) $S_1 = 1.65\lambda_d$

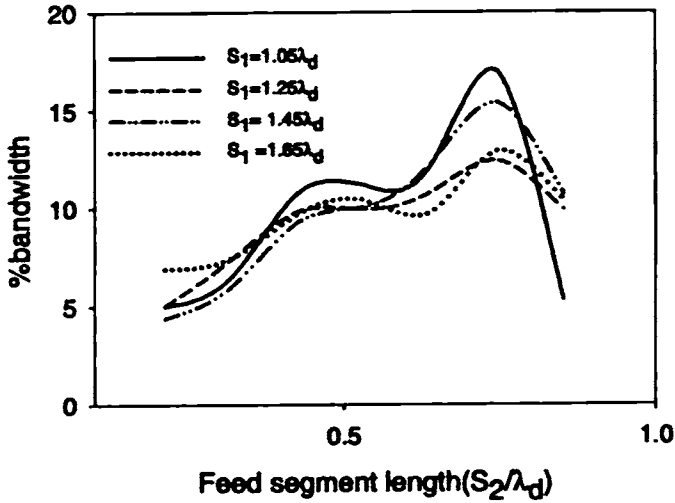


Figure 3.3 Bandwidth variations with feed segment length of L-strip fed circular antenna for different feed lengths

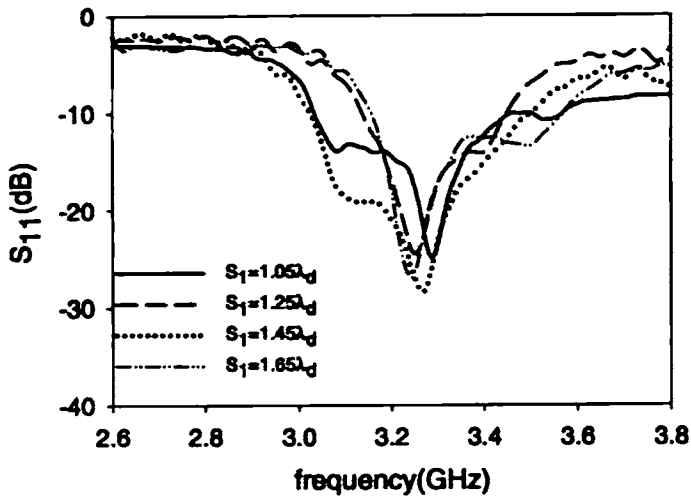


Figure 3.4 Return loss variations with frequency of the antenna for different feed lengths at the maximum bandwidth positions for the patch with $r = 1.22$ cm

Table 3.1 Resonant frequency and bandwidth variations with S_1 and S_2 for patch with radius 1.22cm, $\epsilon_{r1} = \epsilon_{r2} = 4.28$, $h_1 = h_2 = 0.16$ cm.

Feed length (S_1/λ_d)	Feed segment length (S_2/λ_d)	Resonant frequency (GHz)	% bandwidth
1.05	0.209	3.34	5.00
	0.314	3.20	6.50
	0.418	3.20	12.97
	0.523	3.24	10.01
	0.628	3.20	11.00
	0.732	3.28	16.66
	0.837	3.20	5.31
1.25	0.208	3.30	5.02
	0.312	3.20	7.40
	0.415	3.22	9.84
	0.520	3.24	9.73
	0.624	3.25	10.8
	0.728	3.26	12.4
	0.831	3.25	9.90
1.45	0.208	3.32	4.39
	0.312	3.30	6.00
	0.415	3.38	9.31
	0.520	3.38	9.08
	0.624	3.24	12.25
	0.728	3.26	15.39
	0.831	3.28	10.69
1.65	0.207	3.29	6.9
	0.311	3.24	7.46
	0.415	3.36	9.7
	0.518	3.38	10.4
	0.622	3.33	9.77
	0.725	3.25	11.21
	0.829	3.23	10.40

Radiation patterns of the L-strip fed circular patch with radius 1.22cm at different frequencies in the operating band are measured. The patterns are broad with cross polar level better than -30dB in both the principal planes. Figure 3.5 shows the measured radiation patterns.

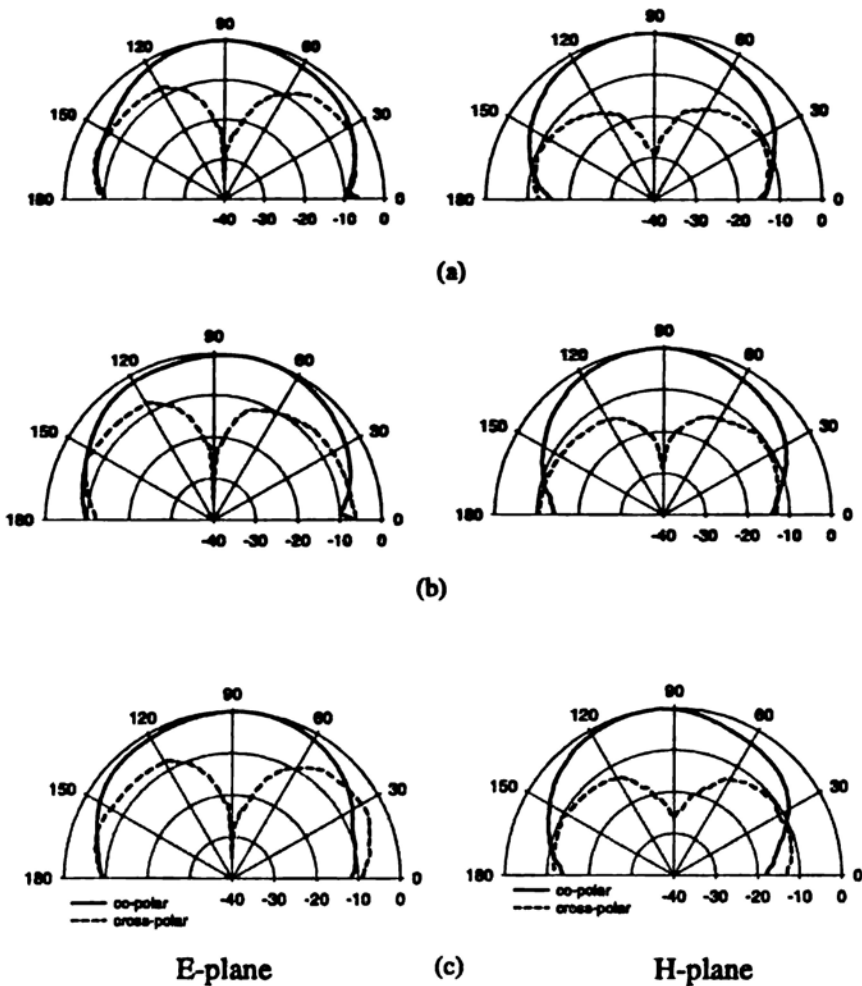


Figure 3.5 Radiation patterns of the antenna at different frequencies in the operating band. $r = 1.22$ cm, $S_1 = 1.05\lambda_d$, $S_2 = 0.732\lambda_d$, $d_1 = 0.01\lambda_d$, $d_2 = 0.251\lambda_d$, $d_3 = 0.209\lambda_d$

(a) 3GHz, (b) 3.28GHz, (c) 3.5GHz

From the experimental studies the following conclusions can be made.

L-strip feeding technique can be used for enhancing the bandwidth of circular patches also. Irrespective of the feed length maximum bandwidth is achieved when the length of the feed segment $S_2 \approx \frac{3}{4}\lambda_d$. The resonant frequency of the patch is shifting down when it is excited with L-strip feed. Maximum bandwidth is achieved with a good resonance curve. Radiation patterns are also broad with low cross polar level.

3.2.2 Circular patch – 2.4 GHz

Experimental study is repeated for circular patch resonating at frequency 2.4 GHz. Effect of feed parameters on the antenna characteristics are studied in detail. When the patch is electromagnetically coupled with a simple microstrip line feed, the antenna offers an impedance bandwidth of 3 % with a down shift in resonant frequency.

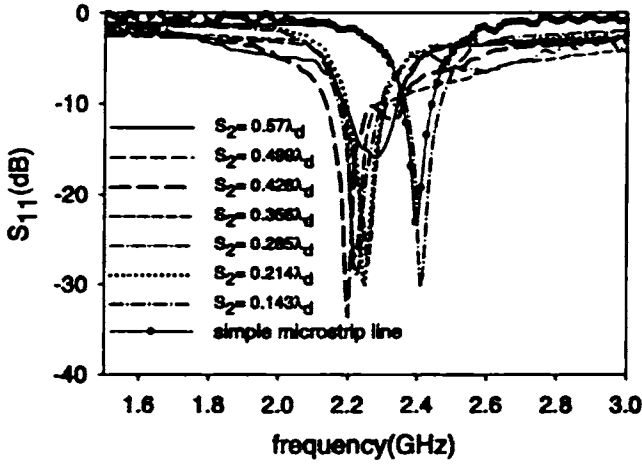
The same patch is excited with L-strip feed and the return loss and bandwidth variations with different S_1 and S_2 are noted. S_1 and S_2 are varied from $0.5\lambda_d$ to $1.5\lambda_d$ and $0.1\lambda_d$ to $1\lambda_d$ respectively. The bandwidth is found to be increasing with shift in the resonant frequency to the lower side.

Figure 3.6(a) shows the return loss variations of the antenna with $S_1 = 0.713\lambda_d$ for different feed segment lengths. Maximum bandwidth of 10.2% is obtained when $S_2/\lambda_d = 0.428$.

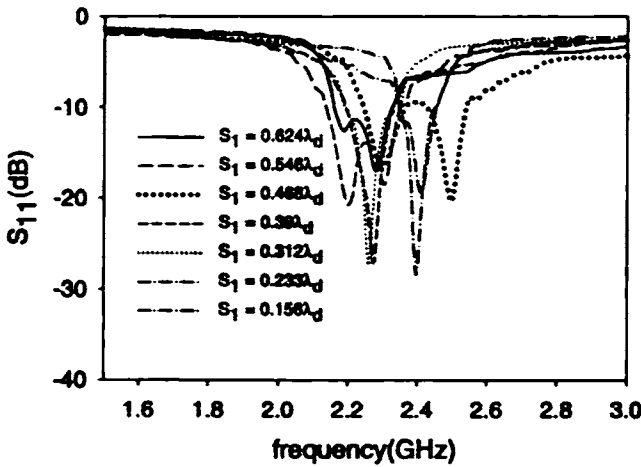
S_1 is increased further to $0.94\lambda_d$ and the return loss variations are measured. Figure 3.6 (b) shows the return loss variations with frequency for different S_2 . Maximum bandwidth of 12.5% is achieved for when S_2 is $0.468\lambda_d$. It is observed that bandwidth is increasing as S_1 is increasing.

Figure 3.6 (c) and (d) shows the return loss variations for different S_2 when the S_1 values are $1.02\lambda_d$ and $1.2\lambda_d$ respectively. Maximum bandwidth of 11.6 % is achieved when $S_1 = 1.2\lambda_d$ and $S_2 = 0.446\lambda_d$. Table 3.2 shows the resonant frequency and bandwidth variations of the circular patch resonating at 2.4 GHz.

From the experimental results it is observed the optimum feed parameters for the antenna resonating at 2.4 GHz is $S_1 = 0.94\lambda_d$ and $S_2 = 0.468\lambda_d$. Resonant frequency of the patch is found to be shifting down. Bandwidth variations with feed lengths are shown in Figure 3.7 indicates that its dependence on feed length is very less.



(a)

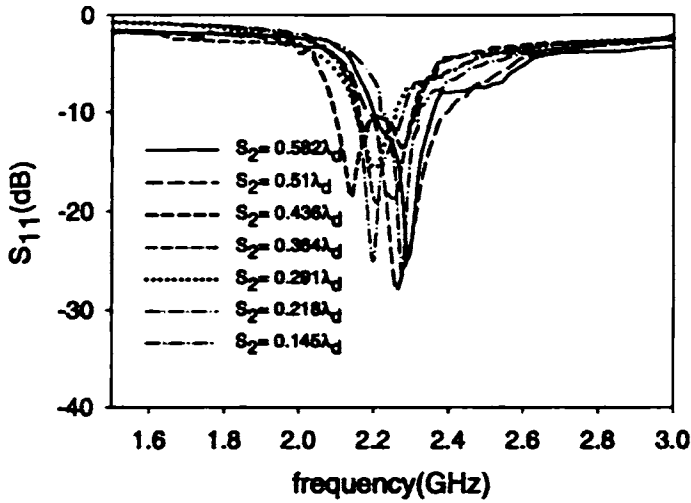


(b)

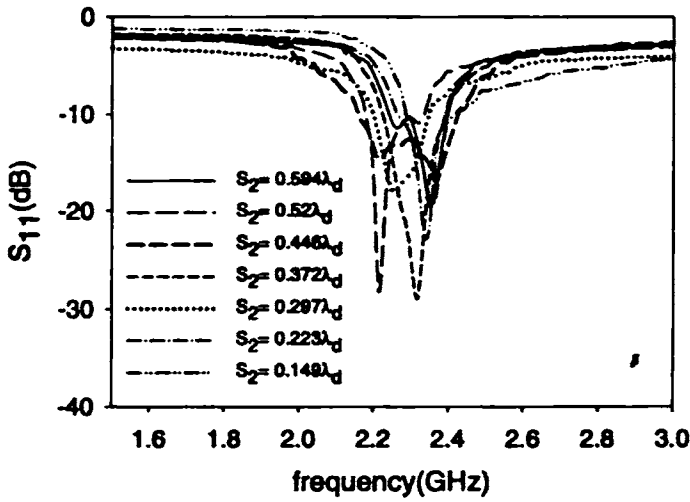
Figure 3.6 Return loss variations of the L-strip fed antenna with $r=1.78$ cm, for different S_2

(a) $S_1 = 0.713\lambda_d$

(b) $S_1 = 0.94\lambda_d$



(c)



(d)

Figure 3.6 Return loss variations of the L-strip fed antenna with $r = 1.78$ cm, for different S_2 .

(c) $S_1 = 1.02\lambda_d$

(d) $S_1 = 1.2\lambda_d$

Table.3.2 Resonant frequency and bandwidth variations with S_1 and S_2 for the circular patch with $r=1.78\text{cm}$, $\epsilon_{r1} = \epsilon_{r2} = 4.28$, $h_1 = h_2 = 0.16\text{cm}$

Feed length (S_1/λ_d)	Feed segment length (S_2/λ_d)	Resonant frequency (GHz)	%Bandwidth
0.713	0.143	2.41	4.35
	0.214	2.245	4.89
	0.285	2.215	5.4
	0.356	2.245	5.72
	0.428	2.20	10.2
	0.499	2.275	7.45
	0.570	2.255	6.6
0.94	0.156	2.395	4.01
	0.233	2.41	4.61
	0.312	2.245	7.99
	0.390	2.275	7.71
	0.468	2.35	12.5
	0.546	2.24	8.07
	0.624	2.275	7.34
1.02	0.145	2.365	4.09
	0.218	2.20	5.78
	0.291	2.204	5.7
	0.364	2.26	6.55
	0.436	2.245	10.01
	0.510	2.26	8.85
	0.582	2.29	6.94
1.2	0.149	2.395	4.89
	0.223	2.335	5.44
	0.297	2.26	6.59
	0.372	2.32	7.28
	0.446	2.293	11.6
	0.520	2.215	7.06
	0.594	2.221	6.55

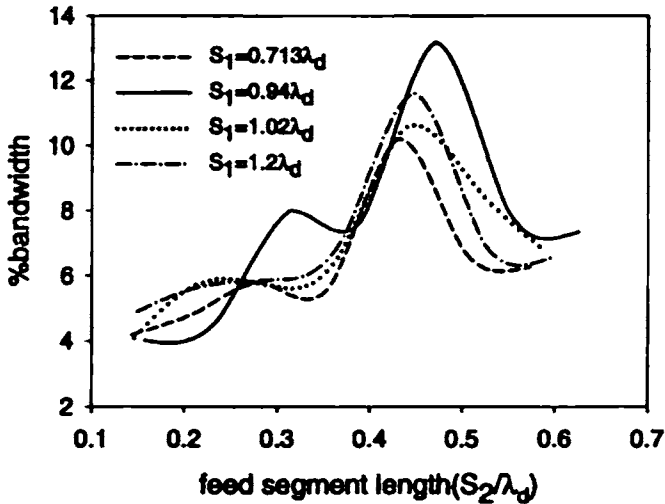
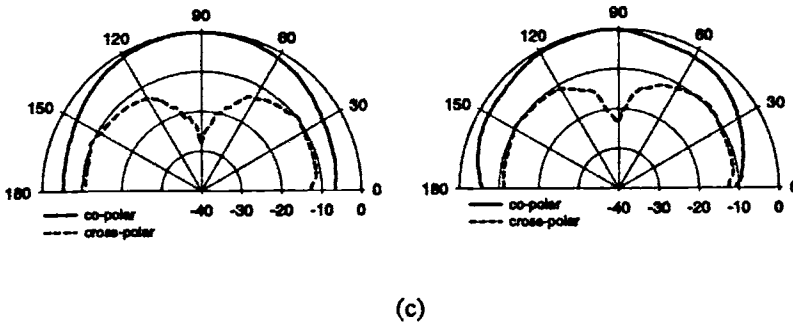
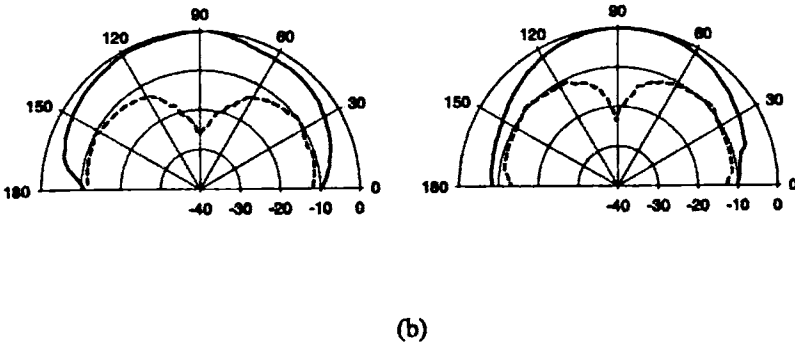
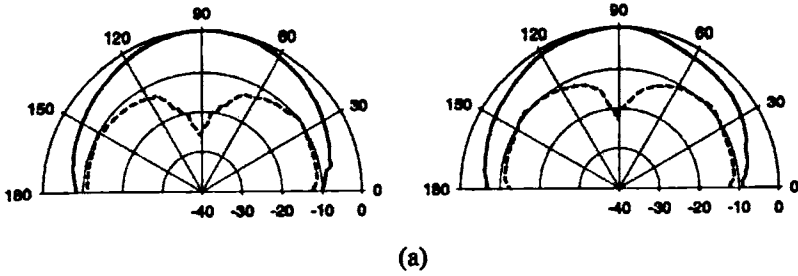


Figure 3.7 Bandwidth variations of the L-strip fed circular patch with $r = 1.78$ cm for different feed lengths

Radiation patterns of the antenna for the maximum bandwidth configuration are measured at different frequencies in the operating band. Measured radiation patterns are shown in Figure 3.8. Cross polar level of the antenna is better than -25 dB.

From the experimental observations it is concluded that for a circular patch resonating at 2.4 GHz maximum bandwidth of 12.5 % is obtained when the feed segment length $S_2 \approx \frac{1}{2}\lambda_d$ with good resonance curve. As the feed length increases the bandwidth has only slight variation and the maximum occurs at nearby values of S_2 for each S_1 .



E-plane

H-plane

Figure 3.8 Radiation patterns of the antenna at the maximum bandwidth position with $r = 1.78$ cm, $S_1 = 0.94\lambda_d$, $S_2 = 0.458\lambda_d$, $d_1 = 0.157\lambda_d$, $d_2 = 0.266\lambda_d$, $d_3 = 0.235\lambda_d$

(a) 2.3 GHz

(b) 2.406

(c) 2.5 GHz

3.2.3 Circular patch – 1.8 GHz

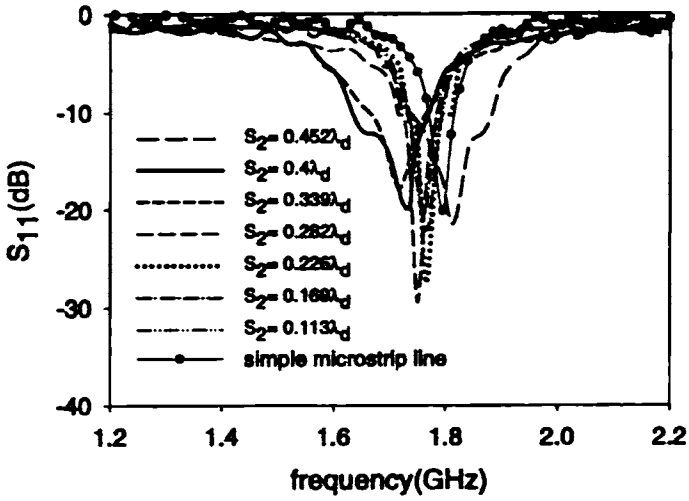
The performance of circular patch resonating at 1.8 GHz is also investigated by exciting with L-strip feed. To study the performance feed length and feed segment lengths are varied from $0.5\lambda_d$ to $1\lambda_d$ and $0.1\lambda_d$ to $0.5\lambda_d$ respectively. Return loss variations of the antenna are measured for different S_1 and S_2 combinations.

Figure 3.9 (a) shows the S_{11} variations of the antenna for different feed segment lengths when the feed length $S_1 = 0.57\lambda_d$. Maximum bandwidth of 8.81% is obtained when $S_2 = 0.4\lambda_d$.

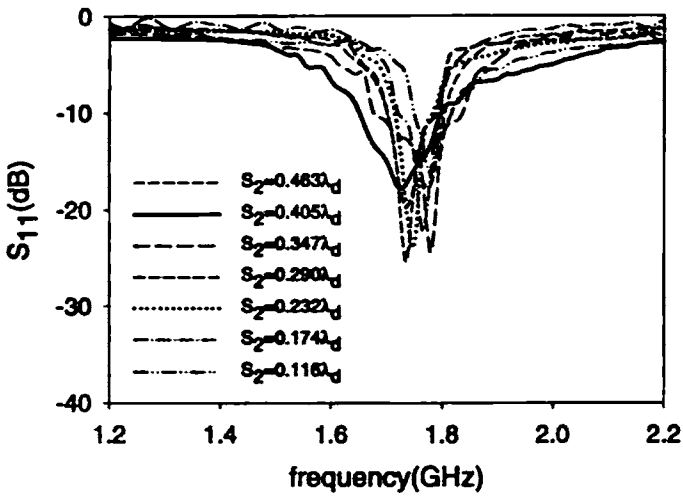
The feed length is increased further to $0.695\lambda_d$ and the return loss and bandwidth variations are noted. Figures 3.9 (b), shows the return loss variations with this S_1 for different S_2 . Maximum bandwidth of 8.12% is obtained when $S_2 = 0.405\lambda_d$

Figures 3.9 (c) and (d) give the return loss variations when the feed lengths are $0.8\lambda_d$ and $0.935\lambda_d$ respectively. Resonant frequency and bandwidth variations are given in Table 3.3. From the Table it is concluded that the resonant frequency has slight variations only as value of feed length increases. Bandwidth variations for different feed lengths obtained are plotted in Figure 3.10. Maximum bandwidth of 10.35% is obtained when $S_1 = 0.8\lambda_d$ and $S_2 = 0.402\lambda_d$.

Maximum bandwidth of the circular patch resonating at 1.8GHz is limited to 8 to 10%. Irrespective of the feed length, maximum bandwidth is achieved when the length of the feed segment is $\approx 0.4\lambda_d$. As the resonant frequency of the patch is lowered bandwidth enhancement can be achieved at lower feed segment lengths. Here also the resonant frequency of the patch shifts to a lower frequency by the L-strip feeding.

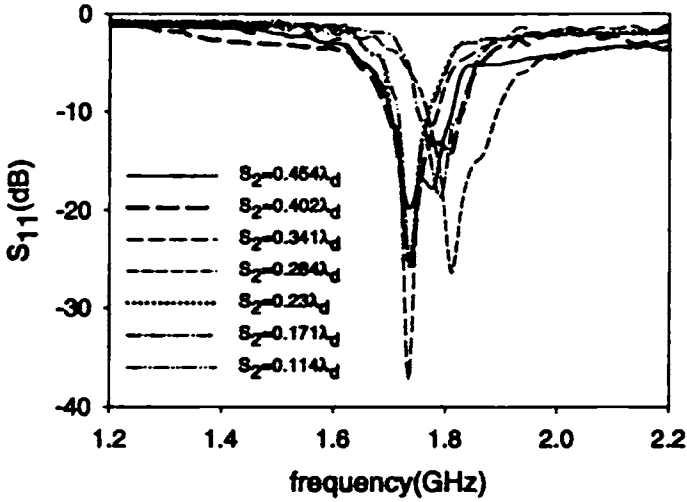


(a)

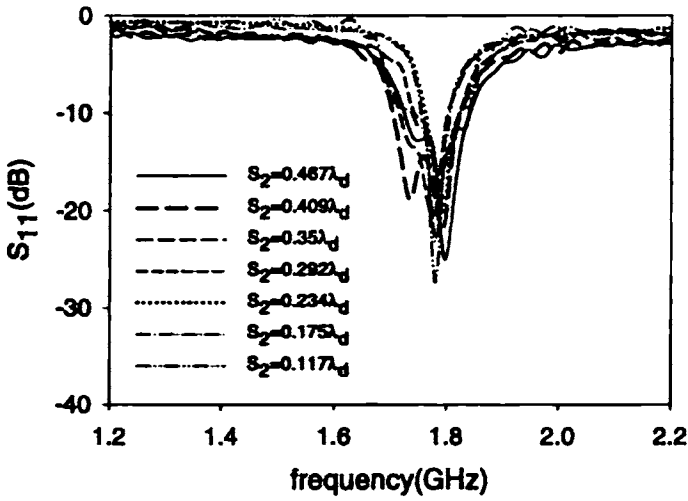


(b)

Figure 3.9 Return loss variations of the L-strip fed circular patch antenna with $r = 2.36\text{cm}$, for different S_2
 (a) $S_1 = 0.57\lambda_d$



(c)



(d)

Figure 3.9 Return loss variation of the L-strip fed circular patch antenna with $r = 2.36\text{cm}$, for different S_2

(c) $S_1 = 0.8\lambda_d$

(d) $S_1 = 0.935\lambda_d$

Table 3.3 Resonant frequency and bandwidth variations with S_2 for different S_1 of the with patch size $r = 2.36\text{cm}$, $\epsilon_{r1} = \epsilon_{r2} = 4.28$, $h_1 = h_2 = 0.16\text{cm}$

Feed length (S_1/λ_d)	Feed segment length(S_2/λ_d)	Resonant frequency (GHz)	%bandwidth
0.57	0.114	1.765	3.5
	0.171	1.765	3.74
	0.228	1.765	4.2
	0.285	1.75	4.5
	0.342	1.735	5.6
	0.40	1.735	8.81
	0.456	1.795	6.36
0.695	0.116	1.78	3.98
	0.174	1.78	4.25
	0.232	1.75	4.6
	0.290	1.75	5.5
	0.347	1.725	6.97
	0.405	1.78	8.12
	0.463	1.795	6.05
0.8	0.114	1.735	3.75
	0.171	1.795	4.01
	0.23	1.735	4.5
	0.287	1.795	4.9
	0.345	1.735	5.69
	0.402	1.735	10.35
	0.454	1.735	6.1
0.935	0.117	1.795	3.75
	0.175	1.78	3.95
	0.234	1.795	4.9
	0.292	1.78	5.5
	0.35	1.78	5.01
	0.409	1.795	6.8
	0.467	1.795	5.2

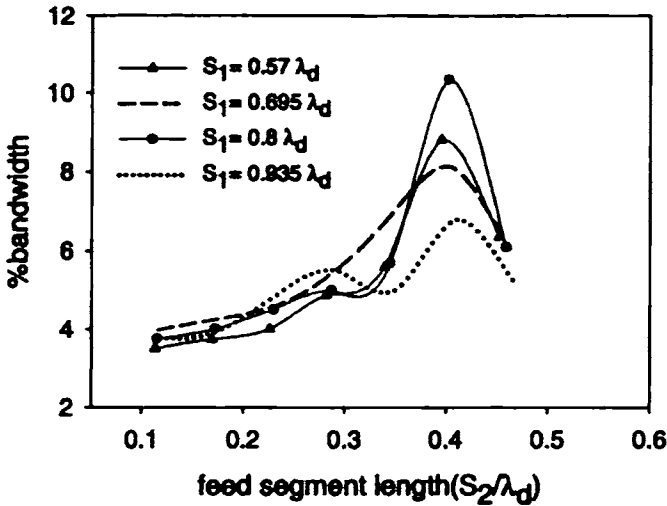


Figure 3.10 Bandwidth variations with S_2 for the patch with $r = 2.36\text{cm}$ for different S_1

3.2.4 Gain

Gain of the antenna at the optimum bandwidth configuration is measured.

Figure 3.11 shows the absolute gain of the antenna. The antenna has a gain of 7.25dBi at the resonant frequency.

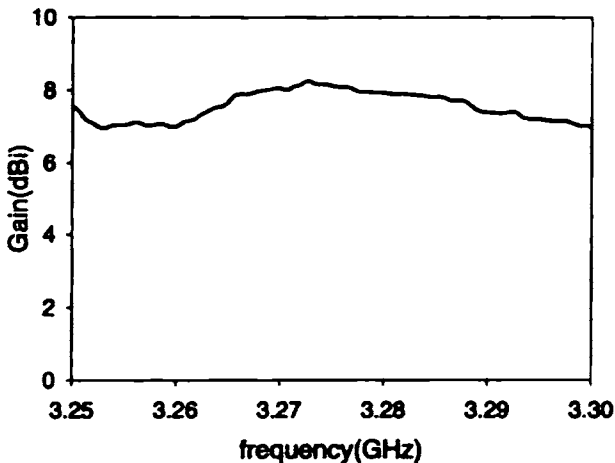


Figure 3.11 Gain plot of the L-strip fed circular patch

3.2.5 Simulated Results

L-strip circular patch configurations which offered maximum bandwidth are simulated using IE3D software. Simulated reflection characteristics are discussed in the following sections.

Experimental and simulated return loss variations of the L-strip fed circular antenna with dimension $r = 1.22$ cm is shown in Figure 3.12. Maximum bandwidth of 12% in the operating band 2.974GHz – 3.364GHz is obtained from simulation. Experimental and simulated resonant frequencies are 3.28GHz and 3.25GHz respectively.

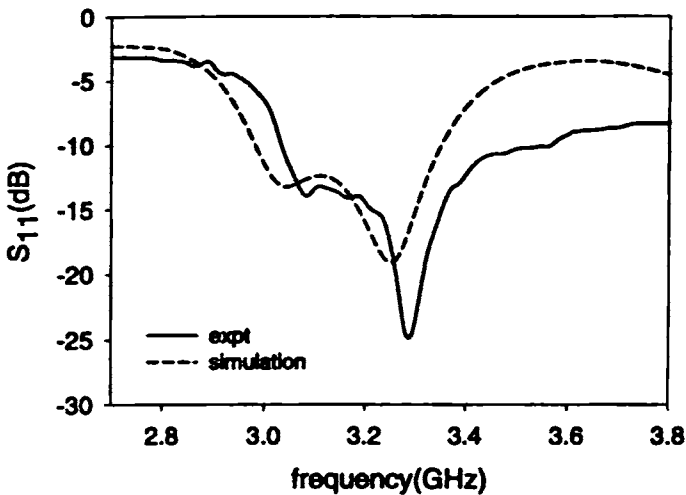


Figure 3.12 Experimental and simulated return loss variations of the antenna with $r = 1.22$ cm, $S_1 = 1.067\lambda_d$, $S_2 = 0.747\lambda_d$, $d_1 = 0.01\lambda_d$, $d_2 = 0.265\lambda_d$, $d_3 = 0.213\lambda_d$

Figure 3.13 shows the experimental and simulated return loss variations of the circular patch with radius $r = 1.78\text{cm}$ with $S_1 = 0.94\lambda_d$ and $S_2 = 0.458\lambda_d$. A maximum bandwidth of 10.97% in the band 2.16GHz- 2.418GHz is obtained from simulation. Experimental resonant frequency is 2.35GHz while that obtained from simulation is 2.358GHz.

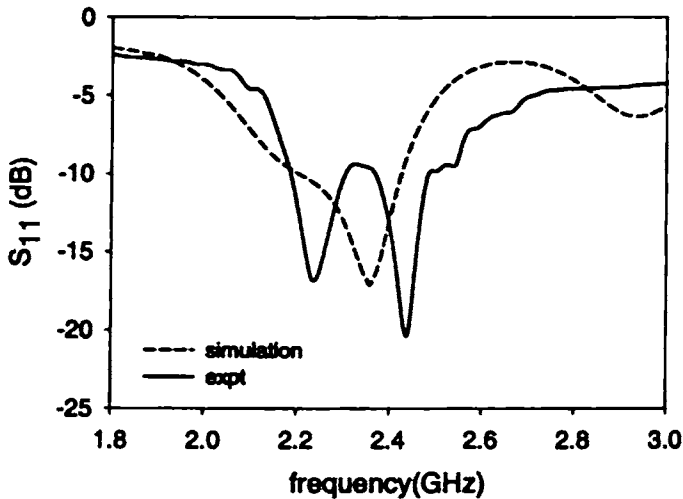


Figure 3.13 Experimental and simulated return loss variations of the L-strip fed circular antenna with $r = 1.78\text{ cm}$, $S_1 = 0.94\lambda_d$, $S_2 = 0.47\lambda_d$, $d_1 = 0.157\lambda_d$, $d_2 = 0.266\lambda_d$, $d_3 = 0.235\lambda_d$

Experimental and simulated return loss variations of the patch with dimension $r = 2.36\text{cm}$ at the maximum bandwidth is shown in Figure 3.14. Maximum bandwidth of 7% is obtained from simulation. Resonant frequencies obtained from experiment and simulations are 1.735GHz and 1.715GHz respectively.

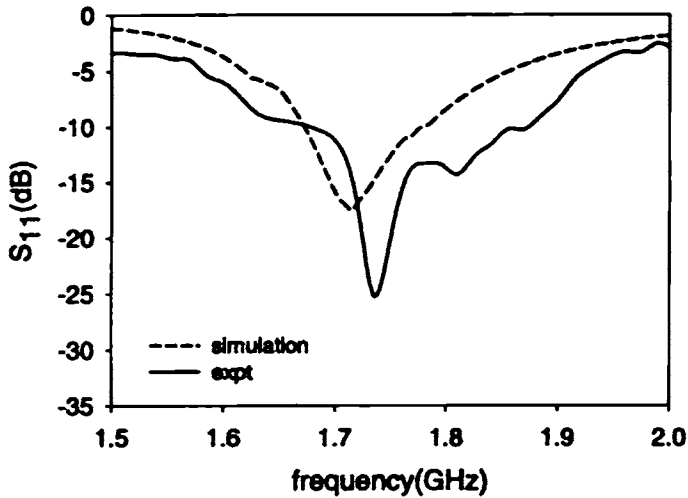


Figure 3.14 Experimental and simulated return loss variation of the antenna with $r = 2.36\text{cm}$, $S_1 = 0.8\lambda_d$, $S_2 = 402\lambda_d$

From the experimental and simulated results it is concluded that L-strip feeding can effectively be used for the bandwidth enhancement of circular patches also. When the resonant frequency of the patch is of the order of 3 GHz, the condition for maximum bandwidth is $S_1 + S_2 \approx 2\lambda_d$ and $S_2 = \frac{3}{4}\lambda_d$ and if the resonant frequency is of the order of 2.4 GHz then the condition for maximum bandwidth is $S_1 + S_2 \approx 1.5\lambda_d$ and $S_2 \approx 0.5\lambda_d$. And if the resonant frequency is lower than that bandwidth enhancement can be achieved at a lower value of S_1 and S_2 combination.

CHAPTER 4

THEORETICAL INVESTIGATIONS

Finite Difference Time Domain Method (FDTD) is employed for the analysis of L-strip fed microstrip antennas. The accuracy of the analysis is validated through experimental results. An FDTD code that can be used for the calculation of scattering parameters, radiation patterns as well as field distribution over the surface of the patch is generated using MATLAB 6.1.

4.1 INTRODUCTION

Theoretical analysis of the L-strip fed microstrip antenna and comparison with the measured results are presented in this chapter. The analysis is based on Finite Difference Time Domain (FDTD) method. It is an efficient tool for directly solving time harmonic Maxwell's equation using finite difference techniques. In the FDTD method the spatial and time derivatives are approximated by centered differences, which are accurate to second order in time or space. With Maxwell's equations reduced to a set of coupled difference equations, the solution is readily obtained by time stepping, where the new value for field components are calculated from the previous values. Hence the method is termed as 'leap-frog' method.

The frequency dependent scattering parameters and radiation patterns have been calculated for the antenna under study. The mode analysis is also done by FDTD. The calculated results are presented and compared with the measured values for the L-strip fed geometry.

4.2 Theoretical Approach

An FDTD algorithm for analyzing the antenna is generated. The antenna geometry is divided into cells for which necessary boundary conditions are applied. The finite difference time domain method permits the analysis of interactions of electromagnetic waves with material bodies of the desired shapes.

4.2.1 FDTD Modeling Theory

The finite difference time domain method was originated by Yee in 1966 [113] and applied to electromagnetic problems in two dimensions. The FDTD method calculates the electric and magnetic fields on a discrete mesh by approximating the first order derivatives in the differential form of Maxwell's vector curl equations. The discrete electric and magnetic fields are interleaved in

space to obtain centered difference approximations to the spatial derivatives. The time derivatives are calculated in a leap-frog manner to obtain the centered differences in time. Space and time discretizations are selected to bind the errors in sampling process and to ensure numerical stability of the problem. The electric and magnetic field components are interleaved in space to permit a natural satisfaction of the tangential field continuity conditions at media interfaces.

Applications of FDTD techniques to various electromagnetic problems are available in literature [114], [116], [120]. In the case of arbitrary shaped patches application of Yee's algorithm has been found to be extremely accurate in finding the current and field distribution across the patch. One practical difficulty with this method is that for devices containing small structures or strongly varying fields, it needs very fine mesh. When using finer meshes it needs longer CPU time and memory. An improved method for reducing the number of time steps is implemented by Lubbers *et al.* [121]. This is based on using a source with an external resistance to excite the circuit.

FDTD method has been used extensively for the solution of two and three dimensional scattering problems. The method has been applied to calculate the frequency dependent characteristics of microstrip discontinuities [122]. Analysis of microstrip discontinuities has great importance, since complicated circuits can be realized by interconnecting the microstrip lines with these discontinuities and using transmission lines and network theory. If the discontinuities are too close to each other the use of network concept will not be accurate due to the interaction of evanescent waves. To analyze the circuits accurately the entire structure has to be simulated in one computation. In time domain analysis a broadband pulse may be used as the excitation and frequency domain parameters may be calculated over the entire frequency range of interest by Fourier Transform of the transient results [120].

The formulation of the FDTD method begins by considering the differential formulae of Maxwell's curl equations which govern the propagation of electromagnetic waves. The media are assumed to be piecewise uniform, isotropic and homogeneous.

$$-\frac{\partial B}{\partial t} = \nabla \times E \quad (4.1)$$

$$\frac{\partial D}{\partial t} = \nabla \times H - J \quad (4.2)$$

$$\text{where } B = \mu H \quad (4.3)$$

$$D = \epsilon E \quad (4.4)$$

In Cartesian co-ordinate system the above equations may be written as

$$-\frac{\partial B_x}{\partial t} = \frac{\partial E_z}{\partial y} - \frac{\partial E_y}{\partial z} \quad (4.5)$$

$$-\frac{\partial B_y}{\partial t} = \frac{\partial E_x}{\partial z} - \frac{\partial E_z}{\partial x} \quad (4.6)$$

$$-\frac{\partial B_z}{\partial t} = \frac{\partial E_y}{\partial x} - \frac{\partial E_x}{\partial y} \quad (4.7)$$

$$\frac{\partial D_x}{\partial t} = \frac{\partial H_z}{\partial y} - \frac{\partial H_y}{\partial z} - J_x \quad (4.8)$$

$$\frac{\partial D_y}{\partial t} = \frac{\partial H_x}{\partial z} - \frac{\partial H_z}{\partial x} - J_y \quad (4.9)$$

$$\frac{\partial D_z}{\partial t} = \frac{\partial H_y}{\partial x} - \frac{\partial H_x}{\partial y} - J_z \quad (4.10)$$

The system of six coupled partial difference equations forms the basis of the FDTD numerical algorithm for electromagnetic wave interaction with general three dimensional objects.

The basic Yee algorithm helps to solve both electric and magnetic fields in time and space using the Maxwell's curl equations. The grid points for the E -field and H -field are chosen as shown in Figure 4.1. The boundary condition for a perfectly conducting surface is that the tangential components of the electric field vanish at the boundary. This implies that the normal component of the magnetic field vanishes on the surfaces. The conducting surfaces will therefore be

approximated by a collection of surfaces of cubes, the sides of which are parallel to the coordinate axes. Plane surfaces are perpendicular to the x -axis will be chosen so as to contain points where E_x and E_y are defined [113].

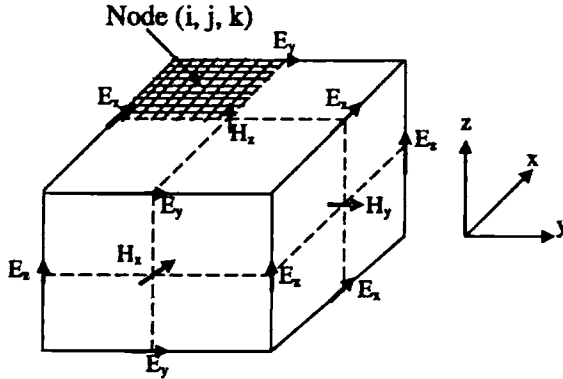


Figure 4.1 Field component placements in the FDTD unit cell

Each Yee cell contains six field components E_x , E_y , E_z and H_x , H_y , H_z . All the fields are offset by half a space step as in figure. The Yee algorithm centers its \bar{E} and \bar{H} components in a three dimensional space so that every \bar{E} component is surrounded by four circulating \bar{H} components and every \bar{H} component by four circulating \bar{E} components.

4.2.2 FDTD Problem Definition

The FDTD method is formulated by discretizing Maxwell's equations over a finite volume and approximating the derivatives with centered difference approximations. Conducting surfaces are treated by setting the tangential electric field components to be zero. The walls are treated separately to prevent reflections from the mesh terminations. In the present analysis, space grids are selected such that the electromagnetic field does not vary significantly over one increment. The notation used for analysis are generalized into three spatial dimensions, space points in a uniform rectangular lattice being represented as,

$$(i, j, k) = (i\Delta_x, j\Delta_y, k\Delta_z)$$

Here Δ_x , Δ_y , and Δ_z are the lattice space increments in the x , y , and z directions.

The aim of the present analysis is to model the L-strip fed antennas accurately and efficiently.

4.2.3 FDTD Principal Equations

The L-strip antenna geometry is divided into fixed rectangular field locations and each conducting surfaces are treated by setting the tangential electric field component to zero. The six field locations are interleaved in space as shown in Figure 4.1, which is a drawing of the FDTD unit cell. The entire computational domain is formed by stacking these rectangular cells into a rectangular volume. The x , y , and z dimensions of the unit cell are Δ_x , Δ_y , and Δ_z respectively. This field arrangement has an advantage that the centered differences are realized in the calculation of each field component and the boundary condition of tangential field component is automatically satisfied at the dielectric material interfaces.

Since there are six field components within the unit cell, six field components touching the shaded upper eighth of the unit cell in the figure are considered to be a unit node with subscript indices (i, j, k) in the x , y , and z directions. The notation implicitly assumes the $\pm 1/2$ space indices and thus simplified the notation. The time step is indicated with subscripts, n . The explicit finite difference approximations to (4.15) to (4.10) are as given by Sheen *et al.* [117]

$$H_x^{n+1/2}{}_{i,j,k} = H_x^{n-1/2}{}_{i,j,k} + \frac{\Delta t}{\mu\Delta z} (E_y^n{}_{i,j,k} - E_y^n{}_{i,j,k-1}) - \frac{\Delta t}{\mu\Delta y} (E_z^n{}_{i,j,k} - E_z^n{}_{i,j-1,k}) \quad (4.11)$$

$$H_y^{n+1/2}{}_{i,j,k} = H_y^{n-1/2}{}_{i,j,k} + \frac{\Delta t}{\mu\Delta x} (E_z^n{}_{i,j,k} - E_z^n{}_{i-1,j,k}) - \frac{\Delta t}{\mu\Delta z} (E_x^n{}_{i,j,k} - E_x^n{}_{i,j,k-1}) \quad (4.12)$$

$$H_x^{n+1/2} = H_x^{n-1/2} + \frac{\Delta t}{\mu \Delta y} (E_z^n{}_{i,j,k} - E_z^n{}_{i,j-1,k}) - \frac{\Delta t}{\mu \Delta x} (E_y^n{}_{i,j,k} - E_y^n{}_{i-1,j,k}) \quad (4.13)$$

$$E_x^{n+1}{}_{i,j,k} = E_x^n{}_{i,j,k} + \frac{\Delta t}{\epsilon \Delta y} (H_z^{n+1/2}{}_{i,j+1,k} - H_z^{n+1/2}{}_{i,j,k}) - \frac{\Delta t}{\epsilon \Delta z} (H_y^{n+1/2}{}_{i,j,k+1} - H_y^{n+1/2}{}_{i,j,k}) \quad (4.14)$$

$$E_y^{n+1}{}_{i,j,k} = E_y^n{}_{i,j,k} + \frac{\Delta t}{\epsilon \Delta z} (H_x^{n+1/2}{}_{i,j,k+1} - H_x^{n+1/2}{}_{i,j,k}) - \frac{\Delta t}{\epsilon \Delta x} (H_z^{n+1/2}{}_{i+1,j,k} - H_z^{n+1/2}{}_{i,j,k}) \quad (4.15)$$

$$E_z^{n+1}{}_{i,j,k} = E_z^n{}_{i,j,k} + \frac{\Delta t}{\epsilon \Delta x} (H_y^{n+1/2}{}_{i+1,j,k} - H_y^{n+1/2}{}_{i,j,k}) - \frac{\Delta t}{\epsilon \Delta y} (H_x^{n+1/2}{}_{i,j+1,k} - H_x^{n+1/2}{}_{i,j,k}) \quad (4.16)$$

The half time steps indicate that \bar{E} and \bar{H} are alternatively calculated in order to achieve centered differences for the time derivatives. This algorithm is referred to as 'leap-frog' algorithm. Here the permittivity and permeability are set to appropriate values depending on the location of each field component. For the electric field component in the air-dielectric interface the average of two permittivities $(\epsilon_0 + \epsilon_1)/2$, where ϵ_0 and ϵ_1 are the permittivity of the free space and medium is used. The error is second order in both space and time steps and are proportional to Δt , and the global error is $O(\Delta t^2)$. The maximum time step is limited by the Courant Stability criterion of the finite difference equations [117]

$$\Delta t \leq \frac{1}{v_{\max}} \left(\frac{1}{\Delta x^2} + \frac{1}{\Delta y^2} + \frac{1}{\Delta z^2} \right)^{\frac{1}{2}} \quad (4.17)$$

where v_{\max} is the maximum velocity of light in the computational volume.

4.2.4 Source Consideration

The time dependence of the source is chosen depending on the problem to be solved. For applications where frequency dependent data is to be generated, a pulse is used such that its frequency content covers the desired frequency range. The usable highest frequency is limited by the size of the Yee's cell. A Gaussian pulse has a smooth waveform in time, and its Fourier Transform is also a Gaussian pulse centered at zero frequency. This unique property makes it a

perfect choice for investigating the frequency dependent characteristics of the microstrip discontinuities via Fourier Transform of the pulse response.

To simulate, a voltage source excitation is necessary to impose the vertical electric field in a rectangular region above the ground plane. The launched wave has a nearly unit amplitude and is Gaussian which is given by

$$f_s(t) = e^{-(t-t_0)^2/T^2} \quad (4.18)$$

where T is the half width and t_0 is the time delay.

The choice of t_0 and T is such that the truncation of the source pulse does not introduce unwanted high frequencies in the spectrum and does not waste computation time on determining values of the fields that are essentially zero. Usually the width of the pulse is chosen to be at least 20 points per wavelength at the highest frequency of interest. However, if we proceed straight way, the computational time is large to achieve the stability condition. Lubbers *et al.* [121] introduced a new concept to reduce the computational time, by introducing a source resistance R_s in series with the voltage source.

The equivalent circuit for a voltage source which includes an internal source resistance R_s is illustrated in Figure 4.2.

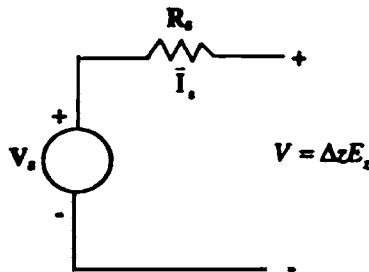


Figure 4.2 FDTD Source with source Resistance ‘ R_s ’

If the source resistance R_s is set to zero then the FDTD electric field at the source is given by

$$E_z^n(i, j, k, t) = V_s (n \Delta t) / \Delta z \quad (4.19)$$

V_s is the Gaussian pulse.

When the source resistance is included, the calculation of source field at each time step is complicated. To determine the terminal voltage V of Figure 4.2, the current through the source must be determined. The current through the source is given by

$$I_z^{n-1/2} = [H_x^{n-1/2}(i, j, -1, k) - H_x^{n-1/2}(i, j, k)]\Delta x + [H_y^{n-1/2}(i, j, k) - H_y^{n-1/2}(i, -1, j, k)]\Delta y \quad (4.20)$$

And the electric source field is given by

$$E_z^n(i, j, k) = V_s(n\Delta t) / \Delta z + I_z^{n-1/2} R_s / \Delta z \quad (4.21)$$

The value of the source resistance cannot be too large or instabilities can occur due to neglecting the displacement current through the FDTD cell containing the source.

Once the pulse amplitude drops, the source voltage becomes essentially zero, any reflections from the antenna which returns to the source, is totally reflected back. The inclusion of an internal resistance to the source provides an additional loss mechanism to dissipate energy introduced into the calculation space that will reduce the computational time appreciably [121].

4.2.5 Absorbing Boundary conditions

Absorbing boundary conditions are applied at the boundary mesh walls of finite difference, to simulate an unbounded space. The most common, and generally most practical, method used to derive absorbing boundary conditions are based on asymptotic expansion of one-way wave equation. Many researchers have developed theories to these approximate boundary conditions [115].

The difference equations cannot be used to evaluate the field components tangential to the outer boundaries since they would require the values of field components outside the mesh. One of the six mesh boundaries is a ground plane and its tangential electric field values are forced to zero. The tangential electric

field components on other five mesh walls are represented in such away that outgoing waves are not reflected using the absorbing boundary conditions. For this structure the pulses on the microstrip line will be considered as incident normally to the mesh walls. This results in a simple approximate continuous absorbing boundary condition that the tangential fields on the outer boundaries will obey the one -dimensional wave equation in the direction normal to the mesh wall. For the y normal wall the one dimensional wave equation is

$$\left(\frac{\partial}{\partial y} - \frac{1}{v} \frac{\partial}{\partial t} \right) E_{\text{wall}} = 0 \quad (4.22)$$

This equation is Mur's first order approximate boundary condition and may be easily discretized using only field components on or just inside the mesh walls, yielding an implicit finite difference equation [117].

$$E_0^{n+1} = E_1^n + \frac{v\Delta t - \Delta y}{v\Delta t + \Delta y} (E_1^{n+1} - E_0^n) \quad (4.23)$$

Here E_0 is the tangential electric field components on the mesh wall and E_1 represents the tangential electric field components one node inside the mesh wall. The normal incidence assumption is not valid for the fringing fields which are propagating tangential to the wall and therefore the side walls should be far away, so that the fringing fields are negligible at the walls. Also the radiation will not be exactly normal to the mesh walls.

Finite difference equations are used with the above boundary and source conditions to simulate the propagation of broadband Gaussian pulse on the microstrip structure. The most important aspects of the time domain algorithm are as follows:

- Initially at $t = n = 0$ all the fields are forced to zero.
- The following steps are repeated until the response is ≈ 0

Gaussian excitation is imposed at port.

$H^{n+1/2}$ is calculated from the finite difference equations.

$E^{n+1/2}$ is calculated from the finite difference equations.

Tangential E is set to 0 on conductors.

Save the desired field quantities

Increment the time $n \rightarrow n+1$

Update the equation

- Compute scattering matrix coefficients from time domain results.

To eliminate the reflections from the circuit, to reflect it again by the source wall, the circuit is placed a sufficient distance away from the source. After the Gaussian pulse has been launched, the absorbing boundary condition is switched on at the boundary walls.

4.2.6 Scattering Parameters

The frequency dependent scattering coefficients can be calculated from $[V]^r = [S] \cdot [V]^i$, where $[V]^r$ and $[V]^i$ are the reflected and incident voltage vectors and $[S]$ is the scattering matrix. To obtain the scattering parameters $S_{11}(\omega)$, the incident and reflected voltage must be known. To obtain the incident waveform the calculation is performed using only the port microstrip line which will be of infinite extent and the incident wave form is noted. This incident waveform is subtracted from total waveform to get the reflected waveform from the port. The scattering parameters, S_{jk} is obtained by calculating the Fourier Transform of these transient waveforms.

$$S_{jk}(\omega) = \frac{FT[V_j(t)]}{FT[V_k(t)]} \quad (4.24)$$

The reference planes are selected far away from the circuit discontinuities to eliminate evanescent waves. These distances are included in the circuit so that no phase correction is performed for scattering coefficients.

4.2.7 Radiation Pattern Calculation

In FDTD, for the calculation of scattering parameters a plane wave

the source usually occupies a fixed location in the workspace and is gradually ramped up in amplitude.

Two types of sources are of primary interest in antenna design. If a finite Gaussian pulse is used as an excitation pulse, the Fourier Transform can be used to convert the time domain information to the frequency domain for computing antenna scattering parameters. Using a single frequency sinusoid as source, the near field in the immediate vicinity of the patch is calculated. From the near field data, the far field pattern at any observation angles can be calculated. A Fourier series summation is done at each point where the fields are sampled over the time of one period. i.e., the first harmonic component

$$E(x', y') = \frac{1}{N} \sum_{n=1}^N E(n) * e^{j(2\pi/N)} \quad (4.25)$$

Where N is equal to the number of time steps in a period of the sinusoid, and $E(n)$ is a tangential component of the E -field measured at time steps n at location (x', y') . This removes the time dependence from the sampled fields [119].

The radiation patterns can be calculated with the following assumptions

- The antenna radiates into the $z > 0$ direction from a planar aperture in the $z = 0$ plane
- $kr \gg 1$
- The field over an aperture is defined such that the transverse electric fields are negligible outside of the aperture region.
- The far field can be written as

$$\bar{E}(r, \theta, \phi) \approx \frac{je^{-jkr}}{\lambda r} \left[\hat{\phi}(P_x \cos \phi + P_y \sin \phi) - \hat{\phi} \cos \theta (P_x \sin \phi - P_y \cos \phi) \right] \quad (4.26)$$

$$\text{where } \begin{Bmatrix} P_x \\ P_y \end{Bmatrix} = \int_{-x}^{+x} \int_{-y}^{+y} \begin{Bmatrix} E_x(x', y', 0) \\ E_y(x', y', 0) \end{Bmatrix} e^{jk(x' \sin \theta \cos \phi + y' \sin \theta \sin \phi)} dx' dy' \quad (4.27)$$

For the radiation pattern calculation the aperture is a plane just above the patch surface as in Figure 4.3(a).

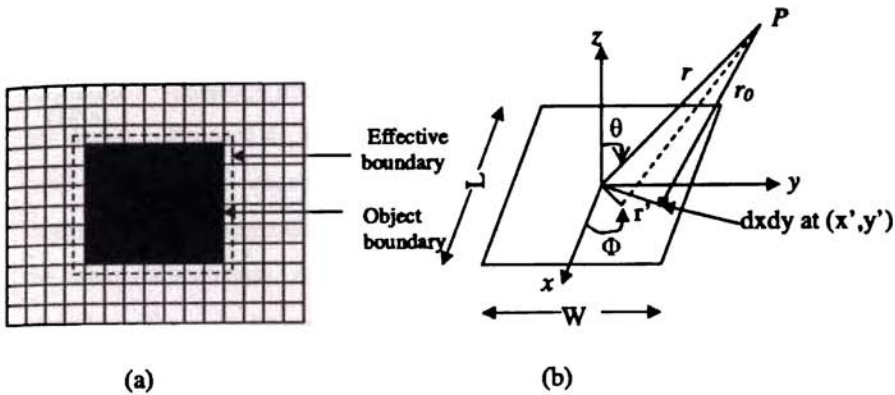


Figure 4.3(a) Aperture boundary layer for pattern calculation
(b) Far field calculation

The electric and magnetic fields at any point $P(r, \theta, \Phi)$ outside the microstrip antenna can be written as [12]

$$\overline{E}^m(r) = -\frac{1}{\epsilon} \nabla \times \overline{F} \quad (4.28)$$

$$\overline{H}^m(r) = \frac{1}{j\omega\mu\epsilon} \nabla(\nabla \cdot \overline{F}) - j\omega\overline{F} \quad (4.29)$$

Where ϵ is the permittivity and μ is the permeability of the medium, the superscript m denotes the field due to magnetic current, and ω is the angular frequency. The electric vector potential \overline{F} over the aperture is defined as

$$\overline{F} = \frac{\epsilon}{4\pi} \iint_{s'} \overline{M}(r') \frac{e^{-k_0(r-r')}}{r-r'} ds' \quad (4.30)$$

Where k_0 is the free space wave number and $\overline{M}(r')$ is the surface magnetic current density at P' , a distance r' from the origin as in Figure 4.3(b).

The only significant field components in the far field are those due to the transverse to the direction of propagation, that is, $\hat{\theta}$ and $\hat{\phi}$ components.

The electric field can be obtained in terms of vector potentials as

$$E_{\theta} = j\omega\eta_0(F_x \sin \phi - F_y \cos \phi) \quad (4.31)$$

$$E_{\phi} = j\omega\eta_0(F_y \cos \theta \cos \phi + F_x \cos \theta \sin \phi) \quad (4.32)$$

4.3 ANALYSIS OF L-STRIP FED RECTANGULAR MICROSTRIP ANTENNA

Simulation of the microstrip patch involves direct application of finite difference equations, along with the source excitation and absorbing boundary conditions. The actual dimensions of the L-strip fed microstrip antenna analyzed are shown in Figure 4.4. To model the thickness (h) of the antenna, Δz is chosen such a way that it exactly matches the thickness. Additional nodes in the z direction are used to model the free space above the antenna. To correctly model the antenna dimensions, Δx and Δy have been chosen so that an integral number of nodes will exactly fit within the rectangular patch.

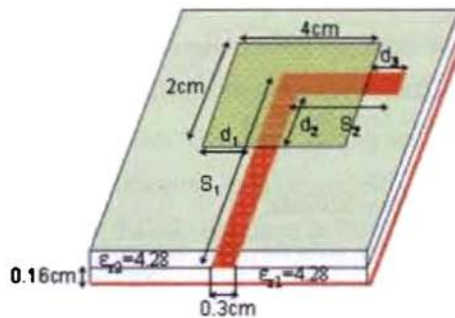


Figure 4.4 L-strip fed rectangular microstrip antenna parameters

The space steps used are $\Delta x = 0.1\text{cm}$, $\Delta y = 0.1\text{cm}$ and $\Delta z = 0.04\text{cm}$ and the total mesh dimensions are $110 \times 110 \times 20 (N_x \times N_y \times N_z)$ in the x , y and z directions. The rectangular patch is thus $40 \Delta x \times 20 \Delta y$. The L-strip feed line width is modeled as $3 \Delta x$. The feed length (S_1) of the L-strip varies from 4cm to 9cm and the feed segment length (S_2) varies from 0.5cm to 4cm. The L-strip feed is modeled as two rectangles each having dimensions $3 \Delta x \times S_1 \Delta y$ and $S_2 \Delta x \times 3 \Delta y$ respectively. Figure 4.5 shows the computational volume of the L-strip fed antenna.

The time step employed for present study is $\Delta t = 1.159\text{ps}$. The Gaussian half-width is $T = 15\text{ps}$, and the time delay t_0 is set to be $3T$ so that the Gaussian will start approximately at time $t = 0$. An internal source resistance of 50Ω is used to reduce the computational time and to enhance the computational efficiency [121]. The simulation is performed for 5000 time steps.

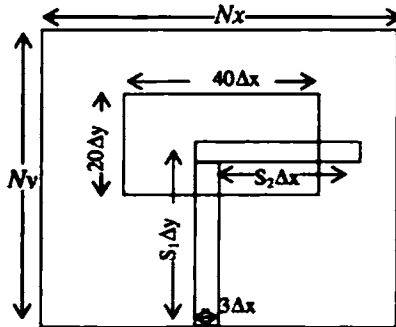


Figure 4.5 FDTD computational domain of the L-strip fed antenna with $L = 4\text{cm}$, $W = 2\text{cm}$

4.3.1 Microstrip Antenna – 3.3GHz

L-strip fed microstrip antenna with dimensions $L = 4\text{cm}$, $W = 2\text{cm}$ is analyzed using FDTD. The FDTD code parameters for the analysis are

Table 4.1 FDTD code parameters

Source excitation	Gaussian pulse ,Half width $T = 15\text{ps}$ Time delay $t_0 = 3T$
Cell dimensions	$\Delta x = 0.1\text{cm}$, $\Delta y = 0.1\text{cm}$, $\Delta z = 0.04\text{cm}$
Time steps	$\Delta t = 1.159\text{ps}$
No. of time steps	5000

Feed lengths used for experimental study are $0.862\lambda_d$, $1.08\lambda_d$, $1.3\lambda_d$, $1.52\lambda_d$, $1.75\lambda_d$ and $1.95\lambda_d$. Same antenna configurations are analyzed theoretically. Theoretical results of the L-strip fed patch with dimension $L = 4\text{cm}$, $W = 2\text{cm}$ with different S_1 values are discussed in the following sections.

4.3.1.1 Feed length – $0.862\lambda_d$

Reflection and radiation characteristics of the antenna with S_1 as $0.862\lambda_d$ are analyzed.

(a) Reflection Characteristics

The input impedance of the antenna is computed as a ratio of the Fast Fourier transform of the voltage derived from E field, over the entire time steps, to the Fast Fourier transform of current derived from the H field values. Reflection coefficient is then computed. The reflection coefficients (S_{11}) computed numerically using FDTD is compared with the measured data. The variations of resonant frequency and bandwidth with S_2 are also studied.

The outcome of the computation of L-strip fed microstrip antenna configuration with $S_1 = 0.862\lambda_d$ are tabulated in the Table 4.2. From the table it is observed that there is good agreement between the measured and calculated data with a maximum of 1.3% error. The slight discrepancies may be due to the truncation effect of ground plane used in the calculation, due to the differences in the measured permittivity of the substrate used in the calculation or due to the thin air gap between the two substrates.

Table 4.2 Theoretical and experimental resonant frequencies with $S_1 = 0.862\lambda_d$, $h_1 = h_2 = 0.16\text{cm}$ and $\epsilon r_1 = \epsilon r_2 = 4.28$

L(cm)	W(cm)	Feed segment length (S_2/λ_d)	Resonant frequency (Theory) GHz	Resonant frequency (Experiment) GHz	%error (wrt expt)
4	2	0.108	3.197	3.205	0.249
		0.215	3.212	3.20	-0.375
		0.323	3.212	3.235	0.71
		0.431	3.18	3.205	0.93
		0.539	3.286	3.33	1.3
		0.647	3.28	3.25	-0.92
		0.754	3.302	3.31	0.30
		0.862	3.302	3.28	-0.6

Return loss variations with frequency at the maximum bandwidth configuration of the antenna obtained by theoretical calculation, and experiment are compared in Figure 4.6. The measured and computed return loss data are almost identical for both the cases. Maximum bandwidth obtained from theory is 15% (3.07GHz-3.565GHz) and that from experiment is 12.6% (3.145GHz-3.565GHz). The corresponding measured and computed resonant frequencies are 3.302 GHz and 3.31GHz respectively.

The analysis can predict the resonant frequency of the patch accurately with in error of only 0.3%. From the figures it is also evident that not only the resonant frequency and bandwidth of operation but also the general shape of the resonance characteristics can also be predicted using the analysis. Theoretical, experimental and simulated variations of resonant frequency of the antenna with feed segment lengths are shown in Figure 4.7.

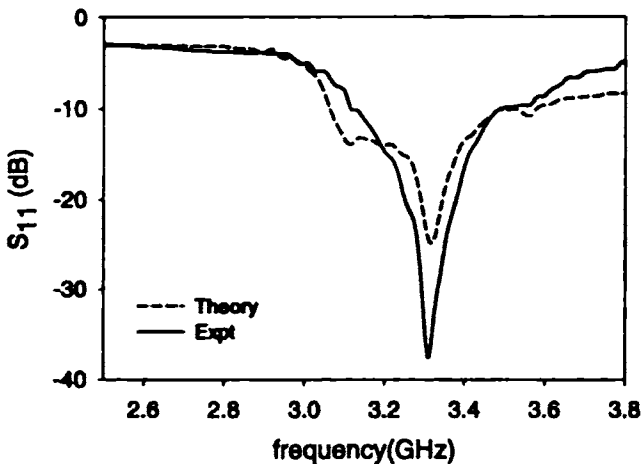


Figure 4.6 Theoretical and experimental variation of S_{11} at the maximum bandwidth position $L = 4\text{cm}$, $W = 2\text{cm}$, $S_1 = 0.862\lambda_d$, $S_2 = 0.754\lambda_d$, $d_1 = 0.258\lambda_d$, $d_2 = 0.323\lambda_d$ and $d_3 = 0.215\lambda_d$. $\Delta x = 0.1\text{ cm}$, $\Delta y = 0.1\text{cm}$, $\Delta z = .004\text{cm}$ and $\Delta t = 1.159\text{ps}$

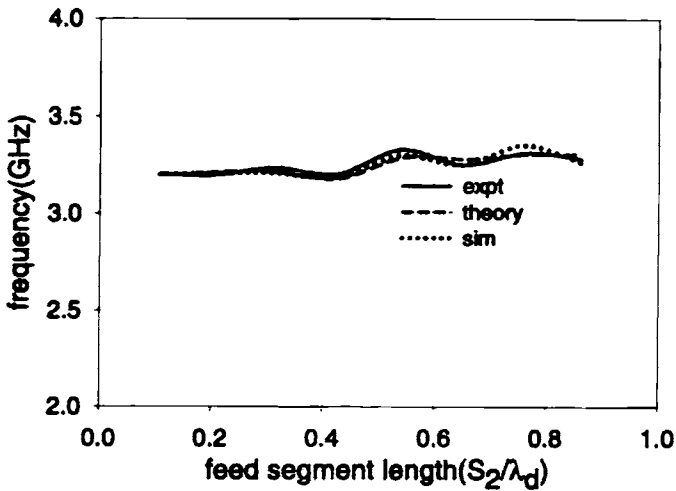


Figure 4.7 Theory, experiment and simulated resonant frequency variations of the antenna with $L = 4\text{cm}$, $W = 2\text{cm}$, $S_1 = 0.862\lambda_d$

(b) Radiation pattern

As per the theory explained in section 4.2.7, for the radiation pattern calculations a sinusoidal excitation is applied at Port 1 instead of a Gaussian pulse. The frequency of the sinusoid is selected as the resonant frequency obtained from the reflection characteristics. The entire simulation is repeated with sinusoidal excitation. The near field is calculated using equation 4.25. From the near-field data the far-field is calculated using the transformation equation 4.26. Radiation patterns obtained from theory is compared with the measured radiation patterns and is shown in Figure 4.8.

It reveals that the theoretical analysis can predict the radiation patterns of the antenna very accurately. The slight discrepancies in the cross-polarization characteristics may be attributed to some reflections from the surroundings. From the theoretical results of both reflection and radiation characteristics discussed above, it is found that the measured and computed data are in good agreement.

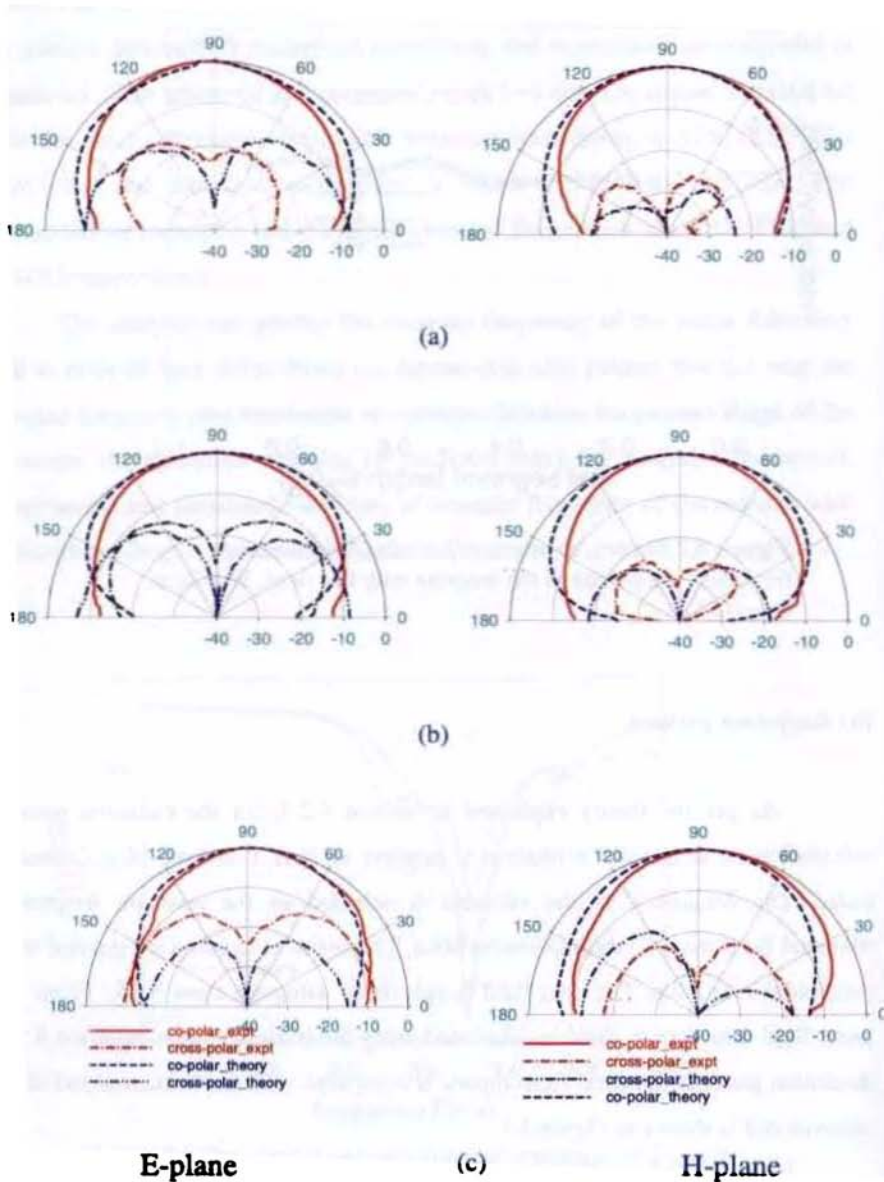


Figure 4.8 Theoretical and experimental radiation patterns of the antenna with $L=4$ cm, $W=2$ cm, $S_1=0.862\lambda_d$, $S_2=0.754\lambda_d$, $d_1=0.258\lambda_d$, $d_2=0.323\lambda_d$ and $d_3=0.215\lambda_d$.
 (a) 3 GHz (b) 3.3 GHz (c) 3.49 GHz

(c) Electric field distribution

The electric field distribution on the patch at the resonant frequency is calculated theoretically and is shown in the Figure 4.9. It shows that the antenna is excited in TM_{01} mode.

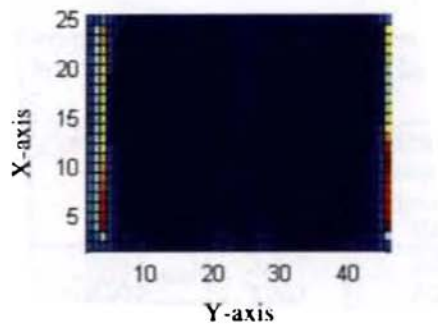


Figure 4.9. Tangential electric field distribution on the patch

(d) Input Impedance

Input impedance of the antenna is computed for the maximum bandwidth configuration theoretically. Figure 4.10 shows the experimental and theoretical impedance loci variations.

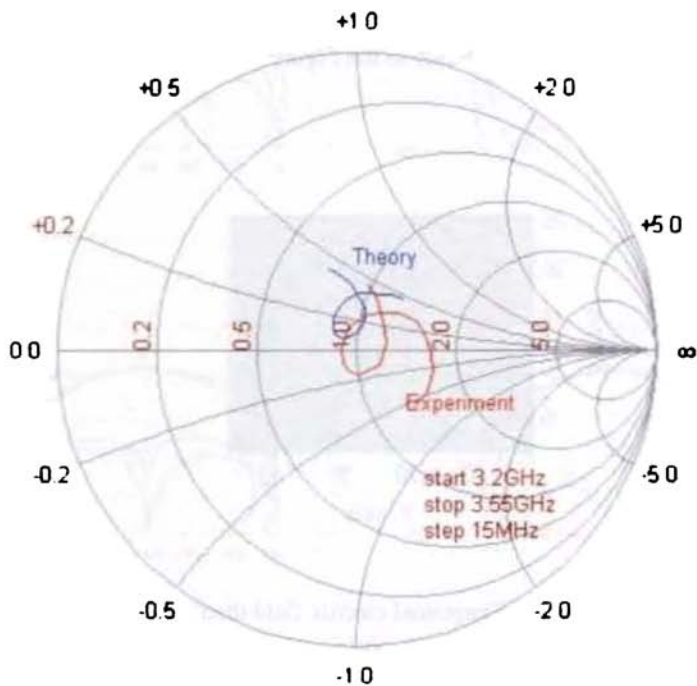


Figure 4.10 Theoretical and experimental impedance variation at the maximum bandwidth position, $L = 4\text{cm}$, $W = 2\text{cm}$, $S_1 = 0.862\lambda_d$, $S_2 = 0.754\lambda_d$, $d_1 = 0.258\lambda_d$, $d_2 = 0.323\lambda_d$ and $d_3 = 0.215\lambda_d$.

4.3.1.2 Feed length – $1.08\lambda_d$

Feed length is increased to $1.08\lambda_d$ and their effects on the antenna characteristics are analyzed using FDTD. The FDTD code parameters for the analysis are same as mentioned in Table 4.1. Reflection and radiation characteristics are studied. Theoretical results are discussed here.

(a) Reflection characteristics

Theoretical return loss and the resonant frequency variations with S_2 of the antenna are computed. The results are given in Table 4.3. It is observed that the calculated and measured data is in good agreement with a maximum error of 1.3%.

Table 4.3 Theoretical and experimental resonant frequencies with $S_1 = 1.08\lambda_d$, $h_1 = h_2 = 0.16\text{cm}$ and $\epsilon r_1 = \epsilon r_2 = 4.28$

L(cm)	W(cm)	Feed segment length (S_2/λ_d)	Resonant frequency (Theory) GHz	Resonant frequency (Experiment) GHz	%error (wrt expt)
4	2	0.108	3.207	3.25	1.3
		0.217	3.207	3.20	0.22
		0.325	3.176	3.20	0.75
		0.433	3.238	3.262	0.73
		0.542	3.238	3.245	0.2
		0.650	3.207	3.245	1.1
		0.758	3.331	3.30	0.8
		0.867	3.302	3.311	-0.6

Theoretical and experimental return loss variations with frequency at the maximum bandwidth configuration are shown in Figure 4.11. Maximum bandwidth obtained from theory for the patch of dimensions $4 \times 2\text{cm}^2$ is 15% while that from experiment is 15.8%. The measured and computed resonant frequencies are 3.31 GHz and 3.331 GHz respectively. The present analysis can predict the resonant frequency and bandwidth of operation with very good accuracy.

Resonant frequency variations of the patches for different feed segment lengths, obtained by theory, experiment and simulation are shown in Figure 4.12 and shows good agreement.

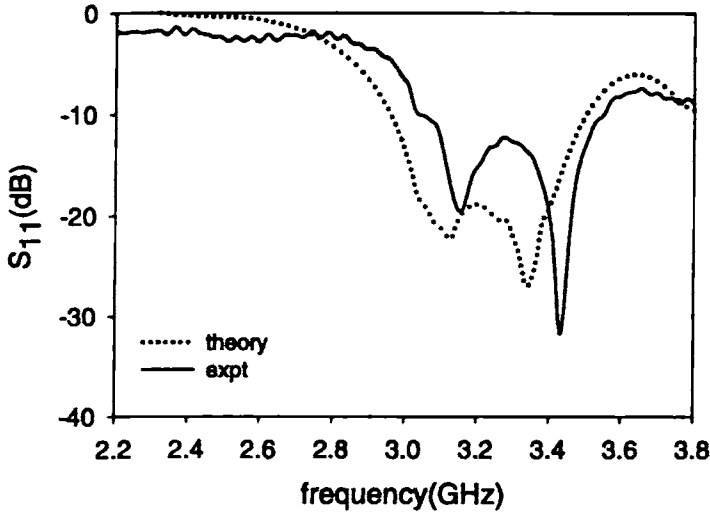


Figure 4.11 Return loss variation of the antenna with $L = 4\text{cm}$, $W = 2\text{cm}$, $S_1 = 1.08\lambda_d$, $S_2 = 0.758\lambda_d$, $d_1 = 0.26\lambda_d$, $d_2 = 0.325\lambda_d$ and $d_3 = 0.217\lambda_d$

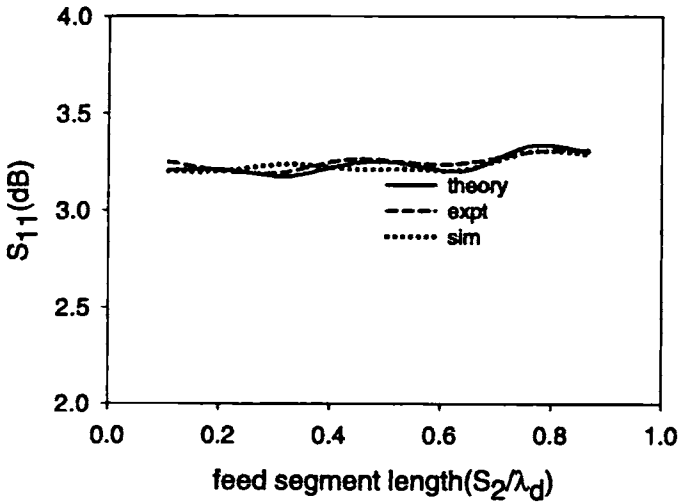


Figure 4.12 Resonant frequency variations of the L-strip fed antenna (theory, experiment and simulation) with $S_1 = 1.08\lambda_d$

(b) Radiation pattern

Radiation patterns of the antenna for this S_1 configuration are computed using the theory mentioned in earlier section. Theoretical and measured radiation patterns are shown in Figure 4.13. Figures indicate that the theoretical analysis can predict the radiation patterns of the antenna very accurately. From the theoretical results discussed above it is found that the return loss and radiation characteristics are in good agreement.

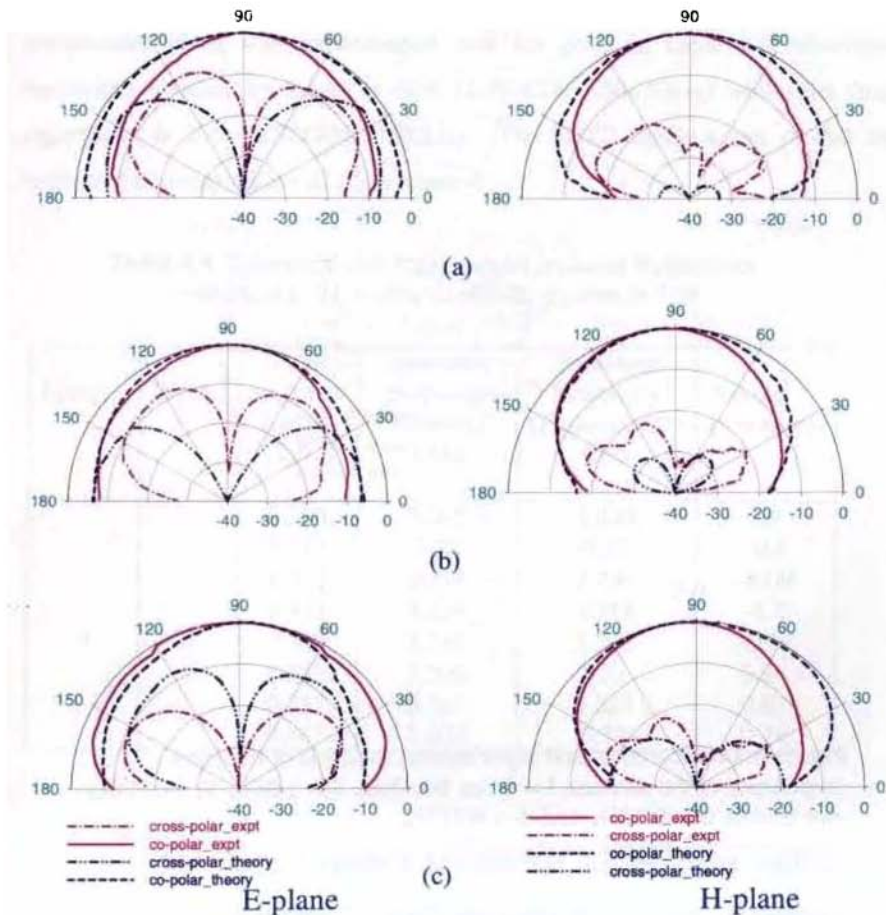


Figure 4.13 Theoretical and experimental radiation patterns of the antenna with $L=4$ cm, $W=2$ cm, $S_1=1.08\lambda_d$, $S_2=0.758\lambda_d$, $d_1=0.26\lambda_d$, $d_2=0.325\lambda_d$ and $d_3=0.217\lambda_d$

(c) Input Impedance

Input impedance of the antenna with $S_1=1.08\lambda_d$ is computed. The impedance variations along with the measured ones are shown in Figure 4.14 and are in good agreement.

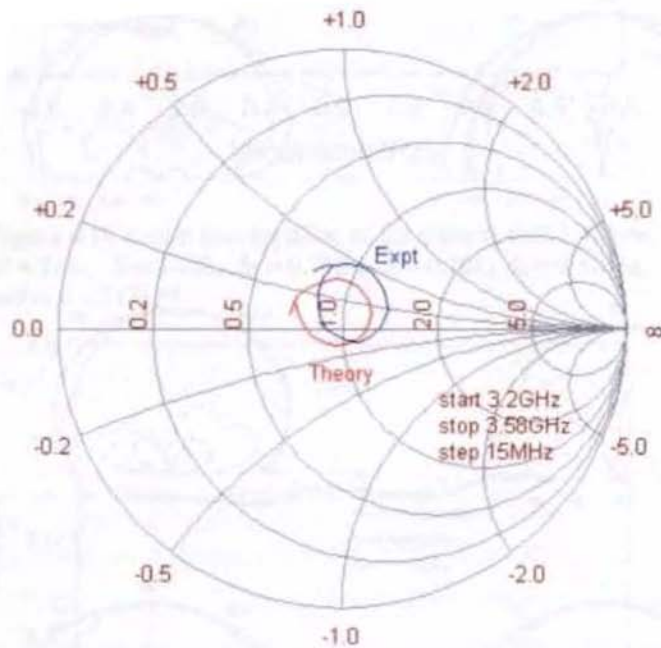


Figure 4.14 Theoretical and experimental variation of the input impedance of the antenna, $L=4\text{ cm}$, $W=2\text{ cm}$, $S_1=1.08\lambda_d$, $S_2=0.758\lambda_d$, $d_1=0.26\lambda_d$, $d_2=0.325\lambda_d$ and $d_3=0.217\lambda_d$

4.3.1.3 Feed length – $1.3\lambda_d$

S_1 value is increased to $1.3\lambda_d$ and the reflection and radiation characteristics of the antenna are studied theoretically. Theoretical results obtained from calculations for this configuration of the antenna are discussed in the following sections.

(a) Reflection characteristics

Results of the resonant frequency variations obtained by theoretical computation along with experimental ones are given in Table 4.4. Maximum bandwidth obtained by theory is 18% (2.987GHz-3.5847GHz) while that from experiment is 20% (2.98GHz-3.67GHz). The FDTD analysis can predict the resonant frequency within $\pm 1.2\%$ accuracy.

Table 4.4 Theoretical and experimental resonant frequencies
with $S_1 = 1.3\lambda_d$, $h_1 = h_2 = 0.16\text{cm}$, $\epsilon r_1 = \epsilon r_2 = 4.28$

L(cm)	W(cm)	Feed segment Length (S_2/λ_d)	Resonant frequency (Theory) GHz	Resonant frequency (Experiment) GHz	%error (wrt expt)
4	2	0.108	3.205	3.235	0.9
		0.217	3.27	3.25	-0.6
		0.325	3.238	3.235	-0.09
		0.433	3.254	3.215	-1.2
		0.542	3.255	3.231	-0.74
		0.650	3.302	3.31	0.24
		0.758	3.302	3.331	0.87
		0.867	3.302	3.32	0.54

From the tabulated results it is concluded that the theory confirms the experiments and the resonant frequency can easily be predicted. Theoretical and experimental resonant frequencies are 3.302GHz and 3.331 GHz respectively.

Return loss variations of the patch at the maximum bandwidth position are shown in Figure 4.15. Resonant frequency variations of the antenna from experiment, theory and simulations are shown in Figure 4.16 and are in good agreement.

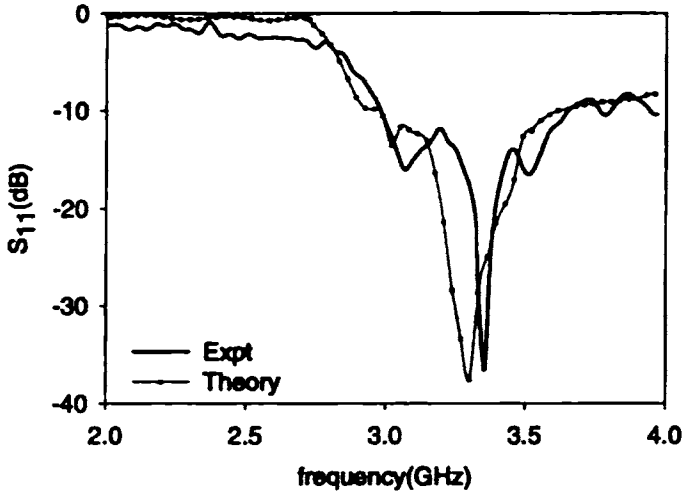


Figure 4.15 Experimental and theoretical variation of return loss at the maximum bandwidth position with $L = 4$ cm, $W = 2$ cm, $S_1 = 1.30\lambda_d$, $S_2 = 0.758\lambda_d$, $d_1 = 0.260\lambda_d$, $d_2 = 0.325\lambda_d$ and $d_3 = 0.217\lambda_d$, $\Delta x = 0.1$ cm, $\Delta y = 0.1$ cm, $\Delta z = .04$ cm and $\Delta t = 1.159$ ps

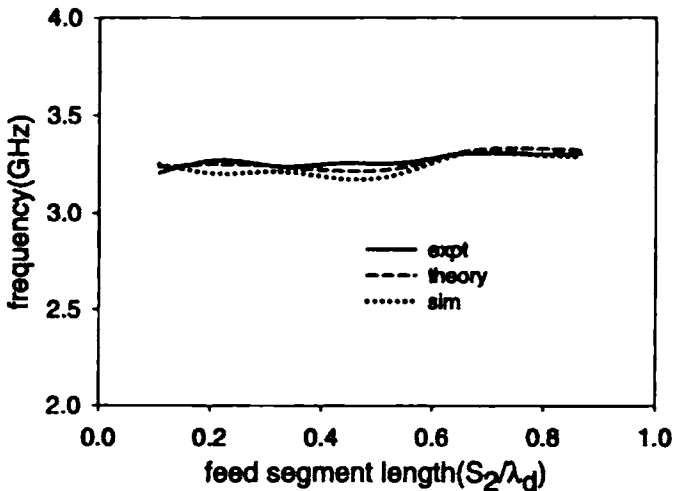


Figure 4.16 Resonant frequency variations of the antenna for different S_2 with $S_1 = 1.3\lambda_d$

(b) Radiation pattern

Theoretical and experimental radiation patterns of the antenna with $S_1 = 1.3\lambda_d$ and $S_2 = 0.758\lambda_d$ are compared in this section. Radiation patterns of the patch at different frequencies in the operating band are shown in comparison in Figure 4.17. It is found that the theory confirms the experimental results.

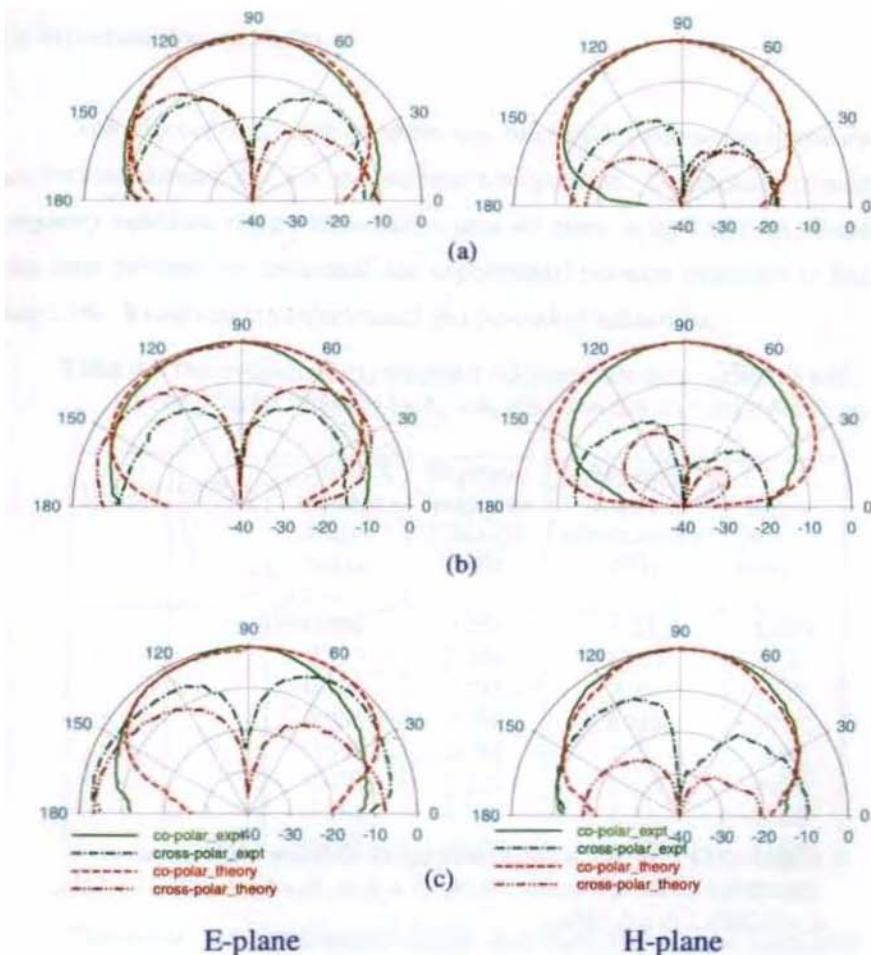


Figure 4.17 Theoretical and experimental radiation patterns of the antenna with $L = 4\text{cm}$, $W = 2\text{cm}$, $S_1 = 1.30\lambda_d$, $S_2 = 0.758\lambda_d$, $d_1 = 0.260\lambda_d$, $d_2 = 0.325\lambda_d$ and $d_3 = 0.217\lambda_d$

(a) 3 GHz (b) 3.33GHz (c) 3.58GHz

(c) Input impedance

Input impedance variation of the antenna with $S_1=1.3\lambda_d$ and $S_2 = 0.758\lambda_d$ configuration is studied theoretically. Figure 4.18 shows the measured and computed input impedance variations.

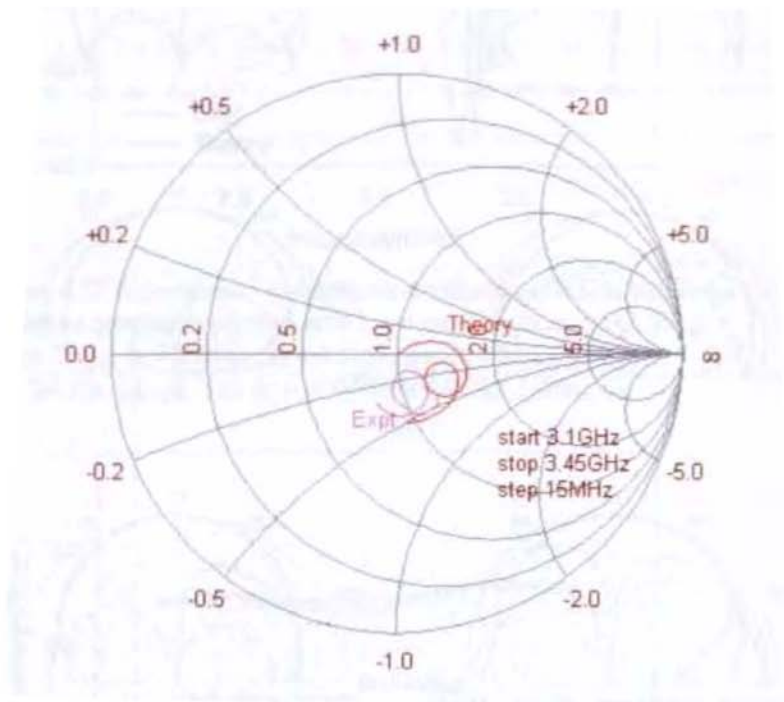


Figure 4.18 Theoretical and experimental variation of the input impedance of the antenna $L = 4\text{cm}$, $W = 2\text{cm}$, $S_1 = 1.30\lambda_d$, $S_2 = 0.758\lambda_d$, $d_1 = 0.260\lambda_d$, $d_2 = 0.325\lambda_d$

4.3.1.4 Feed length – $1.52\lambda_d$

Feed length of the L-strip is further increased to $1.52\lambda_d$ and its effects on antenna characteristics are studied theoretically. Reflection and radiation characteristics of this antenna configuration are discussed in the following sections.

(a) Reflection characteristics

The effect of feed length on return loss, bandwidth and resonant frequency are verified theoretically for the antenna configuration. Theoretical resonant frequency variations along with measured ones are given in the Table 4.5. Worst case error between the theoretical and experimental resonant frequency is less than 1.4%. It confirms the experimental and theoretical validations.

Table 4.5 Theoretical and experimental resonant frequency variations with $S_1 = 1.52\lambda_d$ for different S_2 , $h_1 = h_2 = 0.16\text{cm}$ and $\epsilon r_1 = \epsilon r_2 = 4.28$

L(cm)	W(cm)	Feed segment length (S_2/λ_d)	Resonant frequency (Theory) GHz	Resonant frequency (Experiment) GHz	%error (wrt expt)
4	2	0.108	3.265	3.28	0.457
		0.217	3.226	3.265	1.1
		0.325	3.357	3.31	-1.4
		0.433	3.265	3.295	0.91
		0.542	3.226	3.26	1.04
		0.650	3.212	3.205	-0.22
		0.758	3.351	3.33	-0.63
		0.867	3.31	3.34	0.89

Theoretical and experimental return loss variations at the maximum bandwidth position for this patch are shown in Figure 4.19. Theoretically the antenna offered a bandwidth of 17% (3.050GHz-3.663GHz) while the measured value is 19% (3.04GHz-3.685GHz). Theoretical and experimental return curves

are in found to be in good match. Figure 4.20 shows the variations in resonant frequency with S_2 . From the figure it is clear that the frequency variations are identical.

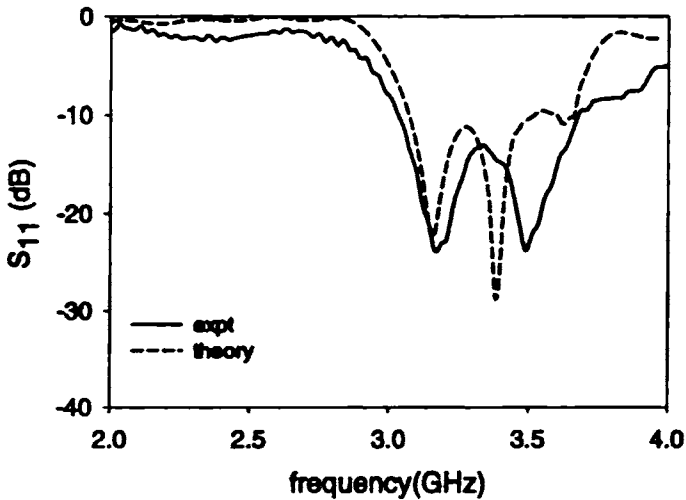


Figure 4.19 Theoretical and experimental return loss variations with frequency with $L = 4\text{cm}$, $W = 2\text{cm}$, $S_1 = 1.52\lambda_d$, $S_2 = 0.758\lambda_d$, $d_1 = 0.260\lambda_d$, $d_2 = 0.325\lambda_d$ and $d_3 = 0.217\lambda_d$.

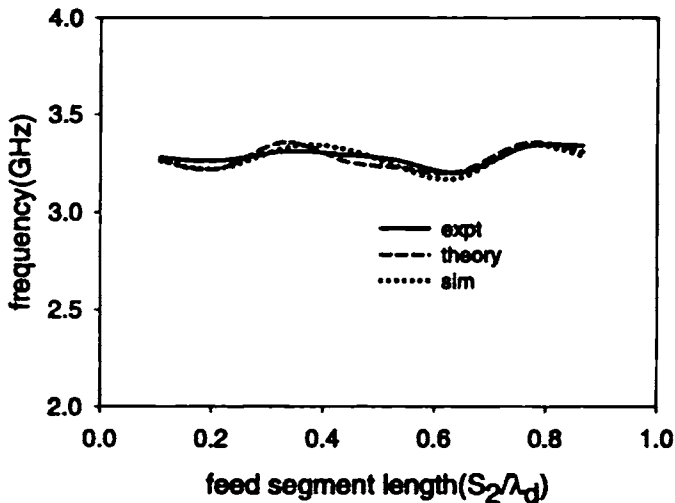


Figure 4.20 Resonant frequency variations obtained by theory, experiment and simulation of the patch $L = 4\text{cm}$, $W = 2\text{cm}$

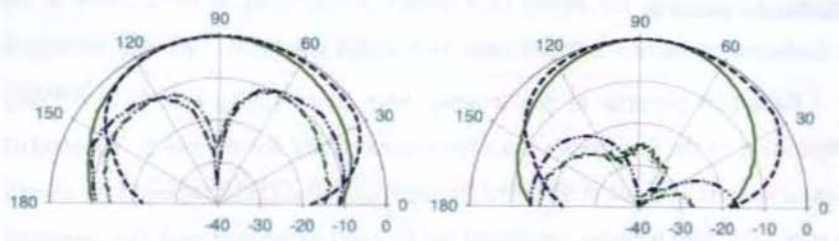
(b) Radiation pattern

Radiation patterns of the antenna with $S_1 = 1.52\lambda_d$ and $S_2 = 0.758\lambda_d$ configuration of the L-strip are calculated numerically for the patch. Theoretical and experimental patterns at different frequencies in the operating band are shown in Figure 4.21. The patterns calculated are in good agreement with the measured ones.

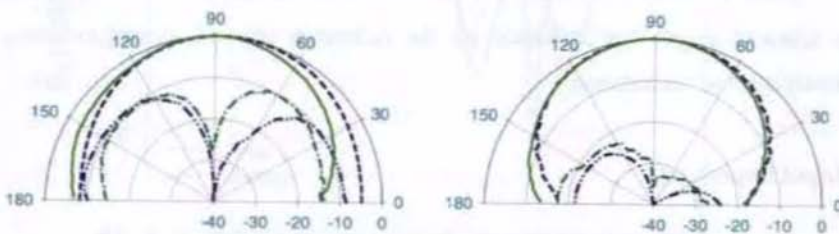
From the theoretical results, it can be concluded that the feed length and feed segment length has influence on the reflection as well as the radiation characteristics of the antenna.

(c) Input impedance

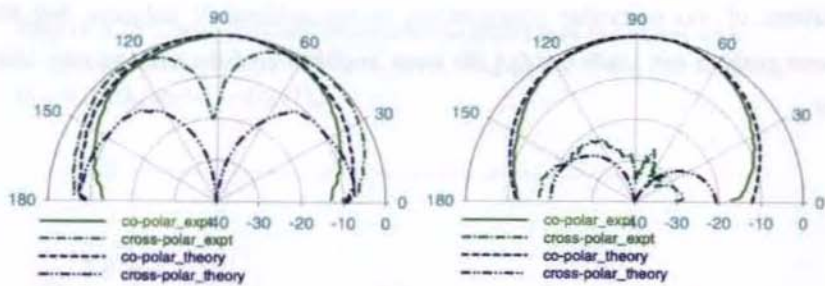
Input impedance variation of the antenna with the feed length $1.52\lambda_d$ is studied theoretically. Figure 4.22 shows the measured and computed input impedance variations of this particular configuration of the antenna. It indicates that the present analysis can easily predict the input impedance of the antenna with least error.



(a)



(b)



E-plane

(c)

H-plane

Figure 4.21 Theoretical and experimental radiation patterns of the antenna with $L = 4\text{cm}$, $W = 2\text{cm}$, $S_1 = 1.52\lambda_d$, $S_2 = 0.758\lambda_d$, $d_1 = 0.260\lambda_d$, $d_2 = 0.325\lambda_d$ and $d_3 = 0.217\lambda_d$.

(a) 3GHz

(b) 3.336GHz

(c) 3.55 GHz

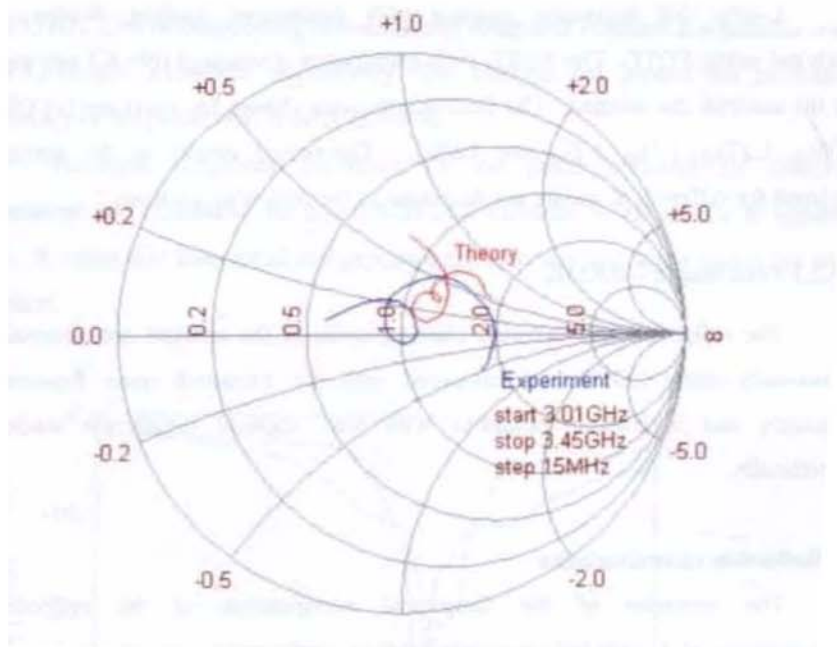


Figure 4.22 Theoretical and experimental variation of the input impedance of the antenna, $L = 4\text{cm}$, $W = 2\text{cm}$, $S_1 = 1.52\lambda_d$, $S_2 = 0.758\lambda_d$, $d_1 = 0.260\lambda_d$, $d_2 = 0.325\lambda_d$ and $d_3 = 0.217\lambda_d$.

4.3.2 Microstrip antenna – 3.2GHz

L-strip fed microstrip antenna with dimensions $L=3\text{cm}$, $W=2\text{cm}$ is analyzed using FDTD. The FDTD code parameters given in Table 4.1 are used for the analysis the antenna. The feed length value chosen for study are $0.833\lambda_d$, $1.06\lambda_d$, $1.27\lambda_d$, $1.5\lambda_d$, $1.7\lambda_d$ and $1.85\lambda_d$. Theoretical results of the antenna obtained for different S_1 values are discussed in the following sections.

4.3.2.1 Feed length – $0.833\lambda_d$

The reflection and radiation characteristics of the antenna are computed numerically using FDTD and compared with the measured ones. Resonant frequency and bandwidth variations with feed segment length are studied theoretically.

(a) Reflection characteristics

The outcome of the theoretical computation of the reflection characteristics of L-strip fed microstrip antenna configuration are tabulated in the Table 4.6. Table shows good agreement between the measured and calculated data with a maximum error of 0.93%.

Table 4.6 Theoretical and experimental resonant frequencies with $S_1 = 0.833\lambda_d$, $h_1 = h_2 = 0.16\text{cm}$ and $\epsilon r_1 = \epsilon r_2 = 4.28$

L(cm)	W(cm)	Feed segment length (S_2/λ_d)	Resonant frequency (Theory) GHz	Resonant frequency (Experiment) GHz	%error (wrt expt)
3	2	0.105	3.199	3.205	0.187
		0.209	3.172	3.16	-0.379
		0.314	3.195	3.205	0.286
		0.419	3.186	3.175	-0.346
		0.524	3.2	3.19	-0.313
		0.628	3.23	3.22	-0.31
		0.734	3.159	3.13	-0.926
		0.838	3.22	3.24	0.617

Return loss variation of the patch at the maximum bandwidth configuration is shown in Figure 4.23. Theoretically, the antenna offered a maximum bandwidth of 11.4% (2.956GHz-3.3174GHz) while measured value is 13% (3.04GHz-3.450GHz). The corresponding measured and computed resonant frequencies are 3.13 GHz and 3.159GHz respectively. The analysis can predict the resonant frequency of the patch with in error of 0.3%.

Resonant frequency variations of the patch obtained by theory, experiment and simulation for $S_1 = 0.833\lambda_d$ for different S_2 are shown in Figure 4.24. It seems that theoretical and experimental resonant frequency variations are identical.

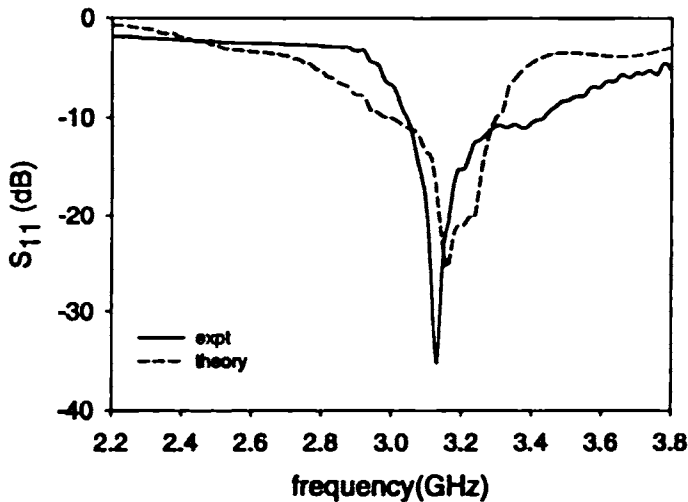


Figure 4.23 Theoretical and experimental variation of S_{11} at the maximum bandwidth position $L = 3\text{cm}$, $W = 2\text{cm}$, $S_1 = 0.838\lambda_d$, $S_2 = 0.734\lambda_d$, $d_1 = 0.146\lambda_d$, $d_2 = 0.209\lambda_d$, $d_3 = 0.314\lambda_d$, $\Delta x = 0.1\text{ cm}$, $\Delta y = 0.1\text{cm}$, $\Delta z = .0.04\text{cm}$ and $\Delta t = 1.159\text{ps}$

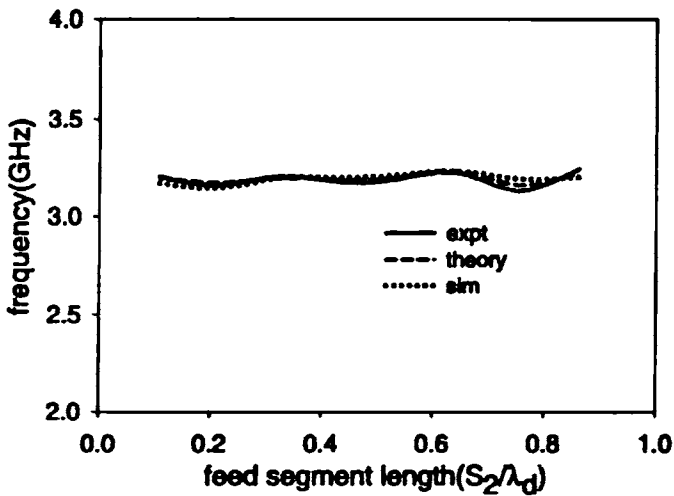


Figure 4.24 Theoretical, experimental and simulation resonant frequency variations of the antenna, with $L = 3\text{cm}$, $W = 2\text{cm}$, $S_1 = 0.833\lambda_d$

(b) Radiation pattern

Radiation patterns of the optimum bandwidth configuration antenna are computed. Theoretical radiation patterns at different frequencies in the operating band are compared with the measured ones and are shown in Figure 4.25. Excellent agreement between theory and experiment is obtained.

From the theoretical results of both reflection and radiation characteristics discussed above, it is found that the measured and computed data are in good agreement.

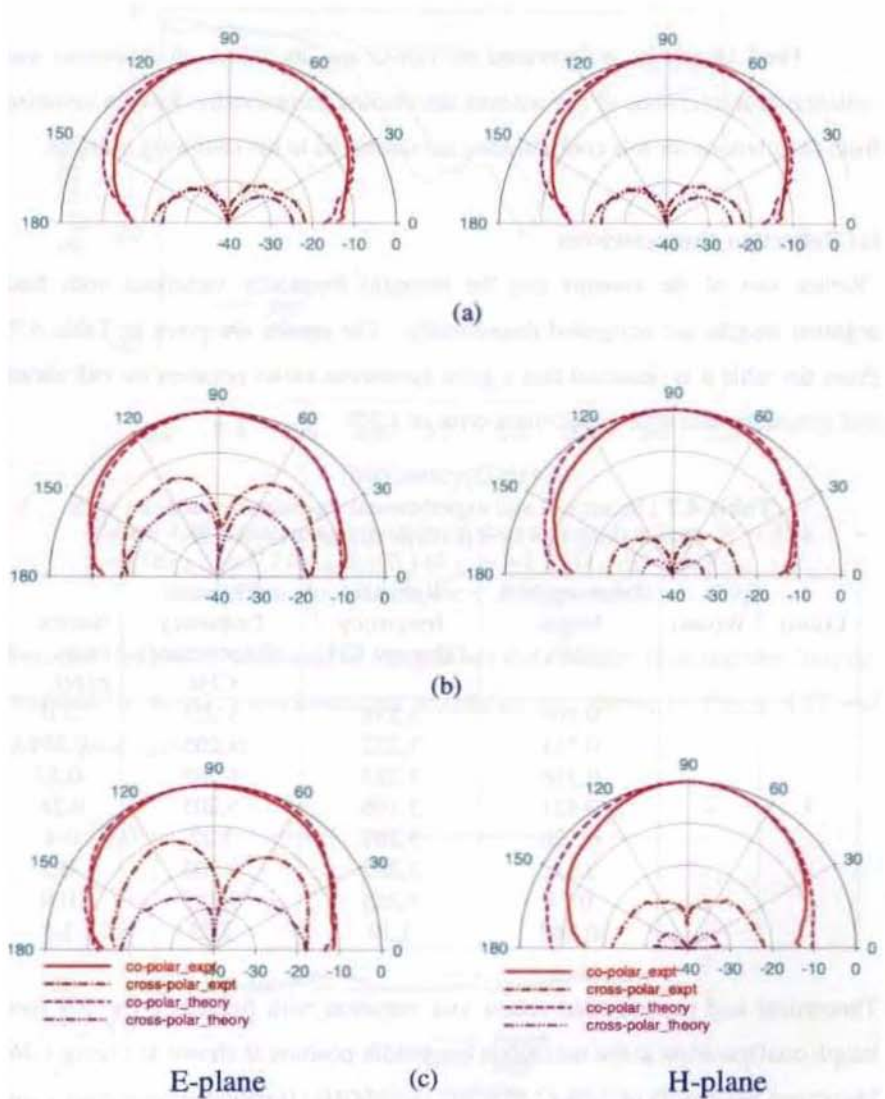


Figure 4.25 Theoretical and experimental radiation patterns of the L-strip fed antenna at different frequencies with $L = 3\text{cm}$, $W = 2\text{cm}$, $S_1 = 0.833\lambda_d$, $S_2 = 0.734\lambda_d$, $d_1 = 0.146\lambda_d$, $d_2 = 0.209\lambda_d$, $d_3 = 0.314\lambda_d$
 (i) 3.1GHz (ii) 3.235GHz (iii) 3.34GHz

4.2.3.2 Feed length – $1.06\lambda_d$

Feed length S_1 is increased to $1.06\lambda_d$ and its effect on reflection and radiation characteristics of the antenna are studied theoretically. Results obtained from calculations for this configuration are discussed in the following sections.

(a) Reflection characteristics

Return loss of the antenna and the resonant frequency variations with feed segment lengths are computed theoretically. The results are given in Table 4.7. From the table it is observed that a good agreement exists between the calculated and measured data with a maximum error of 1.5%.

Table 4.7 Theoretical and experimental resonant frequencies with $S_1 = 1.06\lambda_d$, $h_1 = h_2 = 0.16\text{cm}$ and $\epsilon r_1 = \epsilon r_2 = 4.28$

L(cm)	W(cm)	Feed segment length (S_2/λ_d)	Resonant frequency (Theory) GHz	Resonant frequency (Experiment) GHz	%error (wrt expt)
3	2	0.105	3.238	3.205	-1.0
		0.211	3.222	3.205	-0.379
		0.316	3.285	3.265	-0.53
		0.421	3.196	3.205	0.28
		0.526	3.207	3.22	0.4
		0.632	3.207	3.205	-0.2
		0.74	3.265	3.235	-0.9
		0.842	3.30	3.25	-1.5

Theoretical and experimental return loss variation with frequency for this feed length configuration at the maximum bandwidth position is shown in Figure 4.26. Maximum bandwidth of 14% (2.925GHz -3.385GHz) is obtained from theory and while from the experiment it is 18.12% (2.845-3.43GHz). The measured and computed resonant frequencies are 3.265 GHz and 3.235 GHz respectively. The present analysis can predict the resonant frequency and bandwidth of operation with very good accuracy. Moreover, the overall shape of the resonance curve in theory and experiment are also in good agreement.

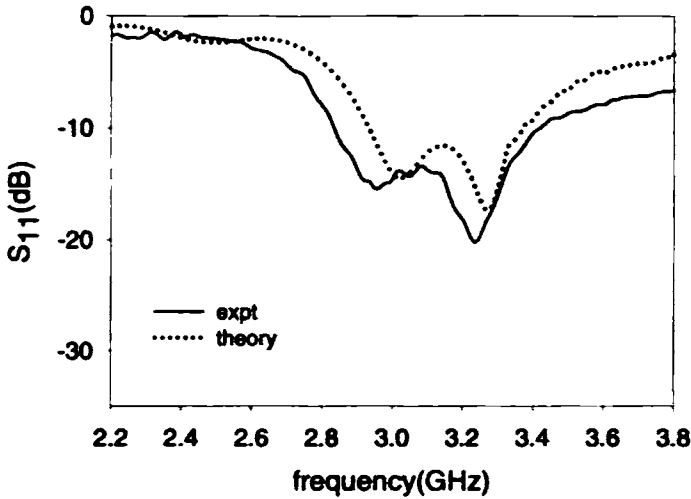
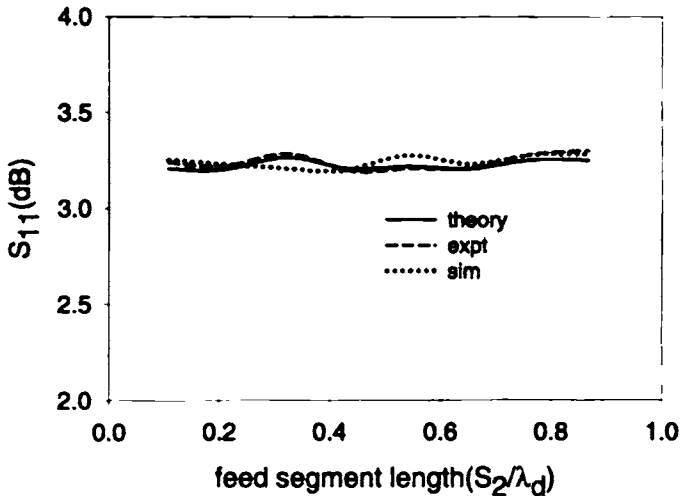


Figure 4.26 Return loss variation of the antenna, $L = 3\text{cm}$, $W = 2\text{cm}$, $S_1 = 1.06\lambda_d$, $S_2 = 0.746\lambda_d$, $d_1 = 0.148\lambda_d$, $d_2 = 0.254\lambda_d$, $d_3 = 0.336\lambda_d$, $\Delta x = 0.1\text{ cm}$, $\Delta y = 0.1\text{cm}$, $\Delta z = .004\text{cm}$ and $\Delta t = 1.159\text{ps}$

Resonant frequency variations of the patches for different feed segment lengths, obtained by theory, experiment and simulation are shown in Figure 4.27 and shows good agreement.



(b) Radiation pattern

Theoretical and measured radiation patterns for this configuration are shown in Figure 4.28. Figures reveal that the theoretical analysis can predict the radiation patterns of the antenna very accurately. From the results discussed above it is found that the return loss and radiation characteristics are in good agreement.

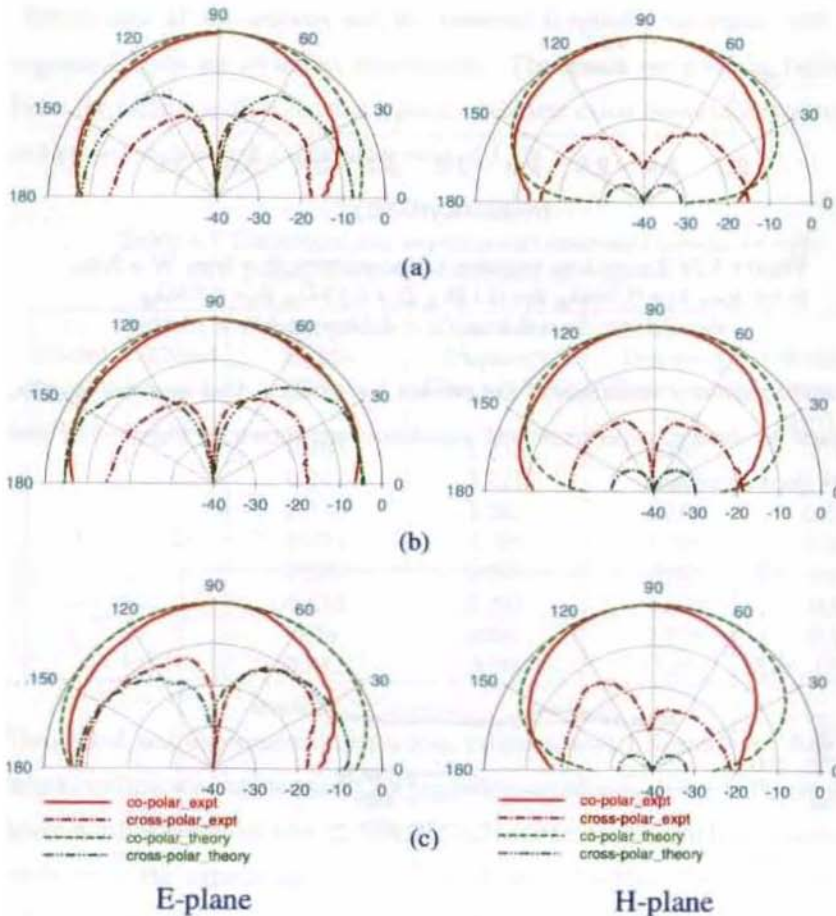


Figure 4.28 Theoretical and experimental radiation patterns of the antenna with $L = 3$ cm, $W = 2$ cm, $S_1 = 1.06\lambda_d$, $S_2 = 0.746\lambda_d$, $d_1 = 0.148\lambda_d$, $d_2 = 0.254\lambda_d$, $d_3 = 0.336\lambda_d$
 (a) 2.9 GHz (b) 3.25 GHz (c) 3.4 GHz

4.3.2.3 Feed length – $1.27\lambda_d$

Feed length of the L-strip increased to $1.27\lambda_d$ and its effect on the antenna characteristics are studied theoretically. Reflection and radiation characteristics of the antenna are analyzed. Results are discussed in the following sections.

(a) Reflection characteristics

Resonant frequency and return loss variations of the antenna with S_1 as $1.27\lambda_d$ for different S_2 are studied. Resonant frequency variations are given in Table 4.8. From the table it is clear that the worst case error is less than 2%. It confirms the experimental results are in agreement with those predicted by theory. Maximum bandwidth obtained with $S_1 = 1.27\lambda_d$ from theory is 11.25% (3.094GHz-3.463GHz) while that from experiment is 14.25% (3.025Hz-3.49GHz). Theoretical and experimental resonant frequencies are 3.278 GHz and 3.254 GHz respectively. Theoretical and experimental return loss variations at the maximum bandwidth position are shown in Figure 4.29. Resonant frequency variations are shown in Figure 4.30.

Table 4.8 Theoretical and experimental resonant frequencies with $S_1 = 1.27\lambda_d$, $h_1 = h_2 = 0.16\text{cm}$ and $\epsilon r_1 = \epsilon r_2 = 4.28$

L(cm)	W(cm)	Feed segment Length (S_2/λ_d)	Resonant frequency (Theory) GHz	Resonant frequency (Experiment) GHz	%error (wrt expt)
3	2	0.106	3.12	3.16	1.2
		0.212	3.133	3.145	0.38
		0.312	3.159	3.19	0.97
		0.423	3.196	3.205	0.28
		0.529	3.207	3.205	-0.06
		0.635	3.207	3.22	0.4
		0.74	3.278	3.254	-0.74
		0.846	3.212	3.26	-1.4

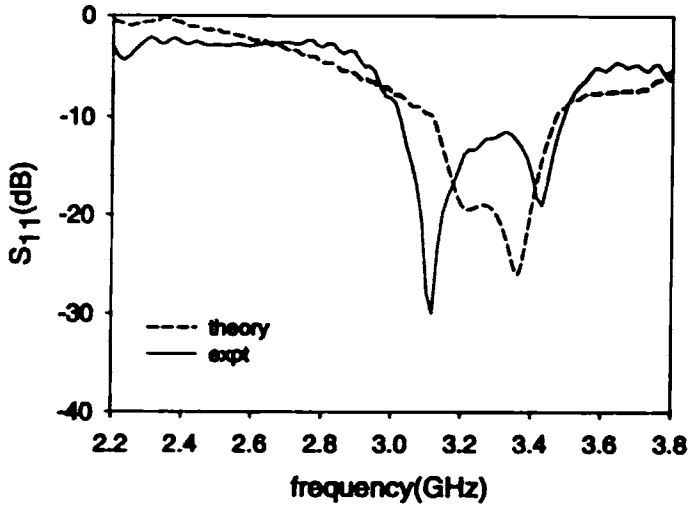


Figure 4.29 Experimental and theoretical return loss variations with frequency, $L = 3 \text{ cm}$, $W = 2 \text{ cm}$, $S_1 = 1.27\lambda_d$, $S_2 = 0.74\lambda_d$, $d_1 = 0.148\lambda_d$, $d_2 = 0.275\lambda_d$ and $d_3 = 0.275\lambda_d$, $\Delta x = 0.1 \text{ cm}$, $\Delta y = 0.1 \text{ cm}$, $\Delta z = .004 \text{ cm}$ and $\Delta t = 1.159 \text{ ps}$

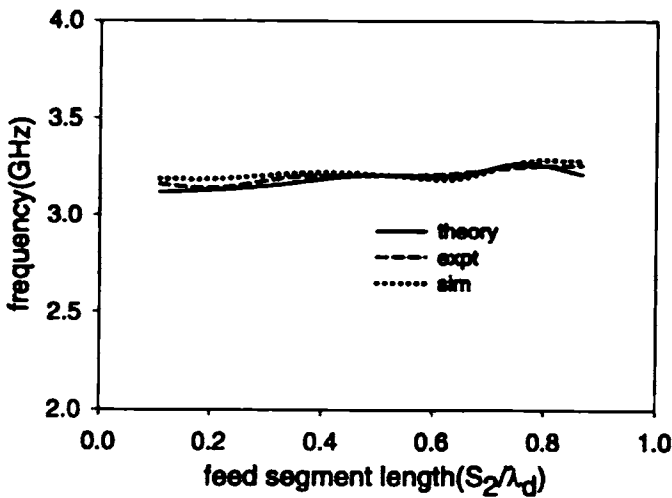


Figure 4.30 Resonant frequency variations of the antenna (experiment, theory and simulation) for S_2 with $S_1 = 1.27\lambda_d$

(b) Radiation pattern

Radiation patterns of the antenna with $S_1=1.27\lambda_d$ and $S_2 = 0.74\lambda_d$ configuration is studied theoretically for different frequencies in the operating band. Experimental and theoretical radiation patterns are shown in Figure 4.31. Except with the discrepancies in the cross-polar patterns all other features of the patterns are in good agreement.

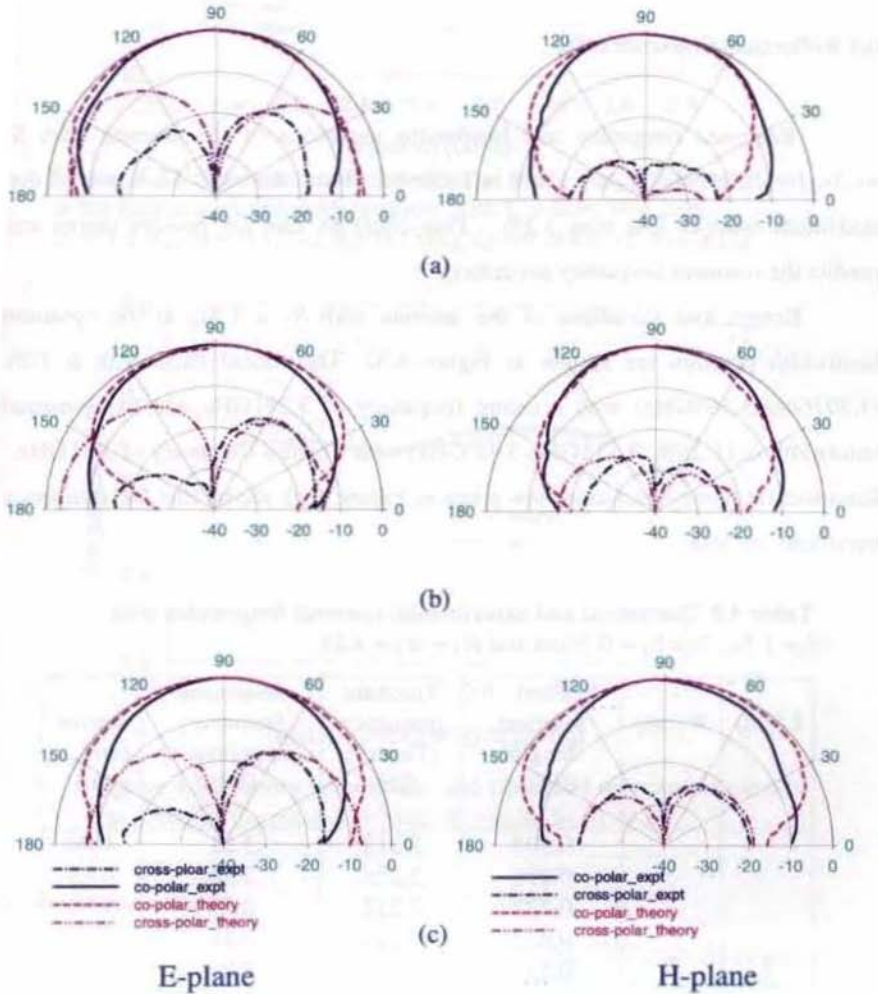


Figure 4.31 Theoretical and experimental radiation patterns of the antenna, $L = 3\text{cm}$, $W = 2\text{cm}$, $S_1 = 1.27\lambda_d$, $S_2 = 0.74\lambda_d$, $d_1 = 0.148\lambda_d$, $d_2 = 0.275\lambda_d$ and $d_3 = 0.275\lambda_d$ (a) 3.1 GHz (b) 3.275GHz (c) 3.45GHz

4.2.3.4 Feed length – $1.5\lambda_d$

Feed length is further increased to $1.5\lambda_d$ to compute the effect of feed length on the antenna characteristics theoretically. Reflection and radiation characteristics of the antenna are studied theoretically and presented in the following parts.

(a) Reflection characteristics

Resonant frequency and bandwidth variations of the antenna with $S_1 = 1.5\lambda_d$ for different S_2/λ_d are given in Table 4.9. From the table it is observed that maximum error is less than 1.2%. This confirms that the present theory can predict the resonant frequency accurately.

Return loss variations of the antenna with $S_1 = 1.5\lambda_d$ at the optimum bandwidth position are shown in Figure 4.32. Theoretical bandwidth is 10% (3.207GHz-3.569GHz) with a centre frequency of 3.291GHz and experimental bandwidth is 11.25% (3.115GHz-3.49 GHz) with a centre frequency of 3.31GHz. Resonant frequency variations are given in Figure 4.33 shows that the frequency variations are less.

Table 4.9 Theoretical and experimental resonant frequencies with $S_1 = 1.5\lambda_d$, $h_1 = h_2 = 0.16\text{cm}$ and $\epsilon_{r1} = \epsilon_{r2} = 4.28$

L(cm)	W(cm)	Feed segment length (S_2/λ_d)	Resonant frequency (Theory) GHz	Resonant frequency (Experiment) GHz	%error (wrt expt)
3	2	0.108	3.212	3.21	-0.06
		0.216	3.226	3.24	0.43
		0.325	3.212	3.22	0.25
		0.433	3.196	3.16	-1.1
		0.541	3.265	3.28	0.46
		0.649	3.302	3.31	0.24
		0.757	3.291	3.32	0.57
		0.866	3.212	3.25	1.17

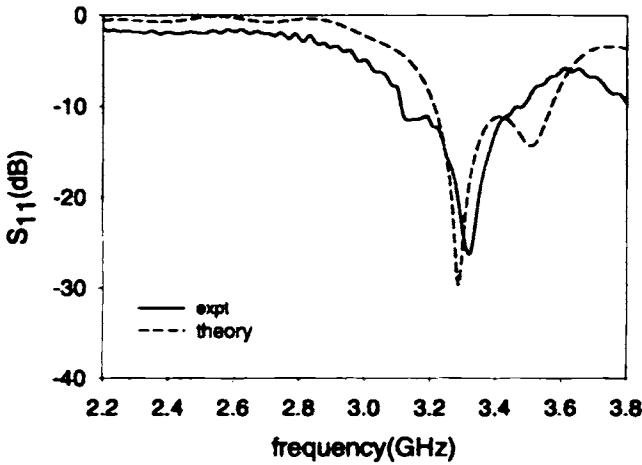


Figure 4.32 Theoretical and experimental return loss variations at the maximum bandwidth position, with $L = 3\text{cm}$, $W = 2\text{cm}$, $S_1 = 1.51\lambda_d$, $S_2 = 0.757\lambda_d$, $d_1 = 0.158\lambda_d$, $d_2 = 0.281\lambda_d$, $d_3 = 0.281\lambda_d$

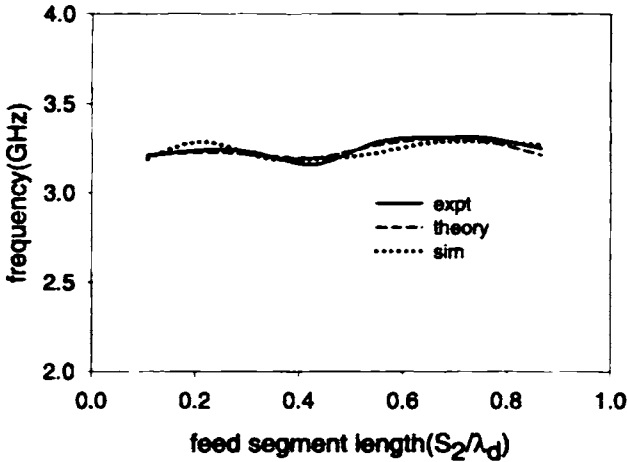


Figure 4.33 Theory, experiment and simulated resonant frequency variations of the patch $L = 3\text{cm}$, $W = 2\text{cm}$, $S_1 = 1.5\lambda_d$

(b) Radiation pattern

Radiation patterns of the optimum bandwidth configuration of the antenna are calculated numerically. Theoretical and experimental patterns at different frequencies in the operating band are shown in Figure 4.34. The patterns calculated

are in good agreement with the measured ones. The discrepancies in the cross-polar levels may be due to the ground reflections.

It can be concluded that the theoretical results support the experimental observations that feed length and feed segment length has influence on the reflection as well as the radiation characteristics of the antenna.

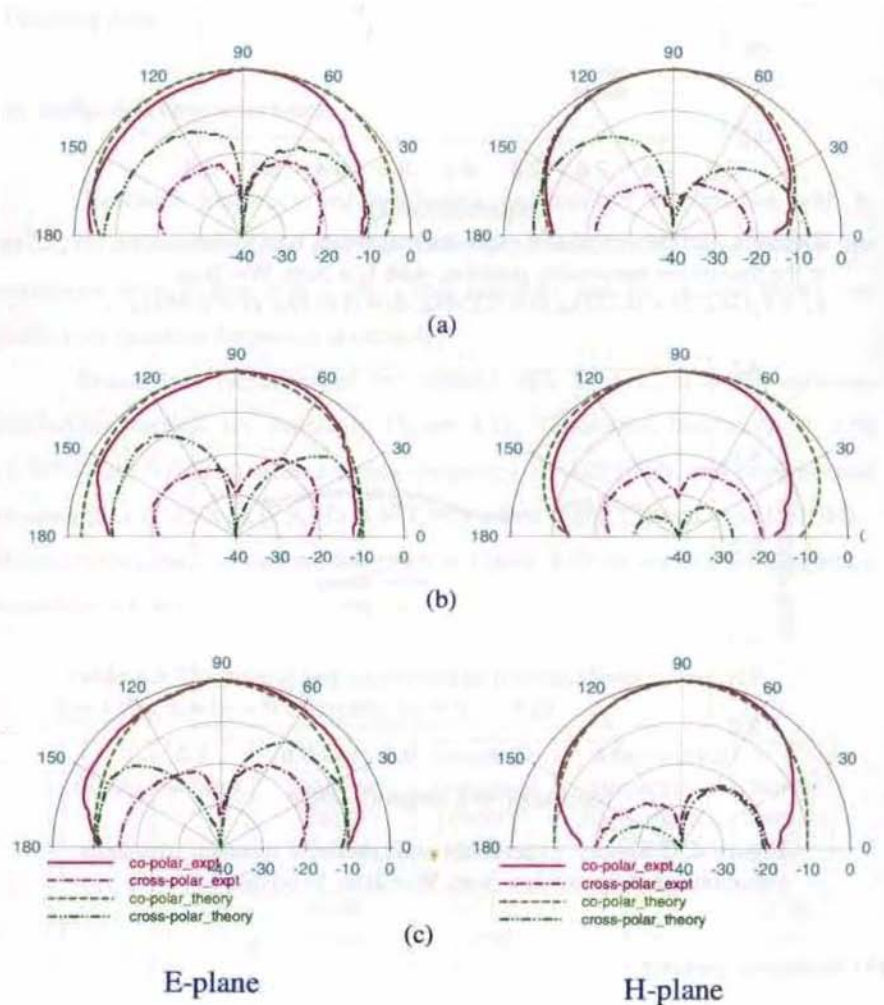


Figure 4.34 Theoretical and experimental radiation patterns of the antenna with $L = 3\text{cm}$, $W = 2\text{cm}$, $S_1 = 1.51\lambda_d$, $S_2 = 0.757\lambda_d$, $d_1 = 0.158\lambda_d$, $d_2 = 0.281\lambda_d$, and $d_3 = 0.281\lambda_d$
 (a) 3.1 GHz (b) 3.235GHz (c) 3.38GHz

4.3.3 Effect of permittivity on bandwidth

Experimental observations discussed in Chapter 3 reveal that permittivity of the patch substrate can also influence the resonant frequency and the bandwidth of the antenna. This section discusses the computed results of the effect of permittivity on the antenna characteristics such as resonant frequency and bandwidth. Patch with size $L \times W = 3.2 \times 2.6 \text{ cm}^2$, resonating at 3.3GHz is fabricated on a substrate having permittivity 2.2, which is fed by L-strip feed fabricated on a substrate having permittivity 4.28 is analyzed using the theory. Theoretical study is repeated for different feed lengths.

(a) Feed length – $0.862\lambda_d$

Return loss characteristics of the antenna with S_1 as $0.862\lambda_d$ is studied theoretically. Experimental and theoretical resonant frequency variations are given in Table 4.10. Return loss variations of the antenna at the maximum bandwidth position are shown in Figure 4.35. Theoretically 5.5% bandwidth is obtained while experimentally it is 6%. It is also evident from the table for the worst case the maximum percentage error in the predicted resonant frequency is 1.2%.

Table 4.10 Theoretical and experimental resonant frequency variations with $S_1 = 0.862\lambda_d$, $\epsilon_{r1} = 4.28$, $h_1 = 0.16 \text{ cm}$ and $\epsilon_{r2} = 2.2$, $h_2 = 0.08 \text{ cm}$

L(cm)	W(cm)	Feed segment length (S_2/λ_d)	Resonant frequency (Theory) GHz	Resonant frequency (Experimental) GHz	%error (wrt expt)
3.2	2.6	0.108	3.265	3.28	0.457
		0.215	3.205	3.19	-0.47
		0.323	3.207	3.18	-0.85
		0.431	3.270	3.295	0.76
		0.539	3.226	3.235	0.278
		0.647	3.212	3.235	0.711
		0.754	3.238	3.235	-0.09
		0.862	3.226	3.265	1.2

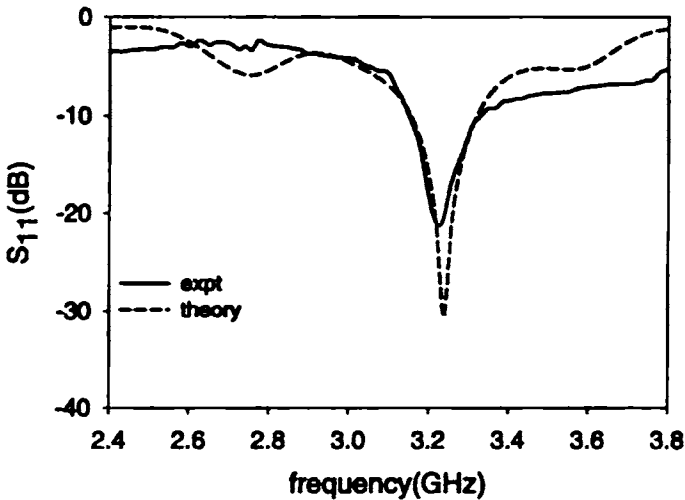


Figure 4.35 Return loss variation of the antenna with
 $S_1 = 0.862\lambda_d$, $S_2 = 0.548\lambda_d$, $\epsilon_{r1} = 4.28$, $h_1 = 0.16\text{cm}$
 $L = 3.2\text{cm}$, $W = 2.6\text{cm}$, $\epsilon_{r2} = 2.2$, $h_2 = 0.08\text{cm}$

(b) Feed length – $1.08\lambda_d$

Feed length of the L-strip is increased to $1.08\lambda_d$ and the reflection characteristics of the antenna are studied. Experiments are repeated with the same patch. Measured and computed resonant frequency variations are given in Table 4.11 and shows good agreement. The maximum percentage error is 1.5%. Return loss variations at the maximum bandwidth position are shown in Figure 4.36. 9.1% bandwidth is obtained from theory while 8.8% bandwidth is obtained from experiment. The measured and computed data are in good agreement.

Table 4.11 Theoretical and experimental resonant frequency variations
 $S_1 = 1.08\lambda_d$, $\epsilon_{r1} = 4.28$, $h_1 = 0.16\text{cm}$ and $\epsilon_{r2} = 2.2$, $h_2 = 0.08\text{cm}$

L(cm)	W(cm)	Feed segment length (S_2/λ_d)	Resonant frequency (Theory) GHz	Resonant frequency (Experiment) GHz	%error (wrt expt)
3.2	2.6	0.108	3.225	3.265	1.2
		0.217	3.27	3.25	-0.62
		0.325	3.192	3.175	-0.54
		0.433	3.270	3.265	-0.15
		0.542	3.317	3.37	1.5
		0.650	3.225	3.265	1.2
		0.758	3.286	3.315	0.87
		0.867	3.226	3.2	-0.81

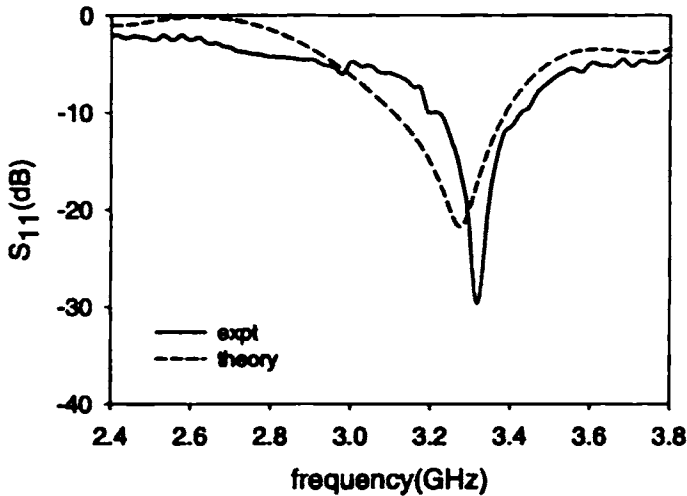


Figure 4.36 Return loss variation of the antenna with $S_1 = 1.08\lambda_d$,
 $S_2 = 0.642\lambda_d$, $\epsilon_{r1} = 4.28$, $h_1 = 0.16\text{cm}$, $L = 3.2\text{cm}$, $W = 2.6\text{cm}$, $\epsilon_{r2} = 2.2$,
 $h_2 = 0.08\text{cm}$, $\Delta x = 0.1\text{cm}$, $\Delta y = 0.1\text{cm}$, $\Delta z = 0.04\text{cm}$ and $\Delta t = 1.159\text{ps}$

(c) Feed length $-1.3\lambda_d$

To find an optimum bandwidth when the feed and patch are fabricated on substrates with different permittivity the feed length is increased to $1.3\lambda_d$ and analyzed theoretically. Reflection characteristics of the antenna is studied and verified theoretically. Results are given in Table 4.12 and shows good agreement. Return loss variations at the maximum bandwidth position are shown in Figure 4.37. Theoretical and experimental bandwidths obtained are 6.14% and 7.7% respectively.

Table 4.12 Theoretical and experimental resonant frequency with $S_1 = 1.3\lambda_d$, $\epsilon_{r1} = 4.28$, $h_1 = 0.16\text{cm}$ and $\epsilon_{r2} = 2.2$, $h_2 = 0.08\text{cm}$

L(cm)	W(cm)	Feed segment length (S_1/λ_d)	Resonant frequency (Theory) GHz	Resonant frequency (Experiment) GHz	%error (wrt expt)
3.2	2.6	0.108	3.226	3.25	0.74
		0.217	3.207	3.205	-0.06
		0.325	3.223	3.205	-0.56
		0.433	3.317	3.295	-0.67
		0.542	3.207	3.235	0.86
		0.650	3.238	3.25	0.37
		0.758	3.226	3.205	-0.65
		0.867	3.254	3.22	-1.05

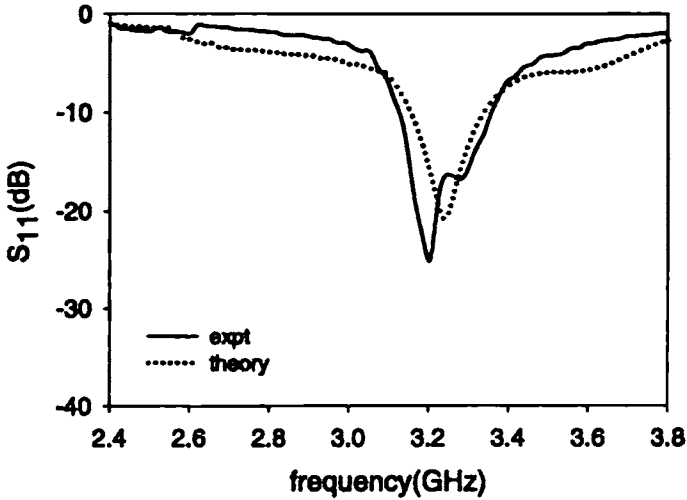


Figure 4.37 Return loss variation of the antenna with $S_1 = 1.3\lambda_d$, $S_2 = 0.543\lambda_d$, $S_3 = 0.5\text{cm}$, $\epsilon_{r1} = 4.28$, $h_1 = 0.16\text{cm}$, $L = 3.2\text{cm}$, $W = 2.6\text{cm}$, $\epsilon_{r2} = 2.2$, $h_2 = 0.08\text{cm}$

(d) Feed length – $1.52\lambda_d$

Experimental results of the effect of permittivity on the bandwidth with the feed length $1.52\lambda_d$ are verified theoretically. Measured and computed resonant frequency variations are given in Table 4.13 and shows good agreement. Return loss variations at the maximum bandwidth position are shown in Figure 4.38. Experimental bandwidth is 9% while that from theory is 7.5%.

The theoretical results explained above reveal that the influence of permittivity of the feed and patch substrates on the bandwidth of the antenna are in same line with the experimental observations. This confirms that the present theory can predict the performance of the antenna when both feed and patch are on substrates with same permittivity and also when they are on substrates with different permittivity.

Table 4.13 Theoretical and experimental resonant frequency with
 $S_1 = 1.52\lambda_d$, $\epsilon_{r1} = 4.28$, $h_1 = 0.16\text{cm}$ and $\epsilon_{r2} = 2.2$, $h_2 = 0.08\text{cm}$

L(cm)	W(cm)	Feed segment length (S_2/λ_d)	Resonant frequency (Theory) GHz	Resonant frequency (Experiment) GHz	%error (wrt expt)
3.2	2.6	0.108	3.207	3.335	1.3
		0.217	3.176	3.295	0.90
		0.325	3.192	3.19	-0.54
		0.433	3.317	3.28	-0.66
		0.542	3.207	3.31	0.86
		0.650	3.238	3.22	0.37
		0.758	3.191	3.325	0.44
		0.867	3.226	3.31	-0.81

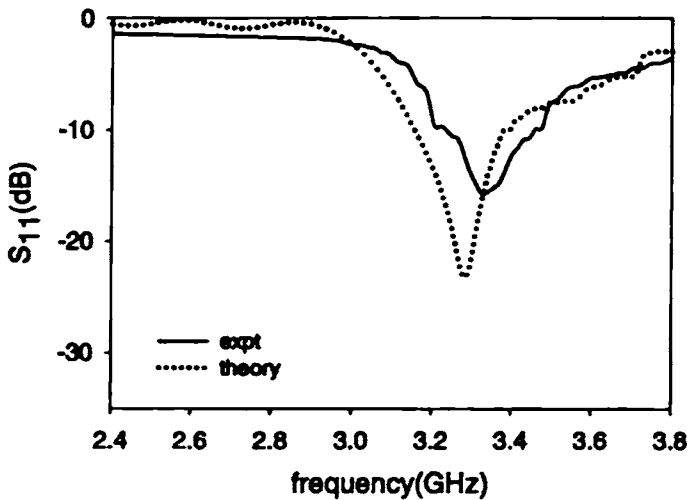


Figure 4.38 Return loss variation of the antenna with $S_1 = 1.52\lambda_d$,
 $S_2 = 0.541\lambda_d$, $\epsilon_{r1} = 4.28$, $h_1 = 0.16\text{cm}$, $L = 3.2\text{cm}$, $W = 2.6\text{cm}$, $\epsilon_{r2} = 2.2$,
 $h_2 = 0.08\text{cm}$

From the theoretical analysis it is concluded that the present analysis can predict the resonant frequency of the L-strip fed antenna accurately within an error of $<2\%$. The difference in the resonant frequencies may be due to the variations in the measured permittivity of the substrates used or due to the air gap in between the substrates used in the experimental measurements. The radiation patterns computed are also in good agreement. The slight discrepancies in the cross-polarization characteristics may be attributed to some reflections from the surroundings.

CHAPTER 5

CONCLUSIONS

This chapter presents the conclusions drawn from the experimental and theoretical investigations carried out on L-strip fed microstrip antennas. Suggestions for further research work in the field are also given.

5.1 INFERENCES FROM EXPERIMENTAL INVESTIGATIONS

The radiation characteristics of different L-strip fed rectangular as well as circular microstrip antenna are studied experimentally and numerically. From the detailed experimental investigations, it is concluded that L-strip feed can successfully be used for bandwidth enhancement of the antenna. It is observed that the resonant frequency of the microstrip antenna shifts towards the lower frequency side when it is excited with L-strip feed. From the Table 3.1 and Figure 3.5 it is clear that with the feed segment length, bandwidth of the patch $3.6 \times 2.6 \text{ cm}^2$ is improved for each feed length. Maximum bandwidth of 17% has been obtained when the feed segment length is $0.4\lambda_d$. From the Table 3.4 and Figure 3.17 it is found that a maximum bandwidth of 20% is obtained for the patch $4 \times 2 \text{ cm}^2$ when the feed segment length is $\frac{3}{4}\lambda_d$. It is also noted that the resonant frequency varies only little with the feed segment length.

Table 3.10 shows the optimized feed parameters for different frequency bands. From these observations, it can be concluded that L-strip feed can effectively be used for bandwidth enhancement of antennas operating in L, S, C and X band frequencies. For all these cases, the antennas offered 11 to 20% bandwidth. This bandwidth enhancement is achieved without deteriorating the radiation characteristics.

Effect of permittivity of the substrates used for fabricating patch and feed on the bandwidth of the antenna is also studied. Figures 3.27 to 31 reveals that permittivity of the patch and feed is also has significant effect on the bandwidth of the L-strip fed antenna. It is found that when the patch and feed are on substrates with different permittivity, bandwidth enhancement is marginal. In this case, maximum bandwidth achieved is only 10-12%. Therefore it is confirmed that bandwidth is maximum if both the patch and feed are fabricated on the substrate having same permittivity.

Radiation patterns of the L-strip fed antennas of the optimum bandwidth configurations have been studied. From Figure 3.32 and Table 3.5, it is clear that

the patterns are similar to those of rectangular patches. The patterns are broad with low cross polar level of the order of -40dB along the bore-sight direction.

Gain of the antenna is also studied in detail. Figure 3.33 gives the absolute gain of the L-strip fed antenna. From the figure, it is found that the gain of the antenna is not much affected as the feed position parameters varies. And maximum gain of the antenna is 8.2dBi . This enhanced gain is attributed as due to the in phase radiation from the L-strip feed.

L-strip feed is used to excite circular patches also. Experimental and simulated results are discussed in Section II. Circular patches resonating at 3.5GHz offered a maximum bandwidth of $\sim 17\%$. And patches resonating at 2.4GHz and 1.8GHz offered a maximum bandwidth of 12% . Radiation patterns of the antenna are also studied. The patterns are similar to those of conventional circular patches. The cross polar level is found to be better than -25dB . Gain of the antenna is also improved. L-strip fed circular antenna has a gain of 7.25dBi . From the experimental analysis, for the moderate bandwidth and optimum gain, L-strip feed is an ideal choice.

6.2 INFERENCE FROM THEORETICAL INVESTIGATIONS

Finite Difference –Time Domain (FDTD) method is used for the analysis of the L-strip fed rectangular patch antennas. The analysis could predict the resonant frequency, electric field variations over the patch surface, radiation patterns, input impedance etc., of the antenna with an error of less than $\pm 2\%$.

The resonance characteristics of the L-strip fed rectangular patches are given in Table 4.2 to Table 4.9. Both the experimental and theoretical results are in good agreement and the maximum error is 2% . Input impedance of the L-strip fed antenna is also computed using FDTD and exactly matching with the experimental results. The discrepancy may be due to the uncertainty in the permittivity of the substrate, non uniformity of the substrate layer and the trapped air between the substrates.

Field distribution over the patch is observed theoretically. From the Figure 4.9, it is clear that the antenna is excited in TM_{01} mode.

Radiation patterns of the antenna are computed theoretically from the calculated near field data. Theoretical and experimental radiation patterns are in good agreement. The slight discrepancies in the cross-polarization characteristics may be due to some reflections from the surroundings. This shows that the present theory can easily predict the radiation patterns of the antenna.

6.3 SCOPE OF FURTHER WORK

L-strip antenna may find applications where wide bandwidth is required. The bandwidth can further be increased by using stepped L-strip. Incorporating photonic band gap ground planes along with L-strip feed would be an interesting topic for future work for bandwidth enhancement along with surface wave reduction. This can improve the overall efficiency of the system.

The effect of air gap between the feed and the radiating patch can be an interesting problem to investigate further. This can considerably increase the bandwidth and gain of the antenna.

Another interesting area to be investigated further is loading the L-strip with Ferro electric materials like BST. By applying suitable potential across BST, the effective dielectric constant can be varied and hence the system can operate at different frequencies.

APPENDIX A

T-STRIP FED WIDEBAND RECTANGULAR MICROSTRIP ANTENNAS

Experimental results of symmetric and asymmetric T-strip fed rectangular microstrip antenna are presented here. Symmetric T-strip fed antenna offered a maximum bandwidth of 23.23% while asymmetric T-strip fed antenna offered 35%. The gain of the antenna is improved with this feeding technique. The antennas are analysed using Finite - Difference Time - Domain method (FDTD). The resonant frequency, return loss, impedance bandwidth and radiation patterns are predicted and are in good agreement with the measured results.

AI INTRODUCTION

L-strip feed has successfully been used for bandwidth and gain enhancement of the rectangular as well as circular patch without affecting the radiation characteristics. Now T-strip feed has been used for exciting rectangular patches. T-strip feed has two versions, with symmetric arms and asymmetric arms. An electromagnetically coupled T-shaped microstrip feed is employed to excite a rectangular microstrip antenna fabricated on another substrate. An impedance bandwidth of ~23% is obtained for symmetric T-strip fed antenna and 35% for asymmetric T-strip fed antenna. The effect of the feed parameters on the radiation and reflection characteristics of the antenna is studied in both the cases. The antenna has a broad radiation pattern with a cross polarization level better than -35 dB. Effect of the feed parameters on the antenna characteristics like resonant frequency, impedance bandwidth, and radiation pattern are theoretically studied. Theoretical results are found to be in good agreement with the experimental ones.

AII SYMMETRIC T-STRIP FED ANTENNA

AII.1 Antenna Geometry

The geometry of the symmetric T-strip fed rectangular microstrip antenna is illustrated in Figure A.1. The feed is fabricated on a substrate with permittivity $\epsilon_r = 4.28$ and height $h = 0.16\text{cm}$. Patch is also fabricated on a similar substrate. The patch is electromagnetically coupled to the feed. The feed parameters that determine the characteristics of the antenna are the length of the two symmetric arms S_2 and S_3 and feed length S_1 of the T-feed.

Effect of feed parameters on the radiation and reflection characteristics of the antenna is studied.

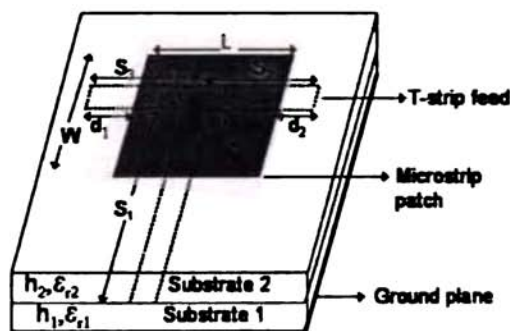


Figure A.1 Geometry of the symmetric T-strip fed rectangular microstrip antenna

AII.2 Experimental observations

Rectangular patches with dimensions $L \times W = 4 \times 2 \text{ cm}^2$ is excited with symmetric T-strip feed. The following antenna characteristics are studied.

- Resonant frequency
- Bandwidth
- Radiation pattern
- Gain

To study the reflection and radiation characteristics, S_1 is varied from $1\lambda_d$ to $1.4\lambda_d$ and S_2 and S_3 from $0.1\lambda_d$ to $1.2\lambda_d$. Resonant frequency and bandwidth variations of the antenna are studied. The measured results are given in the Table A.1. From the table it is clear that the bandwidth is decreasing as S_1 increases. Resonant frequency patch is shifting to the lower side when it is excited with T-strip feed. Feed parameters at the maximum bandwidth position are $S_1 = 1.09\lambda_d$, $S_2 = S_3 = 0.651\lambda_d$, $d_1 = 0.261\lambda_d$, $d_2 = 0.217\lambda_d$ and $a = 0.195\lambda_d$.

Gain of the antenna is measured by gain transfer method at the maximum bandwidth position. The antenna has a gain of 7.8dBi at the resonant frequency.

Table A.1 Resonant frequency and bandwidth variations of symmetric T-strip feed for different S_2 and S_3 , $L=4\text{cm}$, $W=2\text{cm}$, $\epsilon_{r1}=\epsilon_{r2}=4.28$, $h_1=h_2=0.16\text{cm}$

Feed length (S_1/λ_d)	S_2/λ_d	S_3/λ_d	Resonant frequency (GHz)	%bandwidth
1.09	0.217	0.217	3.43	4.02
	0.326	0.326	3.23	6.50
	0.434	0.434	3.27	14.29
	0.543	0.543	3.24	16.56
	0.651	0.651	3.336	23.22
	0.759	0.759	3.34	19.35
	0.868	0.868	3.30	11.24
1.32	0.22	0.22	3.45	4.01
	0.33	0.33	3.38	7.41
	0.44	0.44	3.37	12.47
	0.55	0.55	3.36	12.41
	0.66	0.66	3.38	16.01
	0.77	0.77	3.37	12.13
	0.88	0.88	3.30	6.89

AII.3 Theoretical Investigations

The optimized antenna configuration is investigated using FDTD method. Space steps $\Delta x, \Delta y, \Delta z$ used for computation are 0.1cm, 0.1cm and 0.04cm and the total mesh dimensions are $110 \times 110 \times 20$ in x, y and z directions respectively. Time step Δt is taken as 1.159ps and the Gaussian half-width T as 15ps. The simulation is performed for 5000 time steps. To reduce the number of time steps required for convergence an external source resistance of 50Ω is used. Return loss characteristics, resonant frequency, bandwidth and radiation patterns of the antenna at the maximum bandwidth position are computed theoretically.

S_{11} variation of the antenna at the maximum bandwidth position is shown in Figure A.3. Theoretical and experimental radiation patterns are shown in Figure A.4. The measured and computed cross polar levels are in good agreement.

This reveals that the present theory can predict the radiation patterns of the antenna.

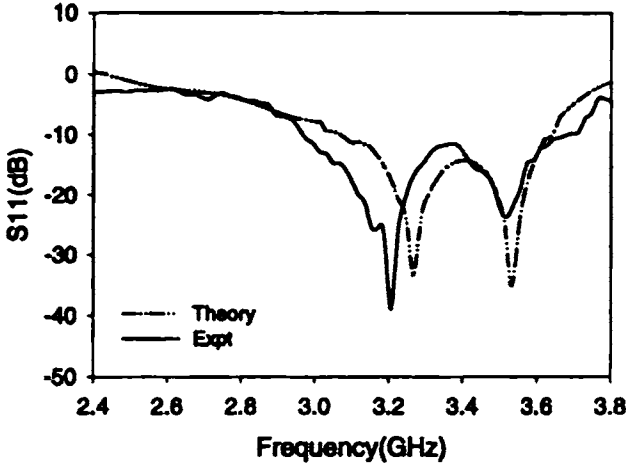


Figure A.3 Theoretical and experimental return loss variation of the antenna ($4 \times 2 \text{cm}^2$), $S_1=1.09\lambda_d$, $S_2 = S_3 = 0.651\lambda_d$, $d_1= 0.261\lambda_d$, $d_2 = 0.217\lambda_d$ and $a = 0.195\lambda_d$

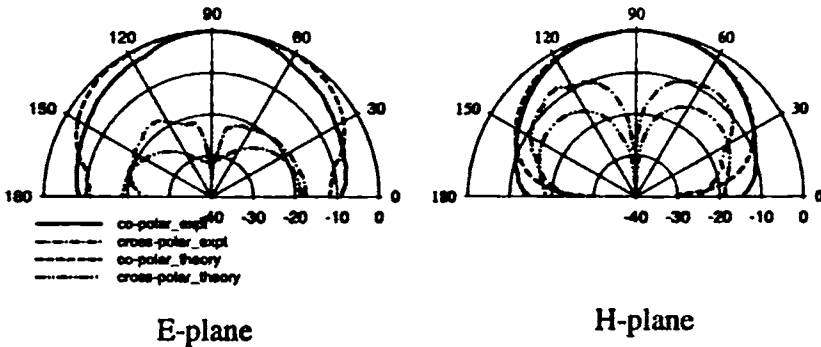


Figure A.4 Radiation patterns of the antenna at the resonant frequency $L = 4 \text{cm}$, $W = 2 \text{cm}$, $S_1 = 1.09\lambda_d$, $S_2 = S_3 = 0.651\lambda_d$, $d_1 = 0.261\lambda_d$, $d_2 = 0.217\lambda_d$, and $a = 0.195\lambda_d$.

AIII. ASYMMETRIC T- STRIP FED ANTENNA

AIII.1 Antenna Geometry

Asymmetric T-strip fed rectangular microstrip antenna geometry is illustrated in Figure A.5. The feed parameters that determine the characteristics of the antenna are the feed length S_1 and two asymmetric feed segment lengths S_2 and S_3 . The feed is fabricated on a substrate with permittivity $\epsilon_r = 4.28$ and height $h = 0.16$ cm. The patch is fabricated on a similar substrate. The patch is electromagnetically coupled to the feed.

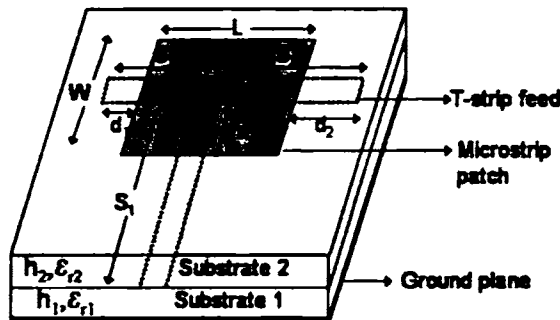


Figure A.5 Geometry of the asymmetric T-strip fed microstrip antenna

AIII.2 Experimental Observations

The performance of an asymmetric T-strip feed on rectangular microstrip patches is studied. The experimental studies are carried out by keeping feed length of the T-strip as $1.052\lambda_d$. The two feed segment lengths S_2 and S_3 are varied. One of the feed segment lengths, S_3 is fixed as $1.158\lambda_d$ and the other feed segment length S_2 is varied from $0.5\lambda_d$ to $1.5\lambda_d$. Experimental studies are conducted on patches of size $L \times W = 4 \times 2$ cm² which is fabricated on a substrate with height 0.16 cm and permittivity 4.28.

S_{11} variations of the antenna for different asymmetric feed segment length S_2 are measured. The feed length S_1 and one of the asymmetric feed lengths S_3 are kept

constant. The bandwidth of the antenna is found to be increasing. Maximum bandwidth of ~35% is obtained when S_2 and S_3 are $1.053\lambda_d$ and $1.158\lambda_d$ respectively. Gain of the optimized antenna configuration is measured and is found that the antenna has again of 7.87dBi at the resonant frequency.

AIII.3 Theoretical investigations

The optimized antenna configuration is analyzed using FDTD. Space steps $\Delta x, \Delta y, \Delta z$ used for computation are 0.1cm, 0.1cm and 0.04cm and the total mesh dimensions are $150 \times 120 \times 20$ in x, y and z directions respectively. Time steps and Gaussian half-width used are as in the above analysis.

Return loss variation of the asymmetric T-strip fed antenna at the maximum bandwidth position is obtained by numerically is shown in Figure A.6 along with experimental result. Theoretically the antenna resonates in the band 2.8569GHz-3.607GHz ($f_r = 3.232$ GHz) with an impedance bandwidth of 23.3% band, while experimental operating band is 2.665GHz-3.805GHz ($f_r = 3.235$ GHz) with a bandwidth of 35.2%. This confirms that the present theory can accurately predict the resonant frequency of the antenna less than an error of 0.09%.

Radiation patterns are also computed at the maximum bandwidth position. Figure A.7 shows the theoretical and experimental radiation patterns of the antenna at the resonant frequency. The differences in the cross-polar levels may be due to the reflections from surroundings.

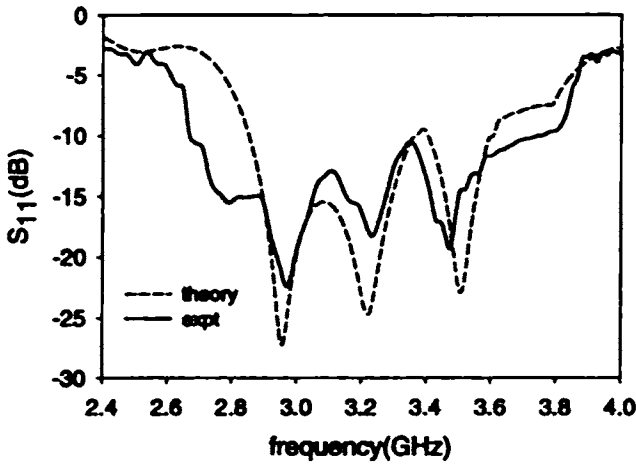


Figure A.6 Experimental and theoretical return loss variations of the antenna at the maximum position
 $L = 4\text{cm}$, $W = 2\text{cm}$, $S_1 = 1.052\lambda_d$, $S_2 = 1.052\lambda_d$, $S_3 = 1.16\lambda_d$
 $d_1 = 0.421\lambda_d$, $d_2 = 0.295\lambda_d$, and $a = 0.211\lambda_d$

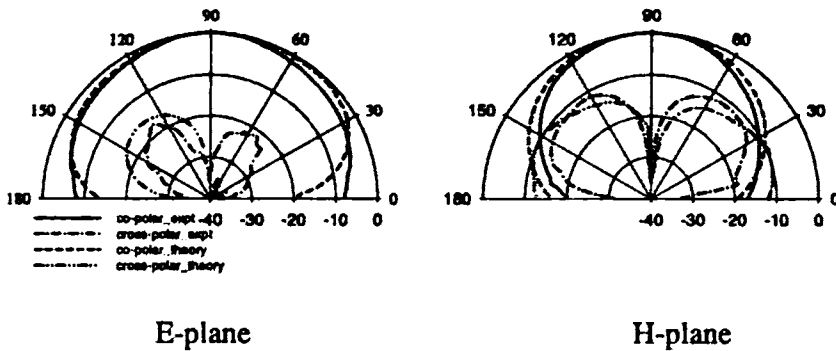


Figure A.7 Theoretical and experimental radiation patterns of the antenna at the resonant frequency, $L = 4\text{cm}$, $W = 2\text{cm}$, $S_1 = 1.052\lambda_d$, $S_2 = 1.052\lambda_d$, $S_3 = 1.16\lambda_d$, $d_1 = 0.421\lambda_d$, $d_2 = 0.295\lambda_d$, and $a = 0.211\lambda_d$

APPENDIX B

WIDE BAND RECTANGULAR MICROSTRIP ANTENNA USING HOOK -STIP FEED

Experimental and theoretical results wideband rectangular microstrip antenna using hook strip feed is presented. Here a hook shaped microstrip line is used to excite the antenna by proximity method. This feeding technique enhances the bandwidth and gain of the antenna without affecting its size. The antenna is excited in TM_{10} mode. This new feeding technique offered a maximum bandwidth of 22% without affecting other characteristics of the antenna.

B.I INTRODUCTION

L-strip and T-strip feed are successfully been applied for the bandwidth enhancement of rectangular microstrip antennas. L-strip feed is modified into hook shaped microstrip line and is used for exciting a rectangular microstrip patch. Experimental and theoretical observations of a hook strip fed rectangular microstrip antenna is discussed in the following sections.

An impedance bandwidth of ~22% is obtained without affecting the antenna characteristics. The effect of the feed parameters on the radiation characteristics of the rectangular patch antenna at resonant frequency is studied. The antenna has a broad radiation pattern with a cross polarization level better than -30 dB. Gain of the antenna is found to be 7.2dBi at the resonant frequency. Experimental results are confirmed by computational results using FDTD.

B.II ANTENNA GEOMETRY

A rectangular patch antenna of dimension $L \times W$ is fabricated on a substrate having dielectric constant $\epsilon_2 = 4.28$ and thickness $h_2 = 0.16\text{cm}$. The antenna is fed by electromagnetic coupling, using a hook shaped microstrip feed, fabricated on another substrate having the same dielectric constant and thickness. The antenna geometry is illustrated in Figure B.1. The feed parameters are feed length S_1 , feed segment length S_2 and hook arm length S_3 , which decides the antenna characteristics.

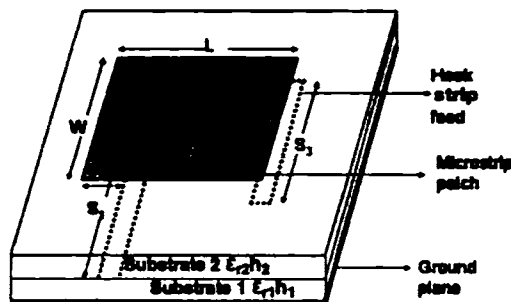


Figure B.1 Geometry of hook strip fed microstrip antenna

B.III RESULTS AND DISCUSSIONS

Hook strip feed is an extension of L-strip feed. The feed length of the hook shaped feed is also fixed as $1.3\lambda_d$ since which gave optimum bandwidth for L-strip. Generally the feed segment length S_2 and hook arm length S_3 are varied from $0.1\lambda_d$ to $0.9\lambda_d$ keeping S_1 fixed.

Microstrip antenna with dimension $4 \times 2 \text{cm}^2$ is used for study. Reflection characteristics of the antenna were studied for different S_2 . For each S_2 , S_3 is varied from $0.1\lambda_d$ to $0.9\lambda_d$. Bandwidth of the antenna is found to be increasing as S_2 increases. The feed parameters are optimized for maximum bandwidth and the radiation characteristics of the optimized antenna are studied. Bandwidth and resonant frequency variations of the antenna for different S_2 and S_3 combinations are given in Table B.1. From the table it is observed that a maximum bandwidth of 21.99% is obtained when $S_2 = 0.763\lambda_d$ and $S_3 = 0.654\lambda_d$. The resonant frequency of the patch is shifting to the lower side as S_2 and S_3 varies.

The experimentally optimized antenna is analyzed using FDTD. Space steps $\Delta x, \Delta y, \Delta z$ used for computation are 0.1cm, 0.1cm and 0.04cm and the total mesh dimensions are $110 \times 110 \times 20$ in x, y and z directions respectively. Time steps Δt is taken as 1.159ps and the Gaussian half-width T as 15ps. The simulation is performed for 5000 time steps. Resonant frequency, bandwidth variations with feed segment length and radiation patterns are computed theoretically. An external source impedance of 50Ω is used for fast convergence.

The return loss and the radiation patterns of the antenna at the optimum position are calculated numerically. Figure B.2 shows the theoretical and experimental S_{11} variations of the antenna at the maximum bandwidth position. Theoretical operating band of the antenna is from 3GHz to 3.558GHz while experimental operating band is 3 GHz to 3.7 GHz.

Figure B.3 shows the theoretical and experimental E-plane and H-plane patterns of the antenna at the resonant frequency. 3 dB beam width of the antenna at the resonant frequency is 92° and 73° in E-plane and H-plane respectively. The cross polarization level is found to be -35dB in the principal planes both in the theory and experiment.

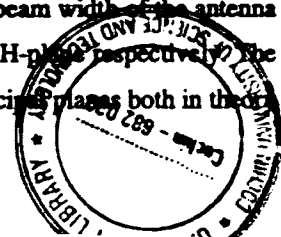


Table B.1 Resonant frequency and bandwidth variations of the hook - strip fed antenna with $L = 4\text{cm}$, $W = 2\text{cm}$, $\epsilon_{r1} = \epsilon_{r2} = 4.28$, $h_1 = h_2 = 0.16\text{cm}$ and $S_1 = 1.3\lambda_d$

Feed segment length S_2/λ_d	Hook arm length S_3/λ_d	Resonant frequency (GHz)	%bandwidth
0.218	0.109	3.4	5.0
	0.218	3.38	6.38
	0.327	3.2	7.3
	0.436	3.35	9.5
	0.545	3.28	9.8
	0.654	3.2	8.5
	0.763	3.38	10.5
	0.872	3.35	7.6
0.327	0.109	3.225	8.59
	0.218	3.375	6.37
	0.327	3.375	7.99
	0.436	3.4	6.72
	0.545	3.425	6.4
	0.654	3.4	7.44
	0.763	3.32	12.3
	0.872	3.38	10.3
0.436	0.109	3.275	5.0
	0.218	3.325	6.06
	0.327	3.26	7.15
	0.436	3.38	8.06
	0.545	3.25	7.05
	0.654	3.275	9.1
	0.763	3.311	12.33
	0.872	3.28	7.84
0.545	0.109	3.325	8.33
	0.218	3.275	8.71
	0.327	3.255	10.47
	0.436	3.26	10.1
	0.545	3.29	12.83
	0.654	3.319	14.59
	0.763	3.38	11.3
	0.872	3.33	10.91

Table B.1 contd.. Resonant frequency and bandwidth variations of the hook -strip fed antenna with $L = 4\text{cm}$, $W = 2\text{cm}$, $\epsilon_{r1} = \epsilon_{r2} = 4.28$, $h_1 = h_2 = 0.16\text{cm}$ and $S_1 = 1.3\lambda_d$

Feed segment length S_2/λ_d	Hook arm length S_3/λ_d	Resonant frequency (GHz)	%bandwidth
0.654	0.109	3.35	11.67
	0.218	3.325	10.18
	0.327	3.275	7.84
	0.436	3.4	10.52
	0.545	3.38	18.5
	0.654	3.34	10.75
	0.763	3.2	9.6
	0.872	3.28	9.10
0.763	0.109	3.4	11.3
	0.218	3.94	16.08
	0.327	3.225	17.04
	0.436	3.38	17.5
	0.545	3.296	18.41
	0.654	3.35	21.99
	0.763	3.39	17.29
	0.872	3.302	12.34
0.872	0.109	3.35	9.709
	0.218	3.275	10.04
	0.327	3.39	8.74
	0.436	3.313	15.48
	0.545	3.36	18.9
	0.654	3.374	17.5
	0.763	3.387	16.97
	0.872	3.28	9.14

B.IV CONCLUSIONS

The effect of hook-strip feed on the characteristics of a rectangular microstrip antenna is studied. The antenna offered a maximum bandwidth of 22% with 7.2dBi gain. The antenna is analyzed using finite difference time domain technique and obtained an excellent agreement with experiment. This antenna may find applications in high speed personal communication systems where large bandwidth is required.

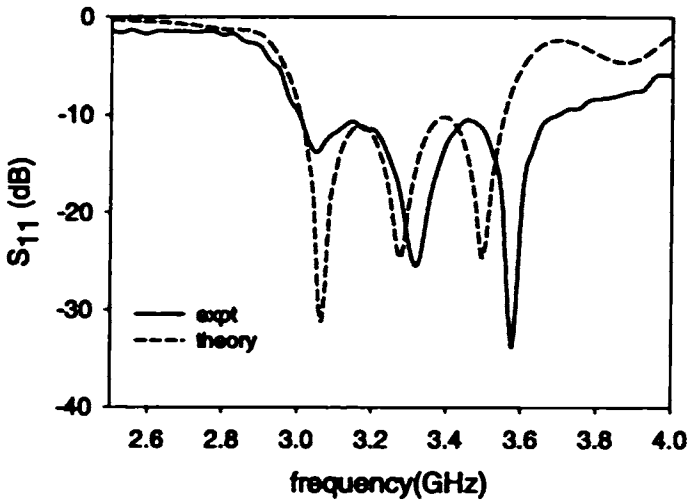


Figure B.2 Experimental and theoretical return loss variation with frequency of the antenna $L = 4\text{cm}$, $W = 2\text{cm}$, $S_1 = 1.3\lambda_d$, $S_2 = 0.763\lambda_d$, $S_3 = 0.654\lambda_d$, $d_1 = 0.109\lambda_d$, $d_2 = 0.371\lambda_d$

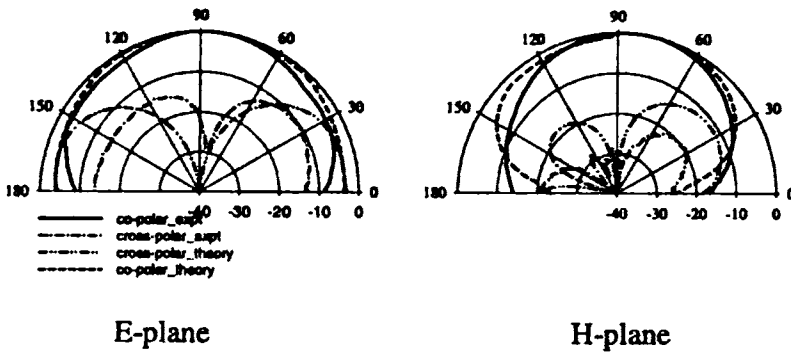


Figure B.3 Theoretical and experimental radiation patterns at the resonant frequency of the antenna, $L = 4\text{cm}$, $W = 2\text{cm}$, $S_1 = 1.3\lambda_d$, $S_2 = 0.763\lambda_d$, $S_3 = 0.654\lambda_d$, $d_1 = 0.109\lambda_d$, $d_2 = 0.371\lambda_d$

APPENDIX C

Appendix C deals with the experimental setup and the measurement techniques employed for the study of radiation characteristics of the developed antennas.

ANTENNA MEASUREMENTS

HP 8510C Vector Network Analyzer is used for the measurement of return loss, resonant frequency, gain and radiated power. Network analyzer can make automatic, rapid and accurate measurements.

C.1 Network Analyzer

A Network Analyzer is swept frequency measurement equipment to completely characterize the complex network parameters without any degradation in accuracy and precision in less time. Two types of network analyzers are available, scalar and vector network analyzers. Scalar network analyzer measures only the magnitude of reflection and transmission coefficients while the vector network analyzer measures both the magnitude and phase.

A vector Network Analyzer consists of the following system

- 1) Microwave Source
- 2) Test Set
- 3) Signal Processor
- 4) Display Unit

The synthesized source or the sweep oscillator provides the RF stimulus. It operates from 45MHz to 50 GHz. It can operate in ramp or in step mode. In the ramp mode the analyzer directs the source to sweep in a linear ramp over the frequency and in the step mode, which provides maximum precision. The schematic diagram of the network analyzer controlled by IBM PC is shown in Figure C.1.

C.II Measurement of return loss, resonant frequency and bandwidth

Network Analyzer is calibrated to one full port and the test antenna is connected to PORT 1 of the S-parameter test set. The measured S_{11} LOGMAG data is acquired and stored in ASCII format in the computer interfaced with the

NWA (Figure C.2), using the software MERL Soft. The resonant frequency is determined from the dip of the return loss curve. The impedance bandwidth is measured by taking the range of frequencies (Δf) over which the return loss is greater than or equal to 10dB. Percentage bandwidth can be calculated using the expression $(\Delta f/f_r) \times 100\%$, where f_r is the center frequency of the operating band.

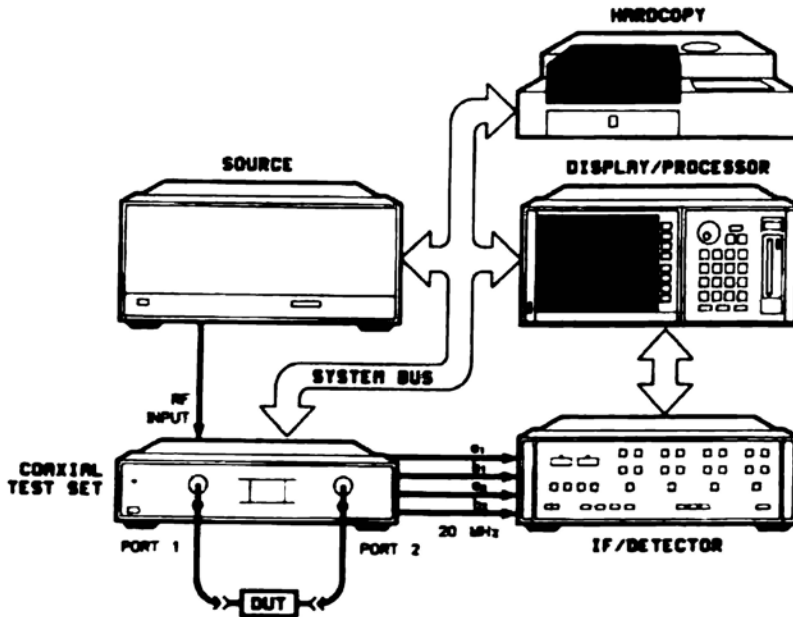


Figure C.1 Schematic diagram of the HP 8510C network Analyzer

C.III Measurement of radiation pattern

Antenna radiation pattern is the spatial distribution of the electromagnetic field radiated by the antenna. Generally patterns in two-principle planes, E and H plane are taken. The principal plane patterns (co and cross polar) of the test antenna are measured by keeping the antenna in receiving mode inside an anechoic chamber. The experimental setup for the measurement of radiation

HP 8510C Network Analyzer, interfaced to an IBM PC, is used for the pattern measurement. The PC is attached to a STIC 310C position controller. The test antenna is mounted on the antenna positioner kept inside the anechoic chamber. A wideband horn antenna is used as the transmitter. The test antenna and the transmitting antenna are connected to Port 2 and Port 1 respectively of the network analyzer. The test antenna is mounted on the Positioner and the transmitting wide band horn antenna is mounted on a stand at the aperture of the Anechoic Chamber. After selecting the start, stop frequencies and number of points in Network Analyzer stimuli menu, the antenna is bore-sighted. The test antenna at the Bore-sight position a thru calibration is done in the Network Analyser. The test antenna is rotated by 90° .

Radiation patterns of the antenna at multiple frequency points can be measured in a single rotation of the test antenna by using antenna position controller and MERL software. The positioner will stop at each step angle and take S_{21} measurement at different frequency points in the operating band. The process will repeat till it reaches the stop angle. The entire measured data is stored in ASCII format and can be used for further processing. The different radiation pattern characteristics like half power beam width, cross-polar level, etc. are obtained after the analysis of the stored data.

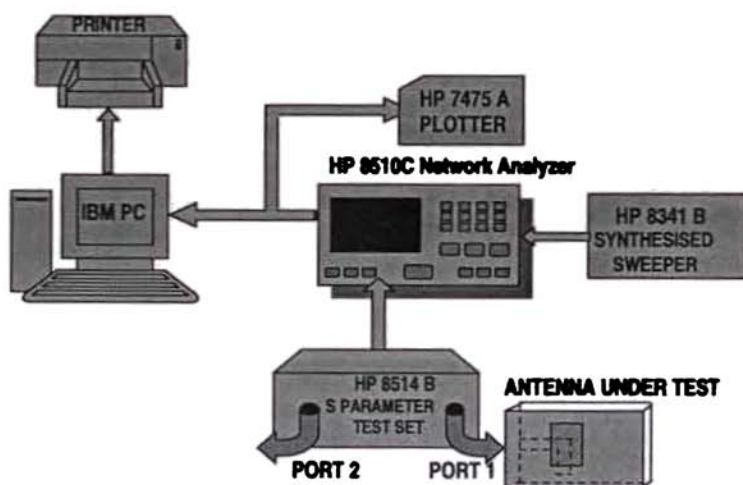


Figure C.2 Experimental setup for the measurement of return loss and cross-polar level.

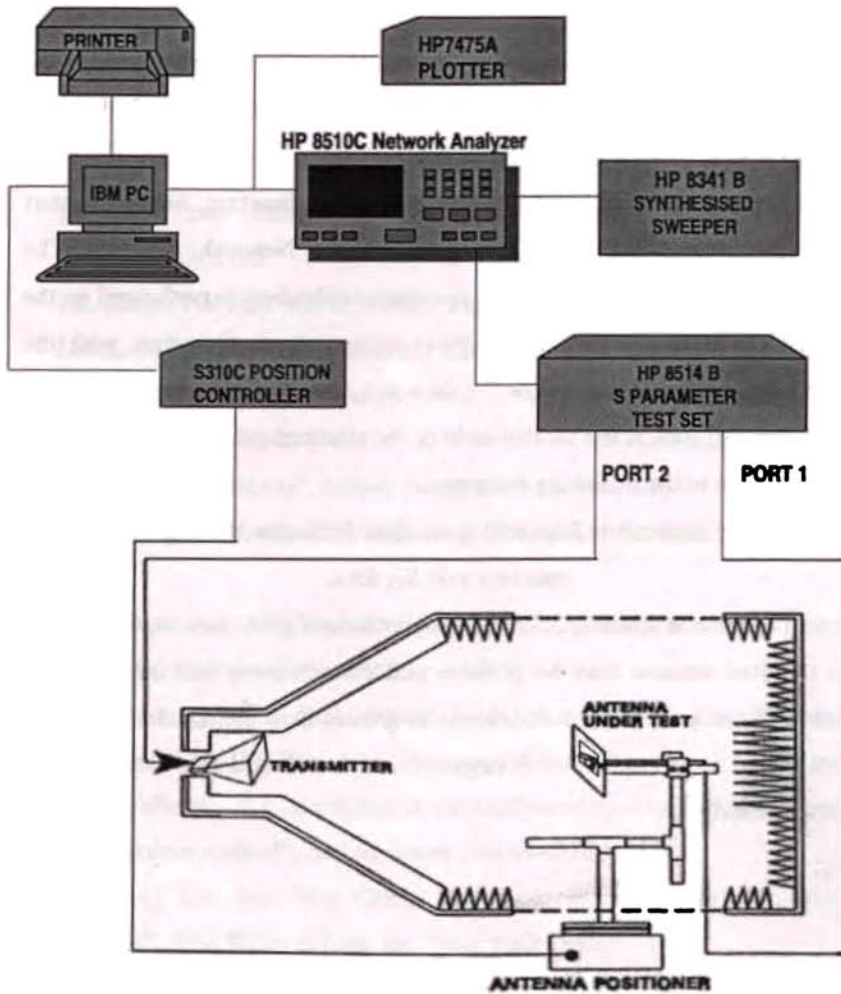


Figure C.3 Experimental setup for the measurement of radiation pattern

C.IV Measurement of Gain

The antenna set up for measuring the radiation pattern can be used for the measurement of gain. Here the gain transfer method is used to calculate the absolute gain of the test antenna.

The test antenna is positioned to the bore-sight direction. Select the start and stop frequencies and number of points in the Network Analyser. The response is switched to S_{22} . A THRU response calibration is performed in the NWA and stored in the CAL SET. Now replace the test antenna with the standard gain antenna. Measure the S_{21} data and store it in the computer. Then the computer will look at the lookup table of the standard gain data and compute the absolute gain in the following manner.

Gain of the test antenna = Standard gain data from the look up table – the standard gain S_{21} data.

If the gain of the test antenna is less than the standard gain antenna, the S_{21} data of the standard antenna may be positive and the computer will calculate the difference. If the gain of the test antenna is greater than the standard antenna, S_{21} data stored in the computer is negative and it will add this data with the standard antenna gain.

REFERENCES

Books

1. L.J. Bahl and Bhartia, "Microstrip Antennas", Artech House, Dedham, MA, 1980.
2. J.R. James, P.S. Hall and C. Wood, "Microstrip antenna-theory and design", London, UK, Peter Peregrinus Ltd., IEE, 1981.
3. C.A. Balanis, "Antenna Theory: Analysis and design", Harper and Row Publishers, New York, 1982.
4. L.V. Blake, "Antennas", Artech House Dedham, MA, 1984.
5. John D. Kraus, "Antenna", McGraw-Hill International Editions, 2nd edition, 1988.
6. K.C. Gupta and Abdelaziz Benalla, "Microstrip antenna design", Artech House, Inc. Norwood MA, 1988.
7. J.R. James and P.S. Hall, "Hand book of microstrip antennas", Peter Peregrinus Ltd., IEE Engineers IV series, 1989.
8. Allen Taflov, "Computational electrodynamics, The finite-difference time-domain method", Artech House, Norwood MA 1995.
9. Kai Fong Lee and Wei Chen, "Advances in microstrip and printed antennas", John Wiley & Sons, Inc. New York 1997.
10. IE3D User's manual, Release 7, Zeland Software, Inc. December 1999.
11. Fidelity User's manual, Release 3, Zeland Software, April 2000.
12. Ramesh Garg, Prakash Bhartia, Inder Bahl and Apisak Ittipiboon, "Microstrip antenna design handbook", Artech House, London, 2001.

JOURNALS /SYMPOSIUM PAPERS

13. G. A. Deshamps, "Microstrip Microwave Antennas", presented at 3rd USAF Symposium on Antennas, 1953.
14. H. Gulston and G. Bassinot, "Flat Aerial for Ultra High Frequencies", French Patent No. 703113, 1955.
15. L. Lewin, "Radiation from Discontinuities in Striplines", Proc.IEE, vol. 107, pp 163-170, 1960.
16. P.S Carter, "Early History of the antenna and Propagations Field until the end of World War I: Part I-Antennas", Proc. IRE, 50:679-682, May 1962.
17. E. V. Byron, "A New Flush Mounted Antenna Element for Phased Array application", Proc. Phased Array Antenna Symp., pp. 187-192, 1970
18. J. Q. Howell, "Microstrip Antennas", IEEE AP-S Int. Symp. Digest, pp.177-180. 1972.
19. R. E. Munson, "Conformal Microstrip Antennas and Microstrip Phased Arrays" IEEE Trans. Antennas Propagation, vol. AP-22, pp. 74-77, 1974.
20. Walter L. Weeks, "Antennas Engineering", Tata Mc Graw-Hill Publishing Company, New Delhi, 1974.
21. G. G. Sanford, "Conformal Microstrip Phased Array for Aircraft Tests with ATS-6", Proc. Nat. Electronic Conf., vol. 29, pp. 252-257, 1974.
22. H. D. Weinschel, "Cylindrical array of circularly polarized microstrip antennas", IEEE Antennas Propagat. Soc. Int. Symp., pp. 177-180, 1975.
23. A.G. Derneryd, "Linear microstrip array antennas", Chalmers Univ. Technol., Goteborge, Sweden, Tech.Report, TR7505, 1975.
24. A. G. Derneryd, "Linearly Polarized Microstrip Antennas", IEEE Trans. Antennas Propagation, vol. AP-24, pp. 846-851, 1976.
25. J. R. James and C. J. Wilson, "Microstrip antennas and arrays Part-I: Fundamental action and limitations", IEE Proc. Microwaves Opt. and Antennas, vol.1, pp. 165-174, 1977.

26. P. K. Agarwal and M. C. Bailey, "An Analysis Technique for Microstrip Antennas", *IEEE Trans. Antennas Propogat.*, vol. AP-25, pp. 756-759, 1977.
27. L. C. Shen, S. A. Long, M. R. Allerting, and M. D. Walton, "Resonant Frequency of a Circular Disc Printed Circuit Antenna", *IEEE Trans. Antenna Propogat.*, vol. AP-25, pp 595-596, 1977.
28. S. A. Long, L. C. Shen, M. D. Walton, and M. R. Allerting, "Impedance of a Circular Disc Printed Circuit Antenna", *Electron Lett.*, vol. 14, pp. 684-686, 1978.
29. J. L. Kerr, "Microstrip Polarization Techniques", in *Proc. Antenna Application Symposium, Allerton Park, IL, September 1978.*
30. E. L. Newman, "Strip antennas in a dielectric slab", *IEEE Trans. Antennas Propogat.*, vol. AP-26, pp. 647-653, 1978.
31. E. L. Newman and D. M. Pozar, "Electromagnetic modeling of composite wire and surface geometries", *IEEE Trans. Antennas Propogat.*, vol. AP-26, pp. 784-787, 1978.
32. Y. T. Lo, D. Solomon and W. F. Richards, "Theory and Experiments on Microstrip Antennas", *IEEE AP-S Symposium (Japan)*, pp. 53-55, 1978.
33. W. F. Richards, Y. T. Lo and D. D. Harrison, "Improved Theory for Microstrip Antennas", *IEE Electron. Lett.*, vol. 15, pp. 42-44, 1979.
34. Y. T. Lo, D. Solomon and W. F. Richards, "Theory and Experiments on Microstrip Antennas", *IEEE Trans. Antennas Propogat.*, vol. AP-27, pp.137-145, 1979.
35. K. R. Carver, "A Modal Expansion Theory for the Microstrip antenna", *Dig. Int. Symp. Antennas Propogat.*, Seattle, WA, pp. 101-104, 1979.
36. K. R. Carver and E. L. Coffey, "Theoretical Investigation of the Microstrip Antenna", *Tech. Rept. PT 00929, Physical Science Lab., New Mexico State Univ., Las Cruces, 1979.*
37. E. L. Coffey and T. H. Lehman, "A New Analysis Technique for Calculating and Self and Mutual Impedance of Microstrip Antennas", *Proc.*

- Workshop on Printed Circuit Antennas, New Mexico State Univ., pp.31/1-21, 1979.
38. P. Hammer, D. Van Bouchante, D. Verschraevan and A. Van de Capelle, "A model for calculating the radiation field of microstrip antennas", *IEEE Trans. Antennas Propagat.*, vol. AP-27, pp. 267-270, 1979.
 39. J. R. Mosig and F. E. Gardiol, "The near field of an open microstrip structure", *IEEE AP-S, Int. Symp. Digest.*, pp. 379-381, 1979.
 40. A.G. Derneryd, "Analysis of the microstrip disc antenna element", *IEEE Trans. Antennas Propagat.*, Vol. AP-27, pp.660-664, 1979.
 41. N. G. Alexopoulos, N. K. Uzunoglu and I. E. Rana, "Radiation by Microstrip Patches", *Dig. Int. Symp. Antennas Propogat.*, pp. 722-727, 1979.
 42. C. M. Butler, "Analysis of a coax-fed circular microstrip antenna", *Proc. Workshop Printed Circuit Antenna Tech., New Mexico State University., Las Cruces*, pp.13/1-17, 1979
 43. C. M. Butler and E. K. Yung, "Analysis of a terminated parallel plate waveguide with a slot in its upper plate", *Ann. Telecommun.*, vol. 34, No.9, 1979
 44. J. W. Mink, "Circular ring microstrip antenna elements", *IEEE Antennas Propogat. Soc. Int. Symp.*, Quebec City, Canada, June 1980.
 45. J.H.Dahelle and A.L.Cullen, " Electric probe measurements on microstrip", *IEEE. Trans. Microwave Theory and Techniques*, vol.MTT-28, no.7, pp.752-755, 1980.
 46. L. C. Shen, "The Elliptical Microstrip Antenna with Circular Polarisation", *IEEE Trans. Antenna Propagat.*, vol. AP-29, pp 95-99, 1981.
 47. R. Chadha and K. C. Gupta, "Green's functions for circular sectors, annular rings, and annular sectors in planar microwave circuits", *IEEE Trans. Microwave Theory Tech.*, vol. MTT-29, pp. 68-71, Jan 1981.
 48. Y. T. Lo and W. F. Richards, "Perturbation Approach to the Design of Circularly Polarized Microstrip Antennas" *Electron. Lett.*, vol. 17, pp. 383-385, 1981.

49. E. H. Newman and P. Tulyathan, "Analysis of microstrip antennas using moment methods", *ibid.*, pp.47-53, 1981.
50. D. H. Schaubert, F.G. Farrar, A. R. Sindors and S.T. Hayca, "Microstrip Antenna with Frequency Agility and Polarisation Diversity", *ibid.*, pp. 118-123, 1981.
51. K. Araki and T. Itoh, "Hankel Transform Domain Analysis of Open Circular Microstrip Radiating Structures", *ibid.*, pp. 84-89, 1981.
52. W. C. Chew and J. A. Kong, "Analysis of a circular microstrip disc antenna with a thick dielectric substrate", *ibid.*, pp.68-76, 1981.
53. T. Itoh and W. Mentzel, "A Full Wave Analysis method for Open Microstrip structures", *ibid.*, pp. 63-67, 1981.
54. E. F. Kuester, R.T. Johak, and D.C. Chang, "The Thin Substrate Approximation for Reflection from the End of the Slab Loaded Parallel Plate Wave Guide with Application to Microstrip patch", *IEEE Trans. Antennas Propagat.*, vol. AP-30, pp. 910-917, 1982.
55. I. J. Bahl, P. Bhartia, and S.S. Stuchly, "Design of a Microstrip Antenna Covered with a Dielectric Layer", *IEEE Trans. Antennas Propogat.*, vol. AP-30, pp. 314-318, 1982.
56. P.S Hall, C. Wood, C. Garrett, "Wide bandwidth microstrip antennas for circuit integration", *IEE Electron. Lett.* ,vol.15, pp. 458-460,1970
57. C. Wood, "Curved microstrip lines as compact wide band circularly polarized antennas", *IEE JMOA*, vol.126, pp.5-13, 1979.
58. C. Wood, "Improved bandwidth of microstrip antennas using parasitic elements", *IEE Proc.*, Pt.H, vol.127, pp.231-234, 1980.
59. A.G. Derneryd and I. Karlsson, "Broad band microstrip antenna element and array", *IEEE Trans. Antennas Propagat.*, vol.AP-24, pp.140-141, 1981.
60. V.N.Pandharipande and K.G Verma, "Wide band microstrip patch array at X-band", *J.Inst.Elec.Telecom.Eng.* , vol.29, pp.497-500, 1983.
61. D.R Poddar, J.S.Chatterjee and S.K.Choudary, "On some broad band microstrip resonators", *IEEE Trans .Antennas Propagat.*, vol.AP-31, pp.193-194,1983.

62. N.Das and J.Chatterjee, "Conically depressed microstrip patch antenna", *IEE Proc.*, Pt.H, vol.130,pp.193-196, 1983.
63. A. Saban, "A new broadband stacked two layer antenna", *Dig. Int. Symp. Antennas and Propagat.*, vol.1,pp.63-66,May 1983.
64. Long. S. A, Mcallister. M. W, and Shen L.C, "The resonant cylindrical dielectric cavity antenna," *IEEE Trans. Antennas Propagat.*, vol. AP - 31, no.3, pp.406 - 412, May 1983.
65. P.S Bhatnagar, J.P Daniel, K. Mahadjoubi and C. Terret, "Experimental study on stacked microstrip Antennas", *IEE Electron. Lett.*, vol.22, pp.864-865,1985.
66. G. Kumar and K.C Gupta, "Non-radiating dges and four edges gap-coupled multiple resonators broad band microstrip antennas", *IEEE Trans. Antennas and Propagat.*, AP-32,pp.1375-1379,1985.
67. T. Hori and N. Nakagima, "Broad band circularly polarized array antenna with coplanar feed", *Trans. Inst. Electron. and Commun. Eng., Jpn, Part B*, vol. J68B, pp.515-522, 1985.
68. CJ Prior and P.S. Hall, "Microstrip disc antenna with a short circuited annular ring", *IEE Electron. Lett.*, vol.21,pp.719-721,1985.
69. C.K Aanandan and K.G Nair, "Compact broadband microstrip antenna," *IEE Electron. Lett.*, vol.22, no.20, pp.1064-1065, 1986.
70. P.S Bhatnagar, J.P Daniel, K.Mahadjoubi and C. Terret, "Hybrid edge gap and directly coupled triangular microstrip antenna", *IEE Electron. Lett.*, vol.22,pp.853-855,1986.
71. T. Huynh and K.F. Lee, "Single layer single patch wideband microstrip antenna", *IEE Electron.Lett.vol.31, no.16, pp.1310-1312, 1995.*
72. L. Gianffret, J.M Labeurte and A. Papiernik, "Experimental and theoretical investigations of new compact large bandwidth aperture coupled microstrip antenna", *IEE Electron.Lett.*, vol.31, no.25, pp.2139-2140, 1995.
73. S.D. Targonski, R.B. Waterhouse and D.M. Pozar, "Wideband aperture coupled stacked patch antenna using thick substrates", *IEE Electron. Lett.*, vol.32, no.21, pp.1941-1942,1996.

74. M. Deepukumar, J. George ,C.K. Aanandan, P. Mohanan and K.G Nair, "Broadband dual frequency microstrip antenna", *IEE Electron.Lett.*,vol.32,no.17,pp.1442-1443.,1996.
75. Kin -Lu Wong and Wen- Hsiu Hsu, "Broadband triangular microstrip antenna with U-shaped slot", *IEE Electron.Lett.*,vol.33,no.25,pp.2086-2087,1997
76. Kin-Lu Wong and Jian-Yi Wu, " Bandwidth enhancement of circularly polarized microstrip antenna using chip resistor loading", *IEE Electron.Lett.*,vol.34,no.2,pp.138-139,1997.
77. K.P Ray and G.Kumar, "Multi frequency and broadband hybrid coupled circular microstrip antennas", *IEE Electron. Lett.*, vol.33, no.6, pp.437-438, 1997.
78. K.M Luck ,K.F. Lee and Y.L Chow , " Proximity coupled stacked circular disc microstrip antenna with slots", *IEE Eelectron.Lett.*,vol.34,no.5,pp.419-420,1998.
79. Chih-Yu Huang, Jian-YiWu, Cheng-FuYang and Kin-Lu Wong, "Gain enhanced compact broadband microstrip antenna", *IEE Electron. Lett.*, vol.34, no.2, pp.138-139, 1998.
80. Yeunjeong Kim, Wansuk Yun and Youngjoong Yoon, "Dual frequency and dual polarization wideband microstrip antenna", *IEE Electron .Lett.*, vol.34, no.15,pp.1442-1443,1998.
81. C.L. Mak, K.M. Luk and K.F. Lee, "Proximity coupled U-slot patch antenna", *IEE Electron.Lett.*vol.34, no.8, pp.715-716, 1998.
82. Jia-Yi Sze and Kin-Lu Wong, "Broadband rectangular microstrip antenna with pair of toothbrush-shaped slots", *IEE Electron. Lett.*, vol.34,no.23,pp. 2186-2187,1998.
83. Shyh- Tirng Fang, Kin-Lu Wong and Tzung- Wern Chuiou , " Bandwidth enhancement of inset microstrip -line -fed equilateral -triangular microstrip antenna", *IEE Electron.Lett.*,vol.34,no.23,pp.2184-2186,1998.
84. K.M Luk, C.L Mak, Y.L Chow and K.F Lee , " Broadband microstrip patch antenna", *IEE Electron. Lett.*, vol.34,no.15,pp.1442-1443,1998.

85. K.M.Luk, Y.X.Guo, K.F.Lee and Y.L.Chow , “ L-probe proximity fed U-slot patch antenna”, IEE Electron. Lett., vol.34,no.19,pp.1806-1807,1998.
86. Kin-Lu Wong and Jen-Yea Jan, “Broadband circular microstrip antenna with embedded reactive loading”, IEE Electron. Lett., vol.34,no.19,pp.1804-1805,1998.
87. Y.X. Guo, K.M Luk and K.F. Lee, “U-slot circular patch antennas with L-probe”, IEE Electron. Lett., vol.35, no.20, pp.1694-1695, 1999.
88. Y.X.Guo, K.M.Luk and K.F.Lee , “ L-probe proximity fed short circuited patch antennas”, IEE Electron.Lett.,vol.35,no.24,pp.2069-2070,1999.
89. R.B Waterhose, “Broadband stacked shorted patch”, IEE Electron. Lett., vol.35, no.2, pp.138-139,1999.
90. Lakhdar Zaid , Georges Kossiavas, Jean -Yves Dauvignac, Josiane Cazajous and Albert Papiernik, “Dual-frequency and broadband antennas with stacked quarter wavelength elements”, IEEE Trans. Antennas and Propagat., vol.47,no.4,pp.654-660,1999.
91. W.K. Lo, J.L Hu, C.H Chan and K.M.Luk , “ Circularly polarized patch antenna with an L-shaped probe fed by a microstrip line”, Microwave Optical Technol. Lett., vol.24,no.6,pp.412-414,2000.
92. Kin-Fai Tong, Kwai-Man Luk, Kai-Fong Lee, Richard Q.Lee, “A broadband U-slot rectangular patch antenna on a microwave substrate”, IEEE Trans. Antennas and Propagat., vol.48,no.6,pp.954-960,2000.
93. Sean M.Duffy, “An enhanced bandwidth design technique for electromagnetically coupled microstrip antennas”, IEEE Trans. Antennas and Propagat., vol.48, no.2, 2000.
94. Jia-Yi Sze,Kin-Lu Wong , “ Slotted rectangular microstrip antenna for bandwidth enhancement”, IEEE Trans. Antennas and Propagat.,vol.48,no.8,pp.1149-1152,2000.
95. J.S. Baligar, U.K. Revankar and K.V Acharya, “Broad band stacked annular ring coupled shorted microstrip antenna”, IEE Electron. Lett., vol.36,no.21,pp.1756-1757,2000.

96. Y.W. Jang, "Broadband cross-shaped microstrip-fed slot antenna", *IEE Electron. Lett.*, vol.36,no.25,pp.2056-2057,2000.
97. Wen-Hsiu Hsu and Kin-Lu Wong, " A wideband circular patch antenna", *Microwave Optical Technol. Lett.*,vol.25,no.5,pp.327-328,2000.
98. M.D. van Wyk and K.D Palmer, "Bandwidth enhancement of microstrip patch antennas using coupled lines", *IEE Electron. Lett.*, vol.37,no.13,pp.806-807,2001.
99. Yong-Xin Guo, Kwai-Man Luk and Kai-Fong Lee , " L-probe proximity fed annular ring microstrip antennas", *IEEE Trans. Antennas and Propagat.*, vol.49,no.1,2001.
100. Yong-Woong Jang, "Wide-band T-shaped microstrip –fed twin slot array antenna", *ETRI Journal*, vol.23, no.1, pp.33-37, 2001.
101. Yong-Woong Jang, "Broadband aperture coupled T-shaped microstrip –fed triangular patch antenna", *Microwave Optical Technol. Lett.*, vol.31, no.4, pp.262-264, 2001.
102. Y.X.Guo, K.M.Luk and K.F.Lee, "Regular circular and compact semicircular patch antennas with a T-probe feeding, *Microwave Optical Technol. Lett.*, vol.31, no. 1, pp.68-71, 2001.
103. A.K. Shackelford, S.Y. Leong and K.F. Lee, "Small size probe fed notched patch antenna with a shorting post", *Microwave Optical Technol. Lett.*, vol.31, no.5, pp.377-379, 2001.
104. Fa-Shian Chang and Kin-Lu Wong, "A broadband probe fed patch antenna for a DCS base station", *Microwave Optical Technol. Lett.*,vol.30, no.5, pp.341-343, 2001.
105. Tong-Woong Jang, "Large bandwidth double T-shaped microstrip –fed single layer single slot antenna", *Microwave Optical Technol.Lett.*, vol.30, no.3, pp.185-187, 2001.
106. B.L.Ooi, C.L Lee and P.S.Kooi, "A novel F-probe fed broadband patch antenna", *Microwave Optical Technol. Lett.*,vol.30, no.5, pp.355-356,2001.

107. Y.K. Guo, K.M. Luk and K.F.Lee, "Small wideband triangular patch antenna with an L-probe feeding", *Microwave Optical Technol. Lett.*, vol.30, no.3, pp.218-220, 2001.
108. Yong-Xin Guo, Chin-Lun Mak, Kwai-Man Luk and Kai-Fong Lee, "Analysis and design of L-probe proximity fed patch antennas", *IEEE Trans. Antennas and Propagat.*, vol.49, no.2, pp. 145-149, 2001.
109. Yong-Xin Guo, Kwai-Man Luk, Kai-Fong Lee and Ricky Chair, "A quarter wave U-shaped patch antenna with two unequal arms for wideband and dual frequency operation", *IEEE Trans. Antennas and Propagat.*, vol.50, no.8, pp.1082-1086, 2002.
110. Patnam Hanumantha Rao, Vincent F. Fusco and Robert Cahill, "Wideband linear and circularly polarized patch antenna using a printed stepped T-feed", *IEEE Trans. Antenna and Propagat.* vol.50, no.3, pp.356-360, 2002.
111. Yong-Woong Jang, "Broadband T and shunt stub shaped microstrip fed slot antenna backed by a ground plane", *Microwave Optical Technol. Lett.*, vol.32, no.4, pp.278-280, 2002.
112. Y.W.Jang, "Broadband T-shaped microstrip fed U-slot coupled patch antenna", *IEE Electron. Lett.*, vol.38, no.11, pp.495-496, 2002.
113. Kane S Yee, "Numerical solution of Initial boundary value problems involving Maxwell's equations in isotropic media", *IEEE Trans. Antennas and Propagat.*, vol. Ap-14, no.8, pp.302-307, 1966.
114. Allen Taflove and Morris E. Brodwin, "Numerical solutions of steady state electromagnetic scattering problems using the time-dependent Maxwell's equations", *IEEE Trans. Microwave Theory and Techn.* vol.MTT-23, no.8, pp.623-630, 1975.
115. Gerrit Mur, "Absorbing boundary conditions for the finite-difference approximation of the time -domain electromagnetic field equations", *IEEE Trans. Electromagnetic Compatibility*, vol.EMC.23, no. 4, pp.377-382, 1981.

116. Alain Reincix and Bernard Jecko, "Analysis of microstrip patch antennas using Finite -Difference Time -Domain method", *IEEE Trans. Antennas and Propagat.* vol. 37, no.11, pp.1361-1369, 1989.
117. David M. Sheen, Sami M. Ali, Mohamed D. Abouzahra and Jin Au Kong, "Application of the three -dimensional Finite-Difference Time-Domain method to the analysis of planar microstrip circuits", *IEEE Trans Antennas and Propagat.*, vol.38, no.7, pp.849-857, 1991.
118. Raymond Lubbers, Li Chen ,Toru Uno and Saburo Adachi , " FDTD calculation of radiation patterns ,impedance and gain for a monopole antenna on a conducting box", *IEEE Trans. Antennas and Propagat .*, vol. 40,no. 12,pp.1577-1583,1992.
119. Martin L. Zimmerman and Richard Q. Lee, "Use of the FDTD method in the design of microstrip antenna arrays", *Int. Journal of Microwave and Millimeter -Wave Computer Aided Eng.*, vol.4, no.1, pp. 58-66, 1994.
120. A.Taflove, "Reinventing Electromagnetics: Emerging applications of FDTD computation, *IEEE Computational Science and Eng.*, pp.24-34, 1995.
121. R.J. Lubbers and H.S Langdon, "A simple feed model that reduces time steps needed for FDTD antenna and microstrip calculations", *IEEE Trans. Antennas and Propagat.*, vol.44, no.7, pp.1000-1005, 1996.
122. Jose A.Perada *et al.*, Numerical dispersion and stability analysis of the FDTD technique in lossy dielectrics", *IEEE Microwave and Guided wave Lett.* Vol.8, no.7, pp.245-248, 1998.

INDEX

Absorbing Boundary -		Electric filed distribution	150
Condition	138	Excitation Techniques	
Active Antennas	2	Aperture Coupling	9
Aperture Antennas	2	Coaxial feed	7
Agarwal	21	Microstrip Line feed	8
Alexopolus	22	Proximity Coupled feed	9
Anechoic Chamber	206,207	FDTD	14, 16, 131-135,137-138, 145-146, 151,156,165
Andre Marie Ampere	1	Finite Element Method	16
Antennas		Fourier Transform	132,136,137,141,146
Dipole	2	Fringe field	4, 12,139
Araki	23	Gain	93
Asymmetric	194,195	Gaiuffret	26
Bahl	24	Gardiol	22
Bailey	21	Gaussian	136,137,139,141,145,148
Bhatnagar	5	Girishkumar	25
Bassinot	21	Glutton	21
Broadband	17, 18, 19, 132,139	Green's function	16, 17,18
Broad side	5, 10	Gupta	23, 25
Butler	23	Hall	24, 25
Byron	21	Hammer	22
Caver	22	Hans Christian Oersted	1
Cavity Model	12, 15	Hankel Transformation	23
Chadha	23	Hertz	1
Chaterjee	25	Helical	2
Chew	23	Homogeneous	132
Coaxial cable	7	Hori	25
Coaxial probe	7	Horn	2
Coffey	22	Howell	2, 21
Conformal	2, 21	Huynh	26
Cross-polarization	32,148	IE3D	97,101
Cullen	23	Input Impedance	37, 146,150,155,159, 162
Current distribution	3,12,17	Impedance Bandwidth	34
Dahelle	23	Isotropic	132
Das	25	Itoh	23, 24
Derneryd	21, 22, 24	Jagadish Chandra Bos	1
Deschamp	2, 21	James	21
Dielectric Constant	33	Karlsson	24
Dipole	2	Kong	23
Efficiency	33	Kraus	2
Electricity	1	Kuester	24
Electromagnetic Coupling	9, 33, 110	Leap-frog	131,132,136
Electromagnetic waves	1,131,132		

Lee	26	Radiating slots	4
Lewin	21	Ray	26
Lo	22, 28	Residuals	16
Long	21, 25	Richard	23
Loss tangent	4, 22	Sabban	25
Lubbers	132	Sanford	21
Luk	26, 27	Satellite communication	6
Magnetic Current	12	Scattering Parameters	131,140,141
Magnetic field	1, 4, 12, 15, 17 131-133,142	Schaubert	23
Mak	27	Shen	23
Marconi	1	Simulation	97, 99,101,127,128
Maxwell	131-134	Sommerfield	2, 16
Method of Moments	16	Stagger tuned	18
Mentzel	24	Symmetric	190,191
Michel Faraday	1	Targonski	26
Microstrip		Transmission Line Model	14
Patch antenna	10	Tulyathan	23
Slot antenna	10	Verma	24
Traveling wave antenna	10	Wood	24
Mink	23	Waterhouse	28
MMIC	2, 18	Weinschel	21
Mobile communication	18	Wilson	21
Modes operation		Yee	131-134,136
TM_{10}	12	Yung	23
TM_{01}	12		
TM_{20}	12		
Monopole	2		
Mosig	22		
Munson	2, 21		
Mur	139		
Nakagima	25		
Network Analyser	34,205,207,209		
Newman	22, 23		
Non-planar	6		
Numerical stability	132		
Palmer	29		
Pandharipande	24		
Parasitic	18		
Patnam Hanumantha Rao	31		
Permittivity	33, 83-86,107,109		
Poddar	25		
Polarization	2,108		
Proximity coupling	35		
Radiation	3, 4		

LIST OF PUBLICATIONS

INTERNATIONAL JOURNAL

1. **B. Lethakumary, Sreedevi K Menon, C.K.Aanandan and P.Mohanan,** "Wide Band Rectangular Microstrip Antenna Using an Asymmetric T-Shaped Feed", *Microwave & Optical Technology Letters*, Vol 37, No. 1, April 5 2003, pp 31-32.
2. **B. Lethakumary, Sreedevi K Menon, C.K.Aanandan, K Vasudevan and P.Mohanan,** "L-strip Excited Wideband Rectangular Microstrip Antenna", *Microwave & Optical Technology Letters*, Vol 42, No. 2, July 20 2004, pp173-175.
3. **B. Lethakumary, Sreedevi K Menon, C.K. Aanandan, K Vasudevan and P.Mohanan,** "FDTD Analysis of a Symmetric T-strip fed Wideband Rectangular Microstrip Antenna", *Microwave & Optical Technology Letters*, Vol 43, No. 4, November 20 2004, pp 332-334.
4. **B. Lethakumary, Sreedevi K Menon, Priya Francis C.K.Aanandan, K Vasudevan and P.Mohanan,** "Wide Band Rectangular Microstrip Antenna with Hook-shaped Feed" , *Microwave and Optical Technology Letters*, Vol.44, No.2, January 20 2005, pp169-171.
5. **Sreedevi K Menon, B Lethakumary, P. V. Bijumon, M. T. Sebastian, and P. Mohanan,** "L-strip Fed Wide Band Rectangular Dielectric Resonator Antenna" *Communicated to Microwave and Optical Technology Letters.*
6. **Sreedevi K Menon, B. Lethakumary, K. Vasudevan and P. Mohanan,** "Wide Band Rectangular Microstrip Antenna Using Symmetric T-Shaped Feed", *Microwave & Optical Technology Letters*, Vol 35, No. 3, November 5 2002, pp 235-236.
7. **Sreedevi K Menon, B Lethakumary, P. Mohanan, P. V. Bijumon and M. T. Sebastian,** "Wideband Cylindrical Dielectric Resonator Antenna Excited using an L-strip feed", *Microwave & Optical Technology Letters*, Vol 42, No: 4, August 20 2004, pp 293-294.
8. **S. Mridula, Sreedevi K Menon, B. Lethakumary, Binu Paul, C.K.Aanandan and P. Mohanan,** "Planar L – Strip Broad Band Microstrip Antenna", *Microwave & Optical Technology Letters*, Vol 34, No.2, July 20 2002, pp 115-117.
9. **Sreedevi. K Menon, Suma M N, B. Lethakumary, K. Vasudevan, C K Aanandan and P.Mohanan** "Comparison of different Electromagnetic

Band gap Structures”(Communicated to *IEEE transactions on Antennas and Propagation*).

10. **B. Lethakumary, Sreedevi K Menon, C.K.Aanandan and P. Mohanan,** “FDTD Analysis of L-strip fed Wideband Rectangular Microstrip Antenna”, (Communicated to *Microwave & Optical Technology Letters*).
11. **B. Lethakumary, Sreedevi K Menon, C.K.Aanandan and P. Mohanan,** “Broad band Rectangular Microstrip Antennas using Modified Microstrip feed”, (Communicated to *Microwave & Optical Technology Letters*).
12. **Sreedevi K Menon, B. Lethakumary, Suma M.N, C.K.Aanandan and P. Mohanan,** “Wideband Circular Microstrip Antennas”, (Communicated to *Microwave & Optical Technology Letters*).

SEMINAR /SYMPOSIA

International

1. **B. Lethakumary, Sreedevi K Menon,, C K Aanandan K. Vasudevan and P Mohanan** “ Wide band rectangular microstrip antenna” Proc., First International Conference on Microwaves, Antennas, Propagation and Remote Sensing (ICMARS 2003), International Centre for Radio Science, Jodhpur, Dec. 15-19 2003.
2. **Sreedevi K Menon, B. Lethakumary, C.K.Aanandan, K. Vasudevan and P. Mohanan,**“ Wide band Rectangular Microstrip Antenna using L-shaped feed”, Proc. 2002 IEEE Antennas and Propagation Society International Symposium, Texas, July 2002.
3. **Sreedevi K Menon, B. Lethakumary, C K Aanandan and P Mohanan,**“ Rectangular microstrip antenna with PBG structured ground plane” Proc., First International Conference on Microwaves, Antennas, Propagation and Remote Sensing (ICMARS 2003), International Centre for Radio Science, Jodhpur, Dec. 15-19 2003.

National Conference

1. **B. Lethakumary, Sreedevi K Menon, C.K.Aanandan, K Vasudevan and P.Mohanan,** “FDTD Analysis of L-strip Fed Microstrip Antenna”, Proc. National Symposium on Antennas and Propagation (APSYM 2002), Cochin, December 9 – 11 2002, pp. 58–60.
2. **B. Lethakumary, Sreedevi K Menon, C.K.Aanandan, K Vasudevan and P. Mohanan,** “L-strip fed Circular Microstrip Antenna”, Proc. National

Symposium on Antennas and Propagation (APSYM 2004), Cochin, December 21-23 2004.

3. Sreedevi K Menon, B Lethakumary, P Mohanan, P V Bijumon, and M T Sebastian "Dielectric Resonator Loaded Microstrip Antenna" Proc. Interactive Integrated Technological Advancement – Recent Trends (IITART), Trivandrum, 5 – 6 July 2002.
4. Sreedevi K Menon, B. Lethakumary, C.K.Aanandan, K Vasudevan and P.Mohanan, "Bandwidth Enhancement of Microstrip Antenna Using Photonic Band Gap Structure", Proc. National Symposium on Antennas and Propagation (APSYM 2002), Cochin, December 9 – 11 2002, pp. 305-308.
5. Sreedevi K Menon, Suma. M.N, B. Lethakumary, C.K.Aanandan, K Vasudevan and P. Mohanan, "Rectangular Microstrip Antenna on EBG ground plane with Unequal Orthogonal Periods", Proc. National Symposium on Antennas and Propagation (APSYM 2004), Cochin, December 21 – 23 2004.

G9049

225

RESUME OF THE CANDIDATE

LETHAKUMARY B



Permanent Address

Puthen Veedu,
Mylode P.O.
Pooyappally
Kollam 691 537
Kerala, India.

Present Address

Lecturer
Dept.of Electronics
University College of Engineering
Muttom P.O.
Thodupuzha
Idukki (Dst)
Kerala, India.

Phone: 91 474 2463752
E-mail: lethasreedharan@yahoo.co.in

Phone: 91 486 2256222
:91 486 2256422

Objective

To involve in the research work in Microwave Electronics with special interest to microstrip antennas, microwave communication, microwave photonics etc.

Research and development activities in the fields related to communication.

EDUCATION

- | | |
|---------------------------|-----------------------------------|
| a) Bachelor of Technology | Kerala University (November 1990) |
| b) Master of Technology | Kerala University (March 1994) |

COMPUTER PROFICIENCY

Programming Languages	FORTRAN, PASCAL, BASIC, C and MATLAB
Simulation Software	IE3D, FIDELITY

AWARDS OBTAINED

National Merit Scholarship – 1985

LIST OF PUBLICATIONS

: 12 International Journal papers and 8 National /International Symposia papers.

Membership in Professional bodies: LM, Indian Society for Technical Education (ISTE)
LM, Energy Conservation Society (ECS)